NAS1.26:3100
COMPLETED
APR 18 1980
ORIGINAL

NASA Contractor Report 3100

Rotary Balance Data for a Typical Single-Engine General Aviation Design for an Angle-of-Attack Range of 8° to 90°

I - Low-Wing Model A

Randy S. Hultberg and William Mulcay

CONTRACT NAS1-14849
FEBRUARY 1980

NASA

383

NASA Contractor Report 3100

Rotary Balance Data for a Typical Single-Engine General Aviation Design for an Angle-of-Attack Range of 8° to 90°

I - Low-Wing Model A

Randy S. Hultberg and William Mulcay
Bihrle Applied Research, Inc.
Jericho, New York

Prepared for
Langley Research Center
under Contract NAS1-14849

NASA
National Aeronautics
and Space Administration

Scientific and Technical
Information Office

1980

I

SUMMARY

Aerodynamic characteristics obtained in a rotational flow environment utilizing a rotary balance located in the Langley spin tunnel are presented in plotted form for a 1/5-scale, single-engine, low-wing, general aviation airplane model. The configurations tested included the basic airplane, various control deflections, tail designs, fuselage shapes and wing leading edges. Data are presented without analysis for an angle-of-attack range of 8° to 90° and clockwise and counter-clockwise rotations covering an $\frac{\Omega b}{2V}$ range from 0 to 0.85.

INTRODUCTION

The NASA Langley Research Center has initiated a broad general aviation stall/spin research program which includes spin-tunnel and free-flight radio control model tests, as well as full-scale flight tests for a number of configurations typical of light, general aviation airplanes. To support this effort, rotary balance wind tunnel force tests covering these same configurations will be conducted to establish a data base for analysis of model and full-scale flight results, and to develop design charts for desirable stall/spin characteristics.

A 1/5-scale, single-engine, general aviation airplane model, referred to as model A, having a low-wing location was tested in a rotational flow environment utilizing a rotary balance located in the Langley spin tunnel. This report presents the data obtained for the basic airplane, various control deflections, tail designs, fuselage shapes and wing leading edges. These data supplement the rotary balance data presented in references 1 and 2.

Reference 1 data is mainly concerned with the fuselage modifications and airplane components previously tested statically (reference 3) at a low and high Reynolds number in the Ames Research Center 12-foot Pressure Tunnel. Data solely relative to leading-edge wing modifications are presented in reference 2. Data for model A having a high-wing location are presented in reference 4.

SYMBOLS

The units for physical quantities used herein are presented in the International System of Units (SI) and U.S. Customary Units. The measurements were made in the U.S. Customary Units; equivalent dimensions were determined by using the conversion factors given in reference 5.

b	wing span, m (ft)
$\bar{c}$	mean aerodynamic chord, cm (in.)
C_L	lift-force coefficient, $\frac{\text{Lift force}}{qS}$
C_N	normal-force coefficient, $\frac{\text{Normal force}}{qS}$
C_A	axial-force coefficient, $\frac{\text{Axial force}}{qS}$
C_Y	side-force coefficient, $\frac{\text{Side force}}{qS}$
C_ℓ	rolling moment coefficient, $\frac{\text{Rolling moment}}{qSb}$
C_m	pitching-moment coefficient, $\frac{\text{Pitching moment}}{qS\bar{c}}$
C_n	yawing moment coefficient, $\frac{\text{Yawing moment}}{qSb}$
q	free-stream dynamic pressure, N/m^2 (lb/ft^2)
S	wing area, m^2 (ft^2)
V	free-stream velocity, m/sec (ft/sec)
α	angle of attack, deg

β	angle of sideslip, deg
Ω	angular velocity about spin axis, rad/sec
$\frac{\Omega b}{2V}$	spin coefficient, positive for clockwise spin
δ_a	aileron deflection, positive when right aileron is down $(\delta_{a_{right}} - \delta_{a_{left}})/2$, deg
δ_e	elevator deflection, positive when trailing edge is down, deg
δ_r	rudder deflection, positive when trailing edge is to left, deg

Abbreviations:

cg	center of gravity
SR	spin radius
TE	trailing edge

TEST EQUIPMENT

A rotary balance measures the forces and moments acting on an airplane while subjected to rotational flow conditions; the background for this apparatus is discussed in reference 1. A photograph and sketch of the rotary balance apparatus installed in the Langley spin tunnel are shown in figures 1 and 2, respectively. The rotating portion of the balance system, mounted on a horizontal supporting boom which is hinged at the wall, is moved from the wall to the center of the tunnel by cables. The rotary arm of the balance system, which rotates about a vertical axis, is attached to the outer end of the horizontal supporting boom and is driven by a drive shaft through couplings and gears.

A test model is mounted on a strain gauge balance which is affixed to the bottom of the rotary balance apparatus. Controls located outside the tunnel are used to activate motors on the rig which position the model to the desired attitude. The angle-of-attack range of the rig is 8 to 90 degrees and the sideslip angle range is ±15 degrees. The spin radius and the lateral displacement motors allow the operator to position the moment center of the balance on the spin axis or at a specific distance from the spin axis. This is done for each combination of angle of attack and sideslip angle. The general practice is to mount the moment center of the balance at the cg location about which the aerodynamic moments are desired. Electrical current from the balance, and to the motors on the rig, is conducted through slip-rings located at the rig head. Examples of how the rig is positioned for different angle of attack and sideslip angles are shown in figures 2a and 2b, respectively.

The model can be rotated up to 90 rpm in either direction. By using different rotational speeds and a specific airflow in the tunnel, the motions of a steady spinning airplane can be simulated. The aerodynamic forces and moments can then be measured for values of $\frac{\Omega b}{2V}$, including the case of $\frac{\Omega b}{2V} = 0$, where static aerodynamic forces and moments can be obtained.

A NASA six-component strain gauge balance is mounted inside the model and measures the normal, lateral and longitudinal forces and the yawing, rolling and pitching moments acting about the model body axis. The interactions that exist between the six components are available from balance calibration tests and are accounted for after the balance voltages are converted to forces and moments.

The data acquisition, reduction and presentation system for the rotary balance set-up is composed of a 12-channel scanner/voltmeter, a mini-computer and a plotter. With this equipment, on-line digital print-out and/or graphical plots of data are possible.

TEST PROCEDURES

Rotary aerodynamic data are obtained in two steps. The first step is to record the inertial forces and moments (tares) acting on the model at different attitudes and rotational speeds. To accomplish this, a covered bird-cage like structure is mounted to the upper rig which encloses the model without touching it. In this manner, the air immediately surrounding the model is rotated with it. As the rig is rotated at the desired attitude and rate, the inertial forces and moments generated by the model are measured and stored on magnetic tape for later use.

The second step in the data-gathering process is to measure aerodynamic and inertial forces at different attitudes and rotational speeds for a selected tunnel velocity with, of course, the cage structure removed. The tares are subtracted from these values, and the remaining aerodynamic forces and moments are then converted to coefficient form and stored on magnetic tape.

MODEL

A 1/5-scale fiberglass/foam/plywood model of a configuration considered to be a typical low-wing, single-engine, light general aviation airplane was tested in the present study. A three-view drawing of this model is shown in figure 3, dimensional characteristics of the model are presented in Table I, and a photograph of the model installed on the rotary balance located in the Langley spin tunnel is presented in figure 1.

The model was fabricated such that various wing, tail and fuselage configurations could be tested. The two tail configurations tested involved different locations of the horizontal tail as shown in figure 4. The fuselage shape and wing leading edge modifications tested are shown in figure 5 and 6 respectively.

The model control surfaces could be set at any position prior to the test. The maximum deflections for the control surfaces were:

Elevator, deg	25 up, 15 down
Rudder, deg	25 right, 25 left
Aileron, deg	25 up, 20 down

TEST CONDITIONS

The tests were conducted in the spin tunnel at a tunnel velocity of 7.62 m/sec (25 ft/sec) which corresponds to a Reynolds number of 128,000 based on the model mean aerodynamic chord. Unless noted otherwise in Table II, all the configurations were tested through an angle-of-attack range of 8 to 90° at a zero sideslip angle with the spin axis passing through the full-scale airplane cg location of $.255\bar{c}$ for angles of attack above 30°. For angles of attack below 35°, the spin axis was set 76.2 cm (30 in.) forward of the cg. Consequently, data was obtained for both a 0 and 76.2 cm (30 in.) spin radius at angles of attack of 30 and 35°. At each spin attitude, measurements were obtained for nominal $\frac{\Omega b}{2V}$ values of .1, .2, .3, .4, .45, .55, .65, .75 and .85 in both clockwise and counter-clockwise directions, as well as for $\frac{\Omega b}{2V}=0$ (static value).

DATA PRESENTATION

Table II identifies the configurations tested and the corresponding appendix figure numbers which present the aerodynamic data. The aerodynamic coefficients vs. $\frac{\Omega b}{2V}$ are presented for each configuration in six sequentially numbered figures in the following order: C_n, C_ℓ, C_m, C_N, C_Y and C_A. Each figure, in turn, consists of four pages which present the subject aerodynamic coefficient vs. $\frac{\Omega b}{2V}$ for the following angles of attack and spin radii, unless noted otherwise in Table II.

a) α= 8, 10, 12, 14, 16 deg SR= 76.2 cm (30 in.)
b) α= 18, 20, 25, 30, 35 deg SR= 76.2 cm (30 in.)
c) α= 30, 35, 40, 45, 50 deg SR= 0
d) α= 55, 60, 70, 80, 90 deg SR= 0

All the moment data are presented for a cg position of $0.255\bar{c}$.

Lift coefficient as a function of angle of attack for zero rotation rate is presented at the end of the Appendix for the configurations cited in Table II.

REFERENCES

1. Bihrle, William, Jr.; Hultberg, Randy S.; Mulcay, William: Rotary Balance Data for a Typical Single-Engine Low-Wing General Aviation Design for an Angle-of-Attack Range of 30° to 90°. NASA CR-2972, 1978.

2. Bihrle, William, Jr.; Mulcay, William: Rotary Balance Data for a Typical Single-Engine General Aviation Design for an Angle-Of-Attack Range of 8° to 35°. III- Effect of Wing Leading-Edge Modifications Model A. NASA CR-3102, 1979.

3. Bihrle, William, Jr.; Barnhart, Billy; Pantason, Paul: Static Aerodynamic Characteristics of a Typical Single-Engine Low-Wing General Aviation Design for an Angle-of-Attack Range of -8° to 90°. NASA CR 2971, 1978

4. Mulcay, William ; Rose, Robert: Rotary Balance Data for a Typical Single-Engine General Aviation Design for an Angle-of-Attack Range of 8° to 90°. II- High Wing Model A. NASA CR-3101, 1979.

5. Mechtly, E.A.: The International System of Units - Physical Constants and Conversion Factors. NASA SP-7012, 1973.

TABLE I.- DIMENSIONAL CHARACTERISTICS OF THE BASIC MODEL

Overall length with tail #4, m (ft)	1.23 (4.05)
Wing:	
Span, m (ft)	1.46 (4.80)
Area, m^2 (ft^2)	0.36 (3.87)
Root chord, cm (in.)	24.54 (9.66)
Tip chord, cm (in.)	24.54 (9.66)
Mean aerodynamic chord, cm (in.)	24.54 (9.66)
Leading edge of $\bar{c}$, distance rearward of leading edge of root chord, cm (in.)	0
Aspect ratio	5.9
Dihedral, deg	5.0
Incidence:	
Root, deg	3.5
Tip, deg	3.5
Airfoil section	NACA 64_2-415 modified
Horizontal tail:	
Span, m (ft)	0.47 (1.53)
Incidence, deg	-3.0
Airfoil section	NACA 65_1-012
Vertical tail:	
Airfoil section	NACA 65_1-012

TABLE II.- CONFIGURATIONS TESTED AND FIGURE INDEX

(Unless noted otherwise, all configurations tested through $\alpha = 8$ to 90° at $\beta = 0^\circ$.)

FIGURE NO.	CONFIGURATION	δ_e deg	δ_a deg	δ_r deg	REMARKS
[a]A1-A6	Basic (#4 Horizontal tail)	0	0	0	
A7-A12	↓		↓	-25	
A13-A18	↓	+15	↓	↓	
A19-A24	↓	-15	↓	↓	
A25-A30	↓	-25	↓	↓	
A31-A36	↓	↓	+22.5	↓	
A37-A42	↓	↓	-22.5	↓	
A43-A48	↓	↓	+22.5	0	
A49-A54	↓	0	0	↓	$\beta = +10^\circ$
A55-A60	↓	↓	↓	↓	$\beta = -10^\circ$
A61-A66	with rounded fuselage bottom aft of wing TE	↓	↓	↓	only $\alpha=30$ to 90°, SR=0
A67-A72	with rounded fuselage bottom aft of engine cowling	↓	↓	↓	only $\alpha=30$ to 90°, SR=0
A73-A78	with rounded fuselage bottom aft of engine cowling and wing fairings removed	↓	↓	↓	only $\alpha=55$ to 90°, SR=0
[a]A79-A84	with full-span leading-edge wing droop	↓	↓	↓	
A85-A90	#3 Horizontal tail	↓	↓	↓	
A91-A96	with rounded fuselage bottom aft of wing TE	↓	↓	↓	only $\alpha=30$ to 90°, SR=0
A97-A102	with rounded fuselage bottom aft of engine cowling	↓	↓	↓	only $\alpha=30$ to 90°, SR=0
A103-A108	with rounded fuselage bottom aft of engine cowling and wing fairings removed	↓	↓	↓	only $\alpha=30$ to 90°, SR=0
A109-A114	with full-span leading-edge wing droop	↓	↓	↓	

---

[a] C_L vs α presented in figure A115.

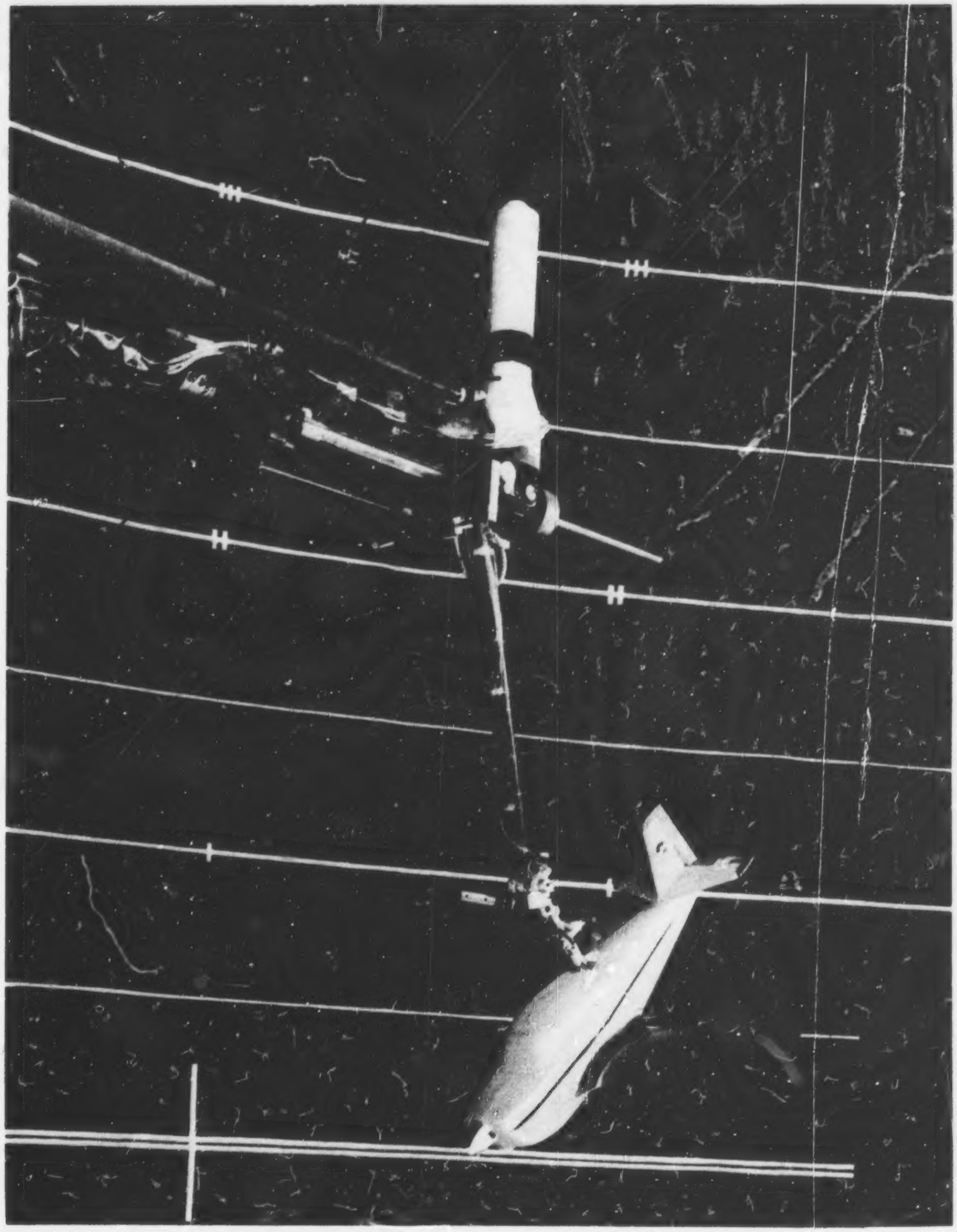

Figure 1.- Photograph of 1/5-scale model installed on rotary balance apparatus.

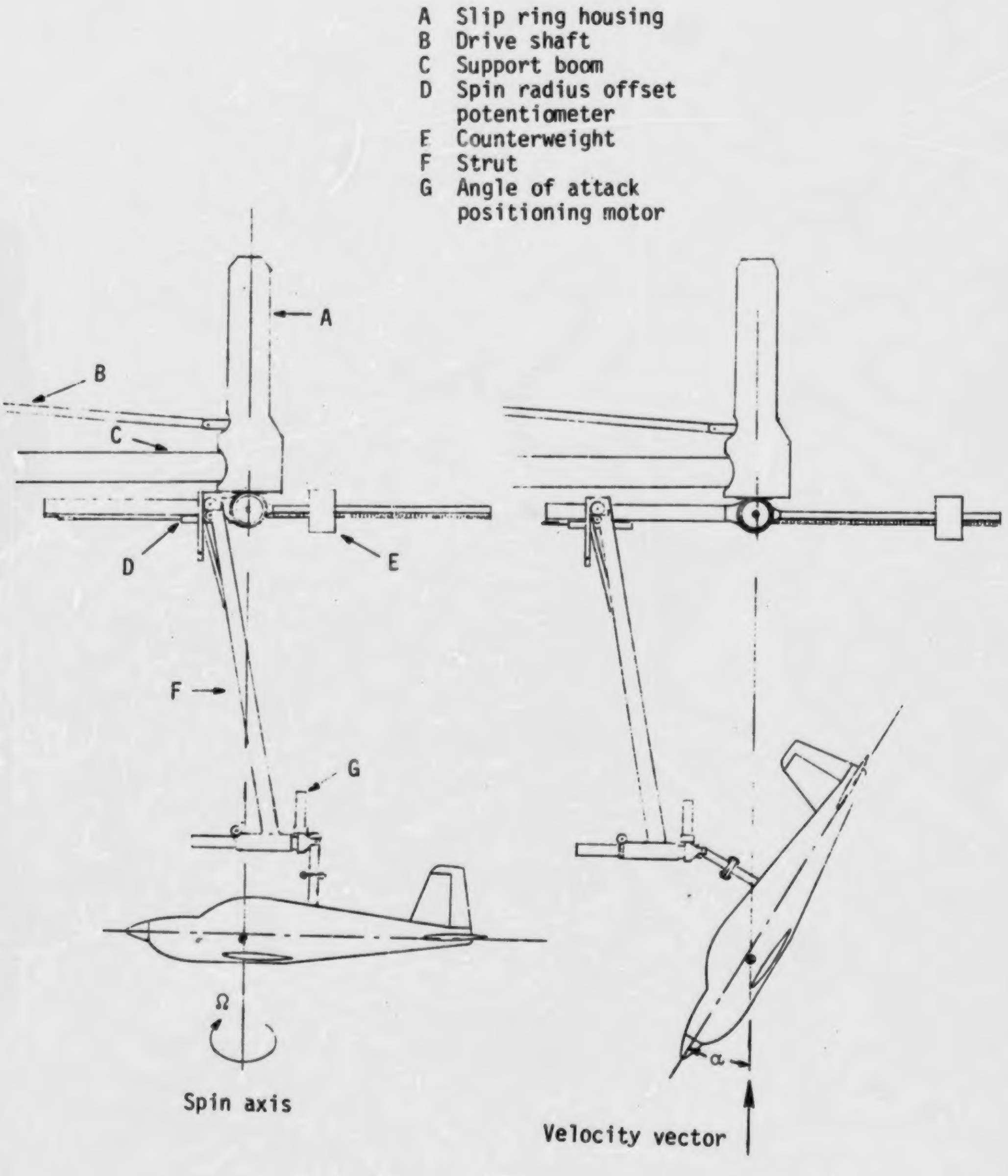
A Slip ring housing
B Drive shaft
C Support boom
D Spin radius offset potentiometer
E Counterweight
F Strut
G Angle of attack positioning motor
A
B
C
D
E
F
G
Ω
Spin axis
α
Velocity vector

(a) Side view of model.

Figure 2.- Sketch of rotary balance apparatus.

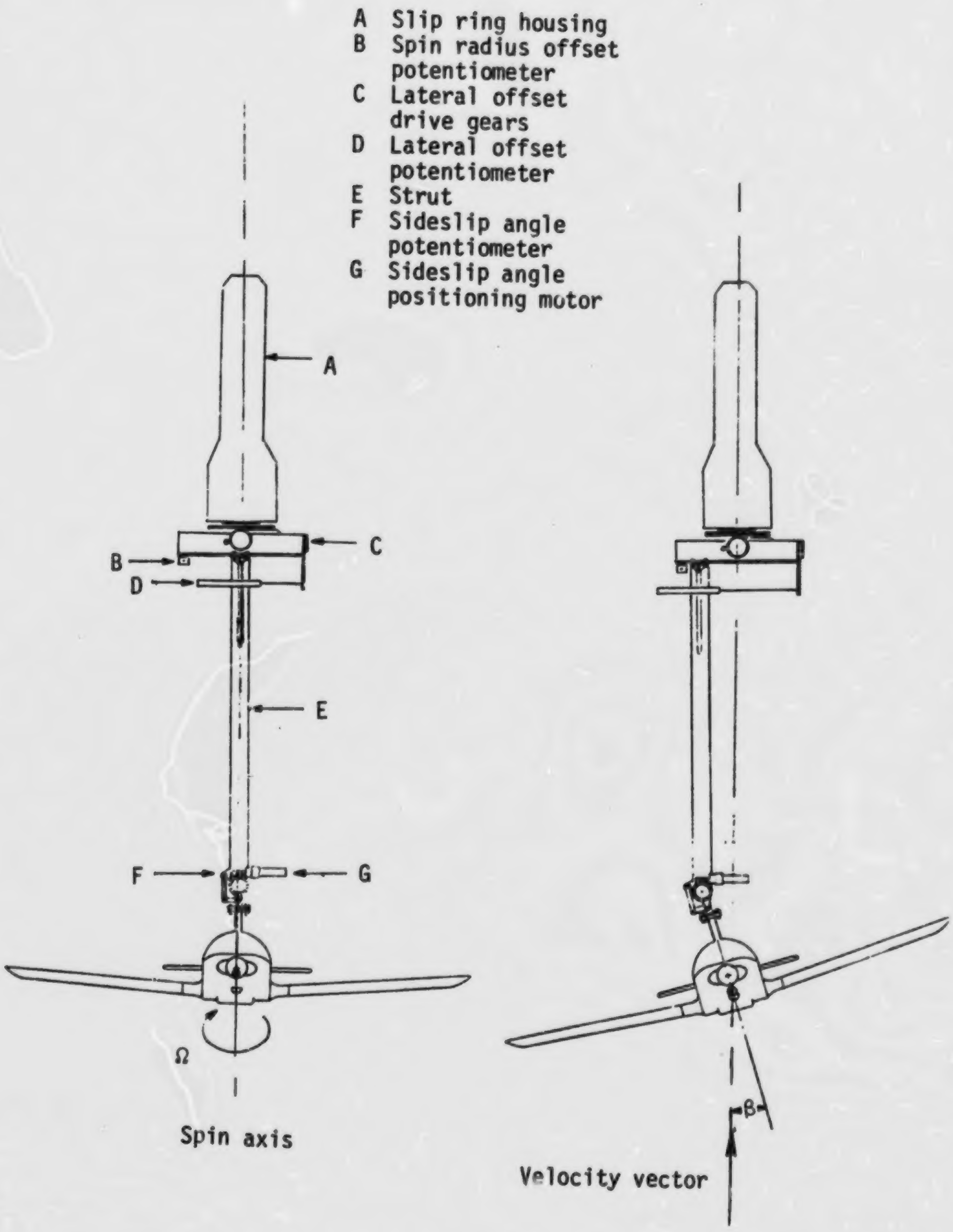
A Slip ring housing
B Spin radius offset potentiometer
C Lateral offset drive gears
D Lateral offset potentiometer
E Strut
F Sideslip angle potentiometer
G Sideslip angle positioning motor
A
B
C
D
E
F
G
Ω
Spin axis
β
Velocity vector

(b) Front view of model.

Figure 2.- Concluded.

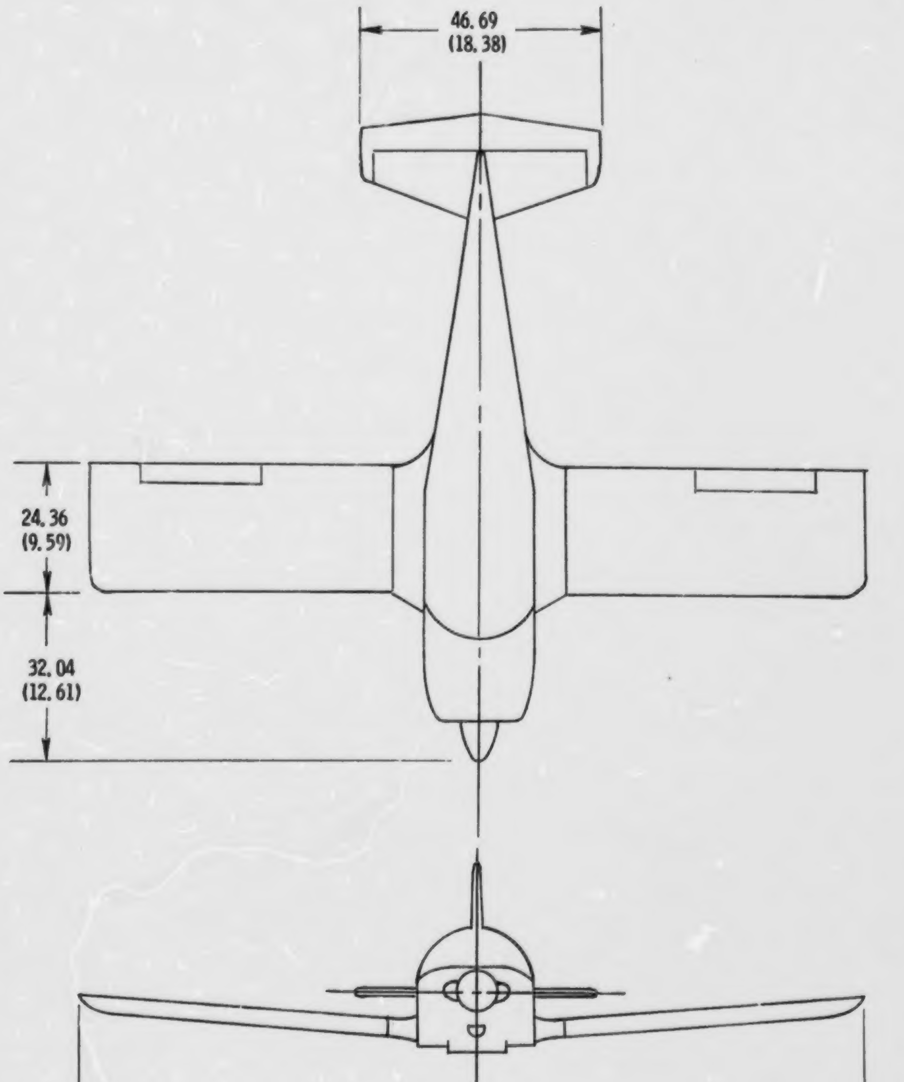
46.69
(18.38)
24.36
(9.59)
32.04
(12.61)
149.10
(58.70)
fuselage
reference
line
38.26
(15.06)
1.07
(.42)
114.97
(45.26)

Figure 3. - Three-view drawing of 1/5-scale low-wing general aviation model A. Center-of-gravity positioned at 0.255c̄. Dimensions are given in centimeters(inches), model scale.

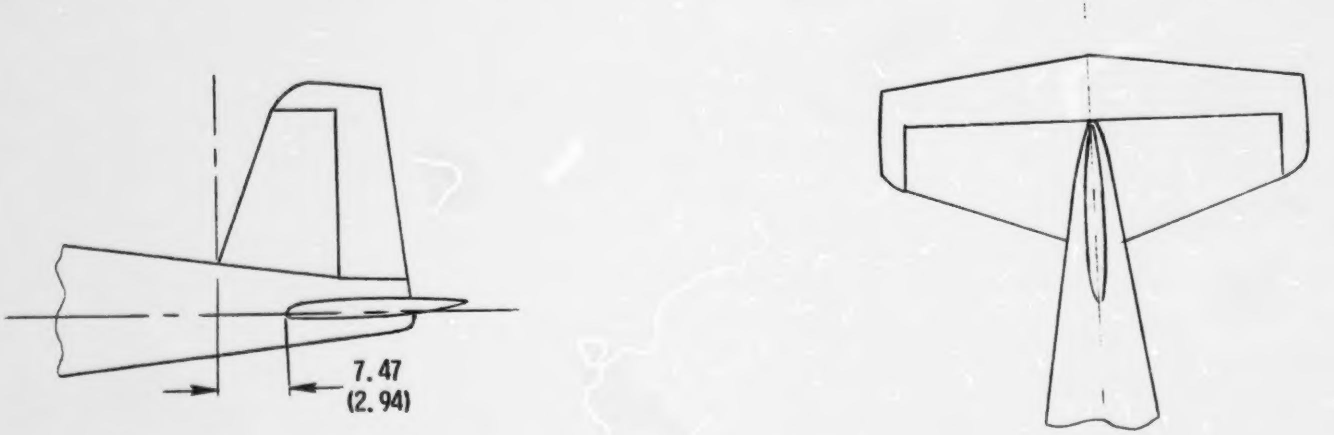

b) Tail 4

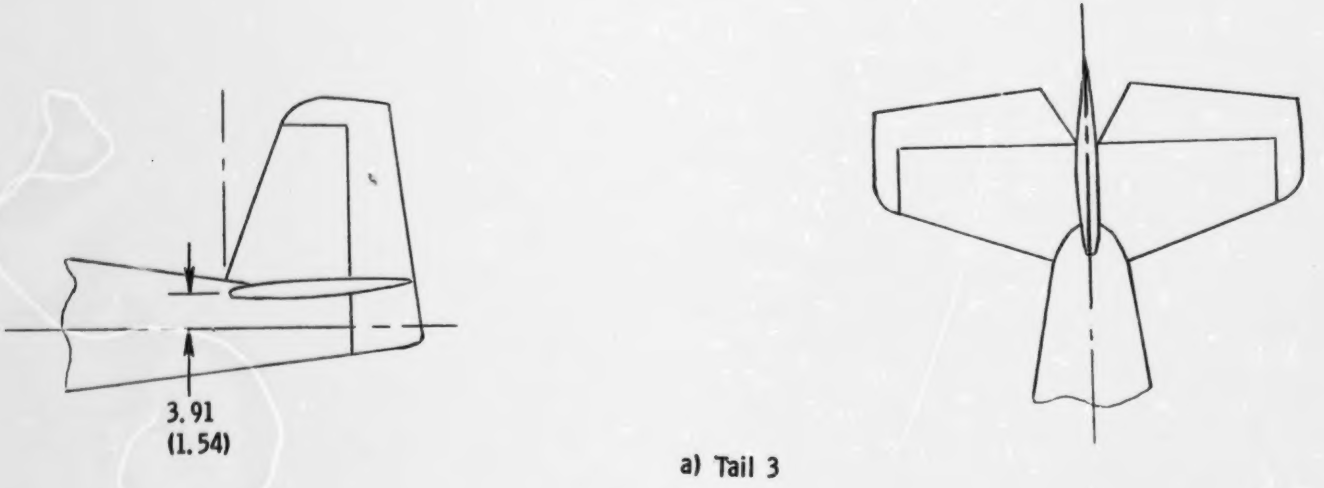

a) Tail 3

Figure 4. -Tail configurations tested on model. Dimensions are given in centimeters (inches), model scale.

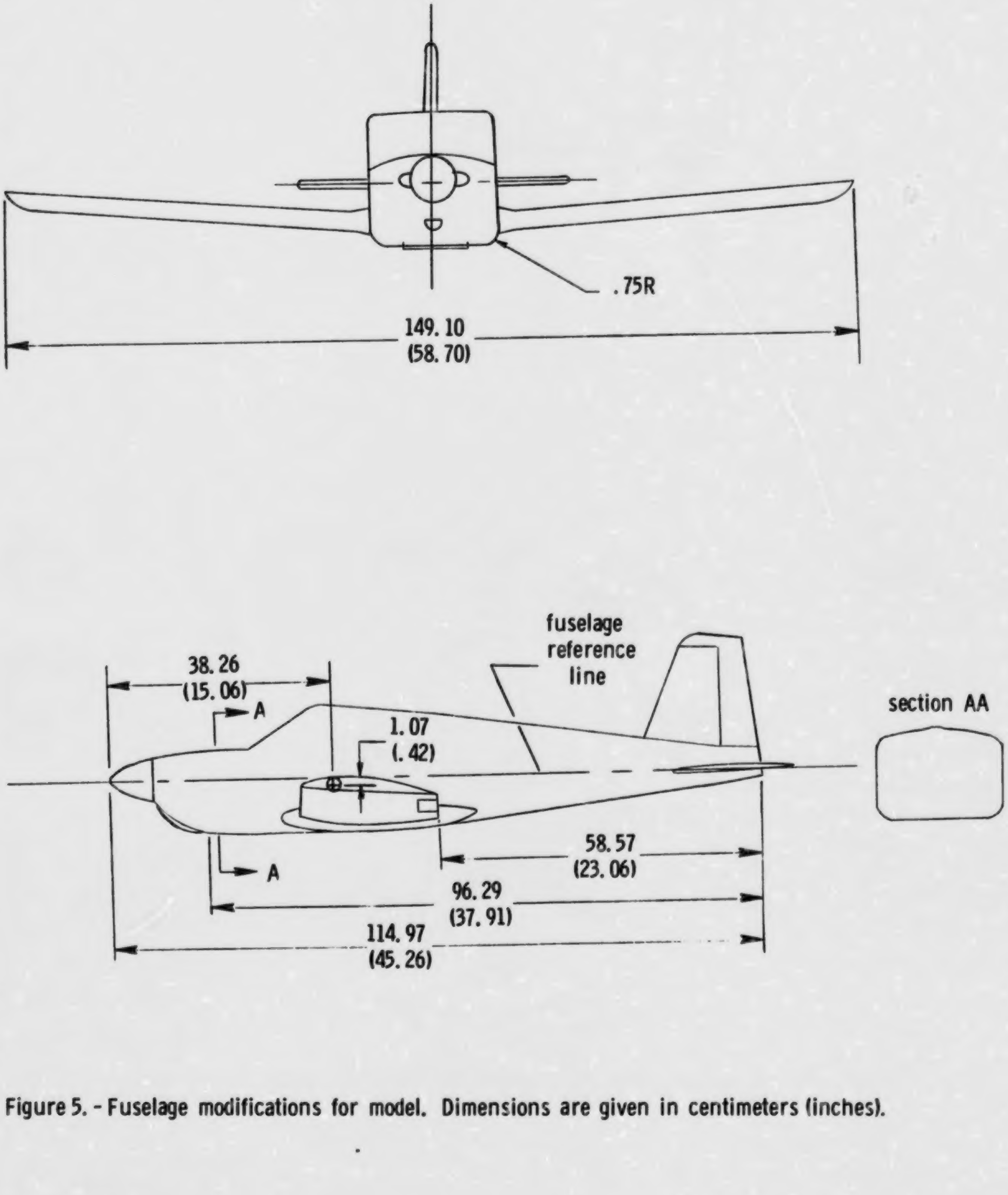
.75R
149.10
(58.70)
fuselage
reference
line
38.26
(15.06)
A
1.07
(.42)
section AA
A
58.57
(23.06)
96.29
(37.91)
114.97
(45.26)

Figure 5. - Fuselage modifications for model. Dimensions are given in centimeters (inches).

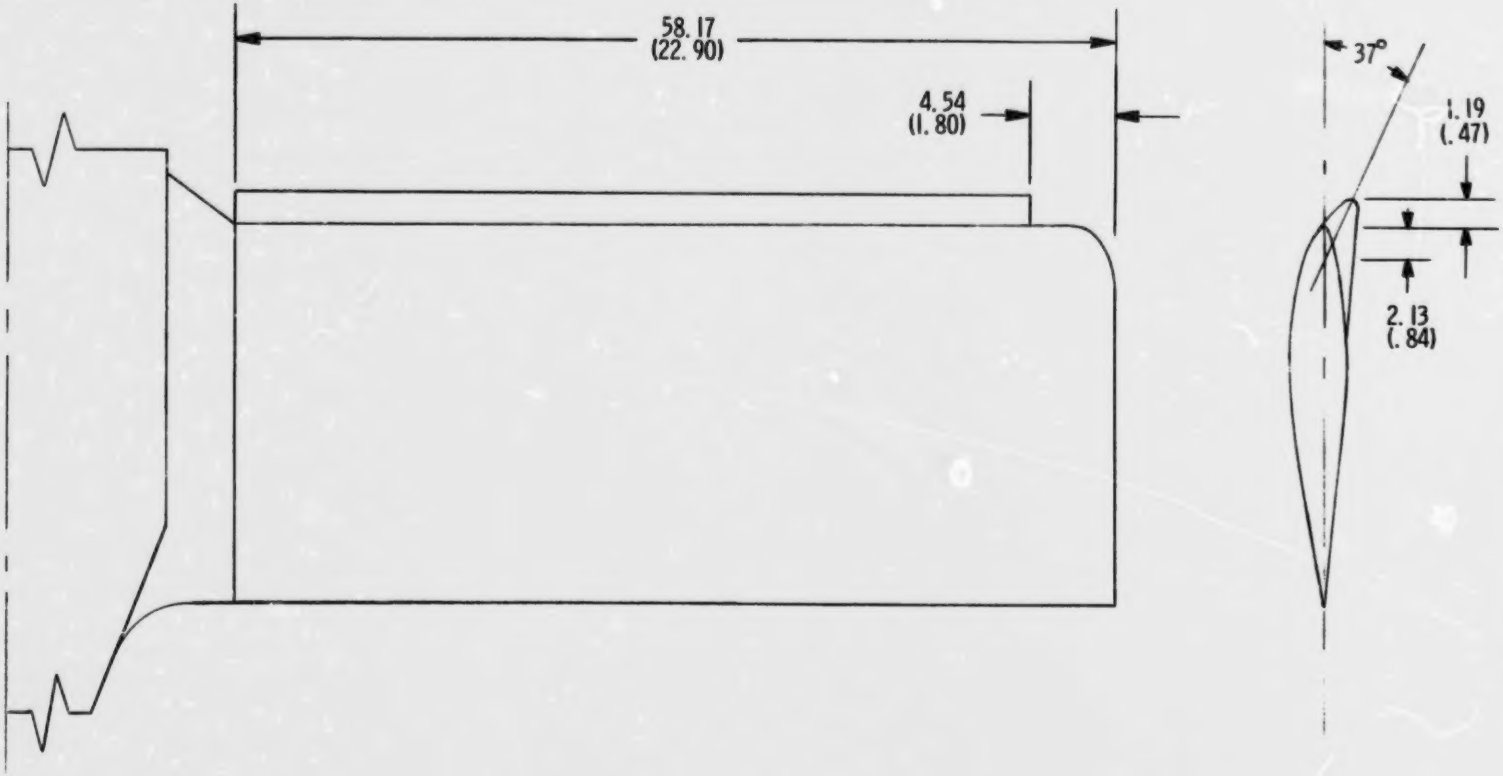
58.17
(22.90)
4.54
(1.80)
37°
1.19
(.47)
2.13
(.84)

Figure 6. - Basic airfoil with leading edge droop tested on model. Dimensions are given in centimeters (inches), model scale.

APPENDIX

A2

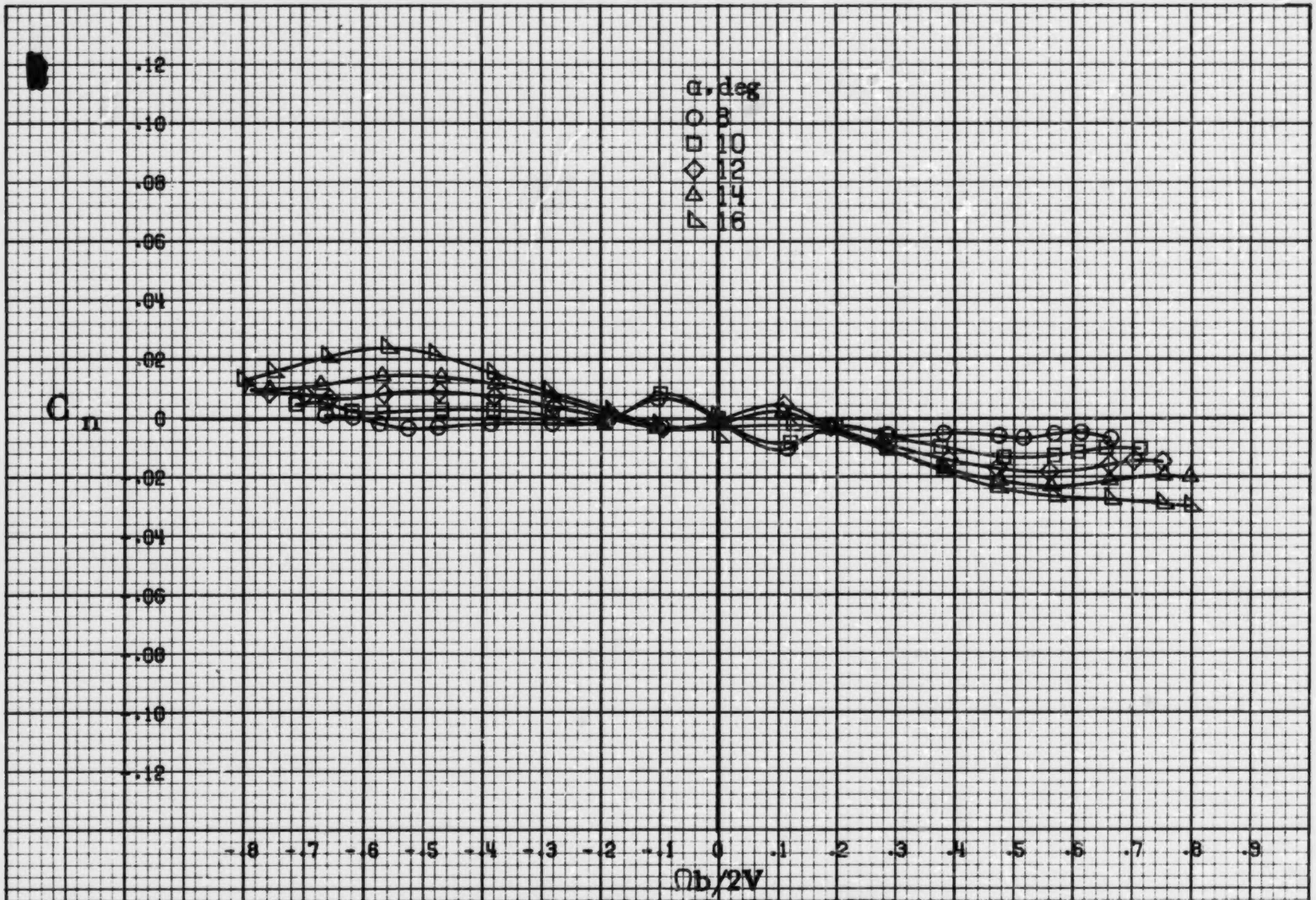

(a) α=8to16deg, SR=76cm(30in).

Figure A1.-Effect of rotation rate and angle of attack on yawing-moment coefficient for basic configuration. $\delta_e = 0°$, $\delta_a = 0°$, $\delta_r = 0°$. $\beta = 0°$.

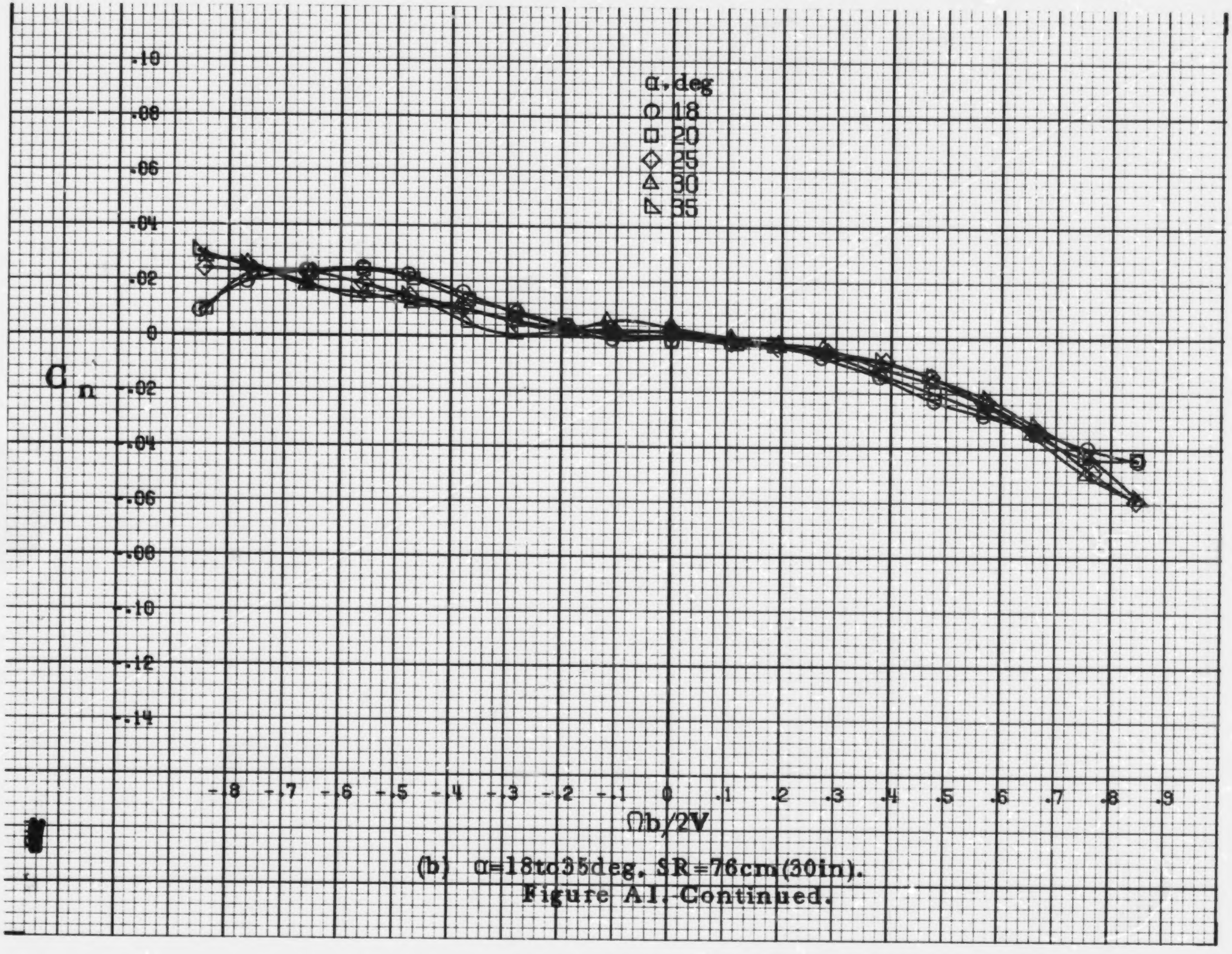

(b) α=18 to 35 deg, SR=76 cm (30 in).

Figure A1. Continued.

BLANK PAGE

BLANK PAGE

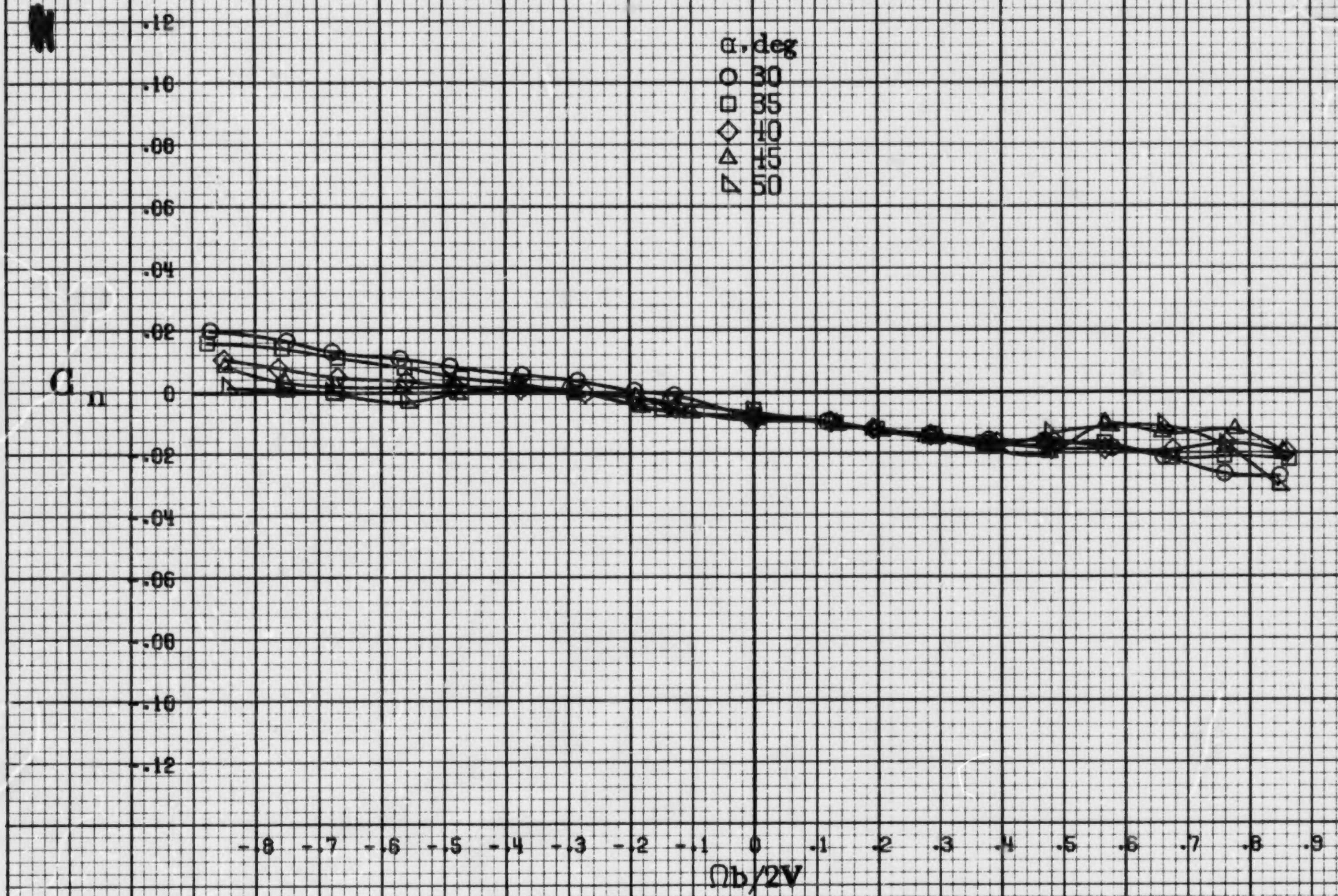

(c) α=30to50deg, SR=0.
Figure A1.-Continued.

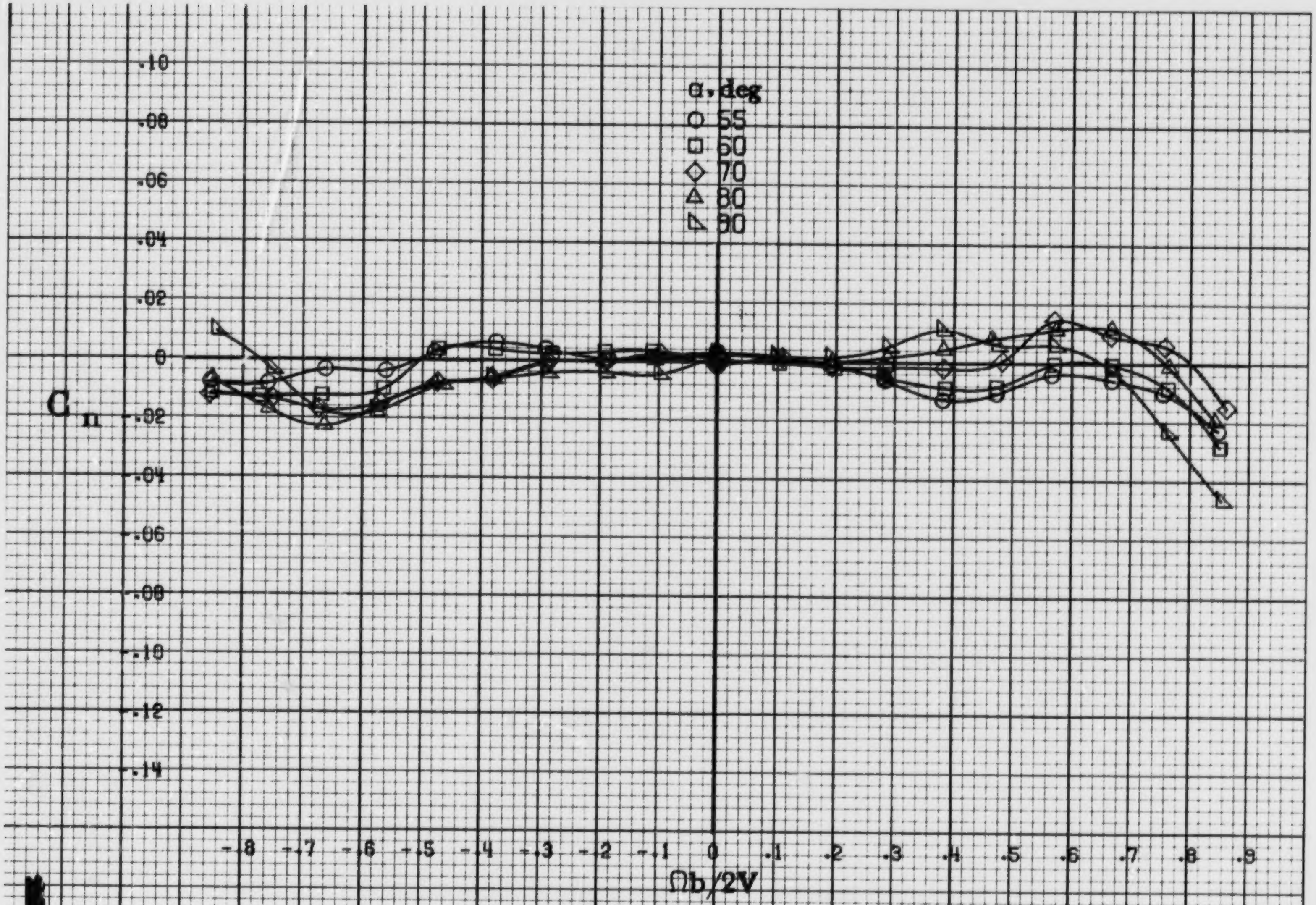

(d) α=55to90deg, SR=0.

Figure A1.-Concluded.

A6

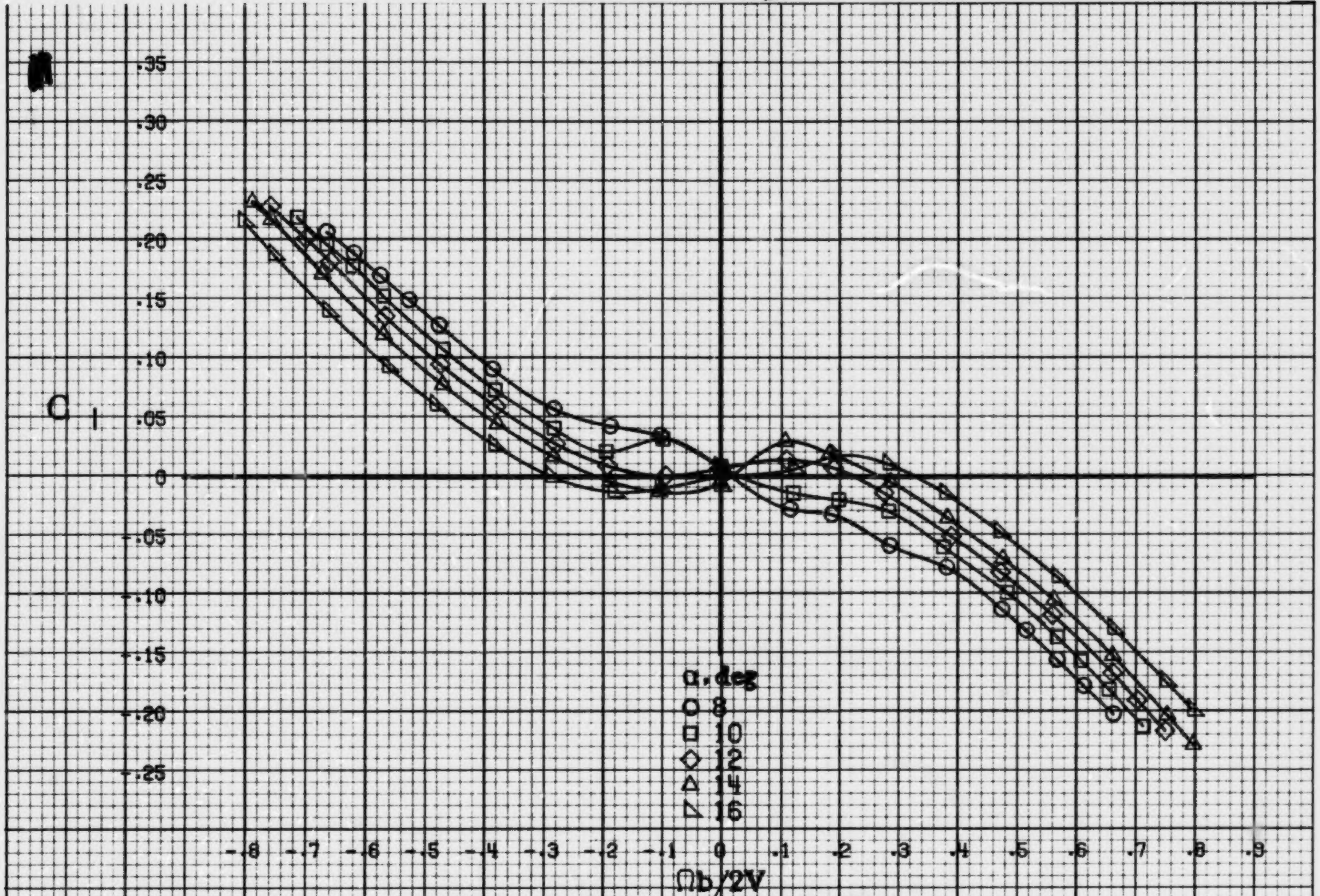

(a) α=8to15deg, SR=76cm(30in).

Figure A2.-Effect of rotation rate and angle of attack on rolling-moment coefficient for basic configuration. $\delta_e = 0°$. $\delta_a = 0°$. $\delta_r = 0°$. $\beta = 0°$.

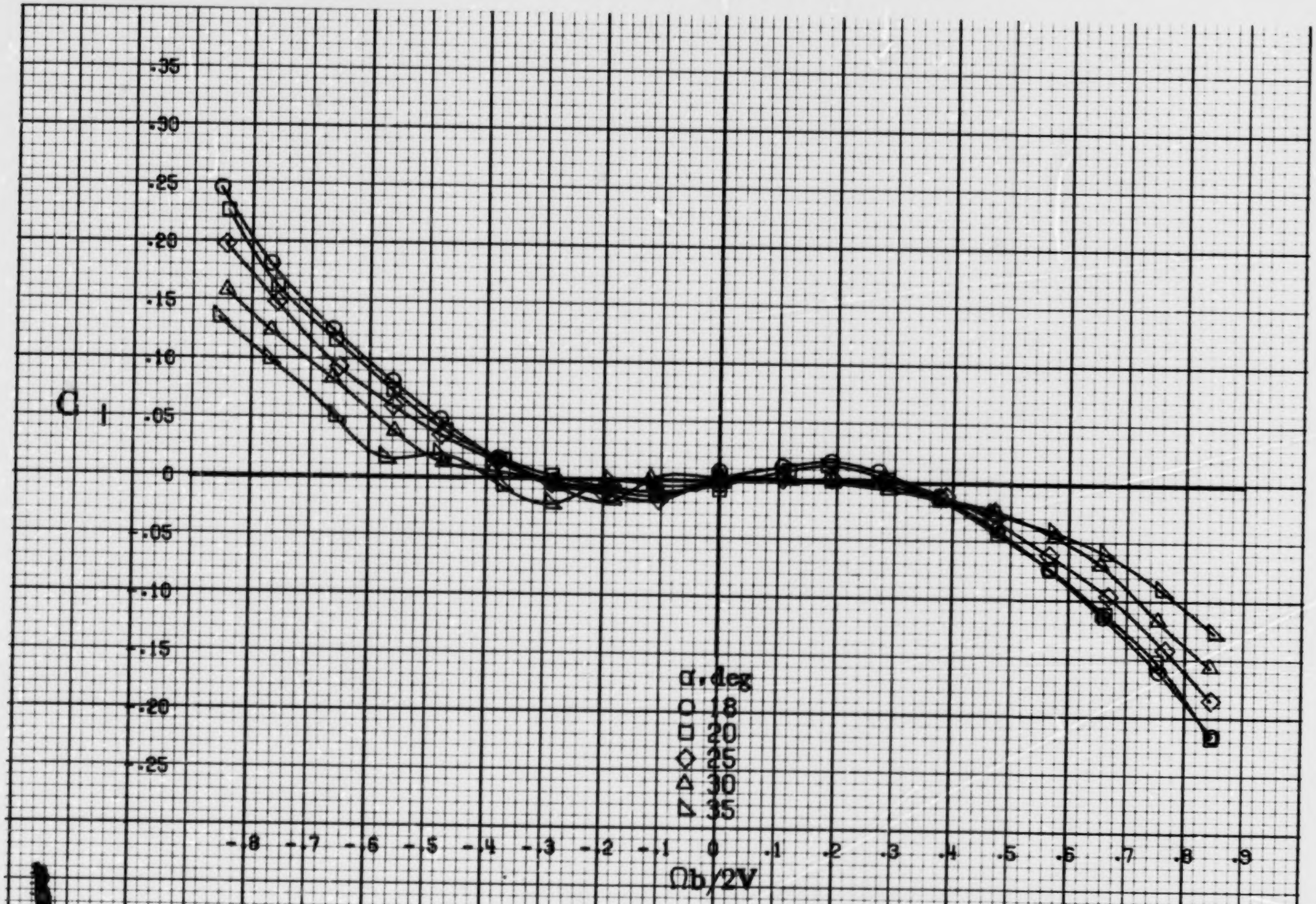

(b) α=18to35deg. SR=76cm(30in).
Figure A2.-Continued.

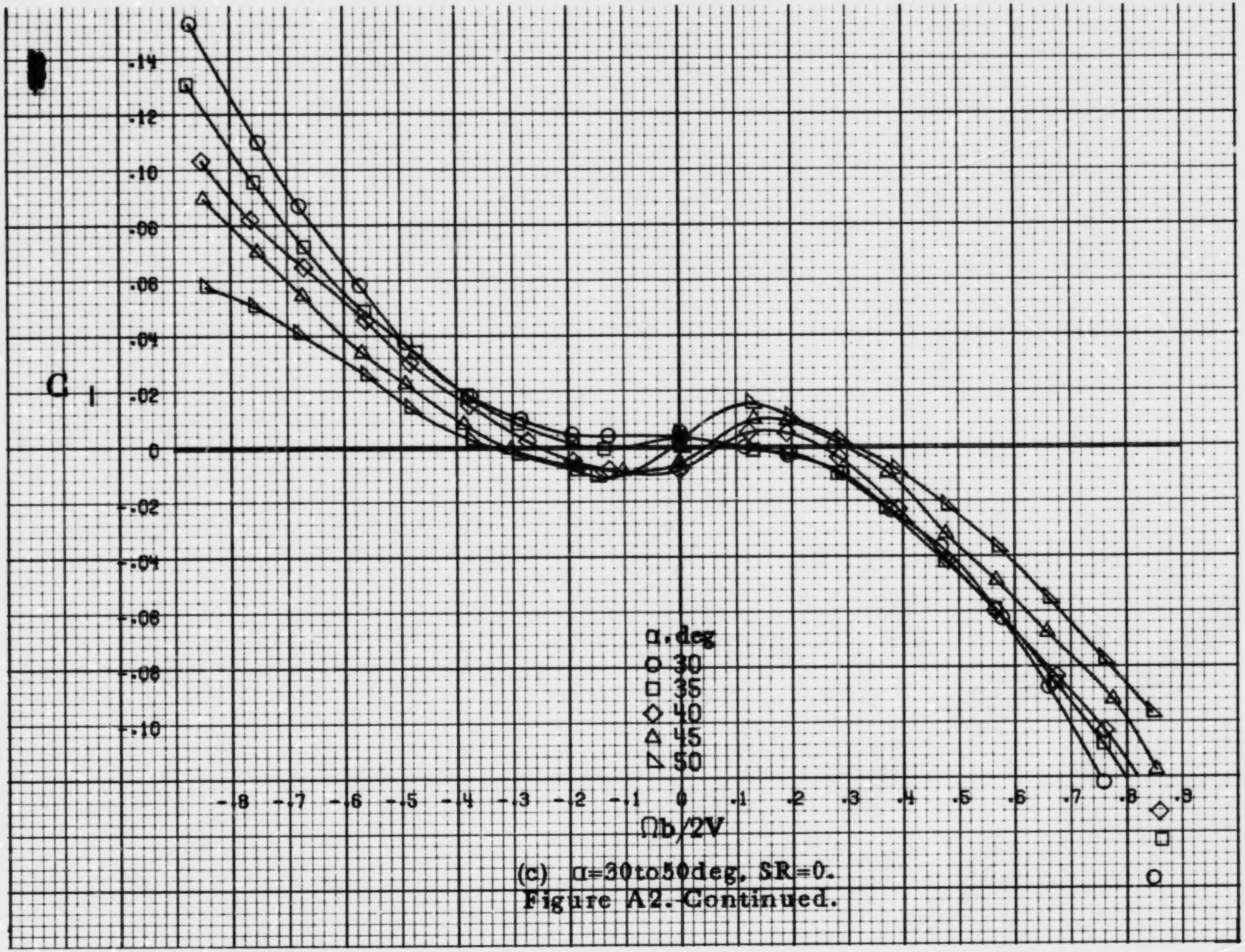

(c) α=30to50deg, SR=0.

Figure A2. Continued.

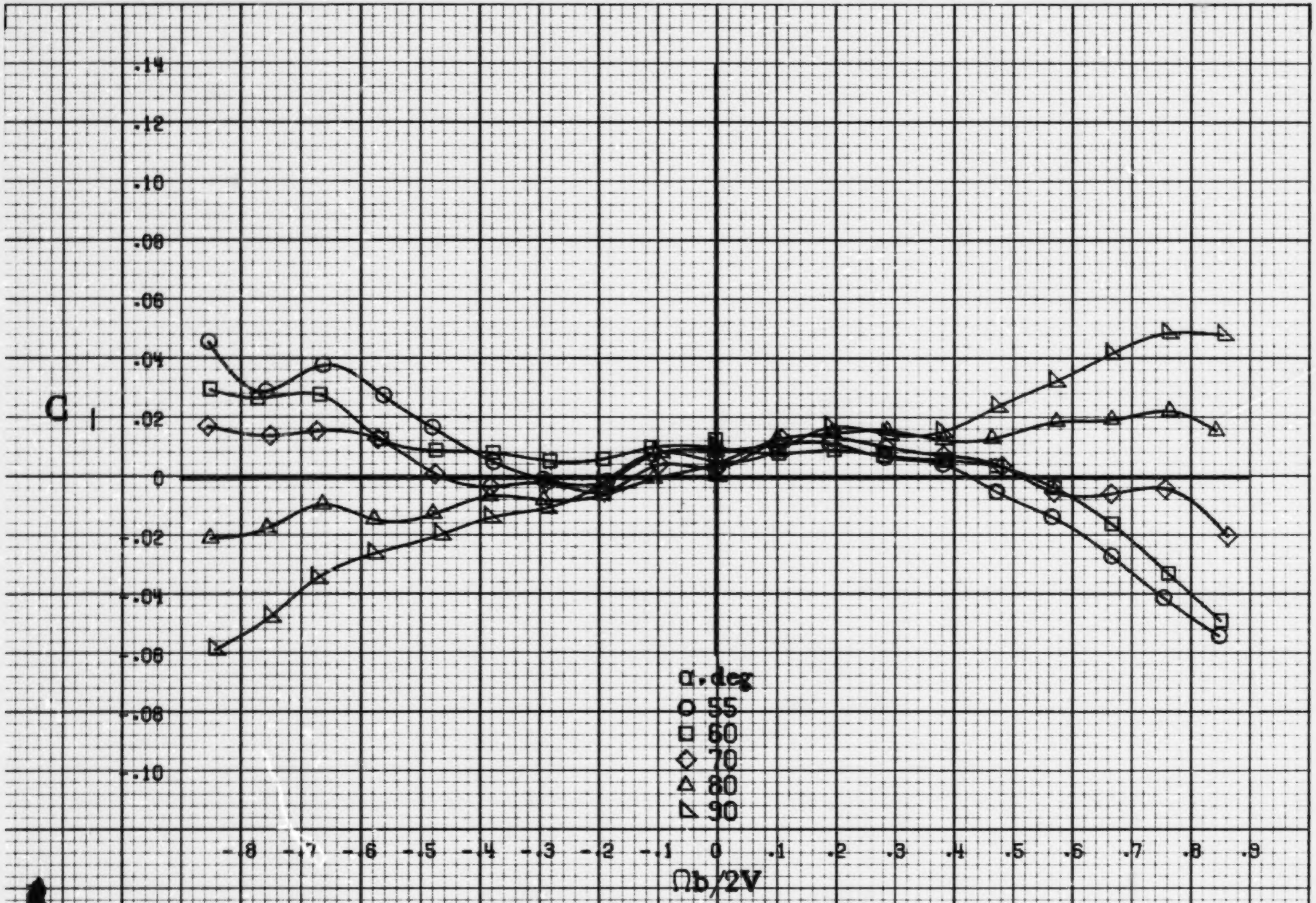

(d) α=55to90deg, SR=0.
Figure A2. Concluded.

A10

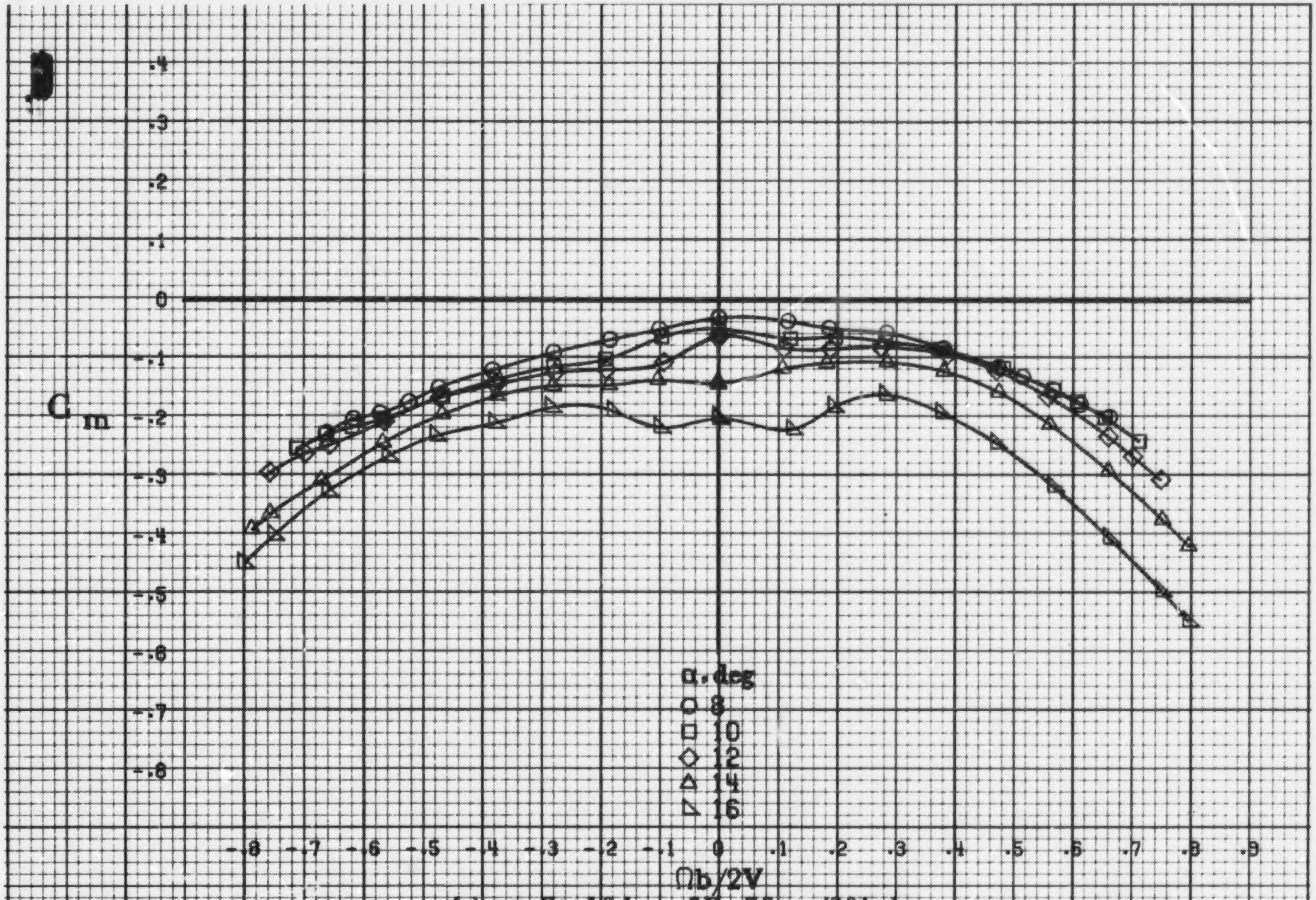

(a) α=8to16deg, SR=76cm(30in).

Figure A3.-Effect of rotation rate and angle of attack on pitching-moment coefficient for basic configuration. δ_e =0°. δ_a =0°. δ_r =0°. β =0°.

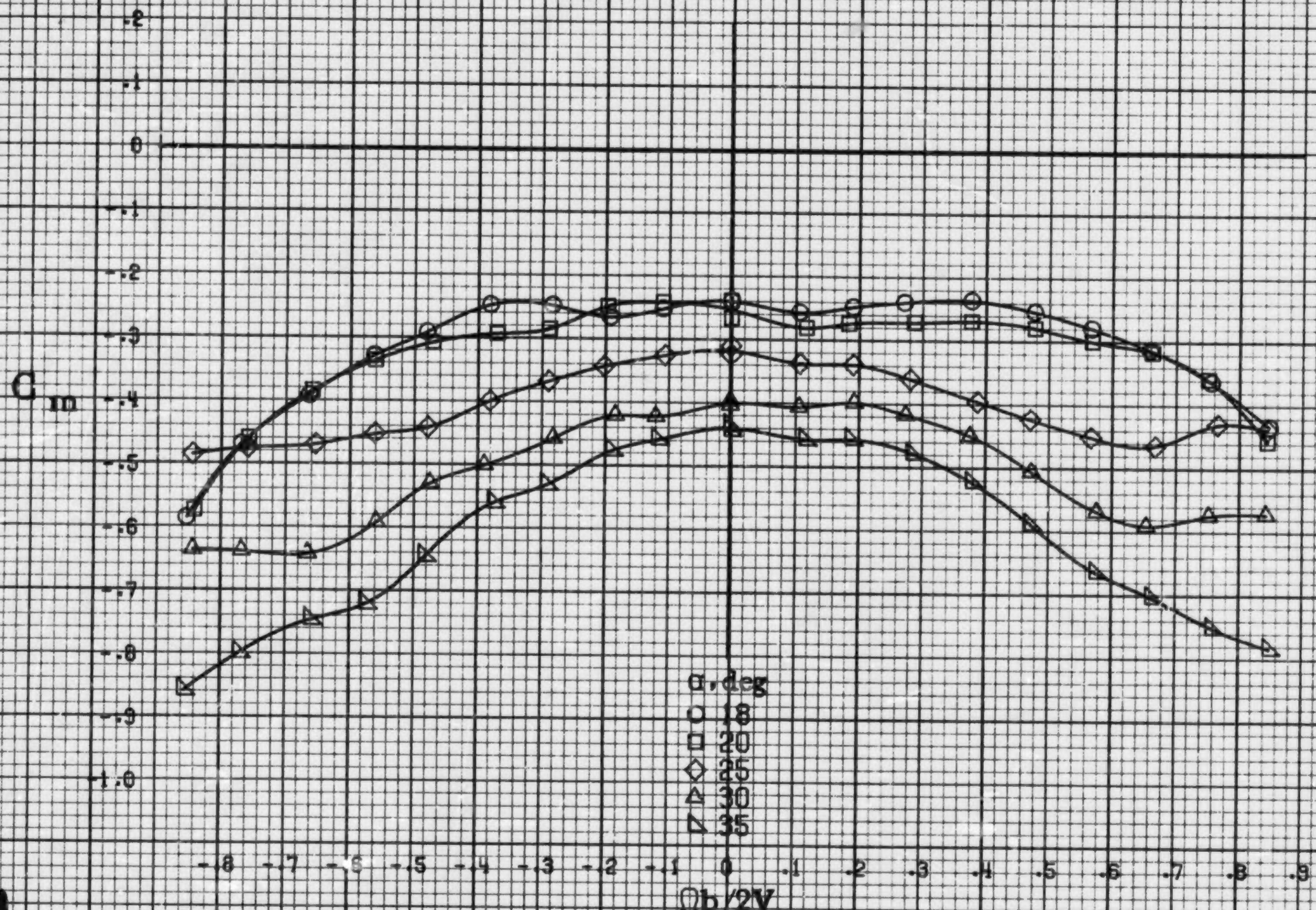

(b) α=18to35deg. SR=76cm(30in).

Figure A3. Continued.

A12

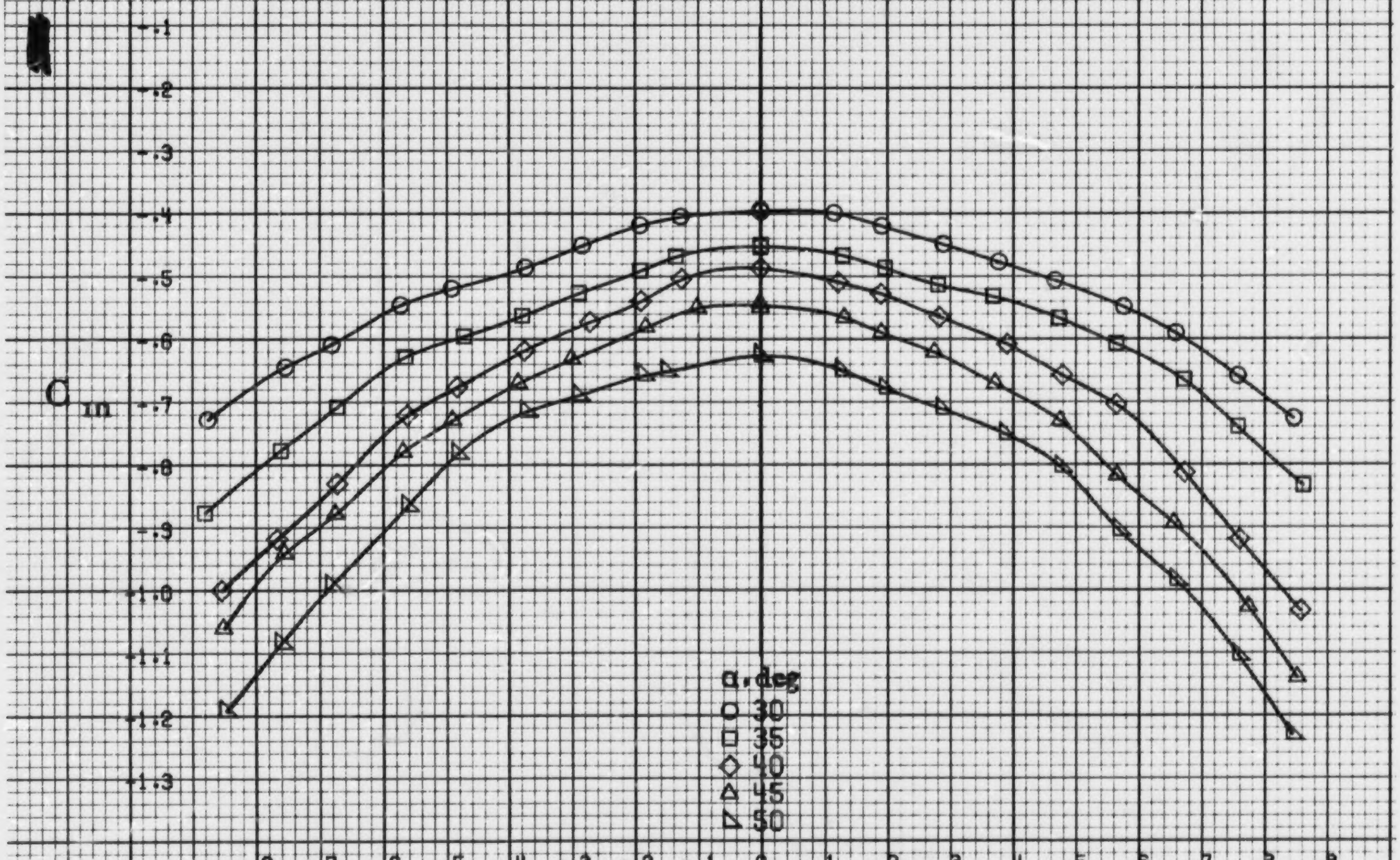

(c) α=30to50deg. SR=0.

Figure A3. Continued.

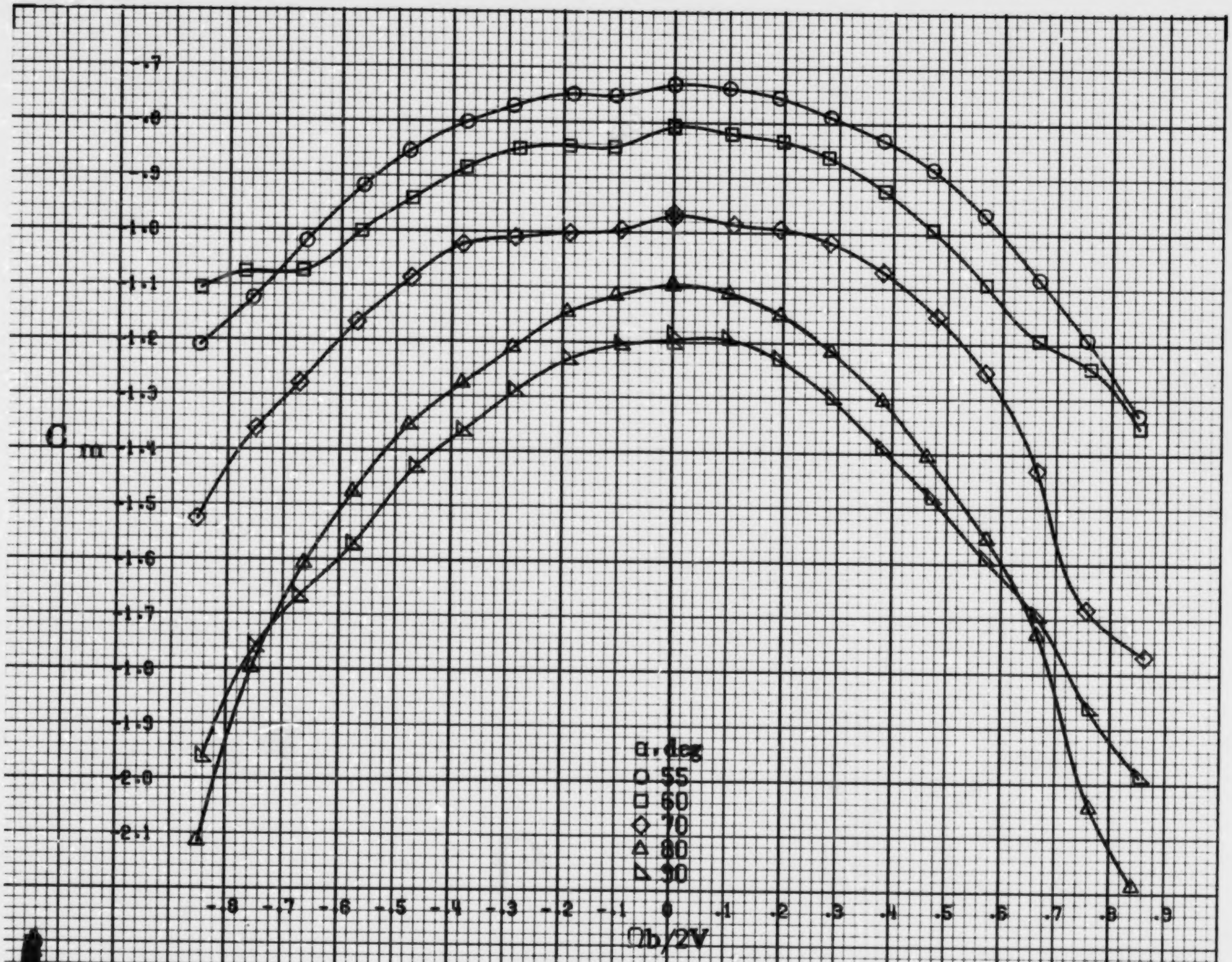

(d) α=55to90deg. SR=0.
Figure A3. Concluded.

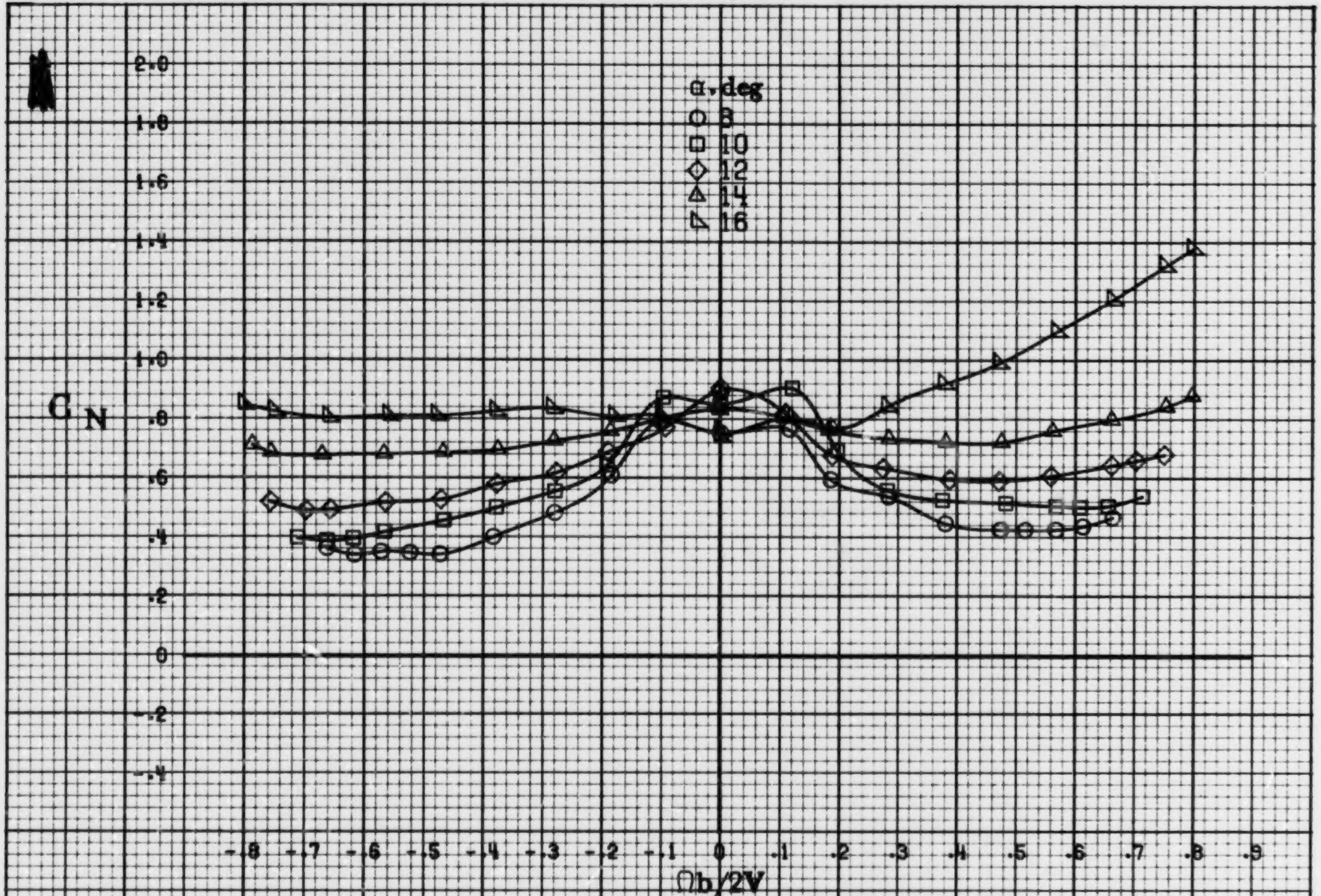

(a) α=8to16deg, SR=76cm(30in).

Figure A4.-Effect of rotation rate and angle of attack on normal-force coefficient for basic configuration. δ_e =0°, δ_a =0°, δ_r =0°. β =0°.

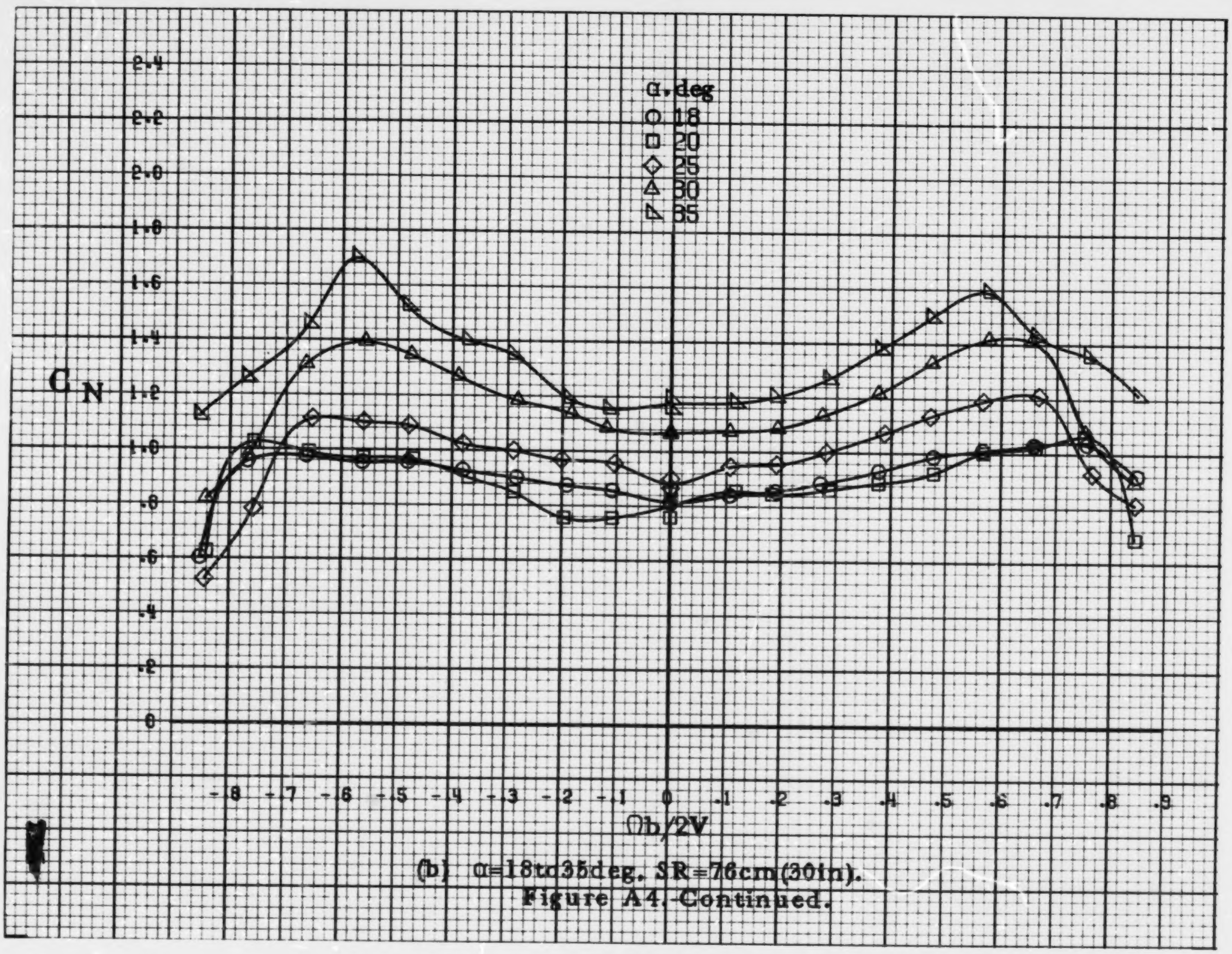

(b) α=18to35deg. SR=76cm(30in).
Figure A4. Continued.

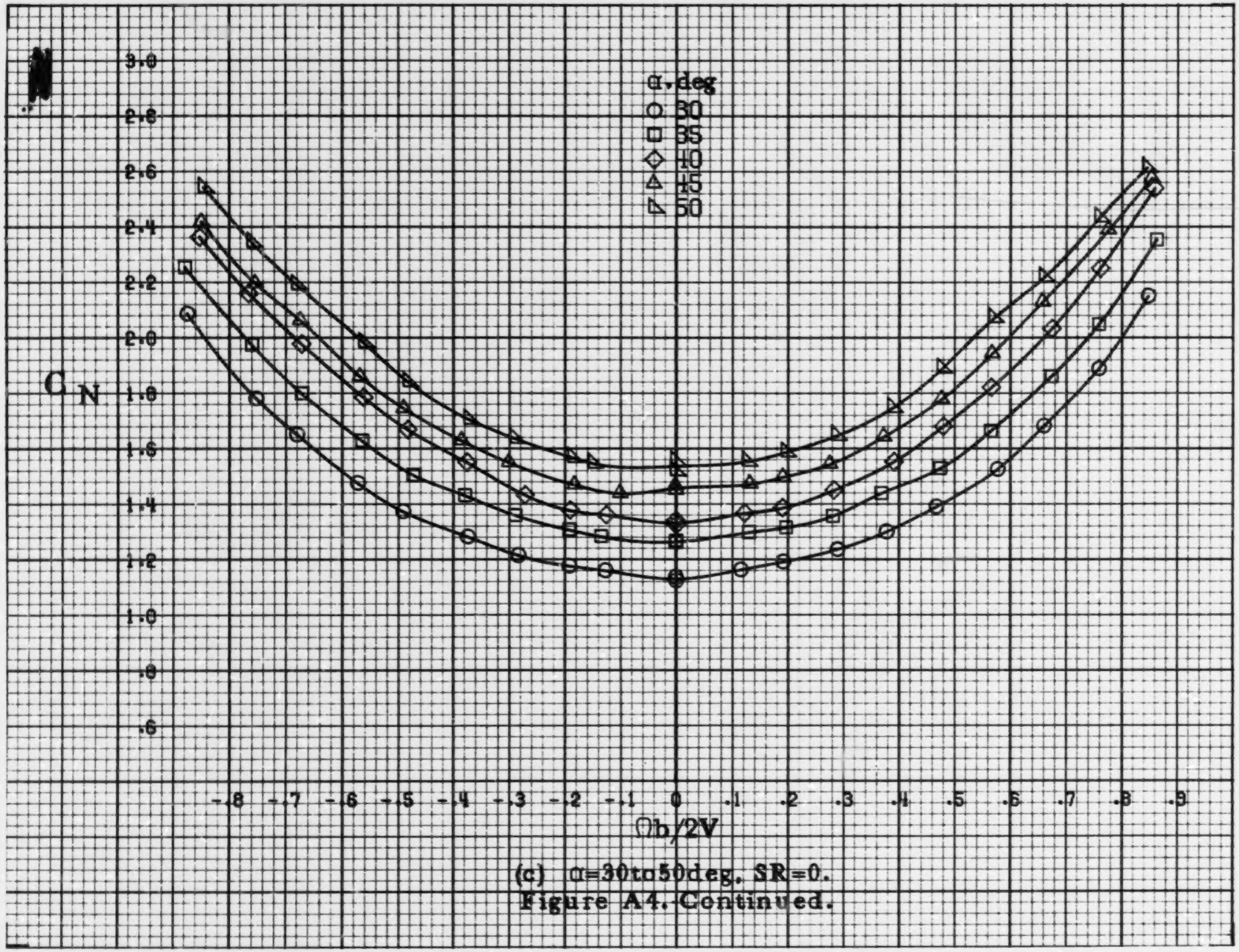

(c) α=30 to 50 deg, SR=0.
Figure A4. Continued.

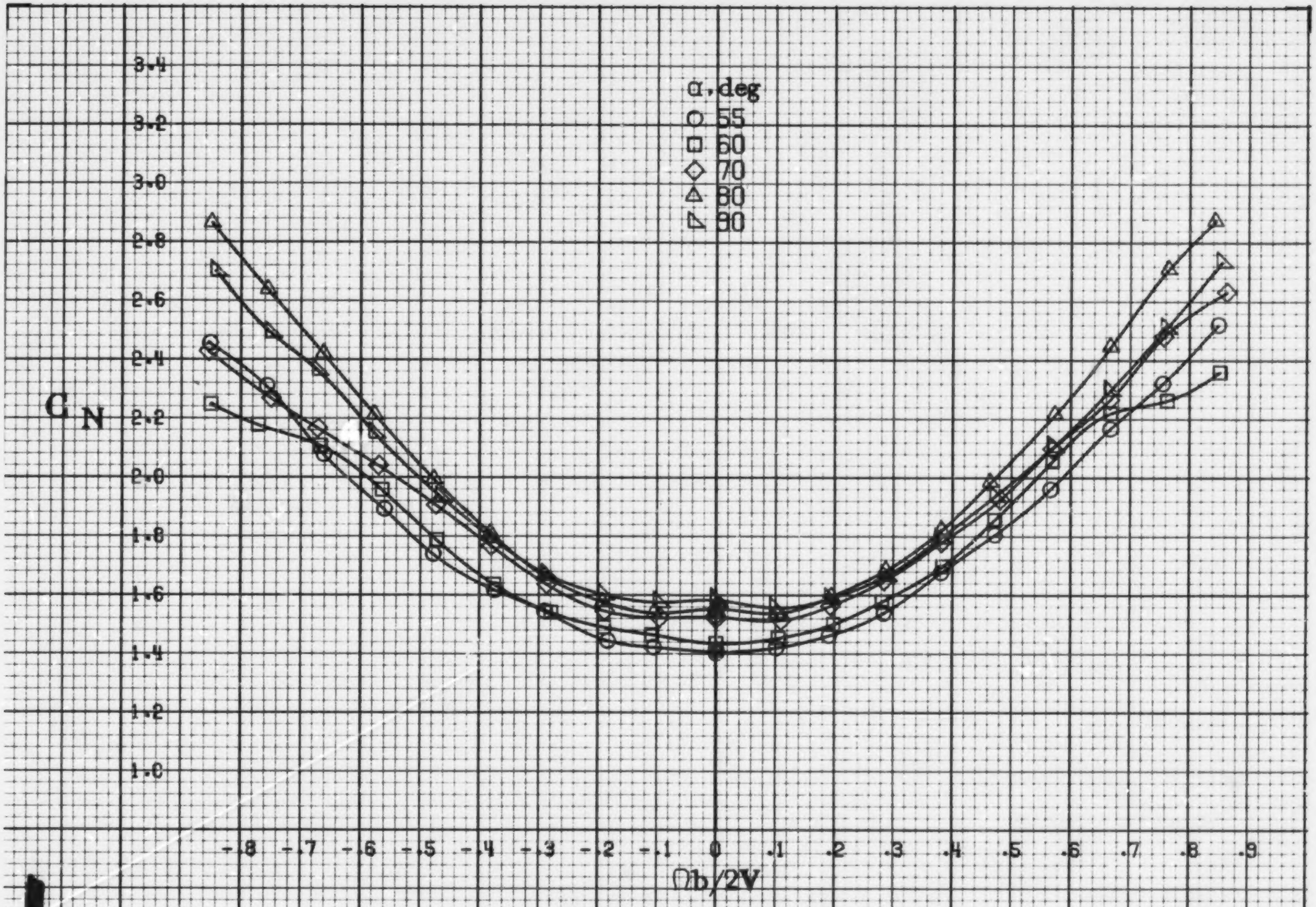

(d) α=55to90deg. SR=0.
Figure A4. Concluded.

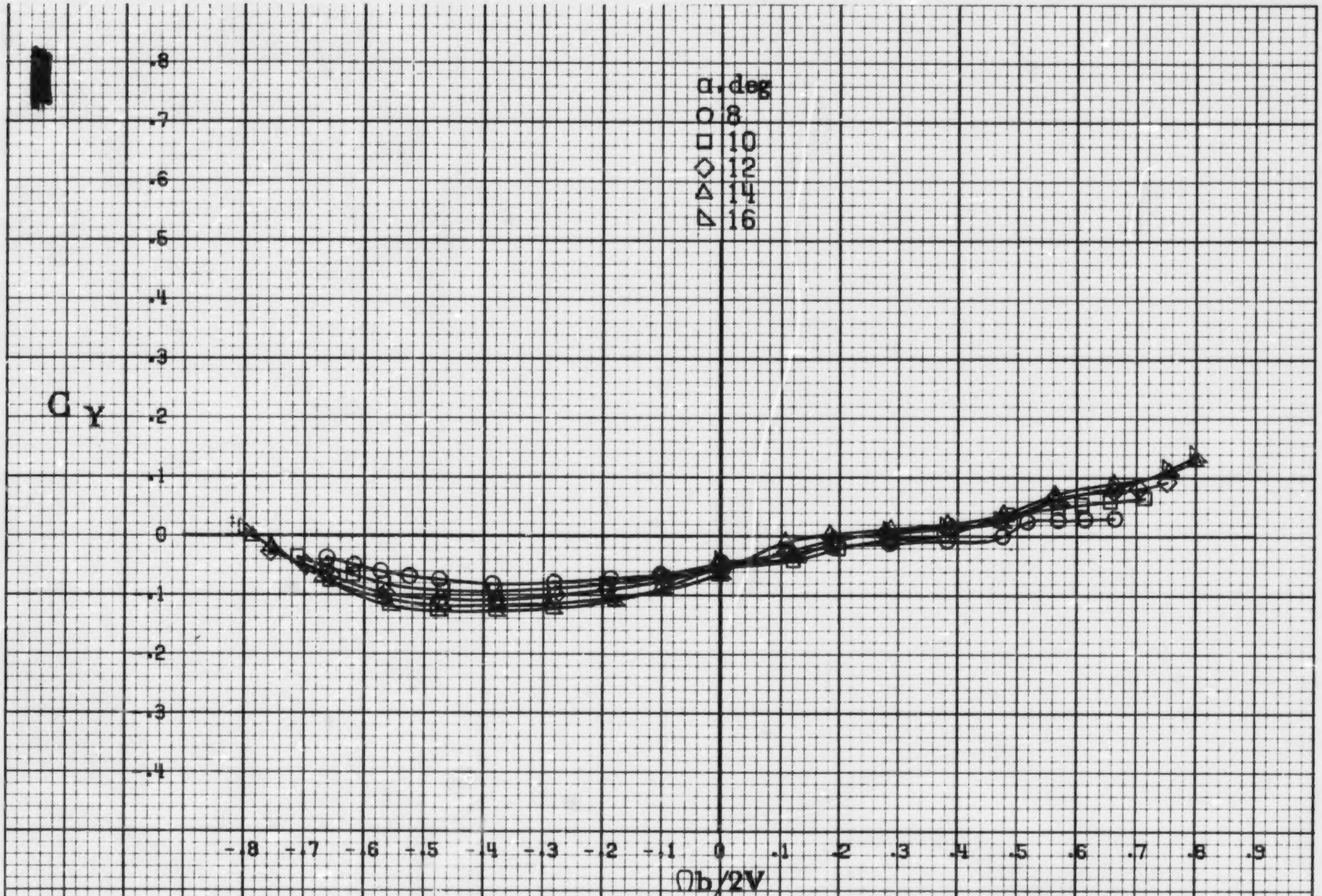

(a) $\alpha = 8$ to 16 deg. SR = 76cm (30in).

Figure A5.-Effect of rotation rate and angle of attack on side-force coefficient for basic configuration. $\delta_e = 0^\circ$. $\delta_a = 0^\circ$. $\delta_r = 0^\circ$. $\beta = 0^\circ$.

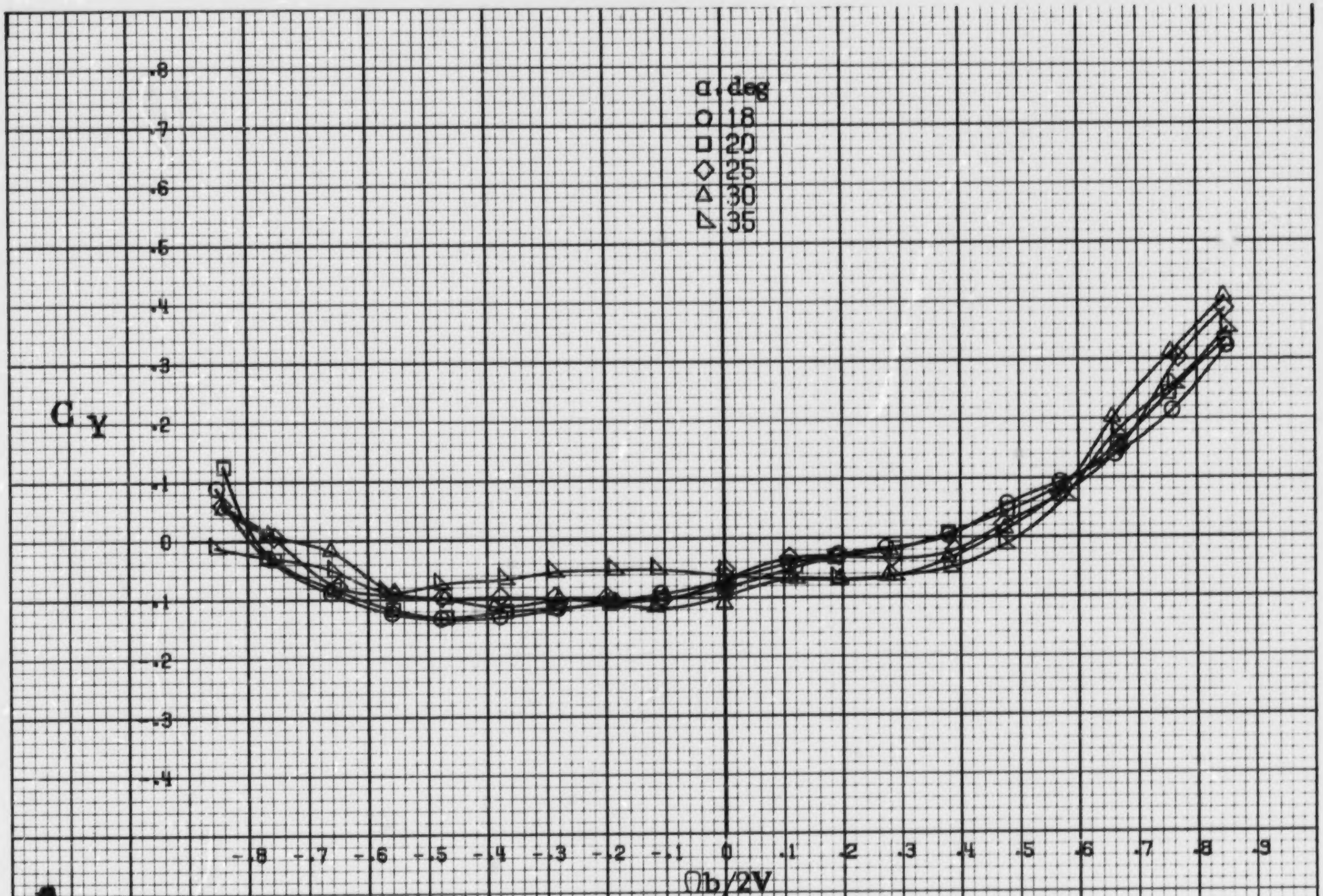

(b) α=18 to 35 deg. SR=76 cm (30 in).

Figure A5.-Continued.

A 30

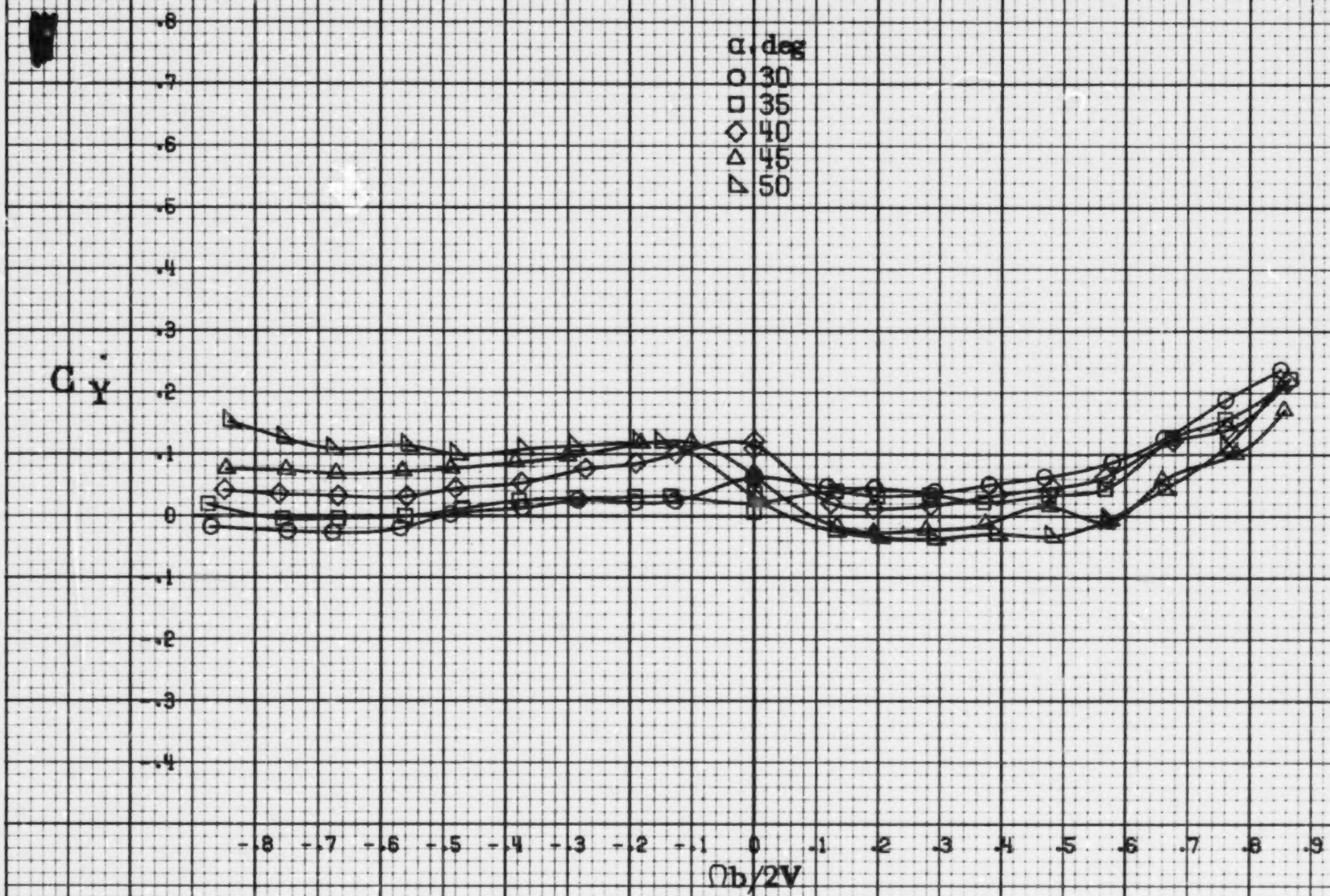

(c) α=30to50deg, SR=0.
Figure A5.-Continued.

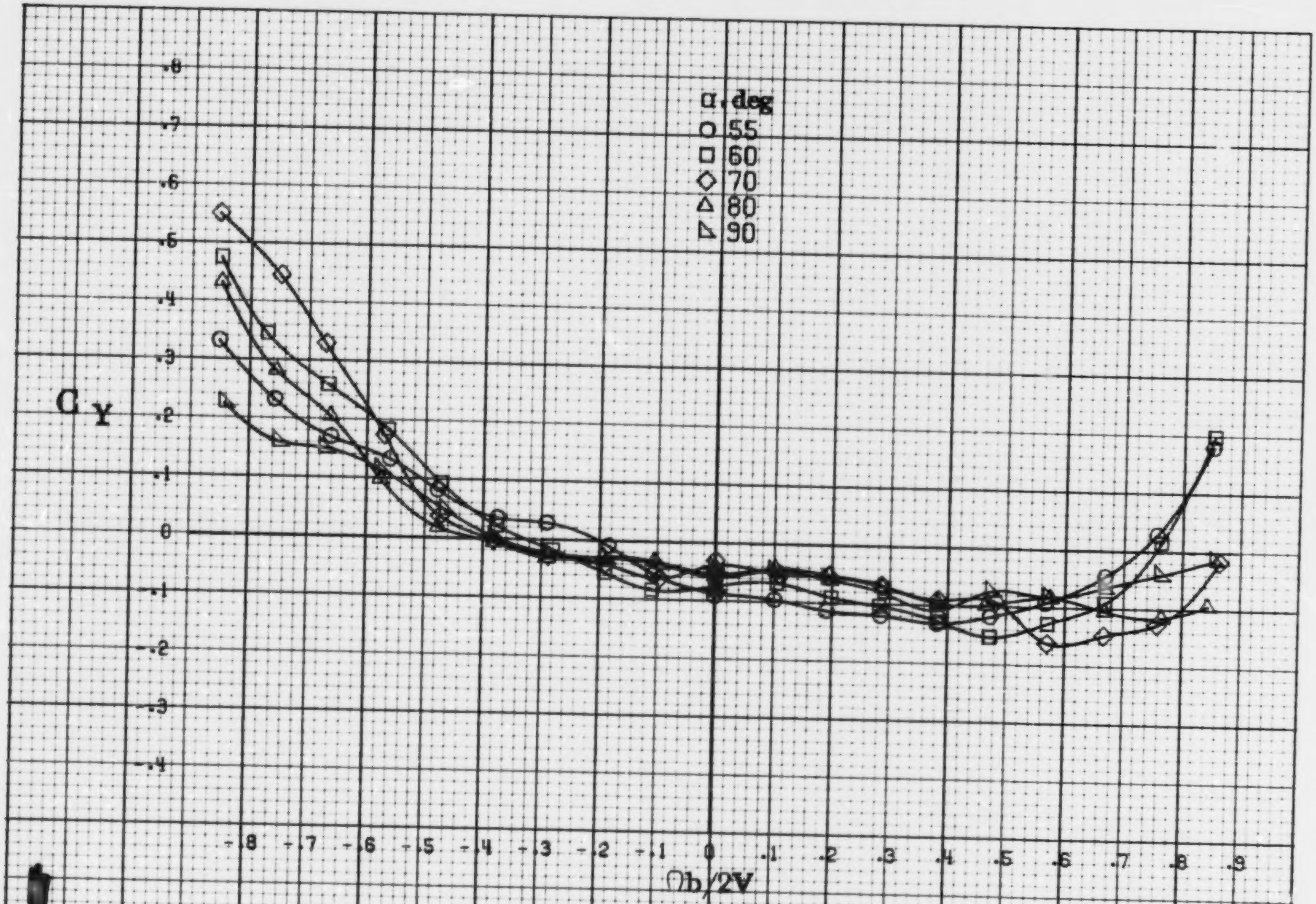

(d) α=55 to 90 deg, SR=0.
Figure A5.-Concluded.

A22

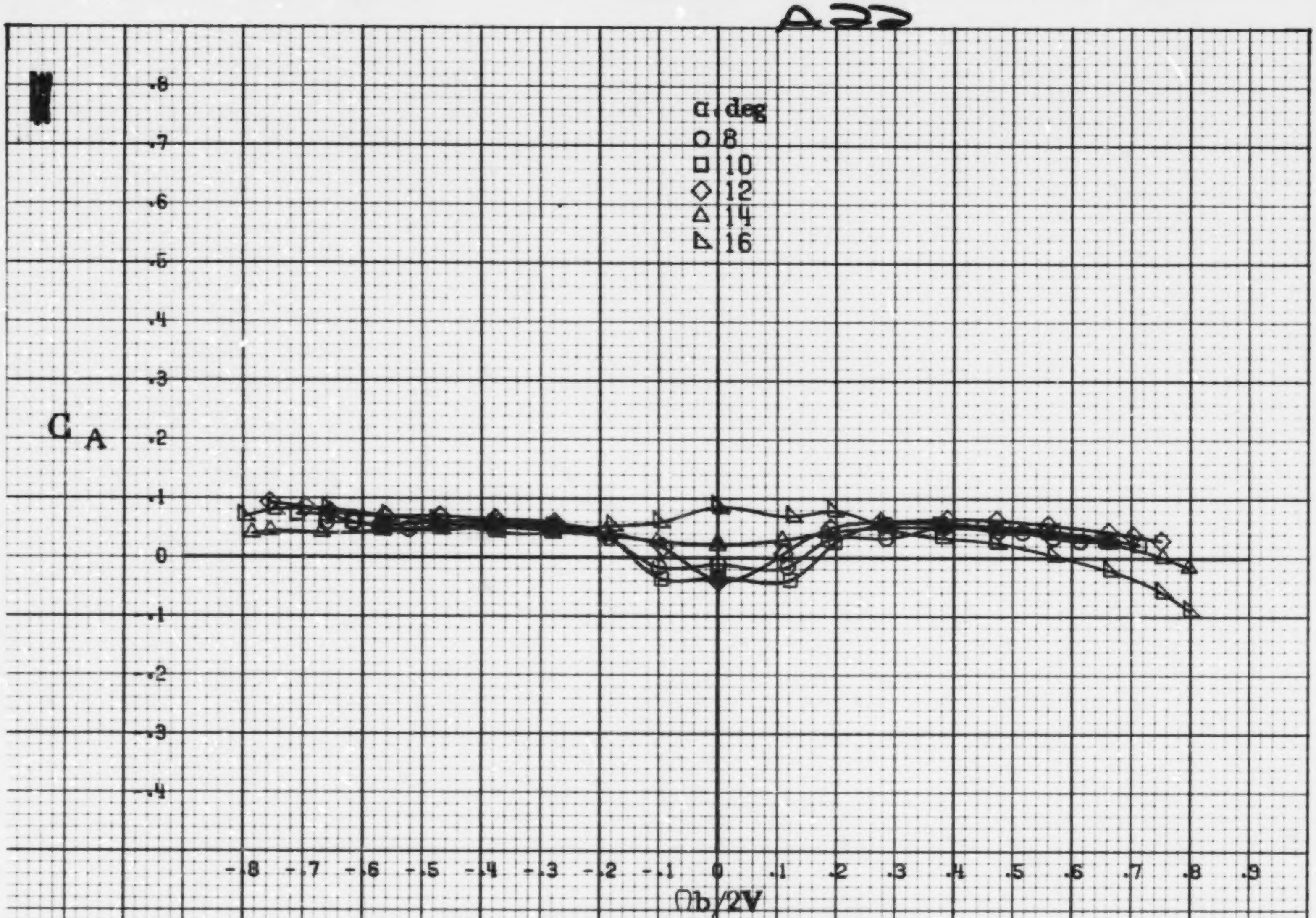

(a) $\alpha = 8$ to 16 deg, SR = 76 cm (30 in).

Figure A6.- Effect of rotation rate and angle of attack on axial-force coefficient for basic configuration. $\delta_e = 0°$, $\delta_a = 0°$, $\delta_r = 0°$. $\beta = 0°$.

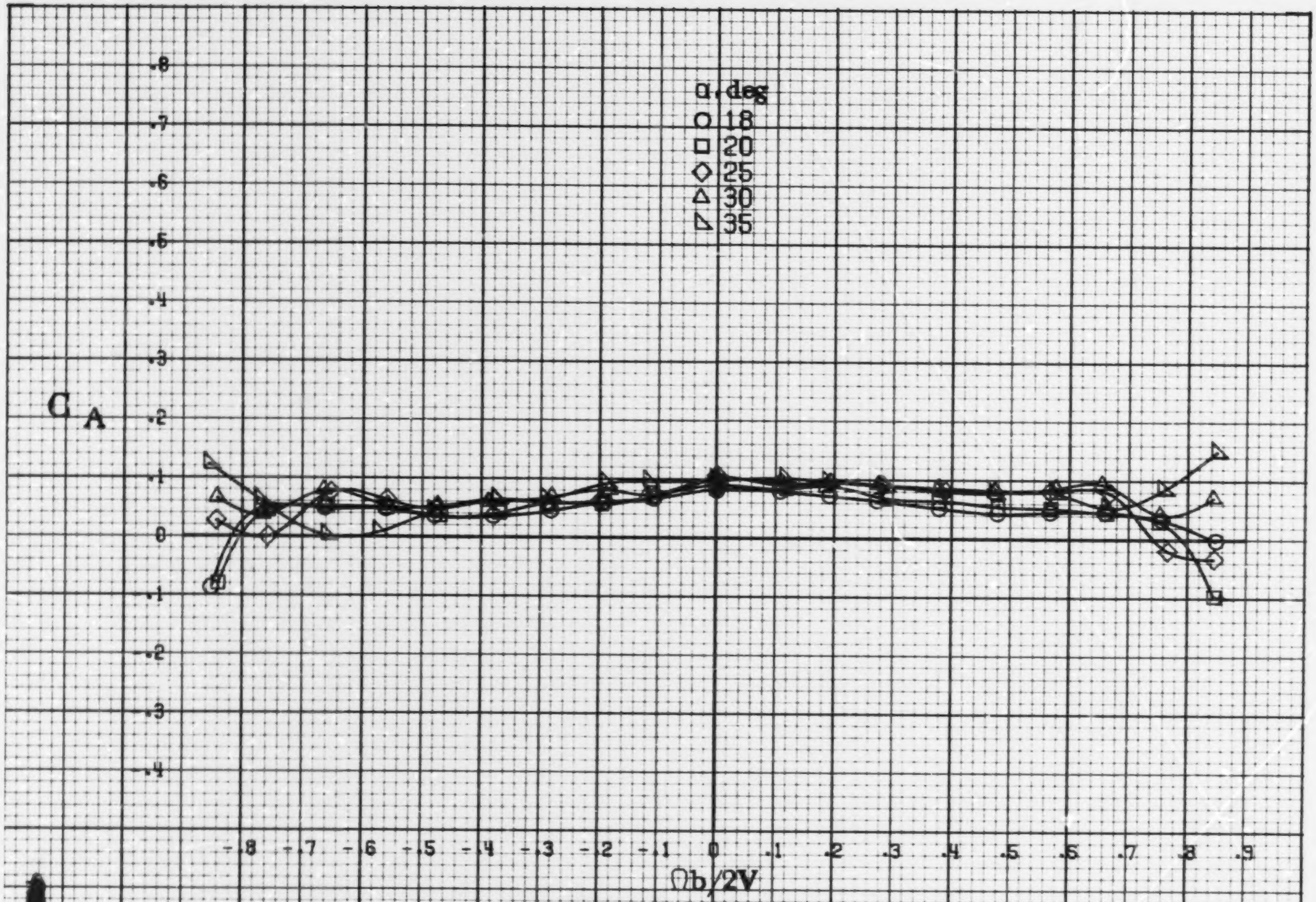

(b) α=18 to 35 deg. SR=76cm(30in).
Figure A6.-Continued.

A 24

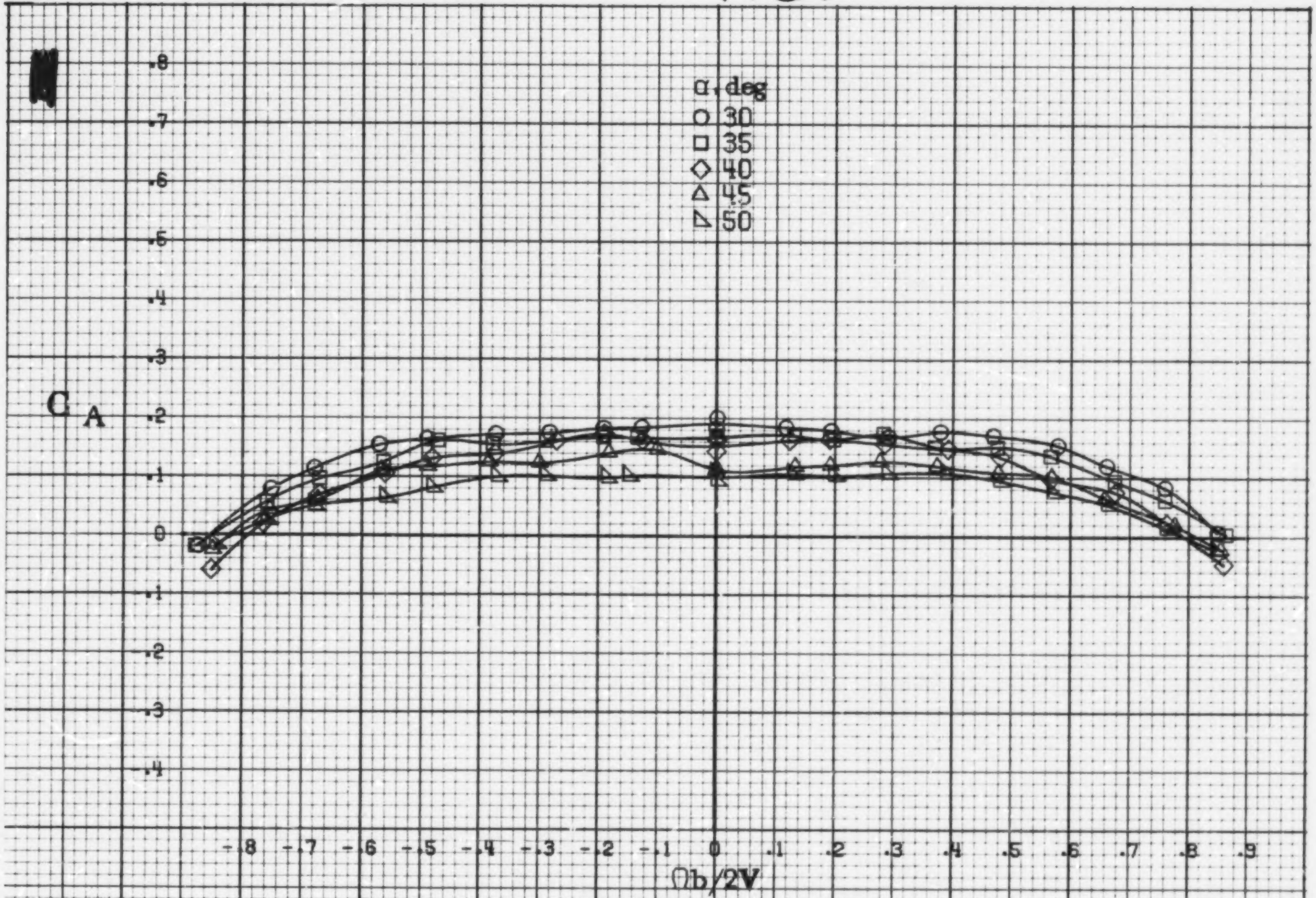

(c) α=30 to 50 deg, SR=0.
Figure A6.-Continued.

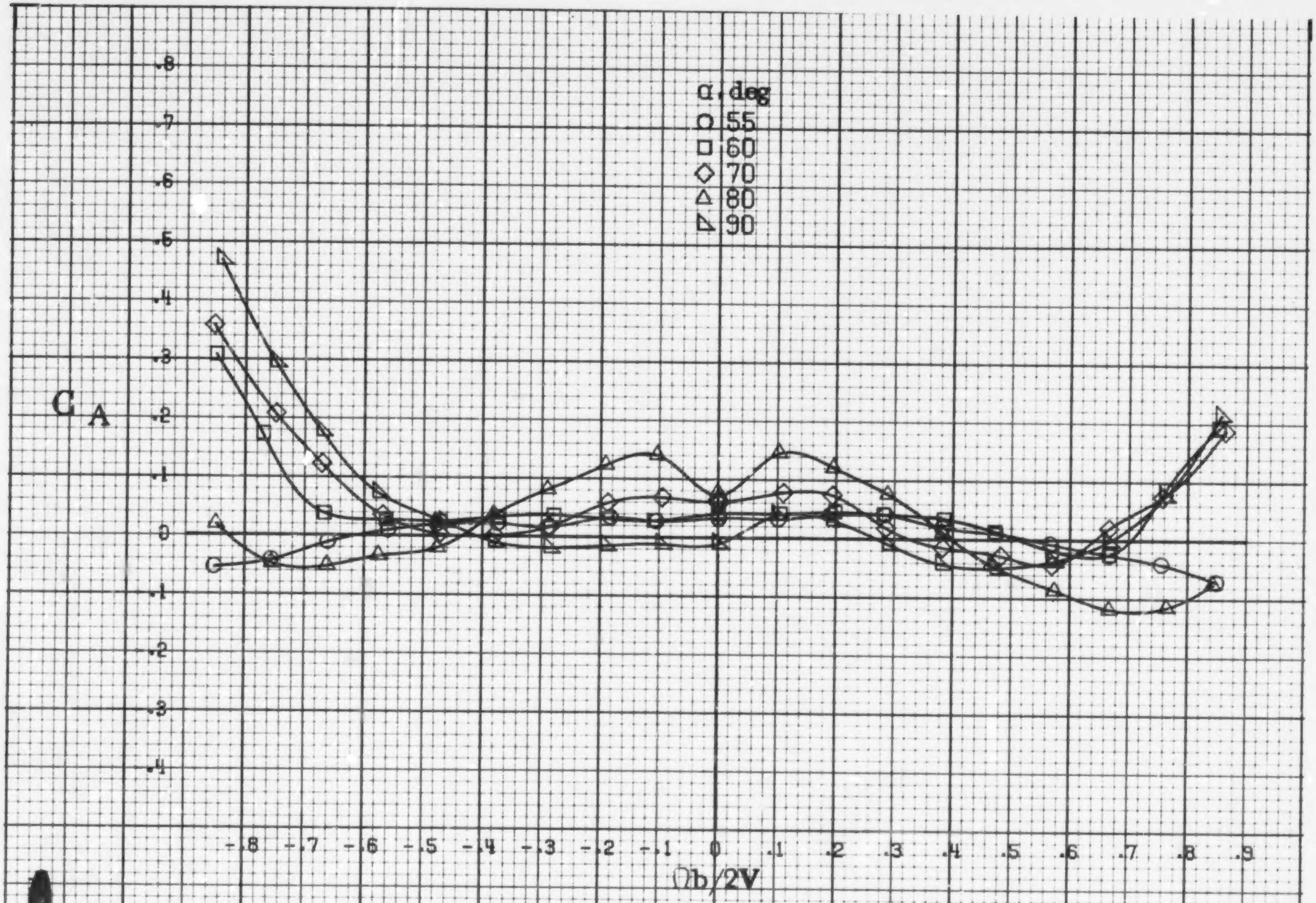

(d) α=55to90deg, SR=0.
Figure A6.-Concluded.

A25

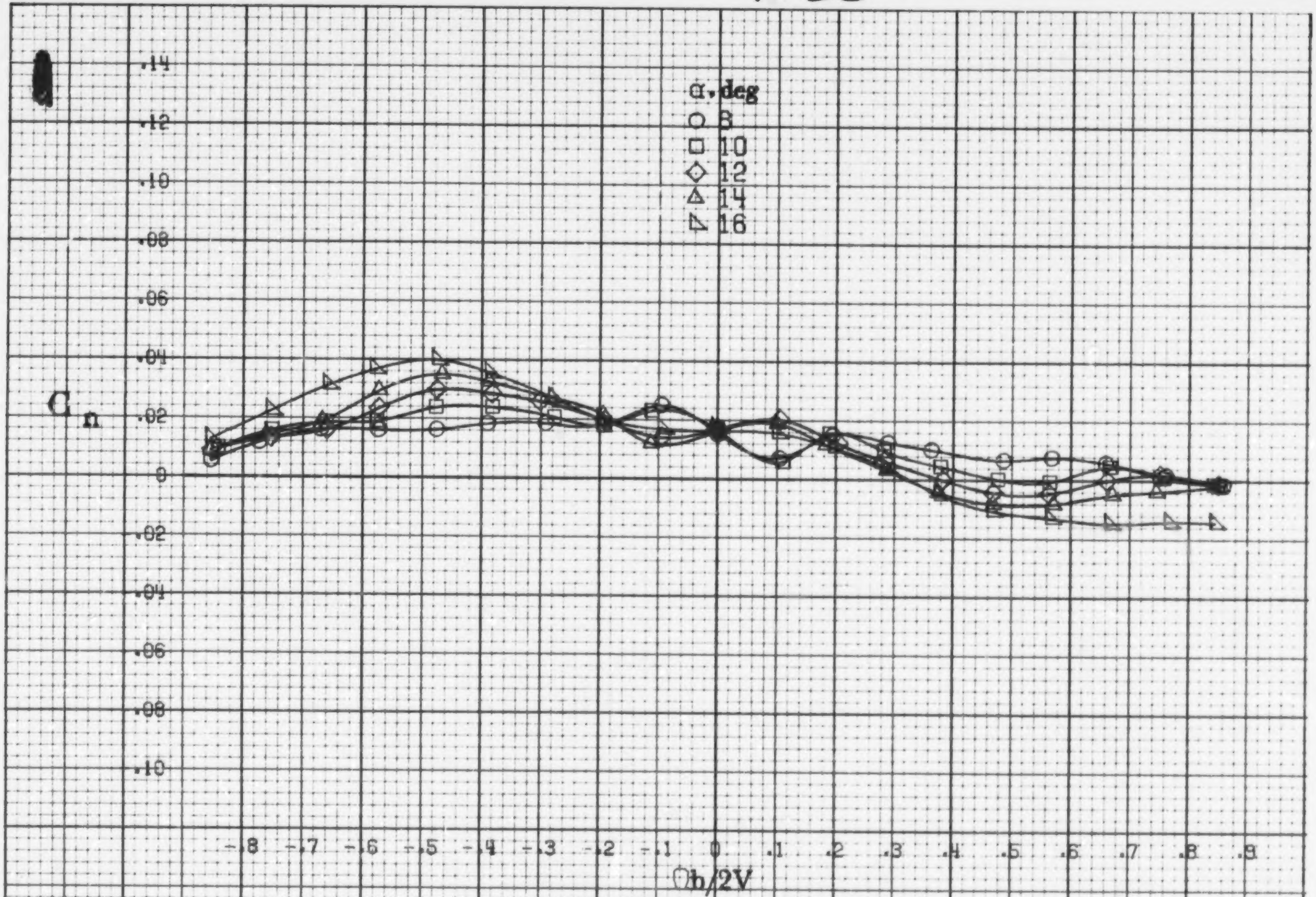

(a) α = 8 to 16 deg, SR = 76 cm (30 in).

Figure A7.-Effect of rotation rate and angle of attack on yawing-moment coefficient for basic configuration. $\delta_e = 0^\circ$, $\delta_a = 0^\circ$, $\delta_r = 25^\circ$, $\beta = 0^\circ$.

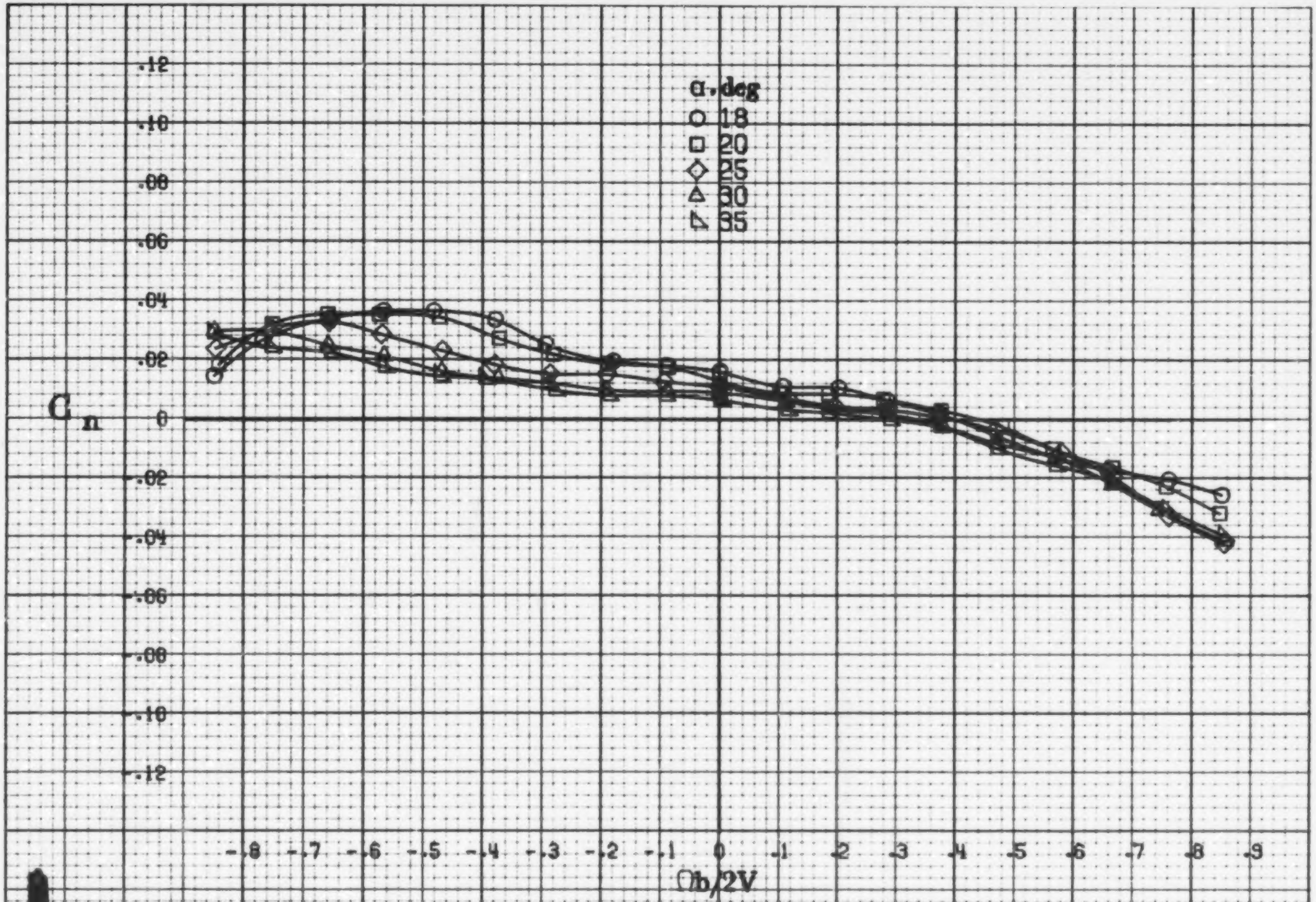

(b) $\alpha = 18$ to 35 deg, SR = 76 cm (30 in).

Figure A7.- Continued.

A28

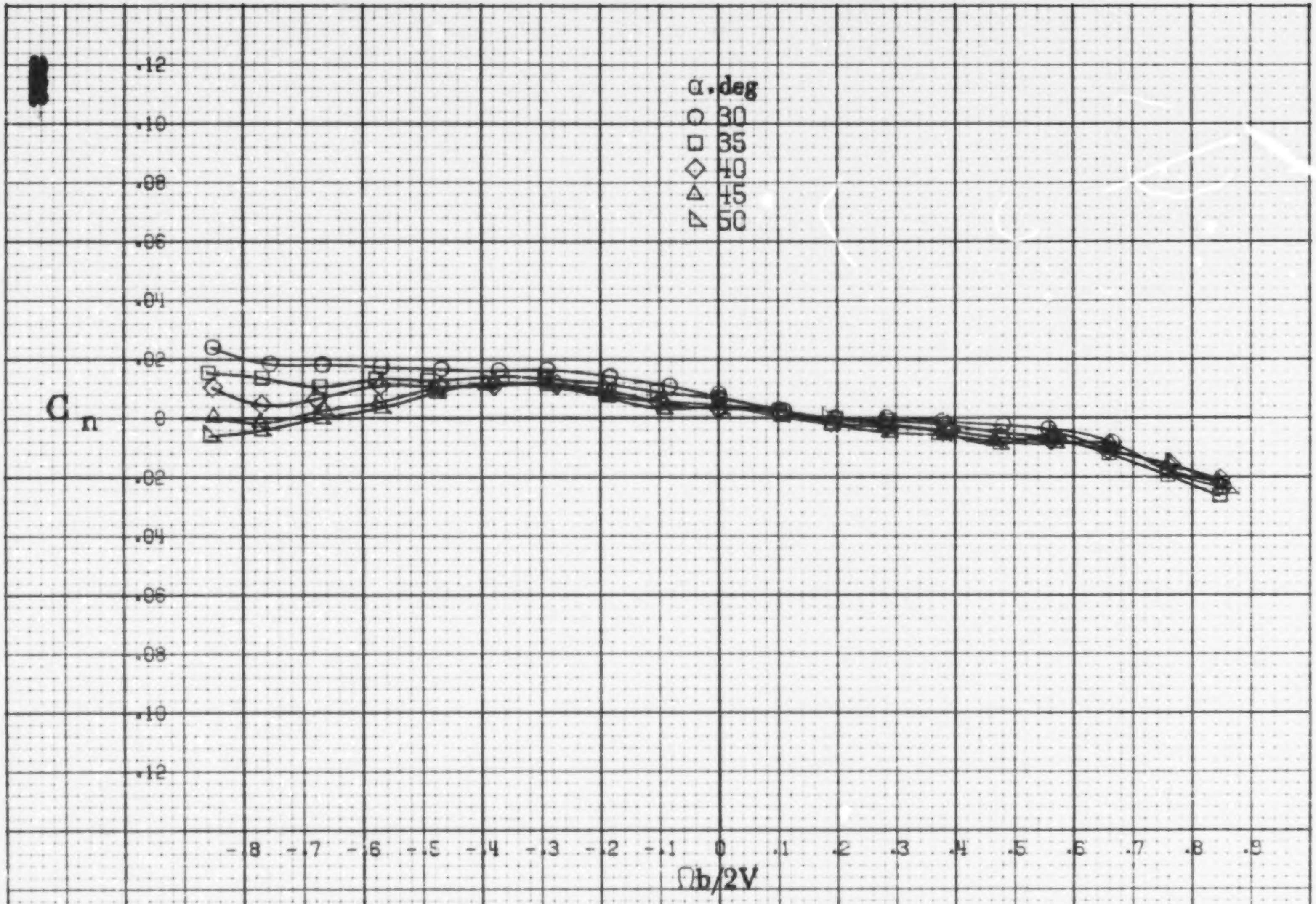

(c) α = 30 to 50 deg, SR = 0.

Figure A7.-Continued.

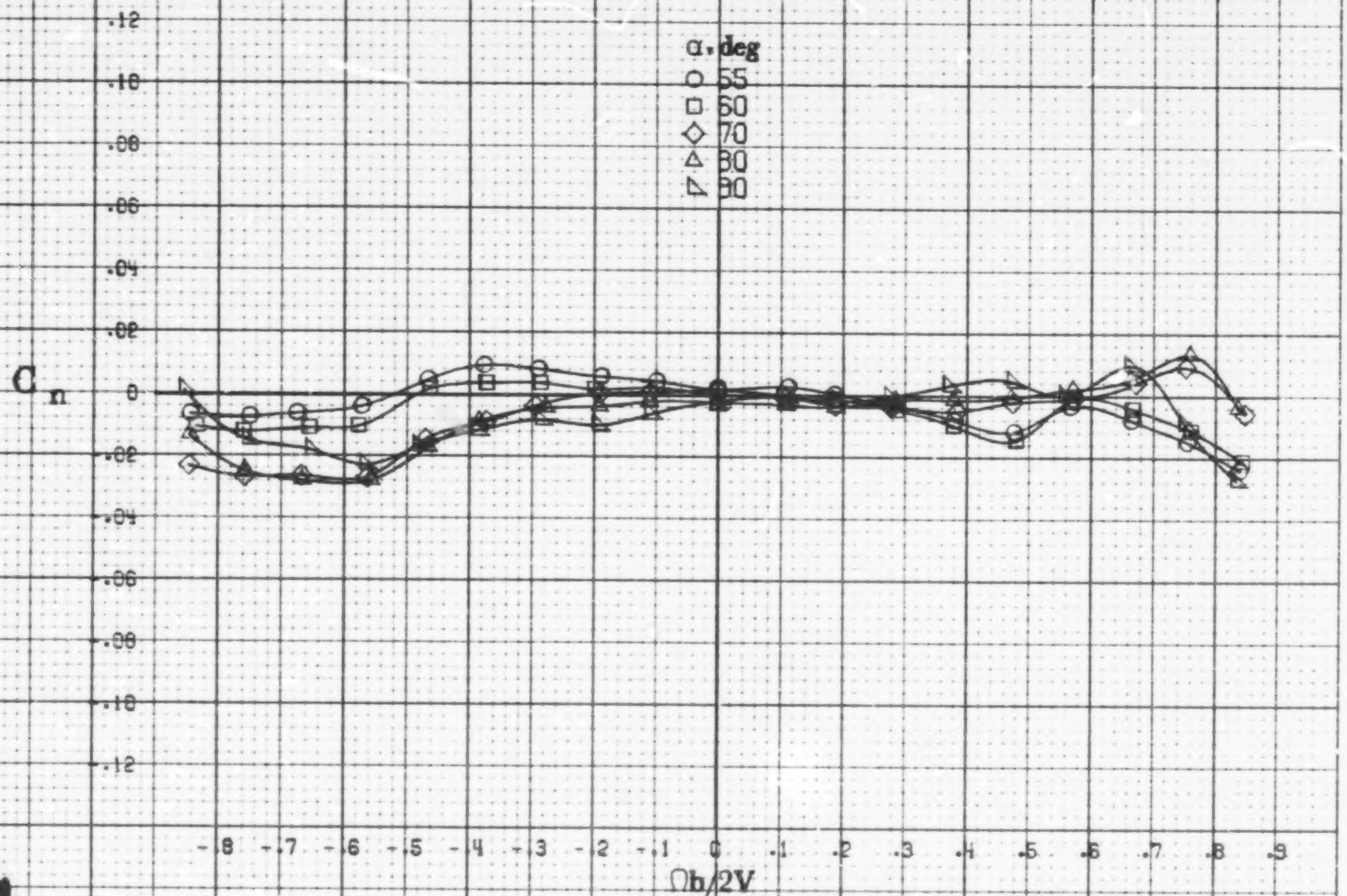

(d) α = 55 to 90 deg, SR = 0.

Figure A7.-Concluded.

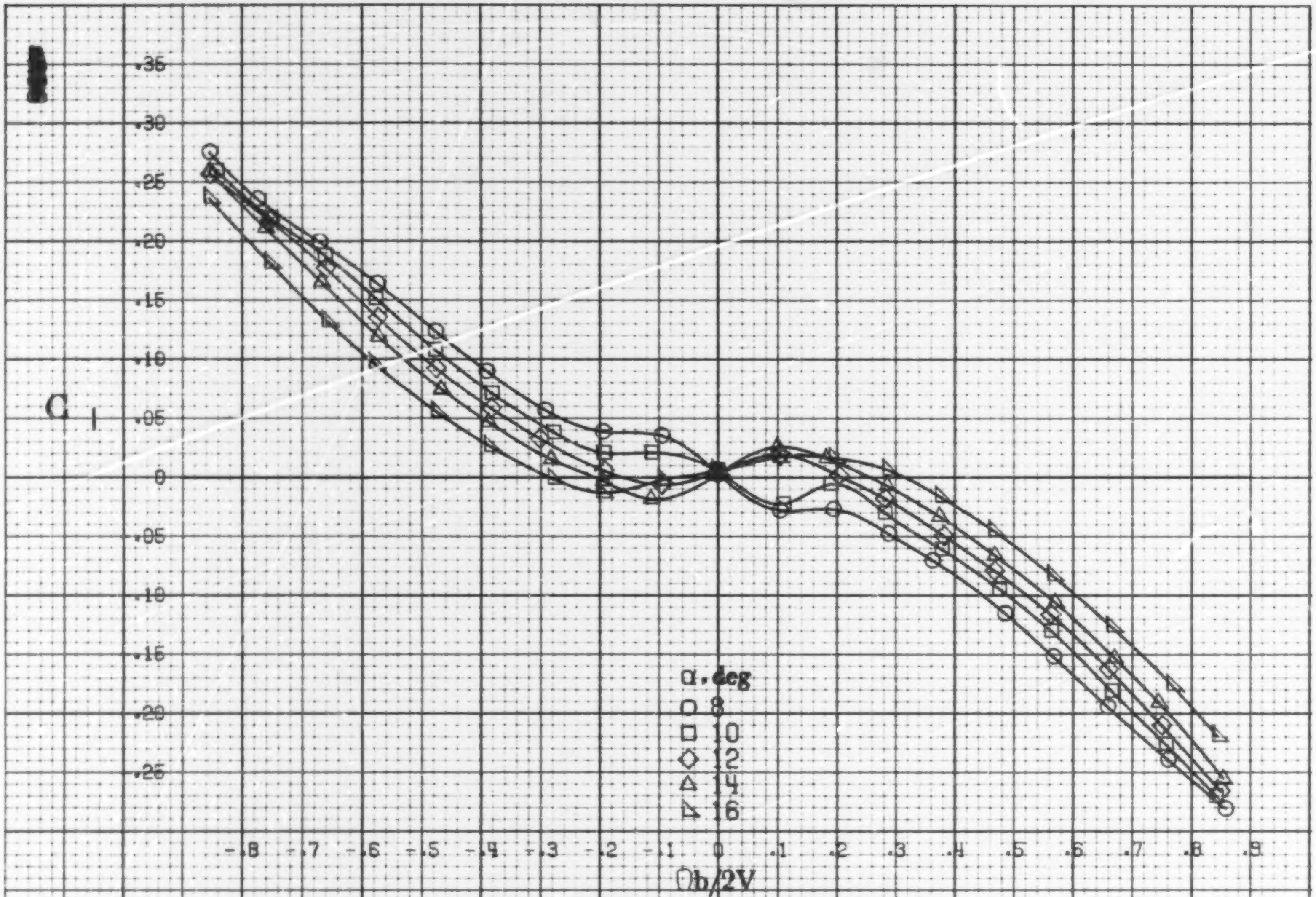

(a) α = 8 to 16 deg, SR = 76 cm (30 in).

Figure A8.-Effect of rotation rate and angle of attack on rolling-moment coefficient for basic configuration. $\delta_e = 0°$, $\delta_a = 0°$, $\delta_r = -25°$, $\beta = 0°$.

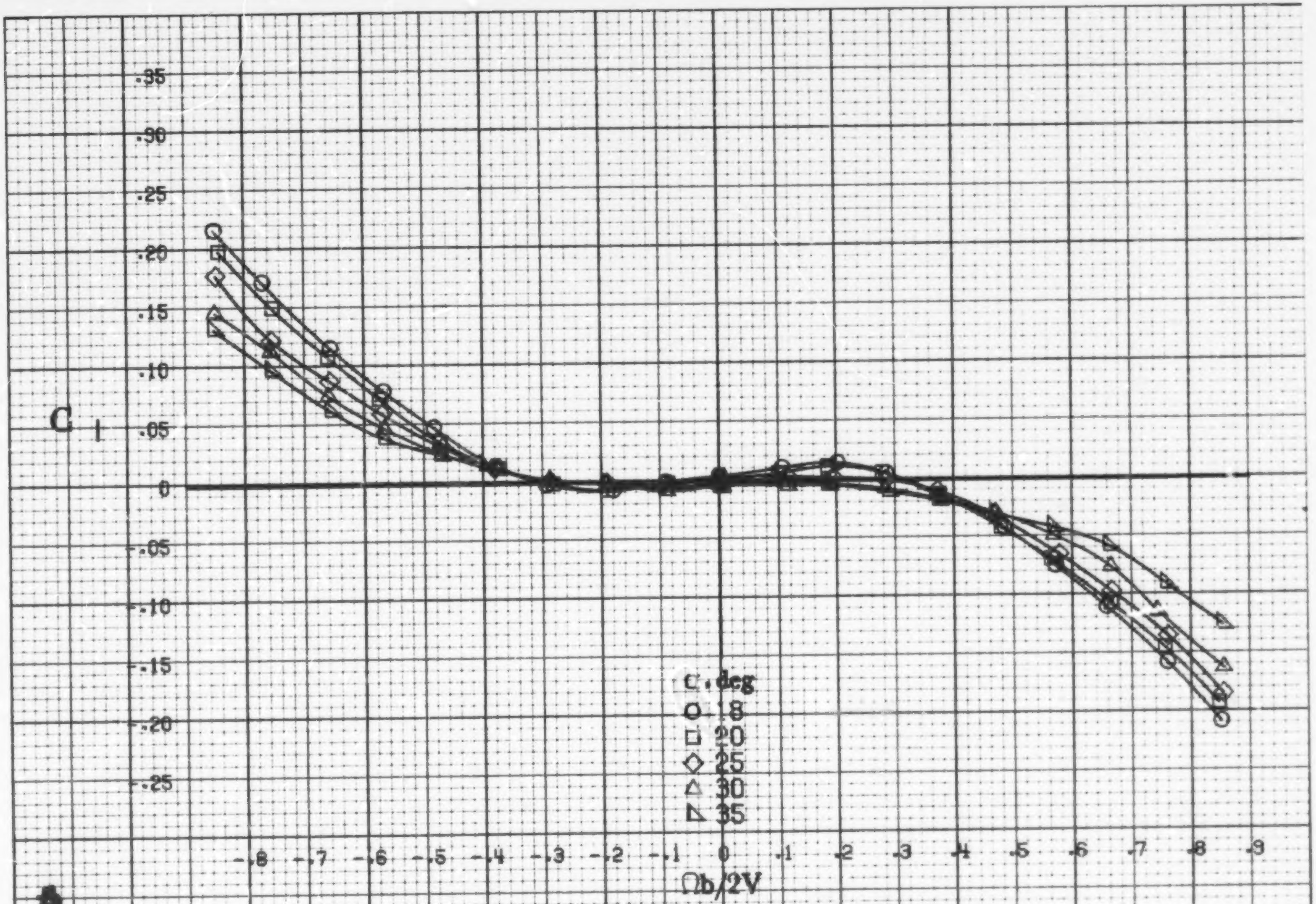

(b) α = 18 to 35 deg, SR = 76 cm (30 in).

Figure A8.- Continued.

A33

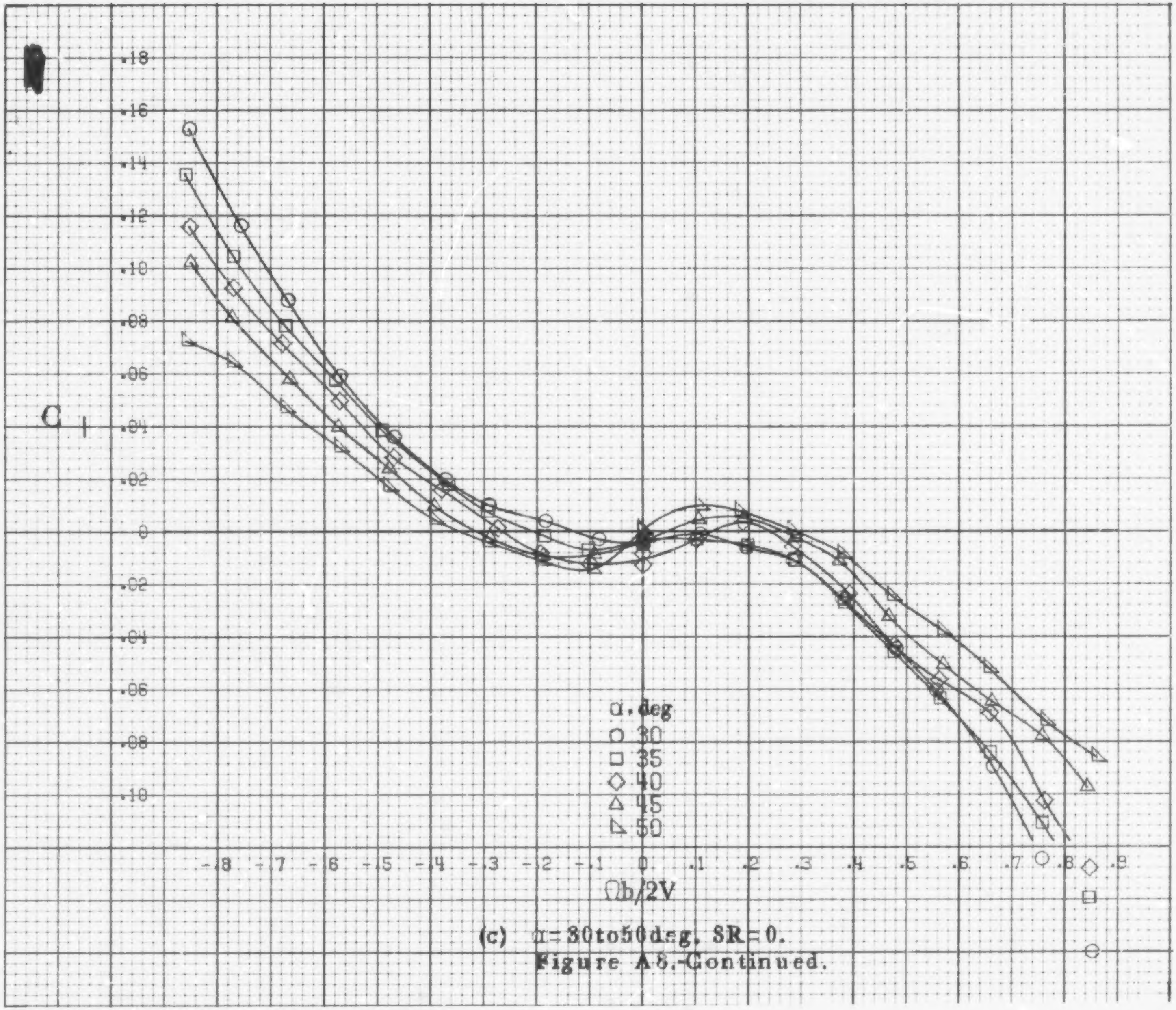

(c) α = 30 to 50 deg, SR = 0.
Figure A8.-Continued.

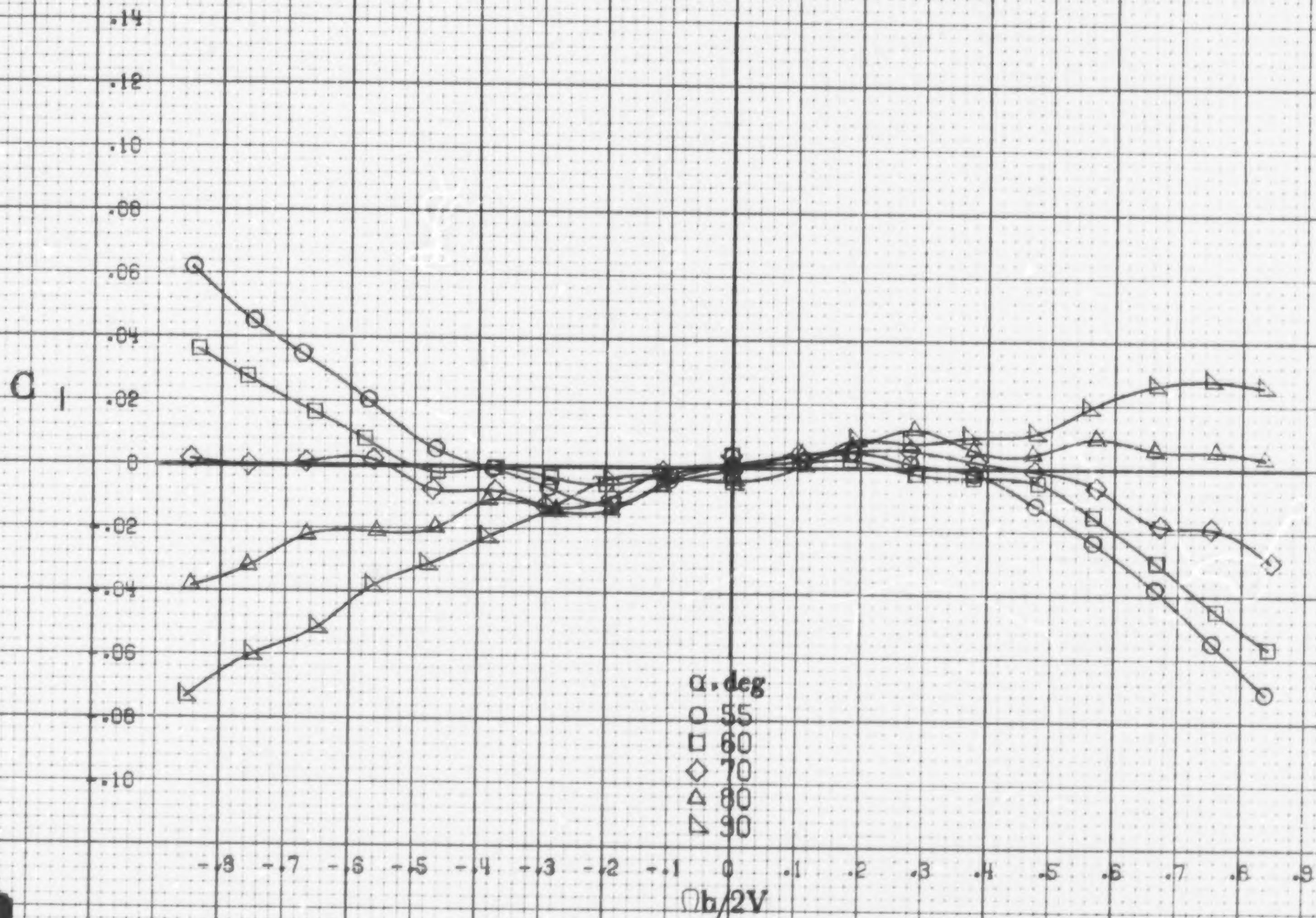

(d) α = 55to90deg, SR = 0.
Figure A8.-Concluded.

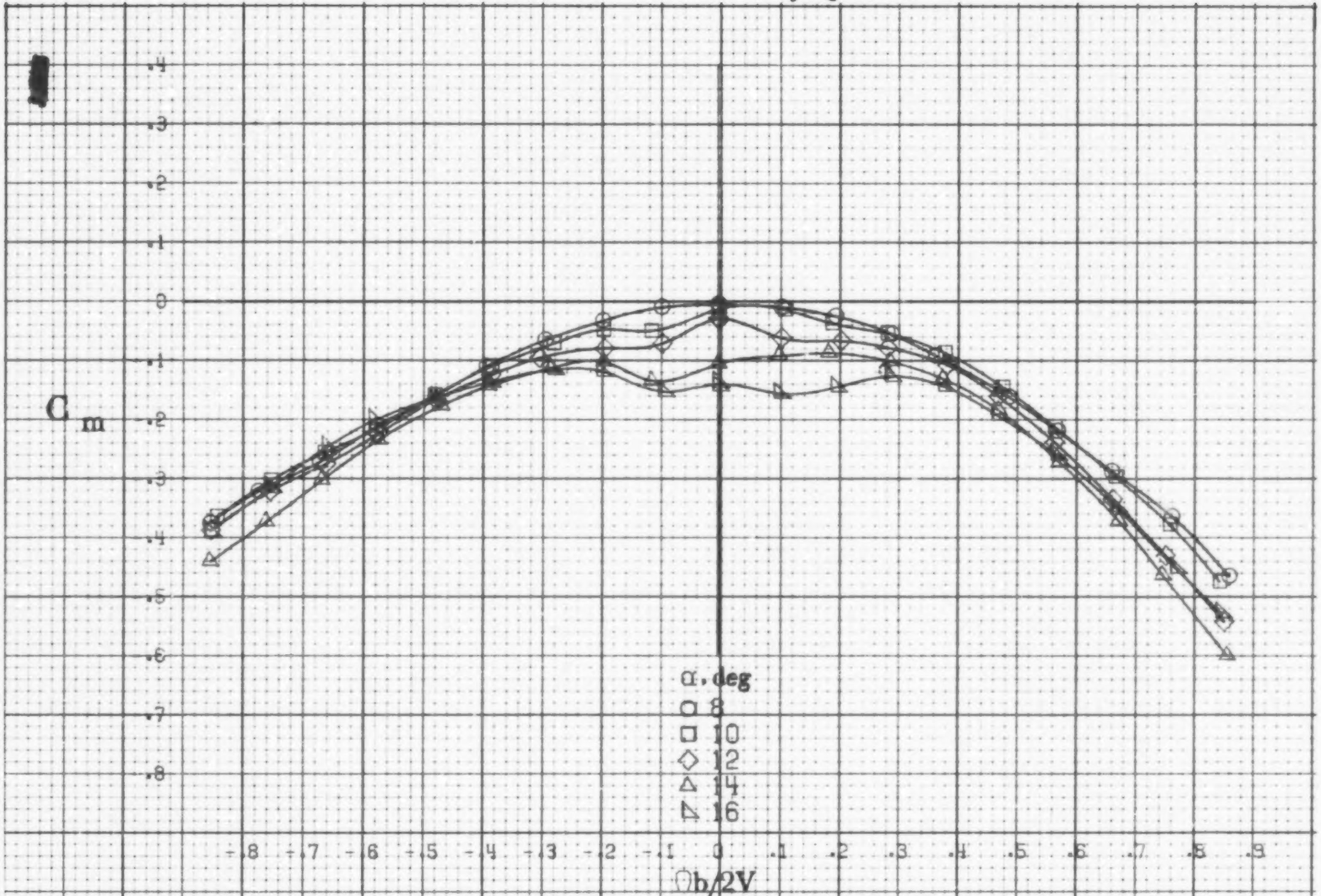

(a) α = 8 to 16 deg, SR = 76 cm (30 in).

Figure A9.-Effect of rotation rate and angle of attack on pitching-moment coefficient for basic configuration. $\delta_e = 0°$, $\delta_a = 0°$, $\delta_r = -25°$, $\beta = 0°$.

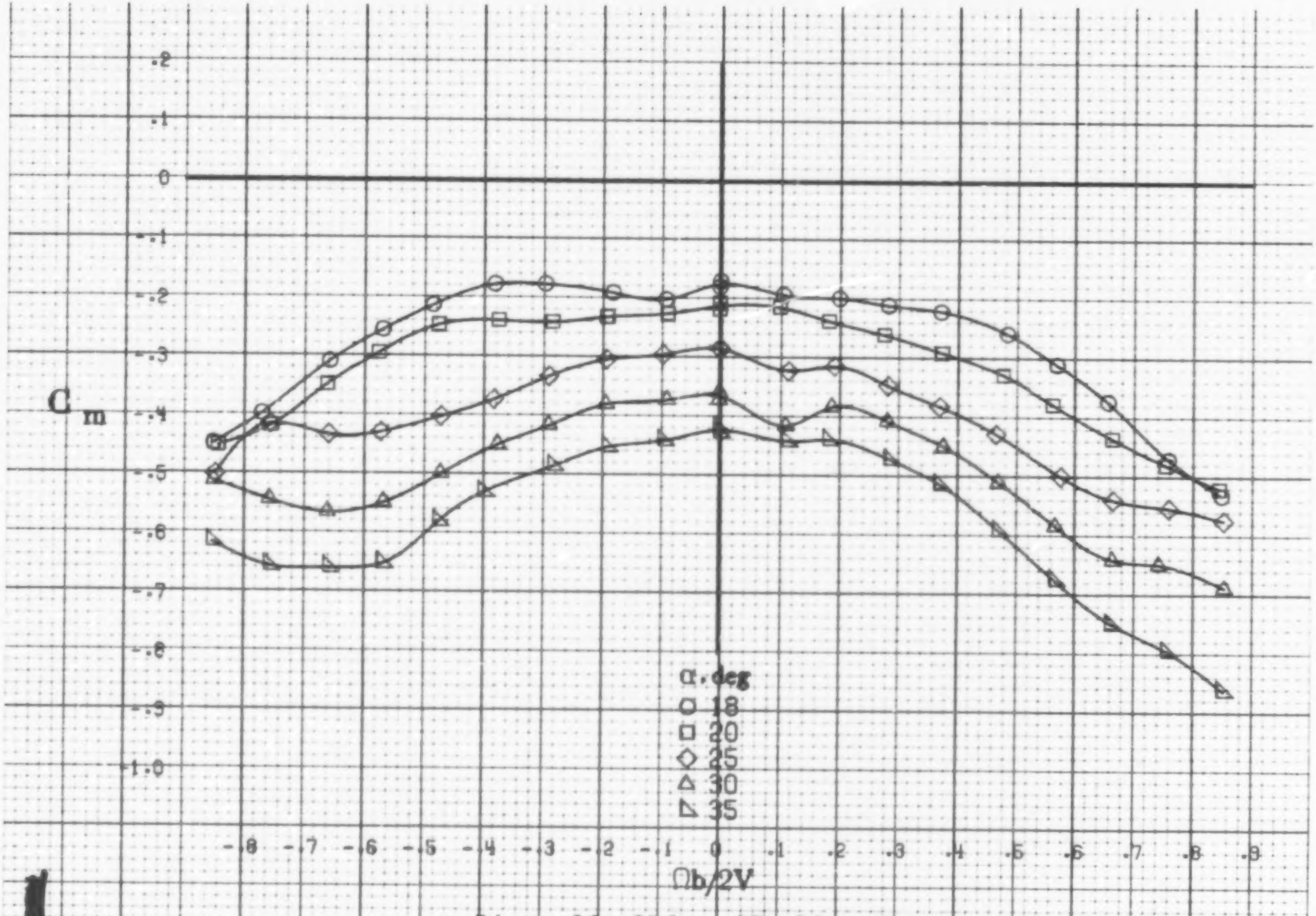

(b) α = 18 to 35 deg, SR = 76 cm (30 in).
Figure A9. Continued.

A 36

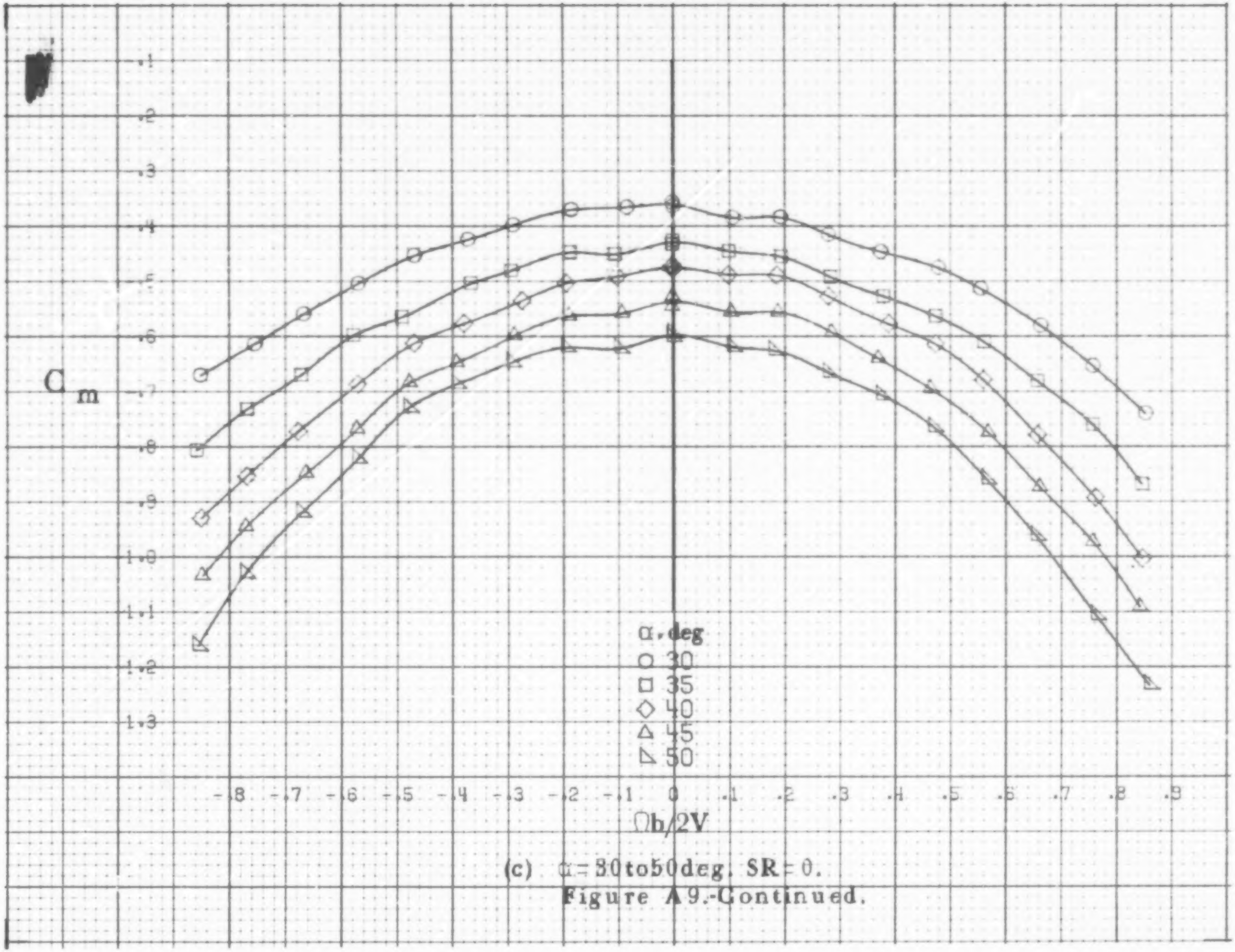

(c) α = 30 to 50 deg. SR = 0.

Figure A9.-Continued.

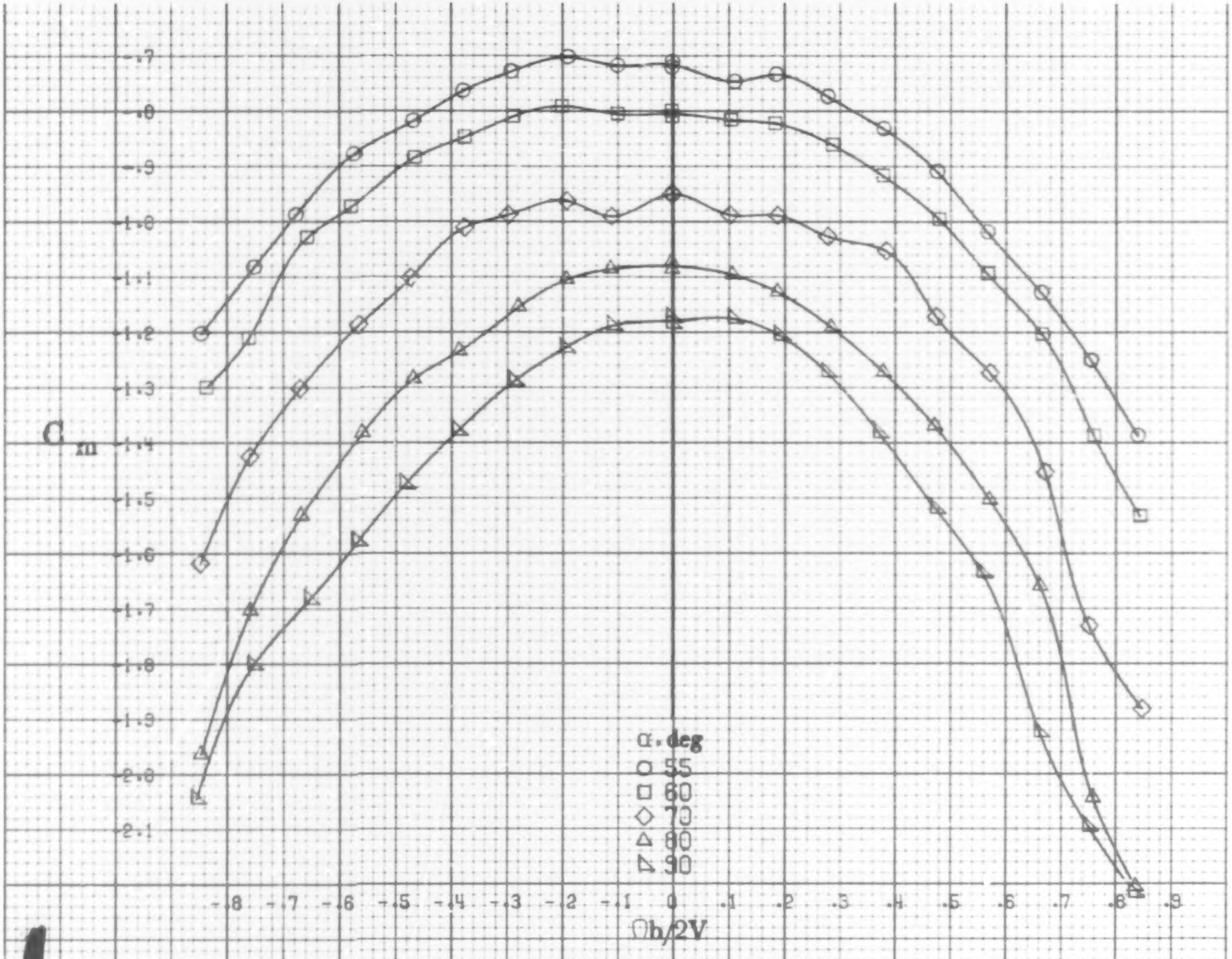

(d) α = 55 to 90 deg, SR = 0.
Figure A9.-Concluded.

A38

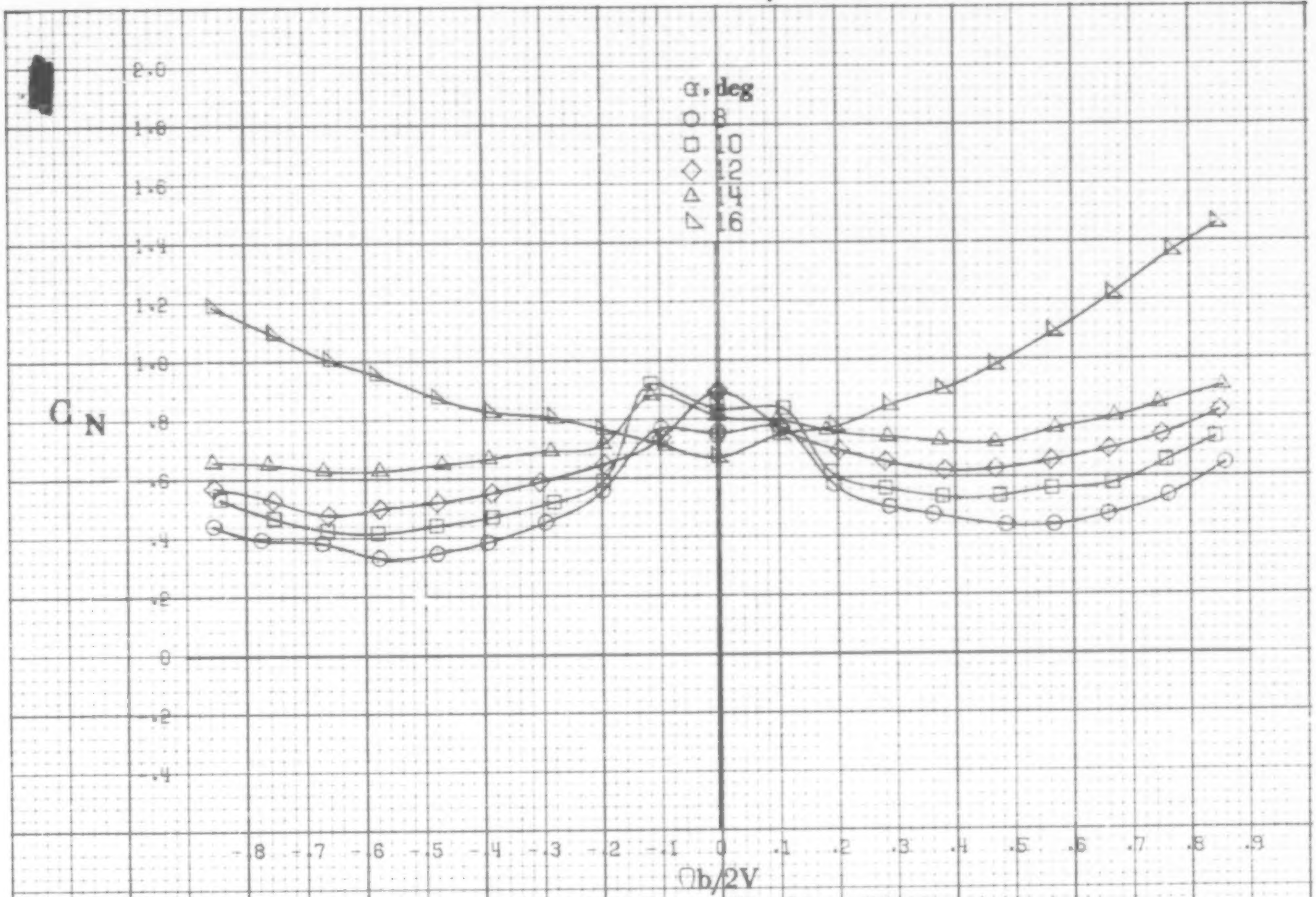

(a) $\alpha = 8$ to 16 deg, SR = 76 cm (30 in).

Figure A10.- Effect of rotation rate and angle of attack on normal-force coefficient for basic configuration. $\delta_e = 0^\circ$, $\delta_a = 0^\circ$, $\delta_r = -25^\circ$, $\beta = 0^\circ$.

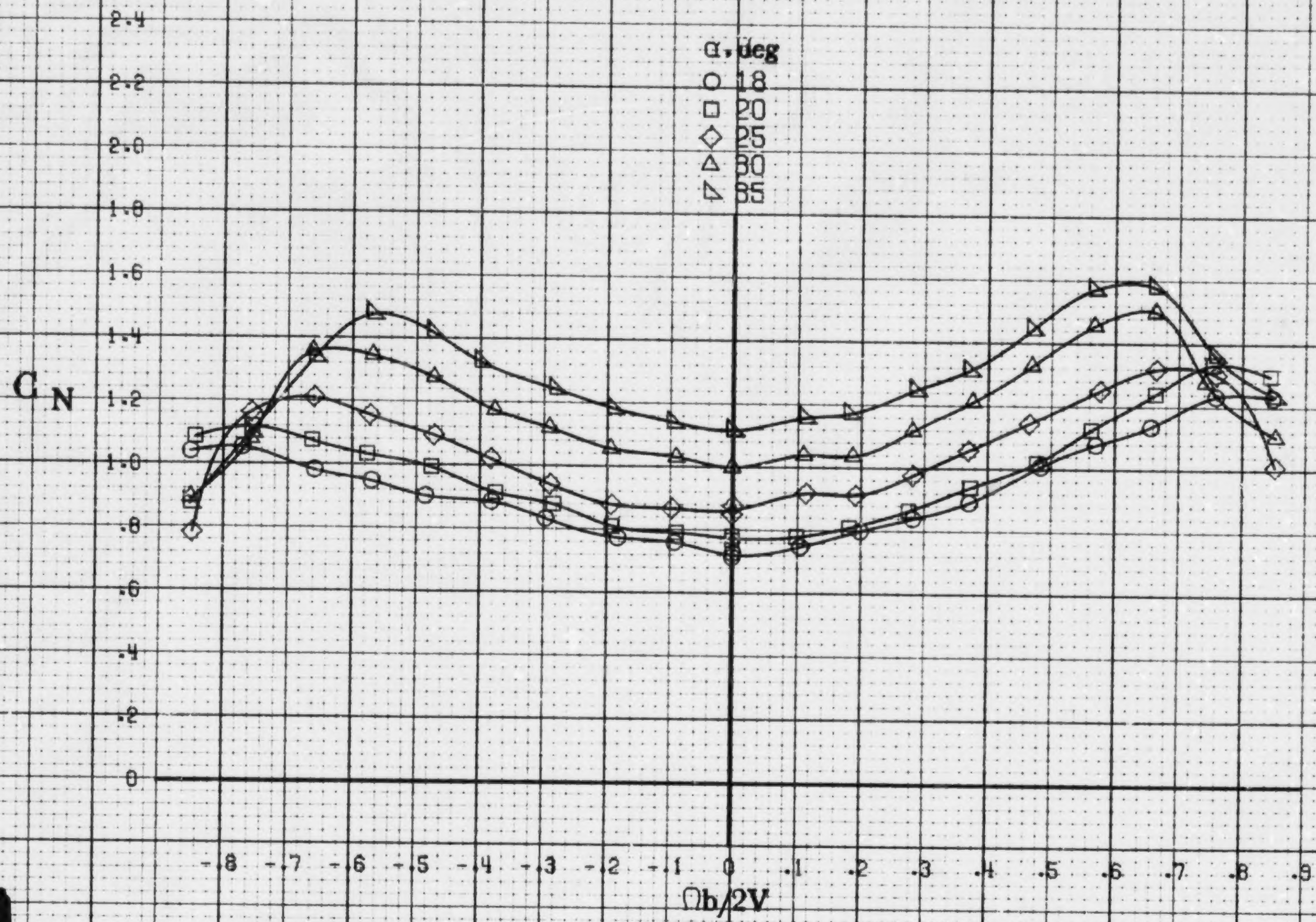

(b) α = 18 to 35 deg, SR = 76 cm (30 in).

Figure A10.-Continued.

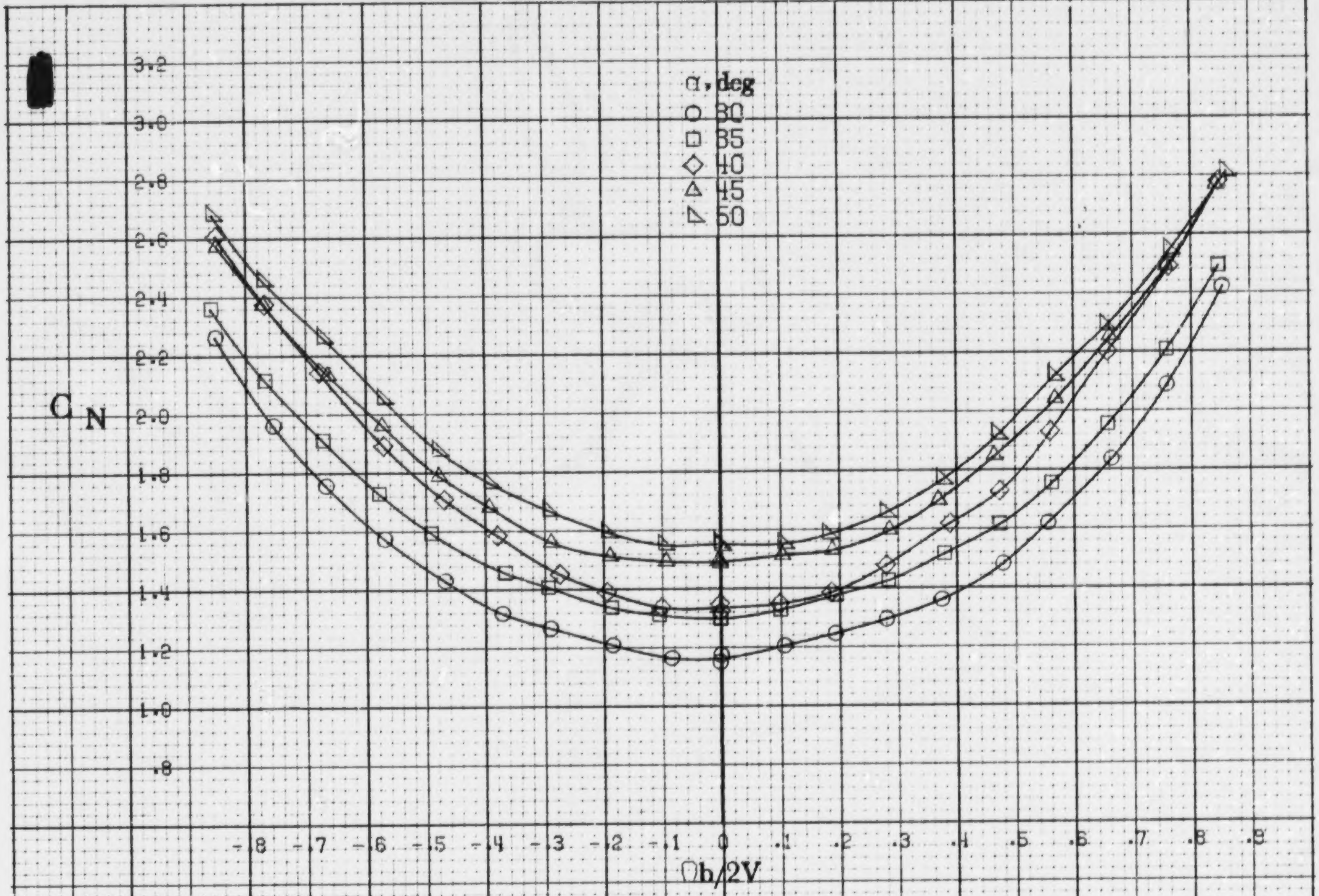

(c) $\alpha = 30$ to 50 deg, SR = 0.

Figure A10.-Continued.

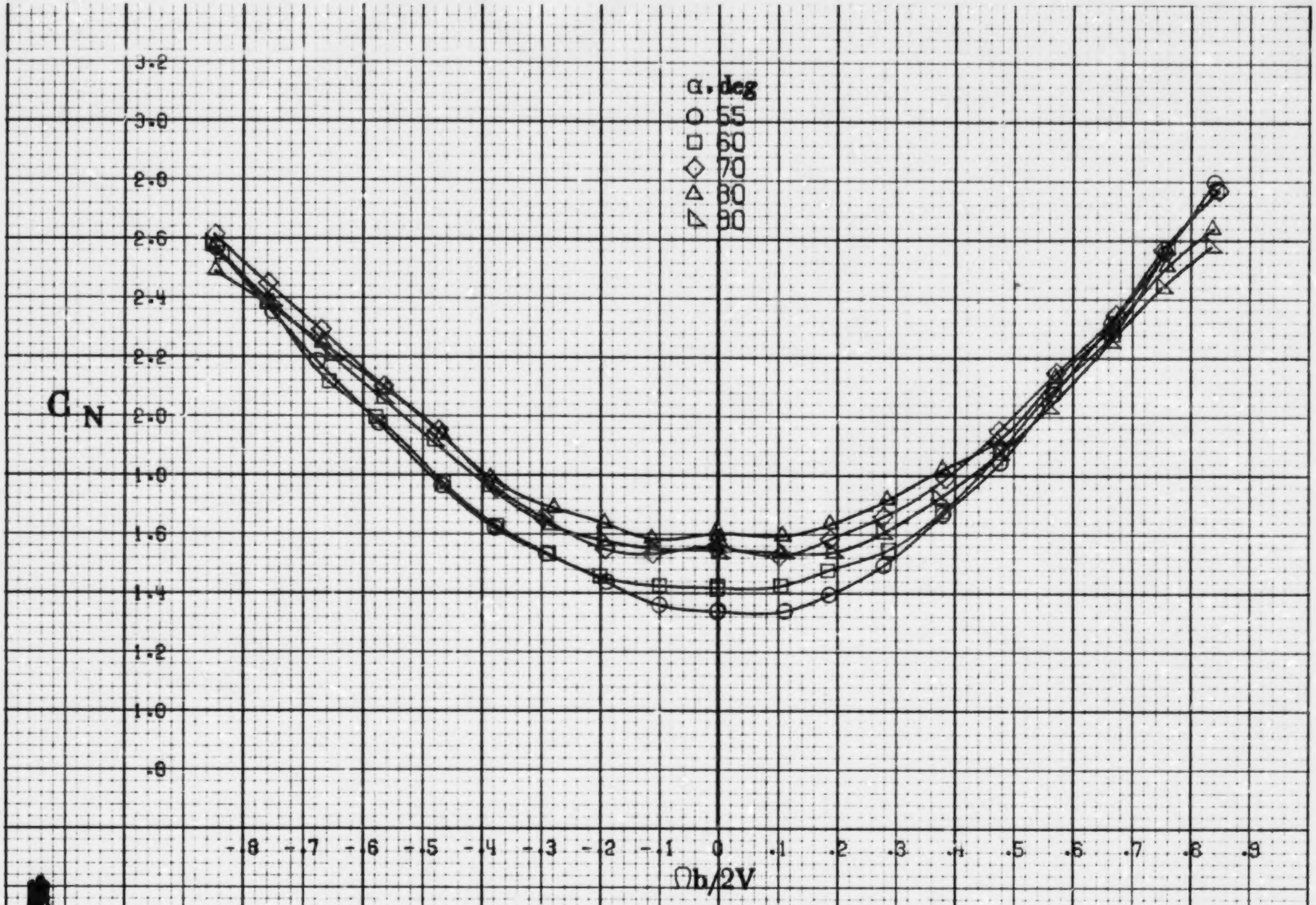

(d) α = 55 to 90 deg, SR = 0.

Figure A10.-Concluded.

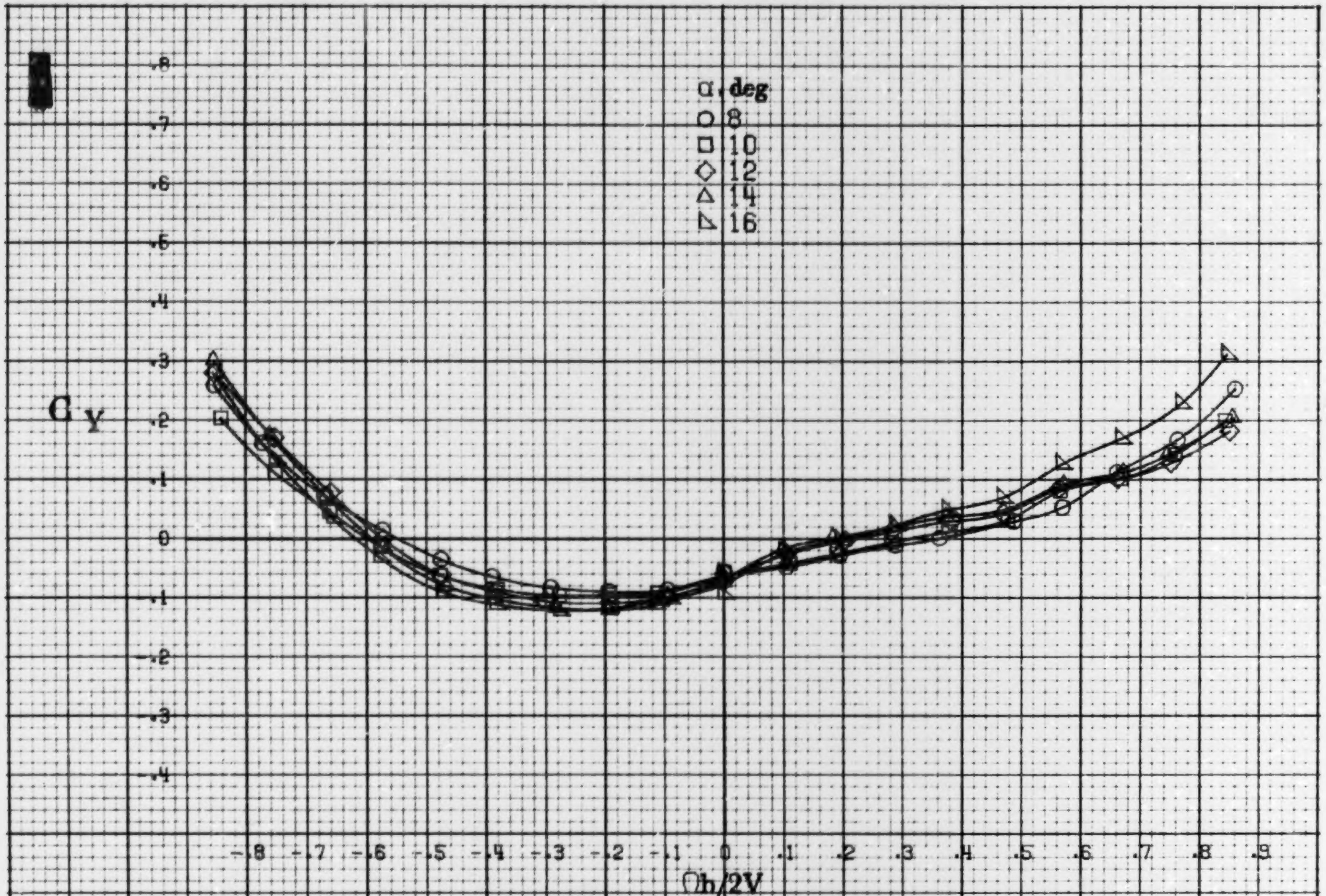

(a) α = 8 to 16 deg, SR = 76 cm (30 in).

Figure A11.-Effect of rotation rate and angle of attack on side-force coefficient for basic configuration. $\delta_e = 0°$, $\delta_a = 0°$, $\delta_r = 25°$, $\beta = 0°$.

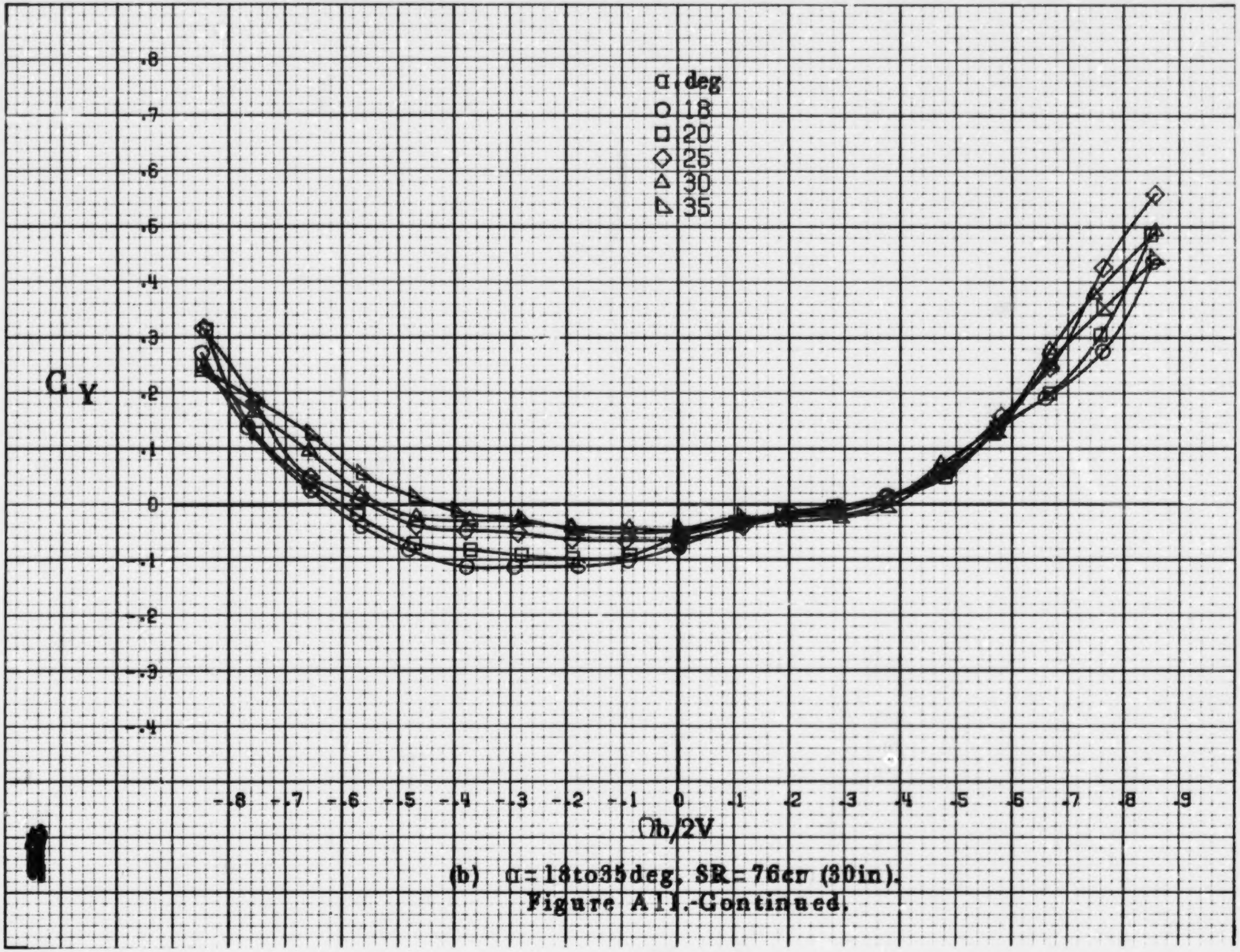

(b) α = 18 to 35 deg, SR = 76 cm (30 in).

Figure A11.-Continued.

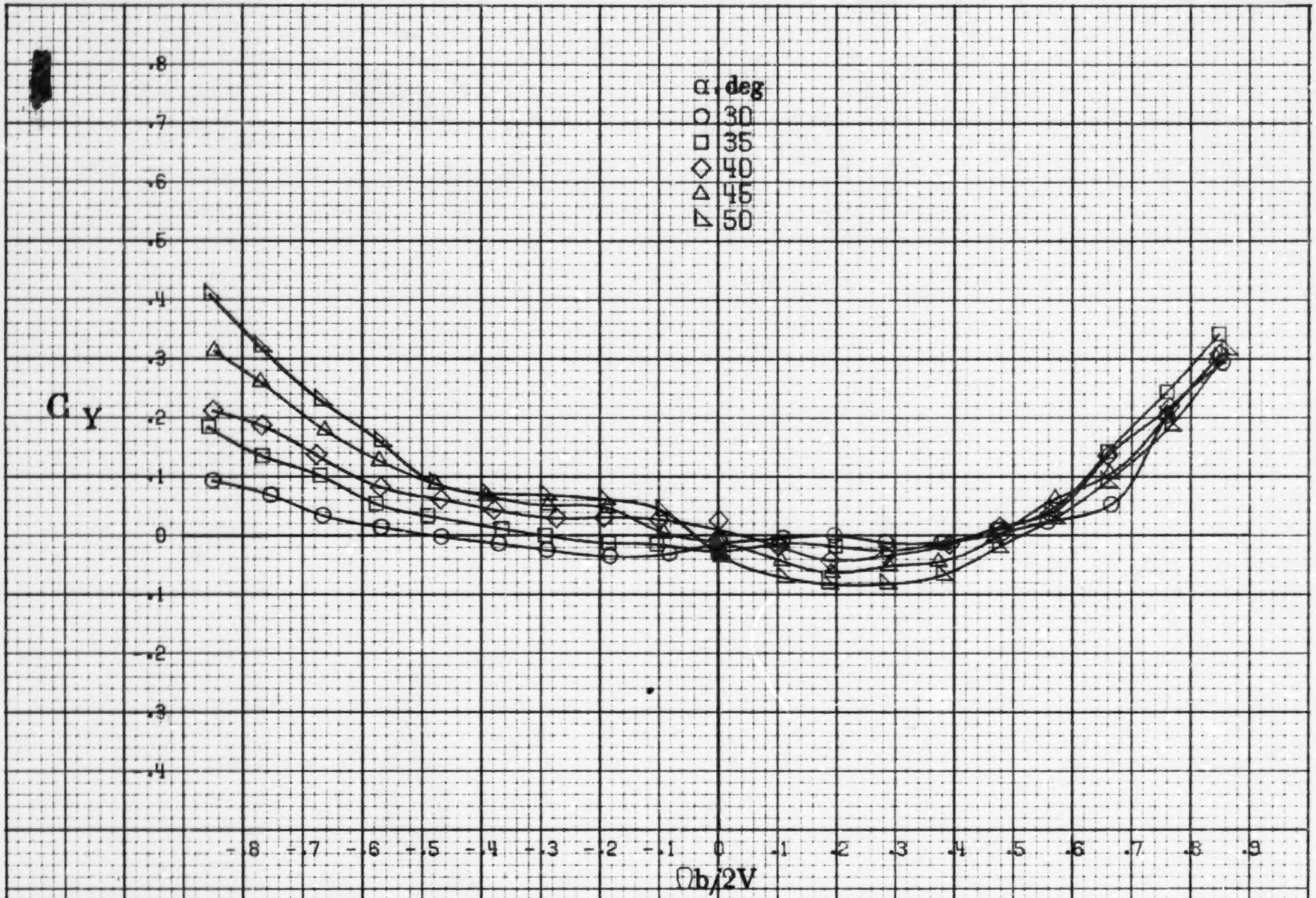

(c) α = 30 to 50 deg, SR = 0.

Figure A11.-Continued.

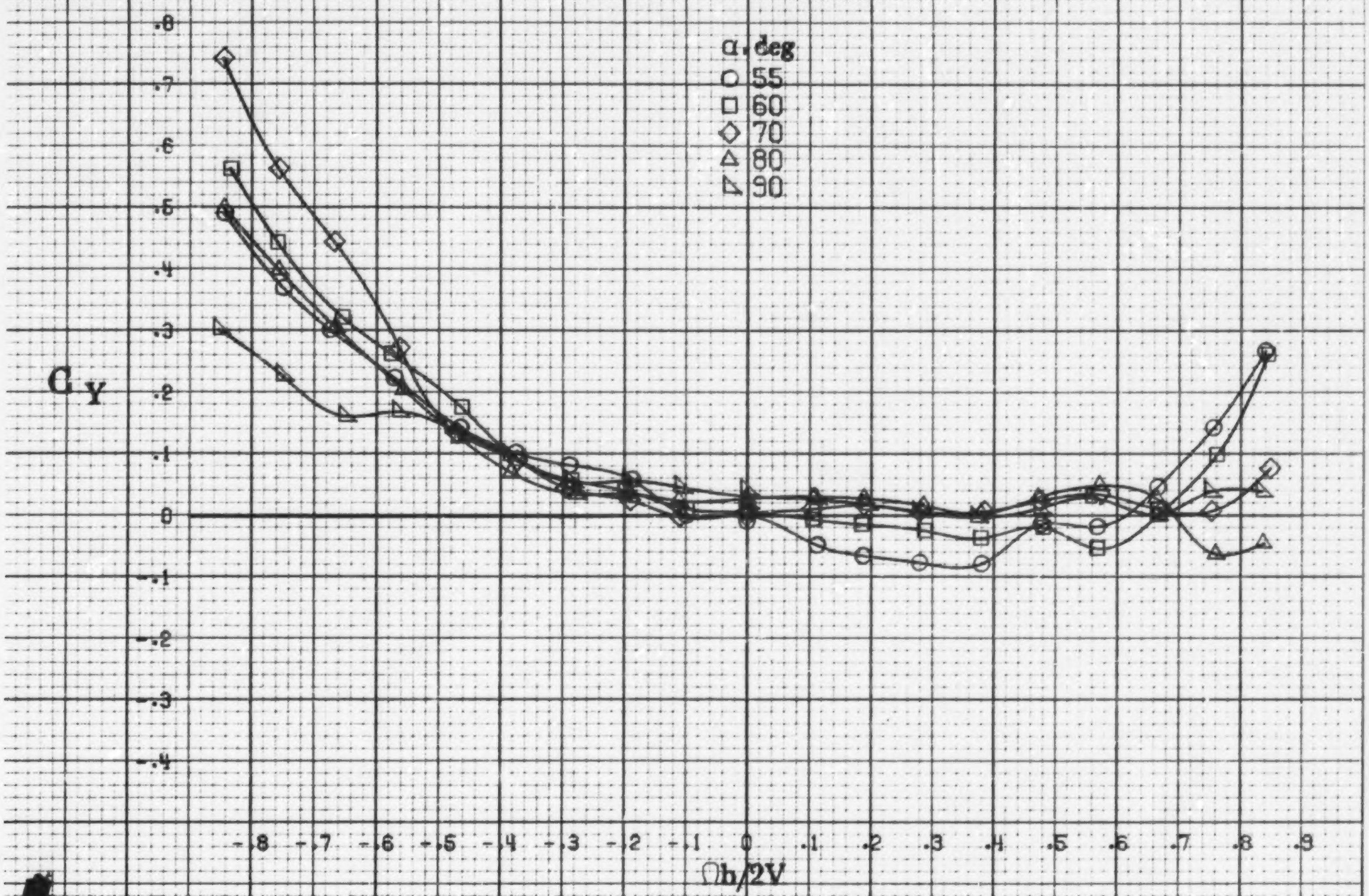

(d) α = 55 to 90 deg, SR = 0.

Figure A11.-Concluded.

A45

A46

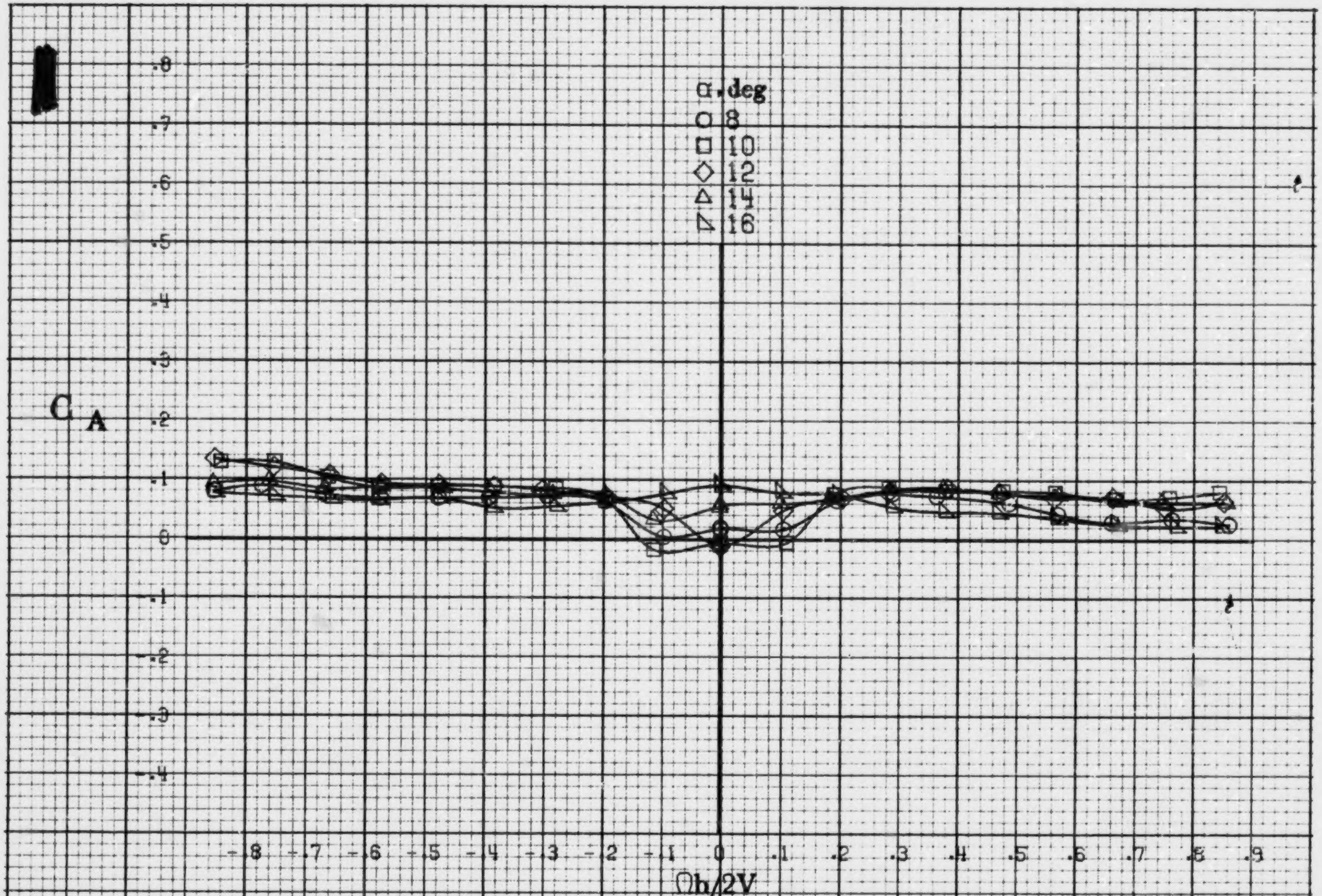

$\Omega h/2V$

(a) $\alpha = 8$ to 16 deg, SR = 76 cm (30 in).

Figure A12.-Effect of rotation rate and angle of attack on axial-force coefficient for basic configuration. $\delta_e = 0°$, $\delta_a = 0°$, $\delta_r = -25°$, $\beta = 0°$.

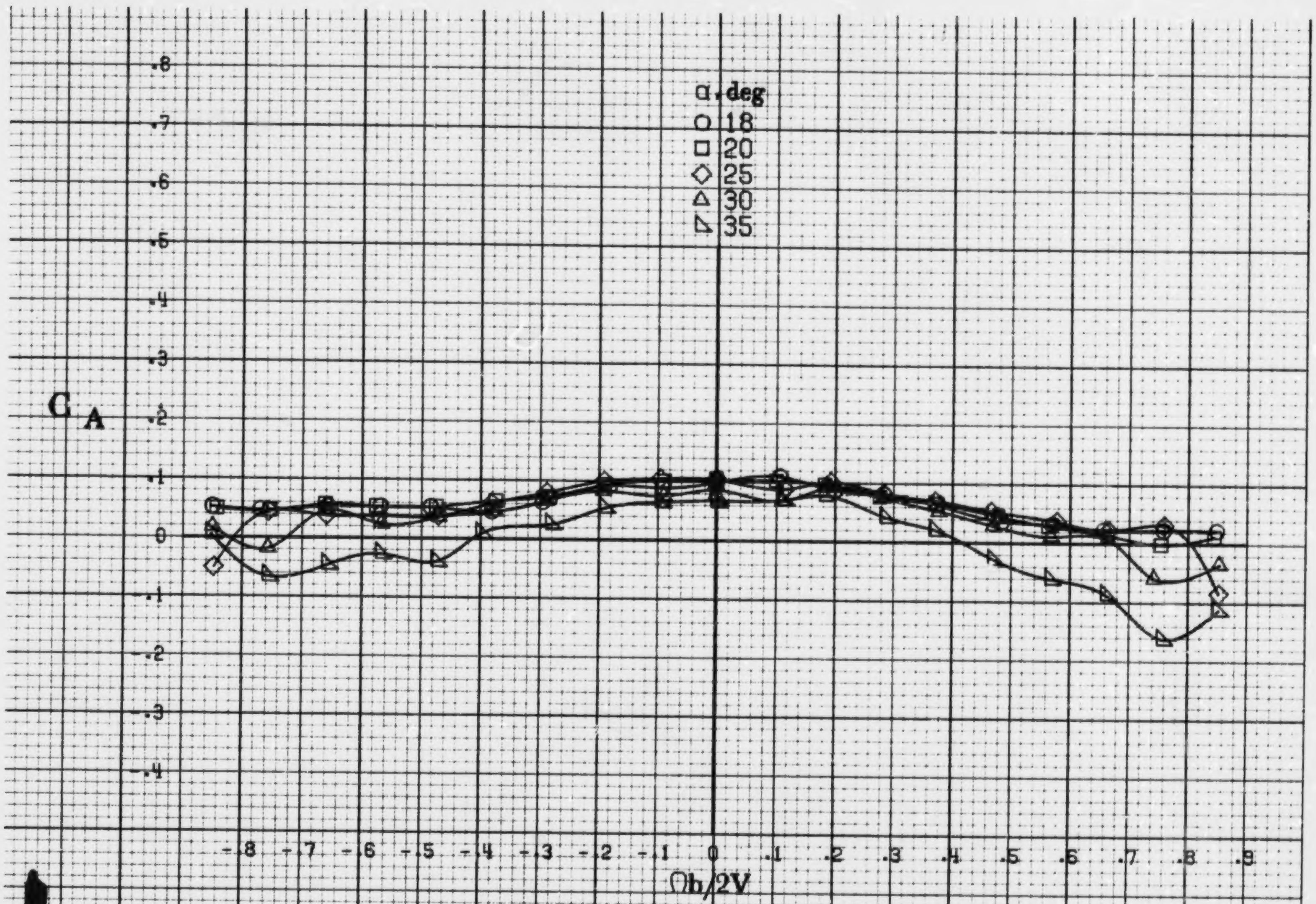

(b) α = 18 to 35 deg, SR = 76 cm (30 in).
Figure A12.-Continued.

A48

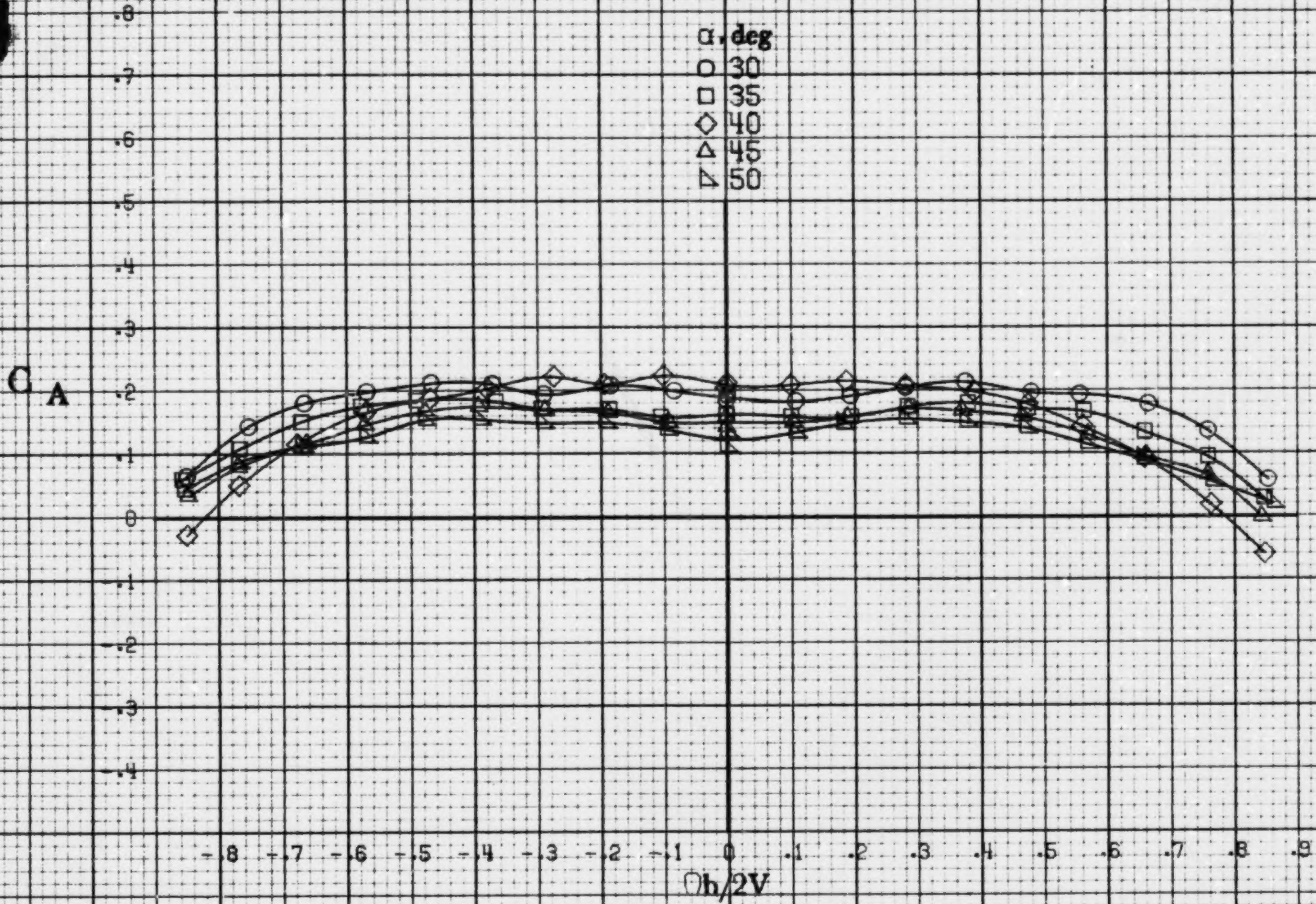

(c) α = 30 to 50 deg, SR = 0.

Figure A12.-Continued.

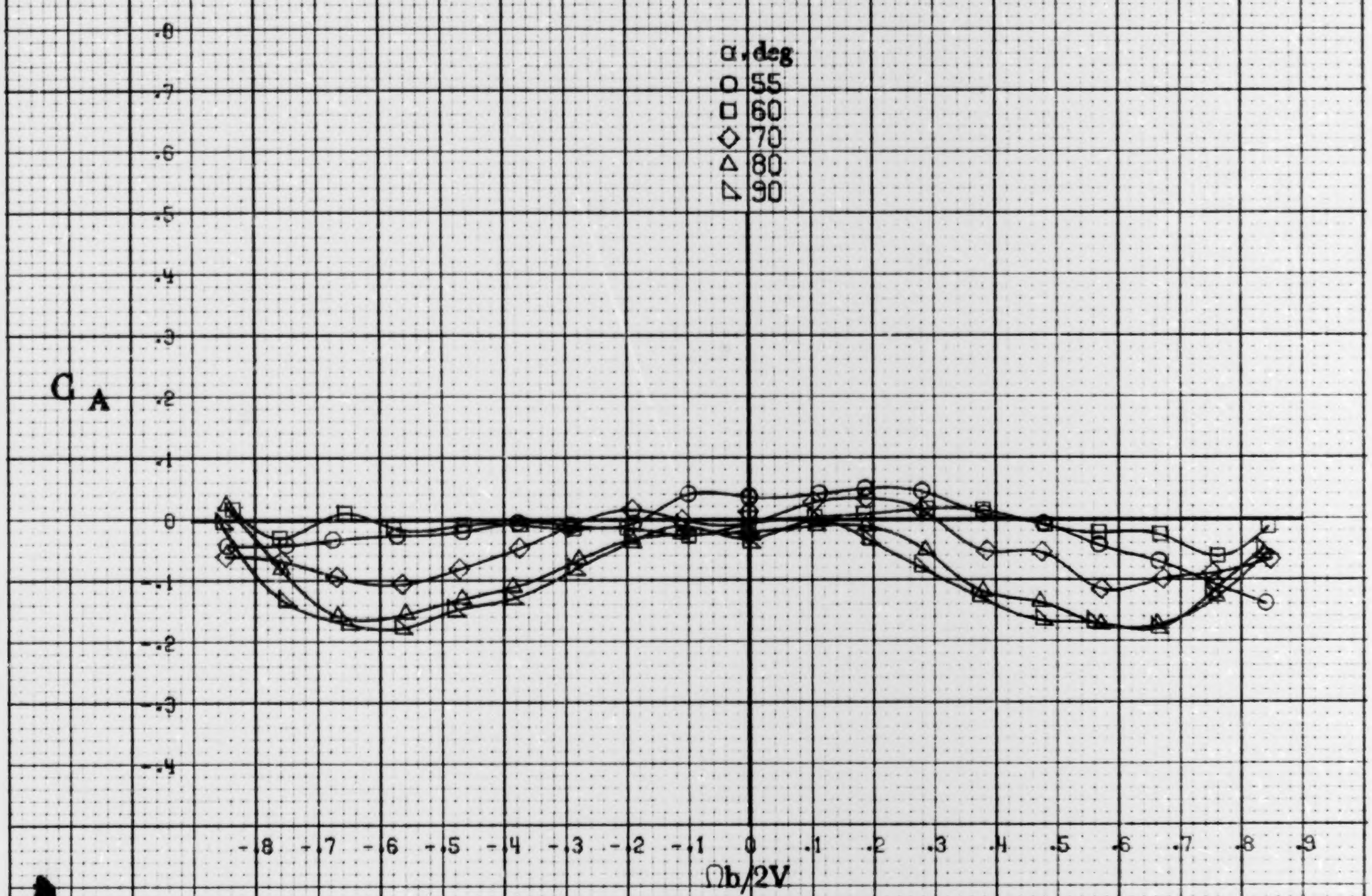

(d) α = 55 to 90 deg, SR = 0.

Figure A12.-Concluded.

A50

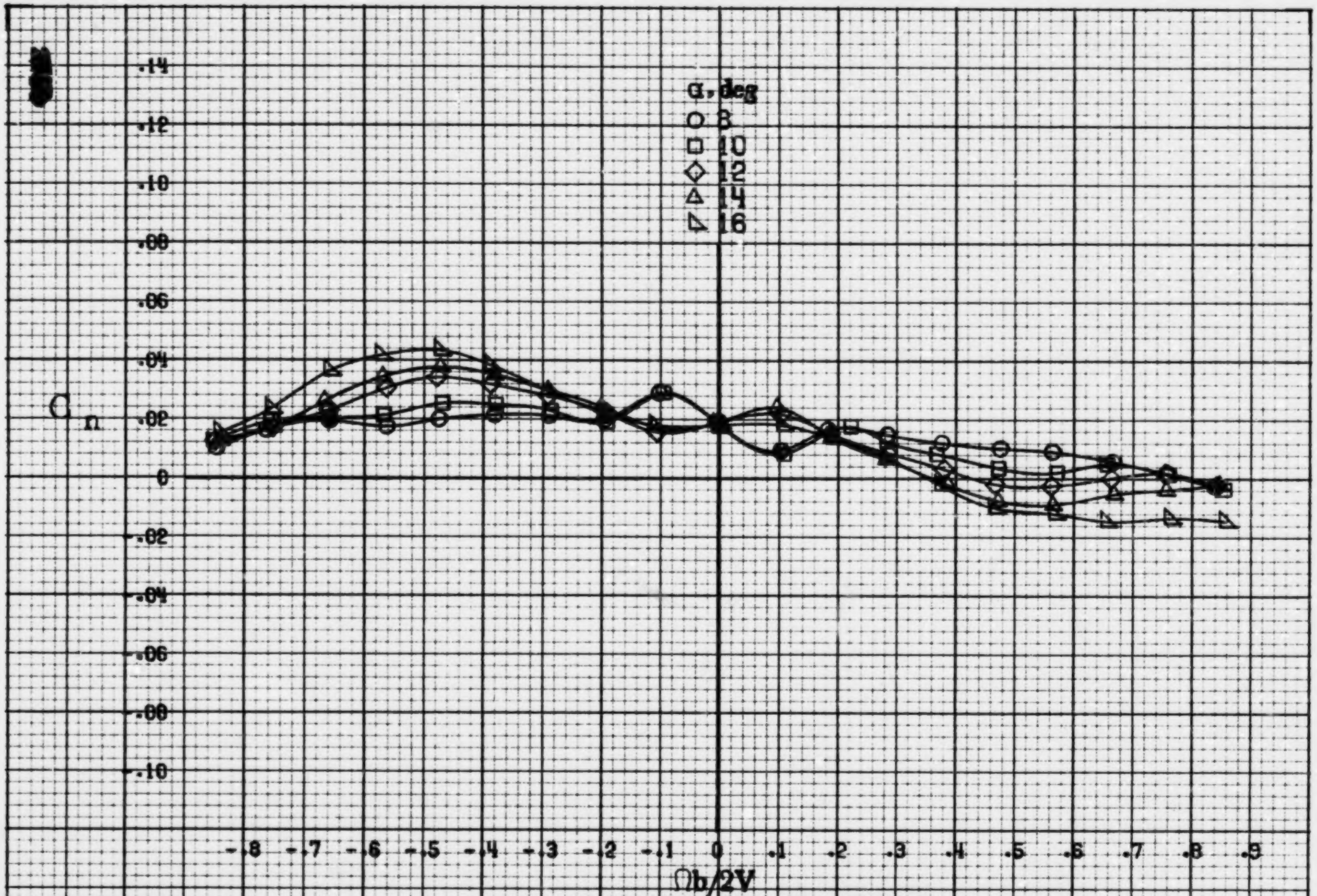

(a) $\alpha = 8$ to 16 deg, SR = 76 cm (30 in).

Figure A18.-Effect of rotation rate and angle of attack on yawing-moment coefficient for basic configuration. $\delta_e = 15°$, $\delta_a = 0°$, $\delta_r = -25°$, $\beta = 0°$.

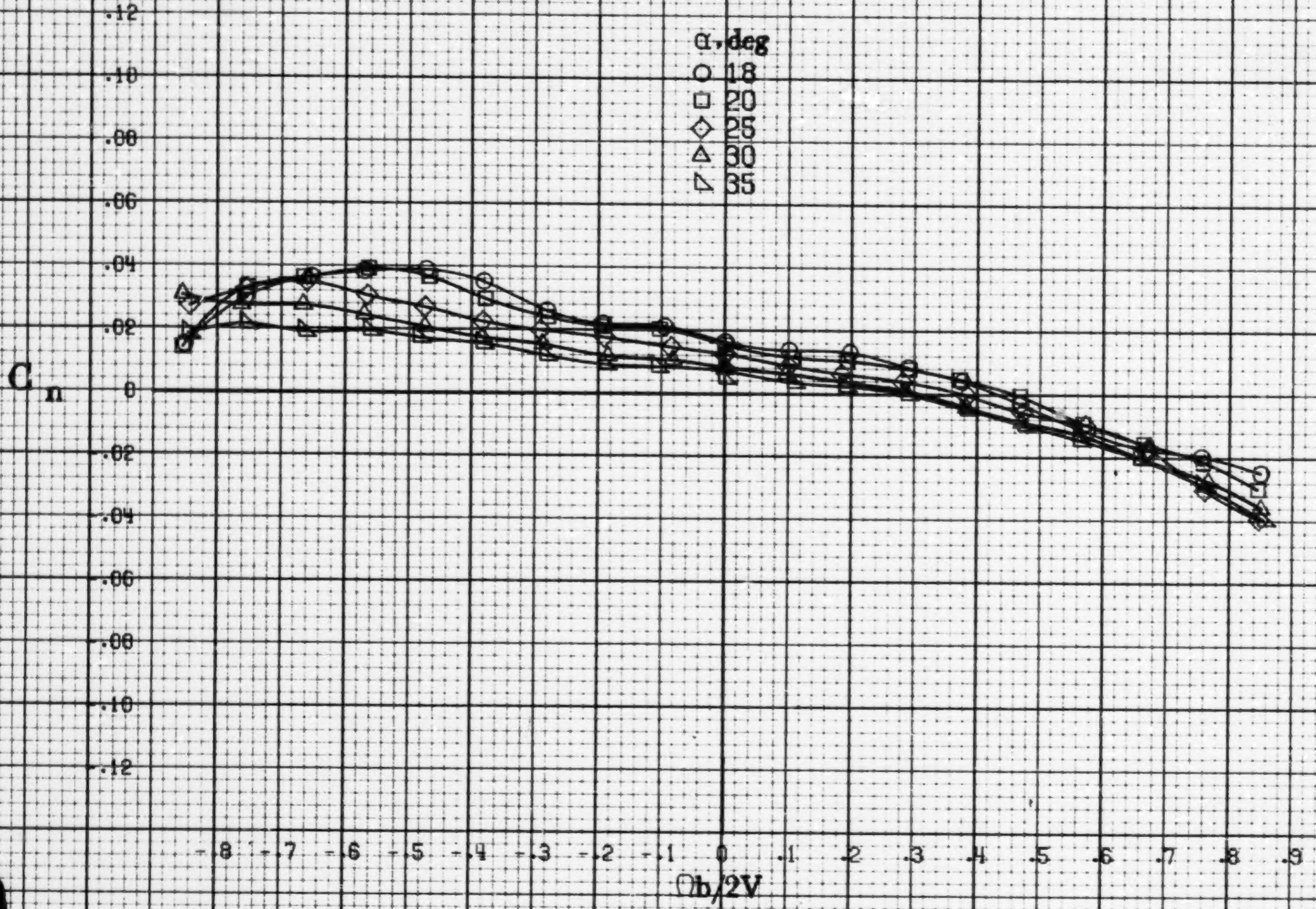

(b) α = 18 to 35 deg, SR = 76 cm (30 in).

Figure A13.-Continued.

A52

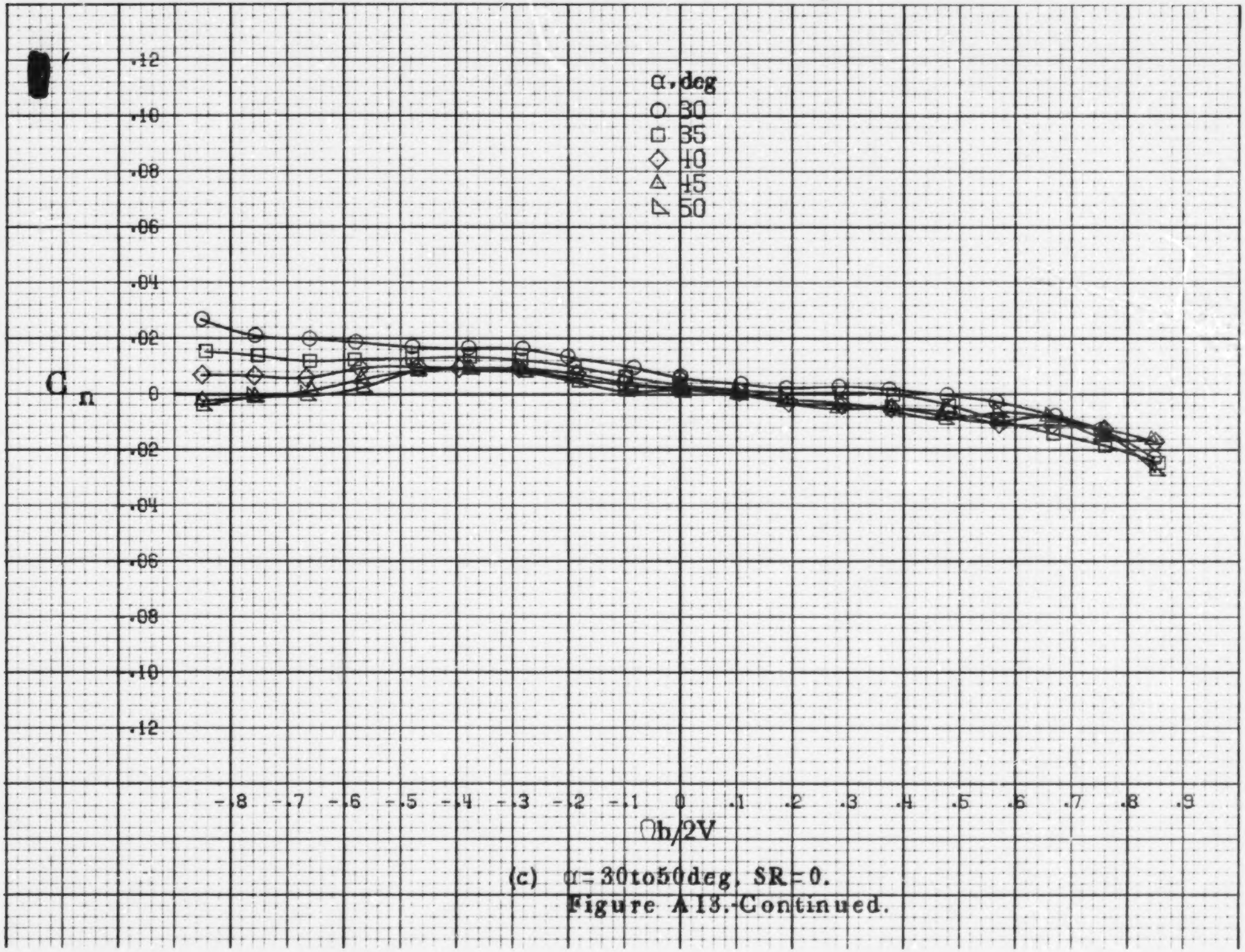

(c) α = 30 to 50 deg, SR = 0.

Figure A13.-Continued.

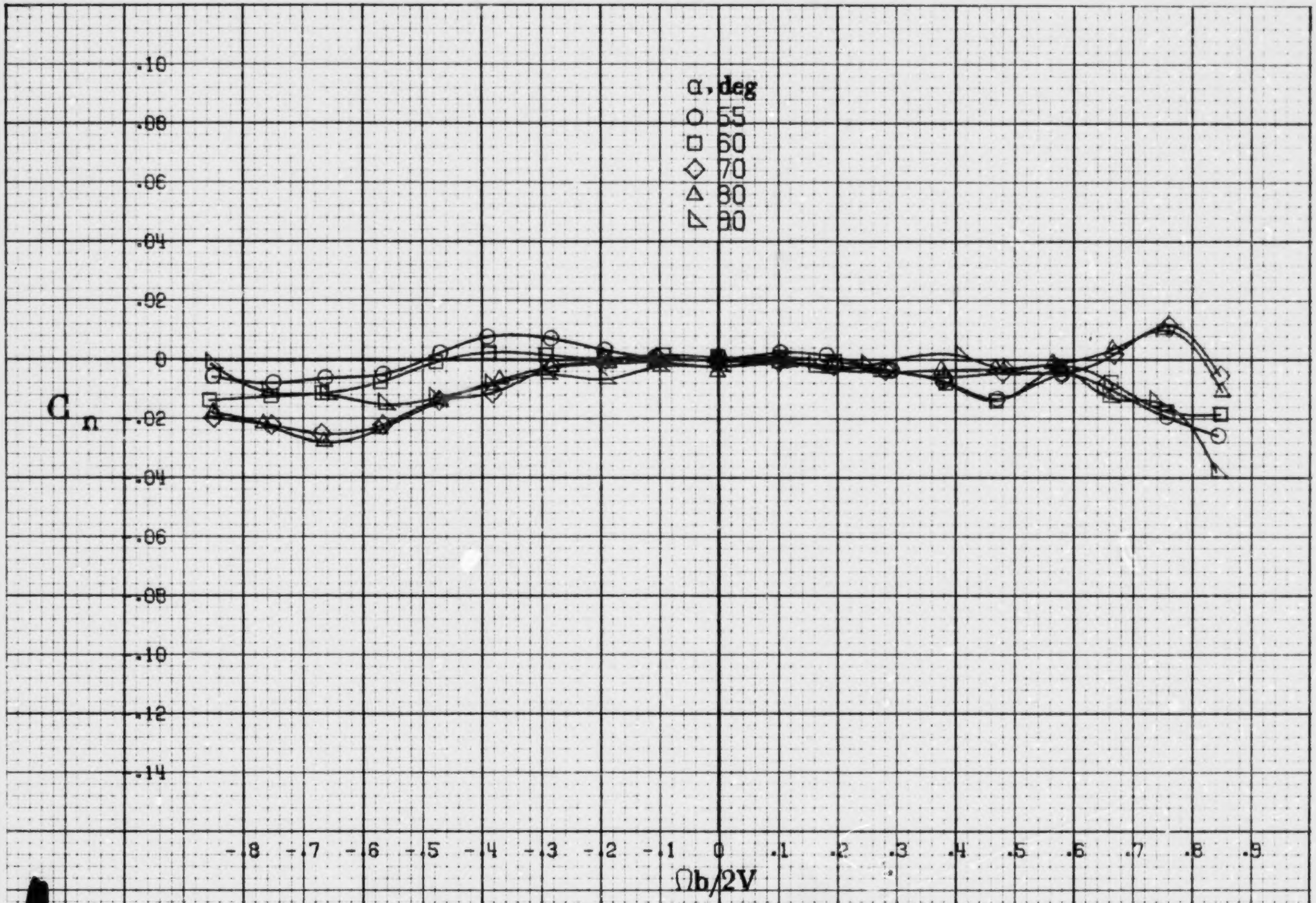

(d) α = 55 to 90 deg, SR = 0.

Figure A13.-Concluded.

A54

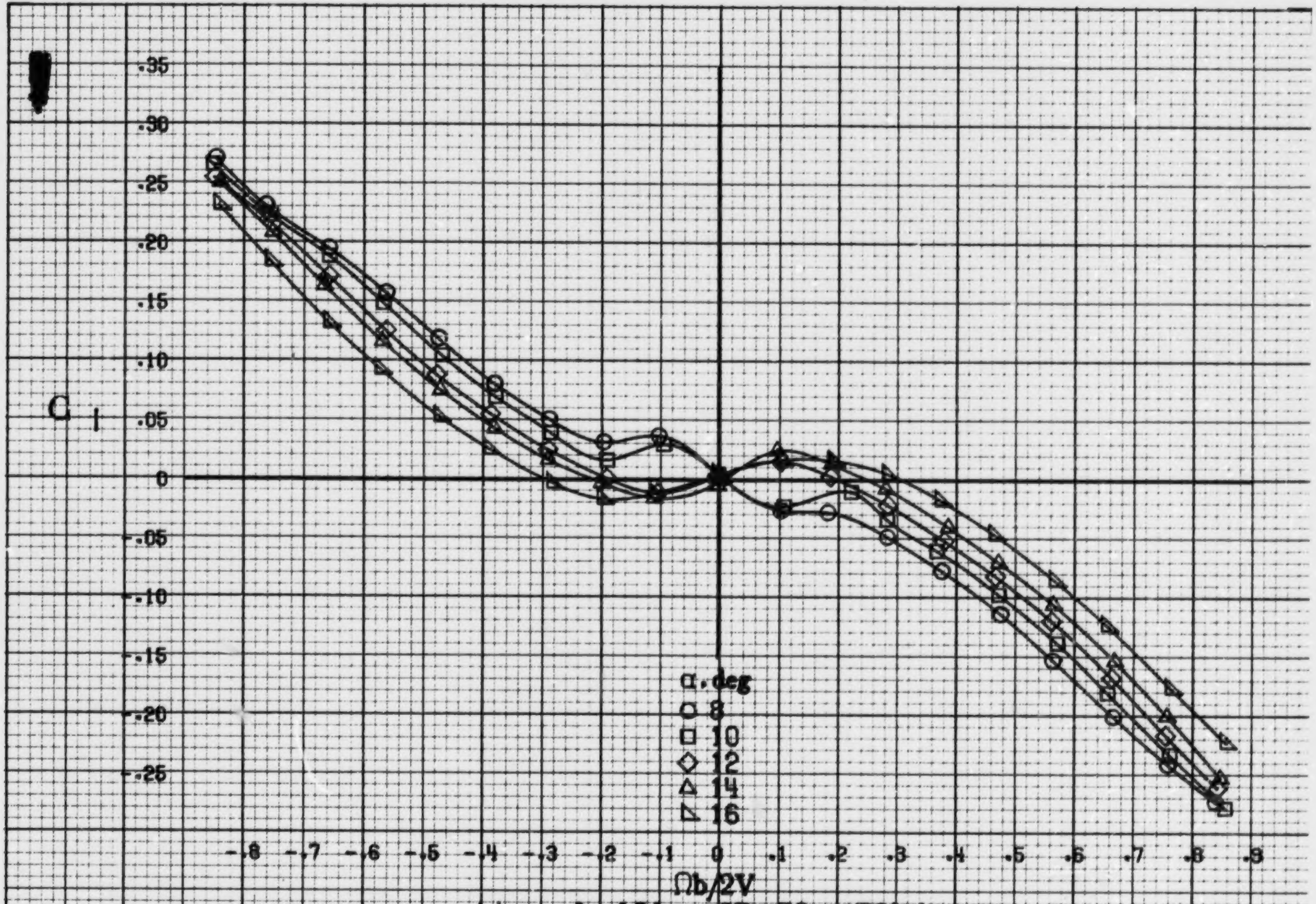

(a) α = 8 to 16 deg, SR = 76 cm (30 in).

Figure A14.- Effect of rotation rate and angle of attack on rolling-moment coefficient for basic configuration. $\delta_e = 15°$, $\delta_a = 0°$, $\delta_r = -25°$, $\beta = 0°$.

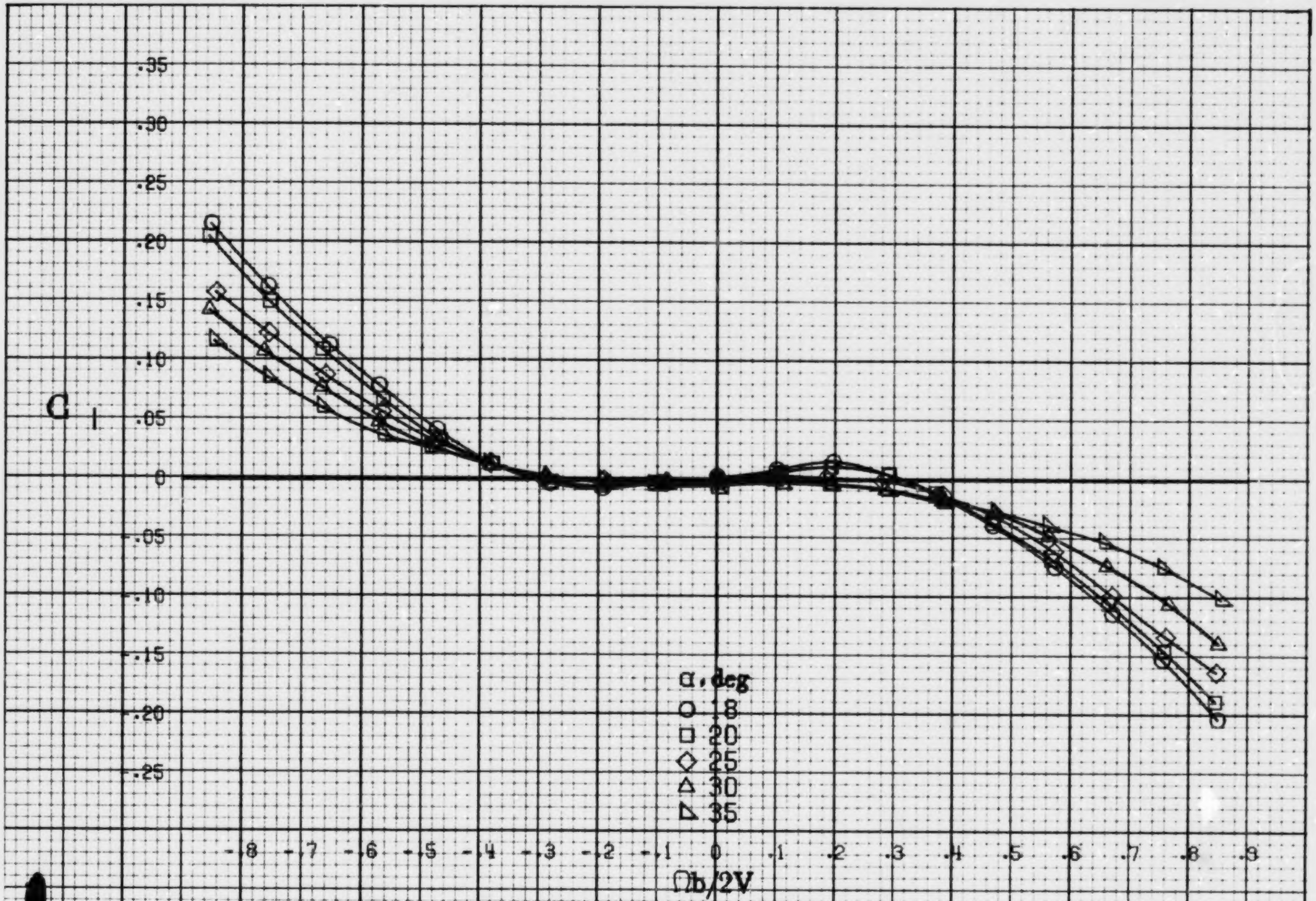

(b) α= 18to35deg, SR= 76cm (30in).

Figure A14.-Continued.

AS6

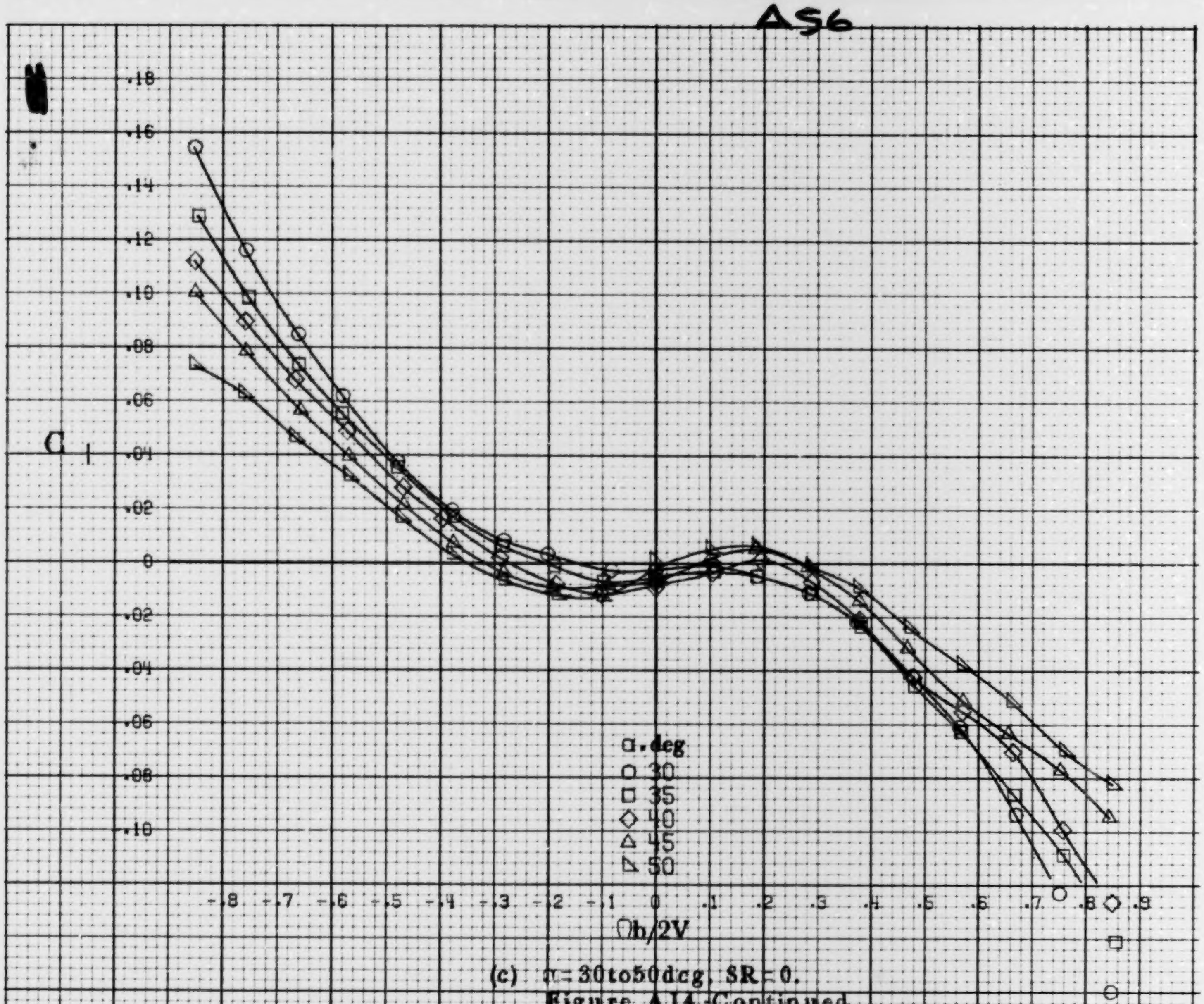

(c) α = 30 to 50 deg, SR = 0.
Figure A14.-Continued.

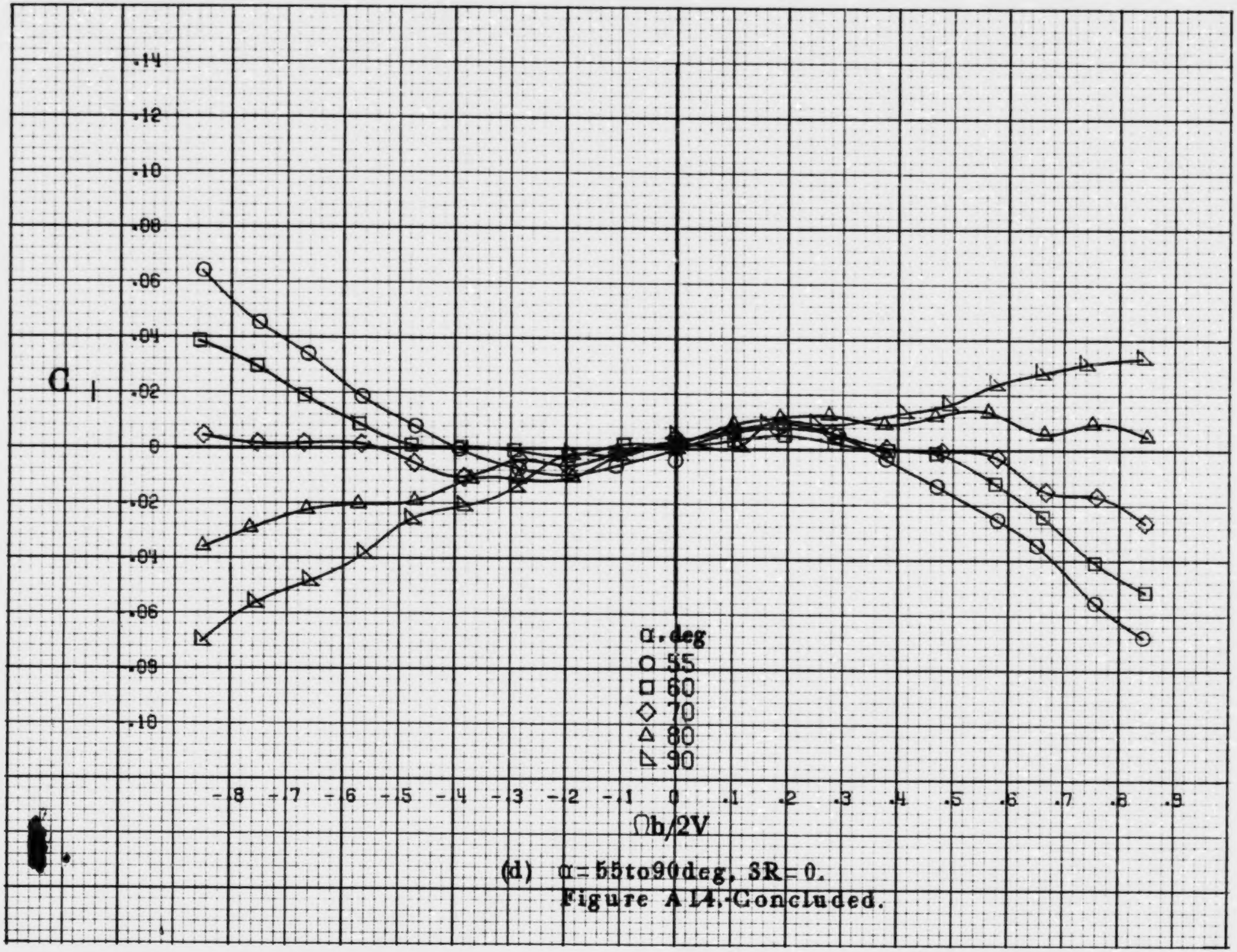

(d) α = 55 to 90 deg, SR = 0.

Figure A14.-Concluded.

A58

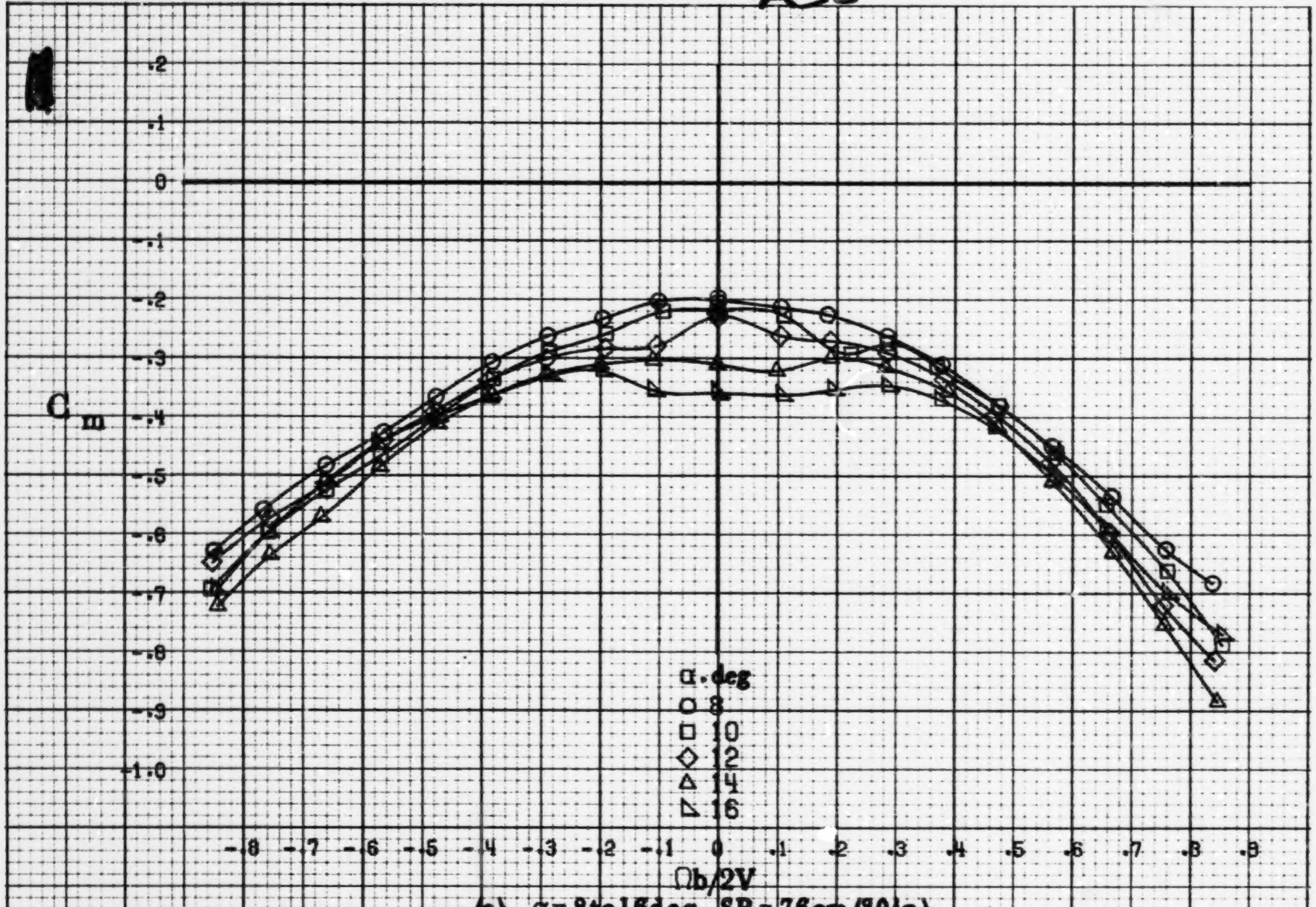

(a) α = 8 to 16 deg, SR = 76 cm (30 in).

Figure A15.- Effect of rotation rate and angle of attack on pitching-moment coefficient for basic configuration. $\delta_e = 15°$, $\delta_a = 0°$, $\delta_r = \pm 25°$, $\beta = 0°$.

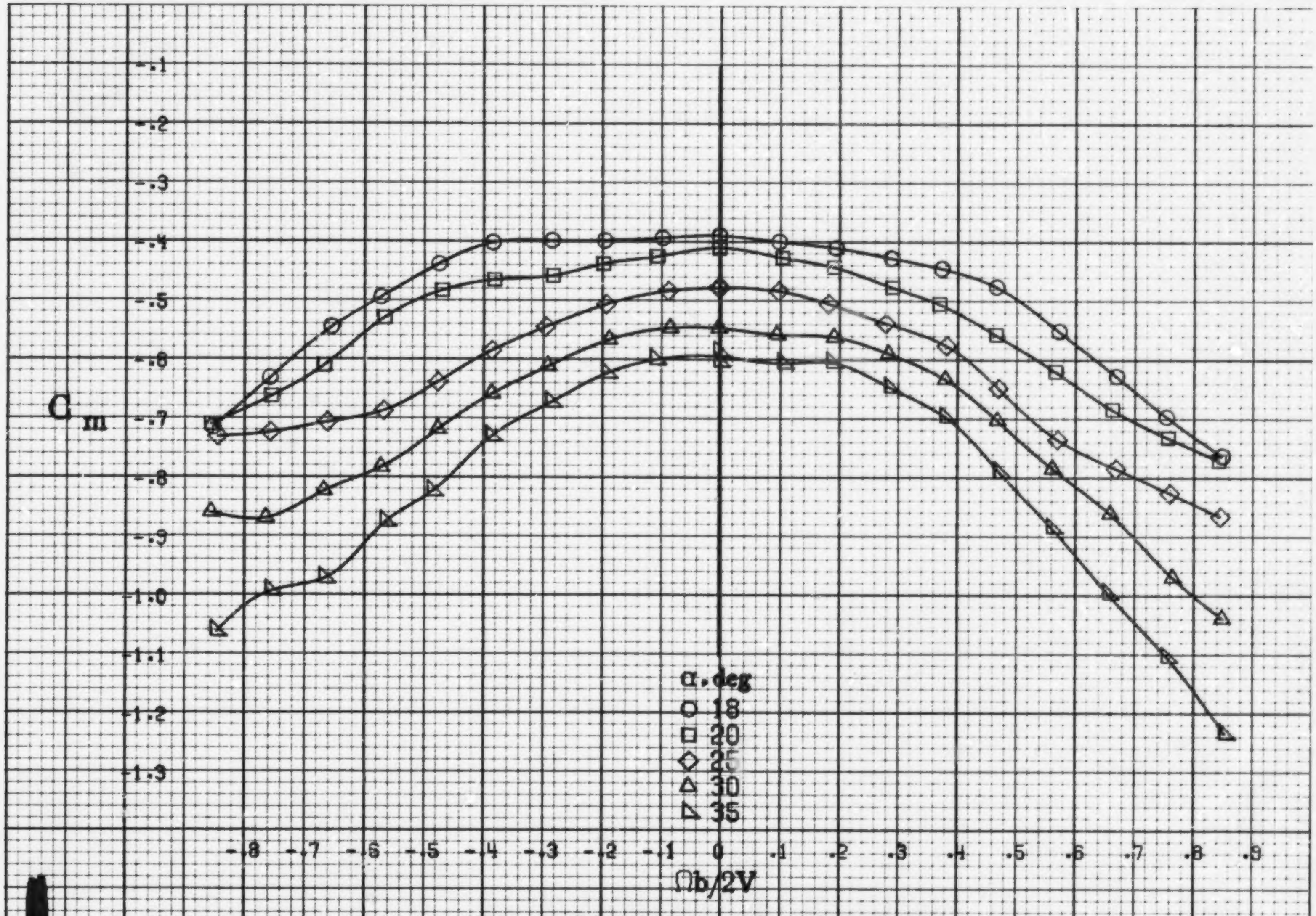

(b) α = 18 to 35 deg, SR = 76 cm (30 in).

Figure A15.- Continued.

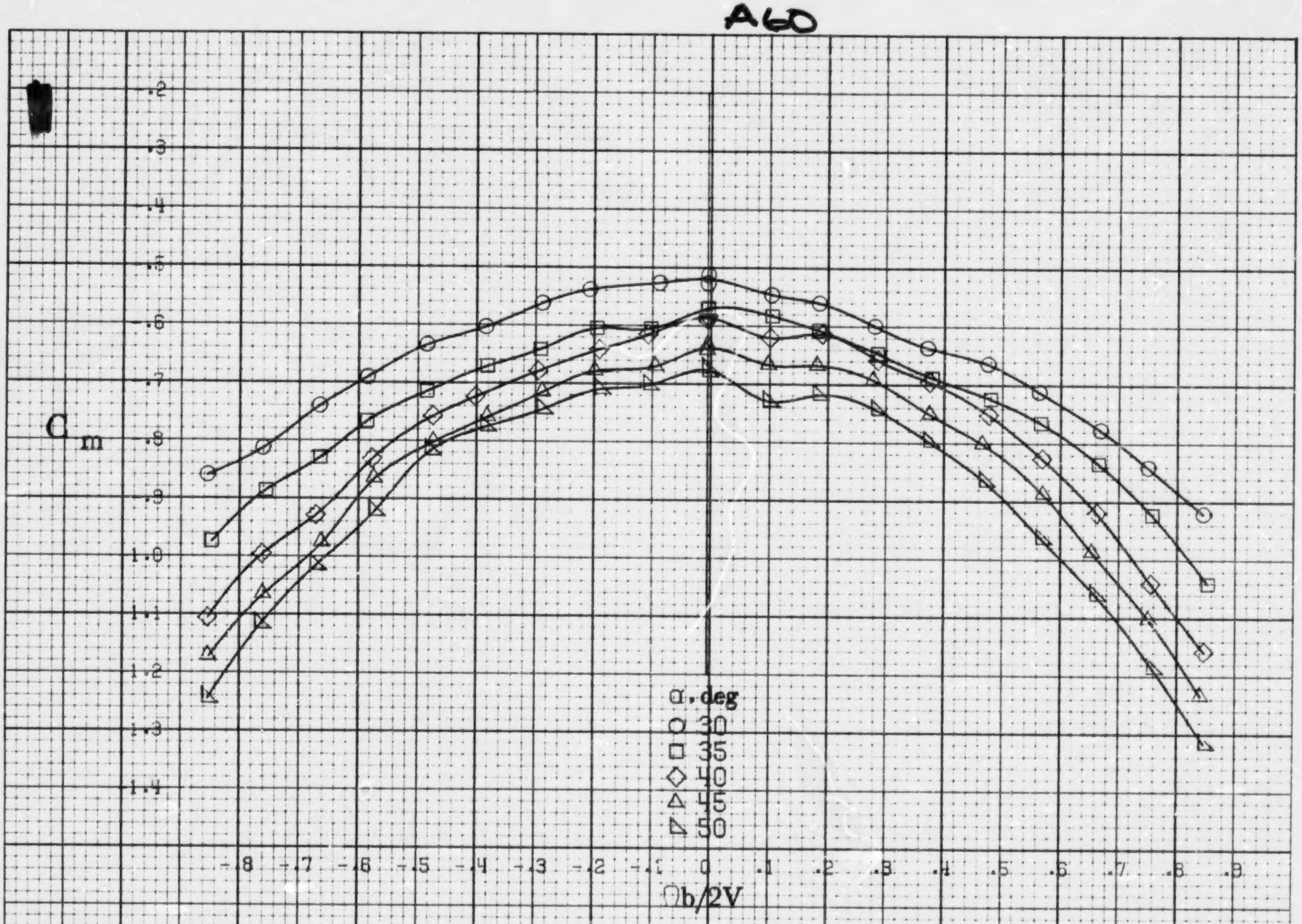

(c) α = 30 to 50 deg, SR = 0.

Figure A15.-Continued.

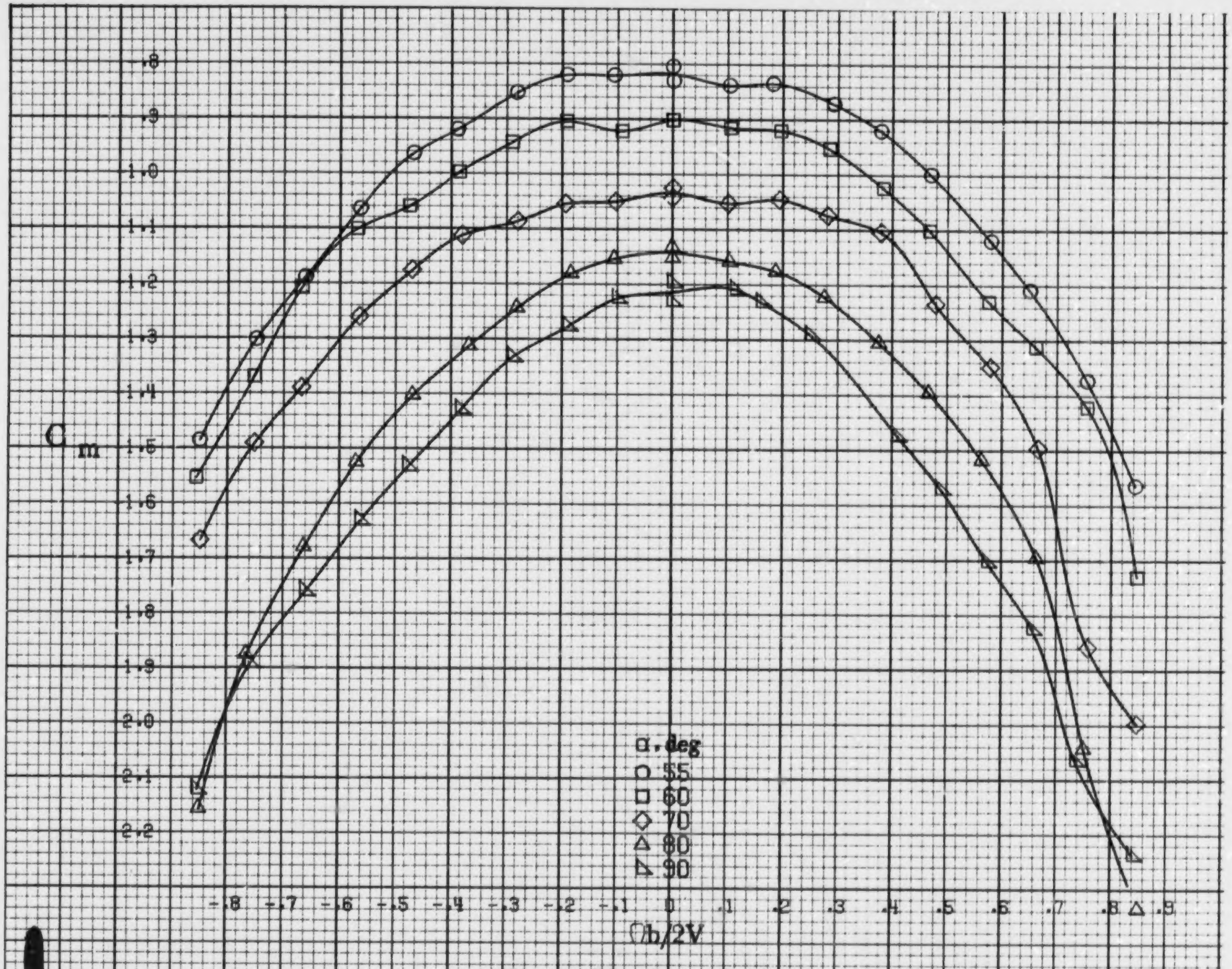

(d) $\alpha = 55$ to 90 deg, SR = 0.
Figure A15.-Concluded.

A62

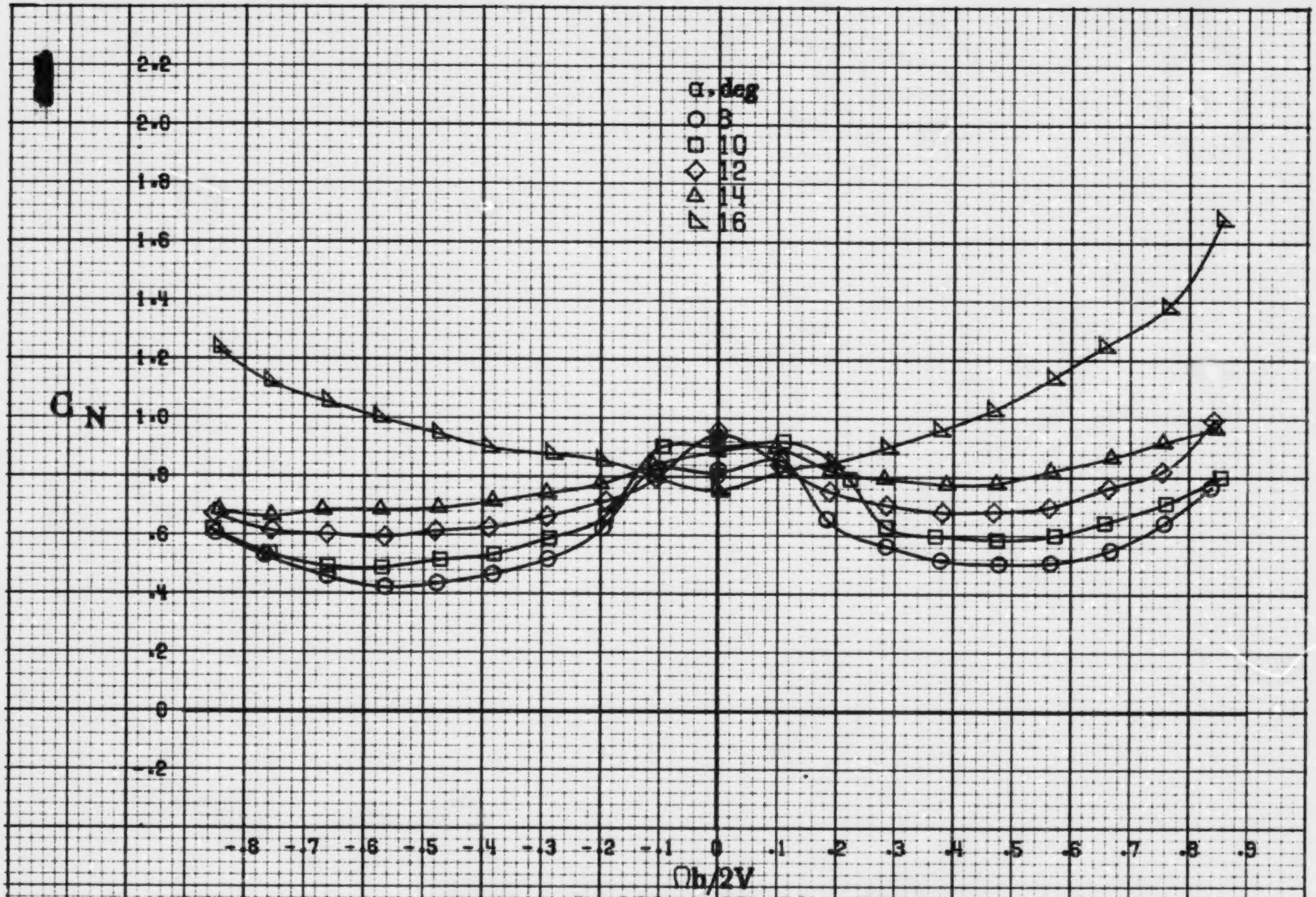

(a) α = 8 to 16 deg, SR = 76 cm (30 in).

Figure A16.-Effect of rotation rate and angle of attack on normal-force coefficient for basic configuration. $\delta_e = 15°$, $\delta_a = 0°$, $\delta_r = \pm 25°$, $\beta = 0°$.

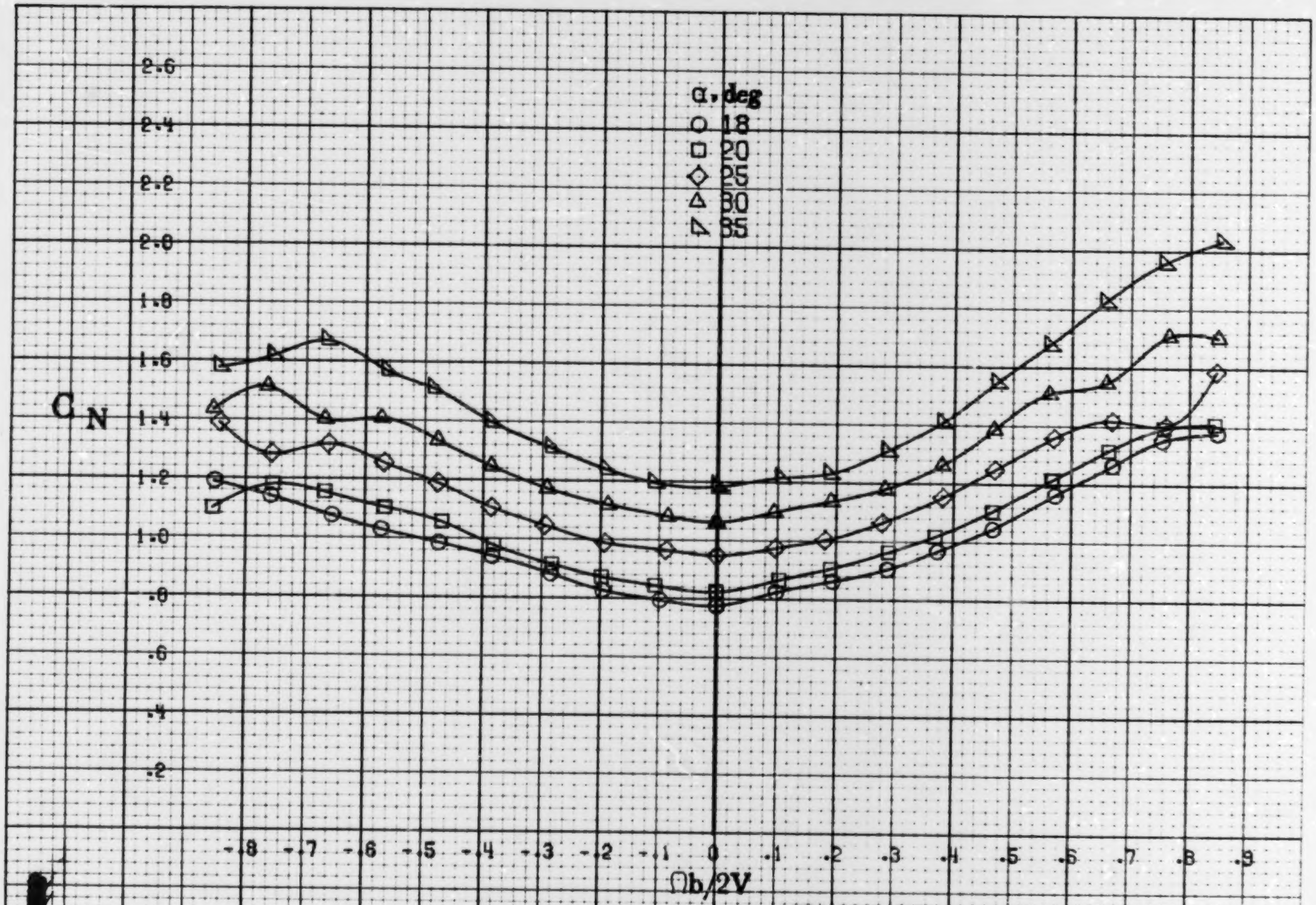

(b) α = 18 to 35 deg, SR = 76 cm (30 in).

Figure A16.-Continued.

A64

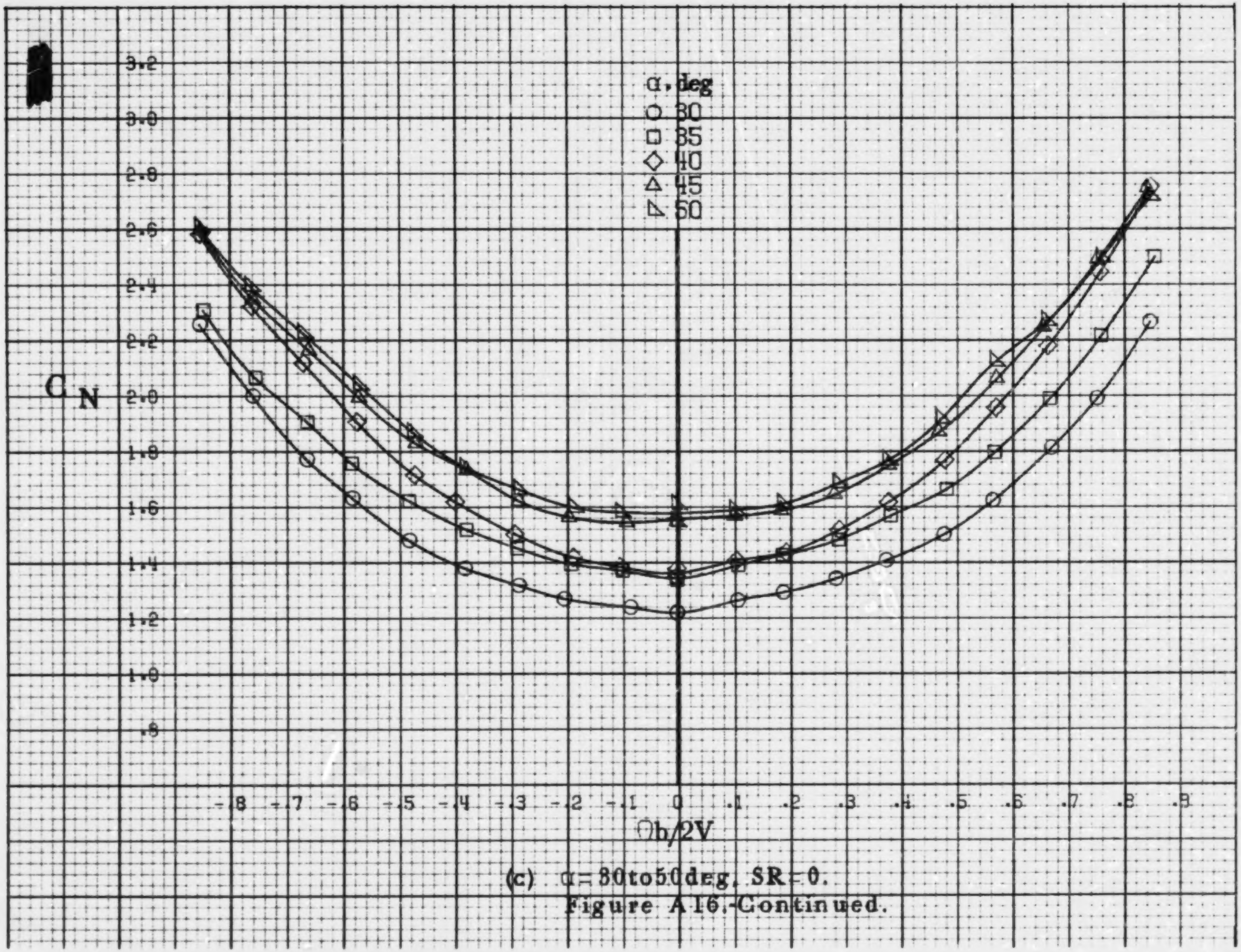

(c) α = 30 to 50 deg, SR = 0.

Figure A16.- Continued.

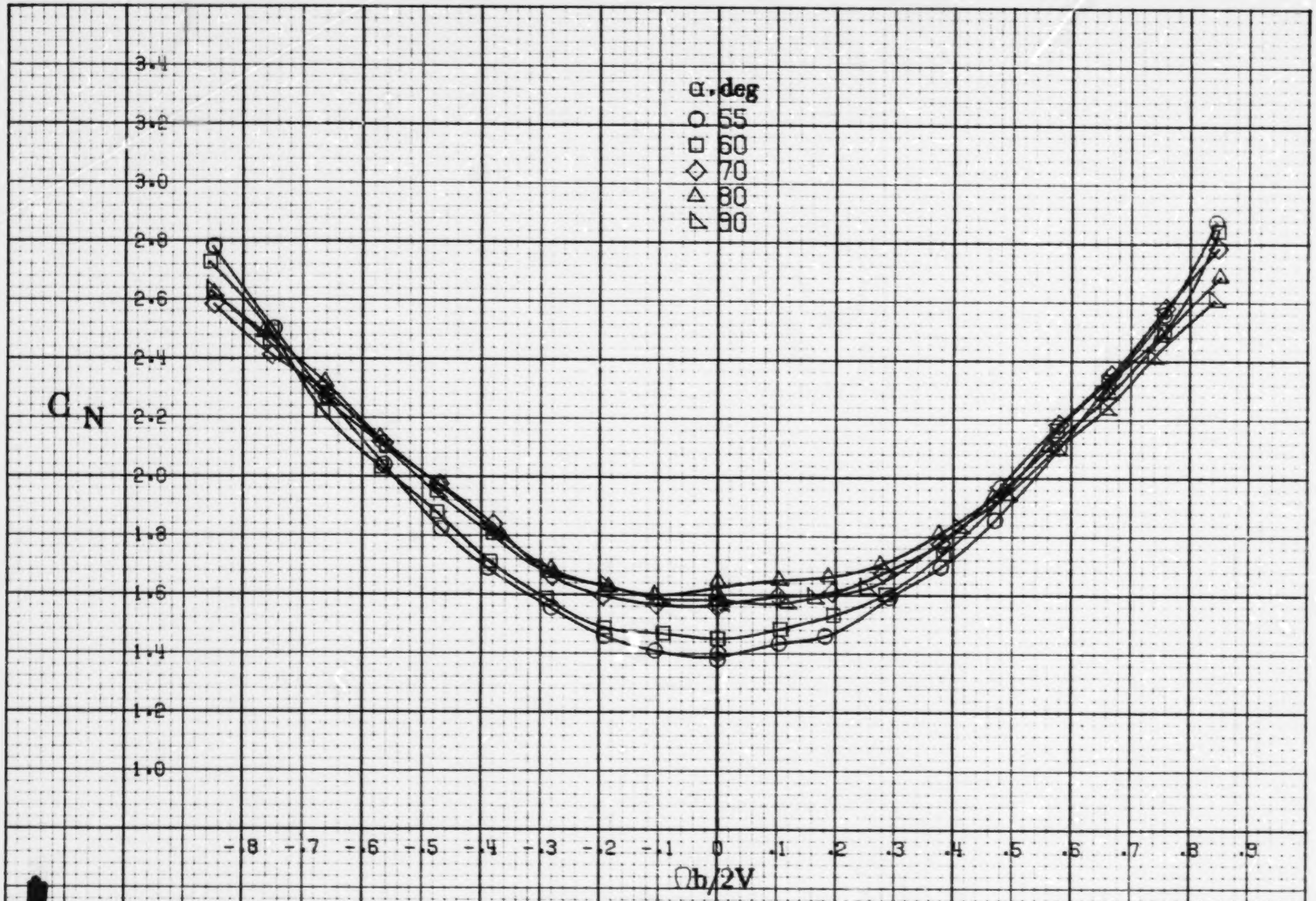

(d) α= 55 to 90 deg, SR= 0.

Figure A16.-Concluded.

A66

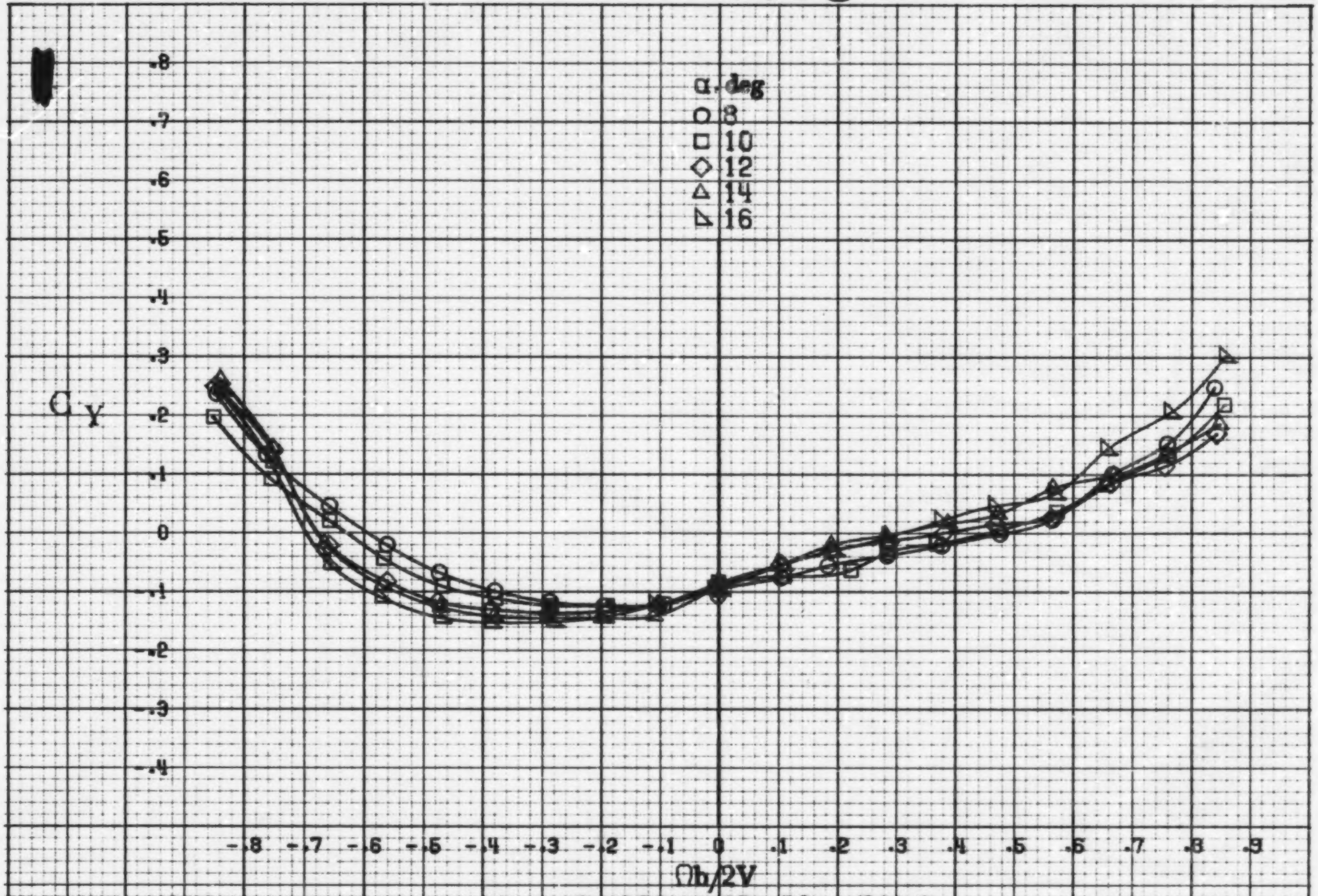

(a) $\alpha = 8$ to 16 deg, SR = 76 cm (30 in).

Figure A17.-Effect of rotation rate and angle of attack on side-force coefficient for basic configuration. $\delta_e = 15^\circ$, $\delta_a = 0^\circ$, $\delta_r = -25^\circ$, $\beta = 0^\circ$.

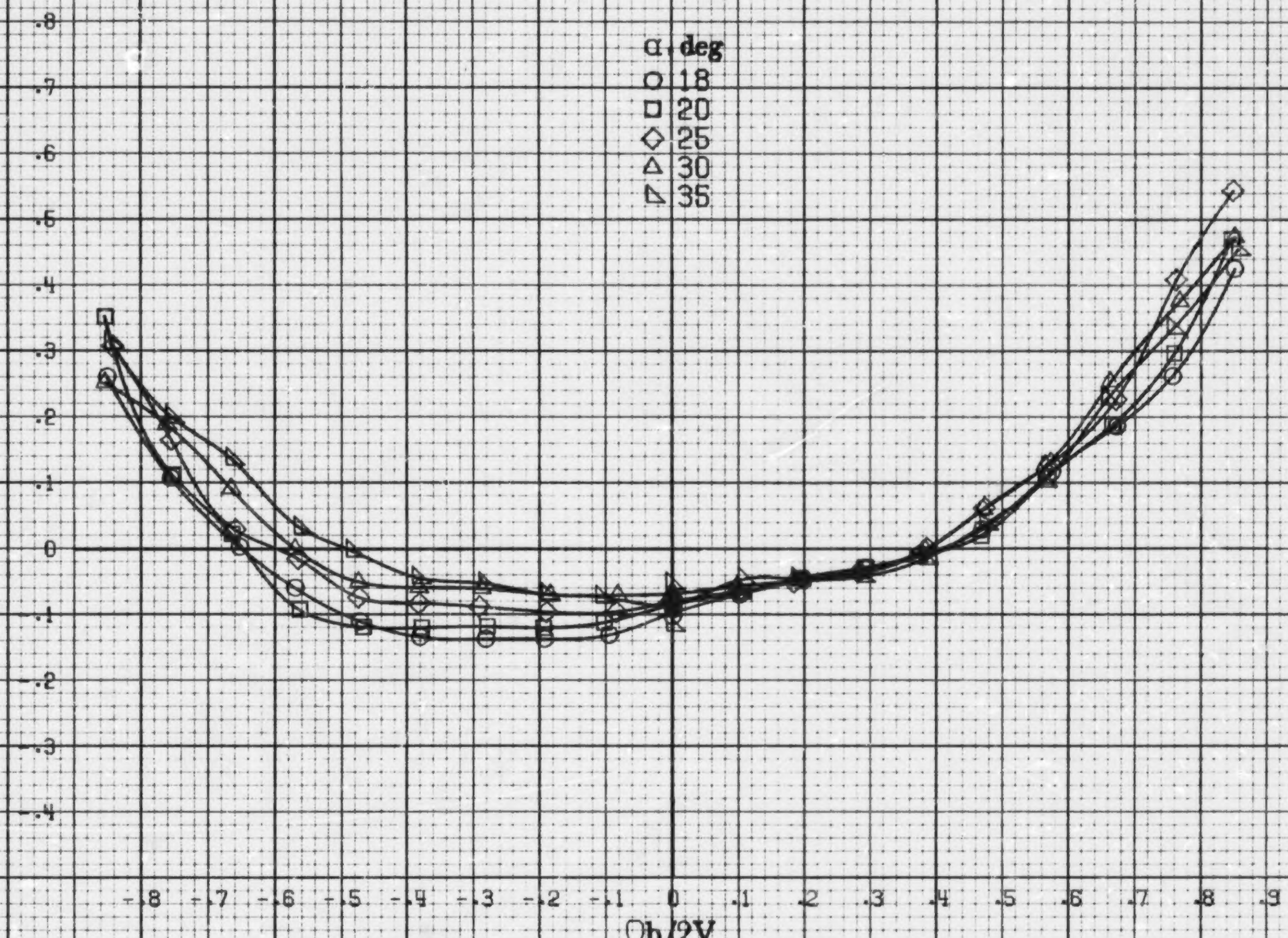

(b) α = 18 to 35 deg, SR = 76 cm (30 in).

Figure A17.-Continued.

A68

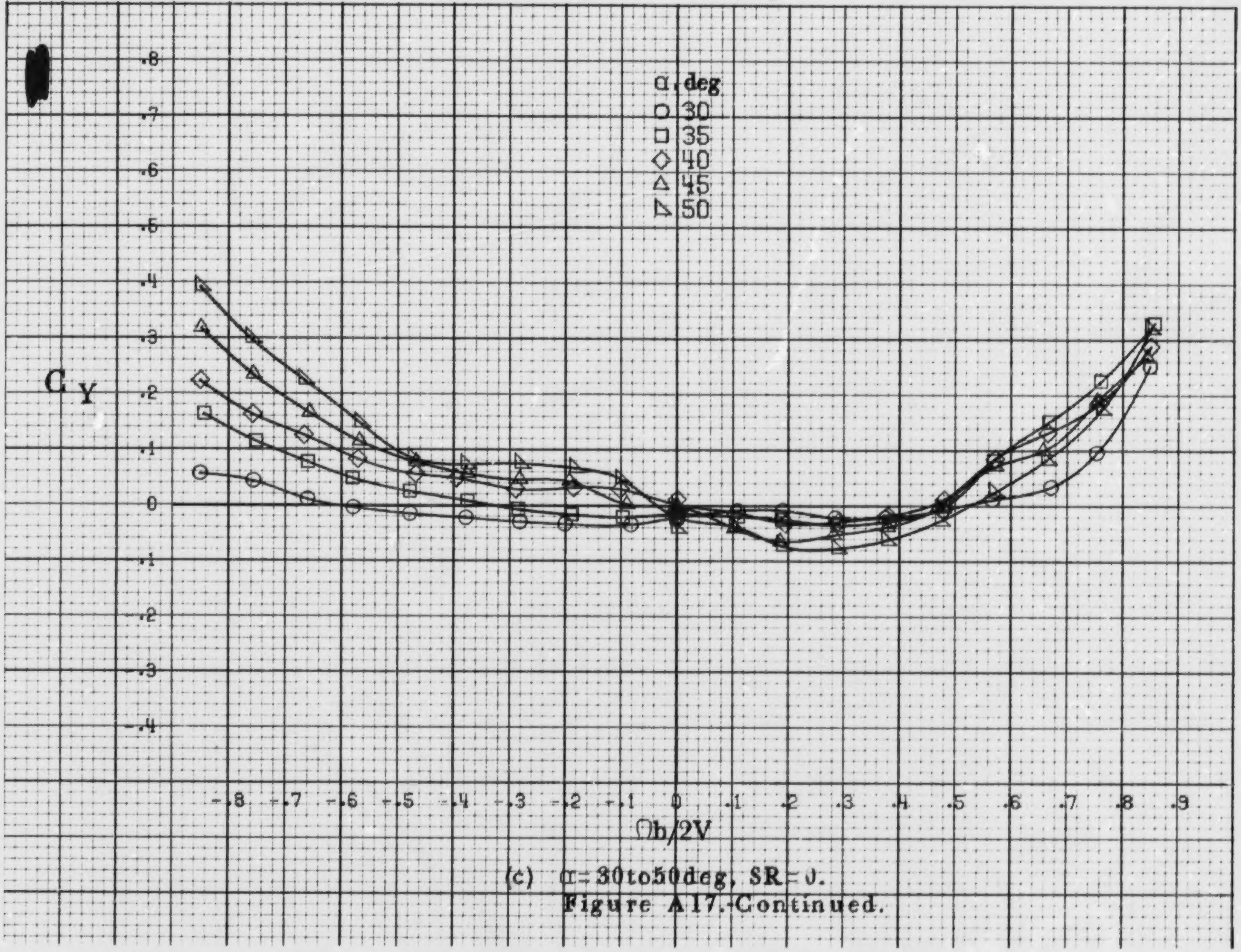

(c) α = 30 to 50 deg, SR = 0.

Figure A17.-Continued.

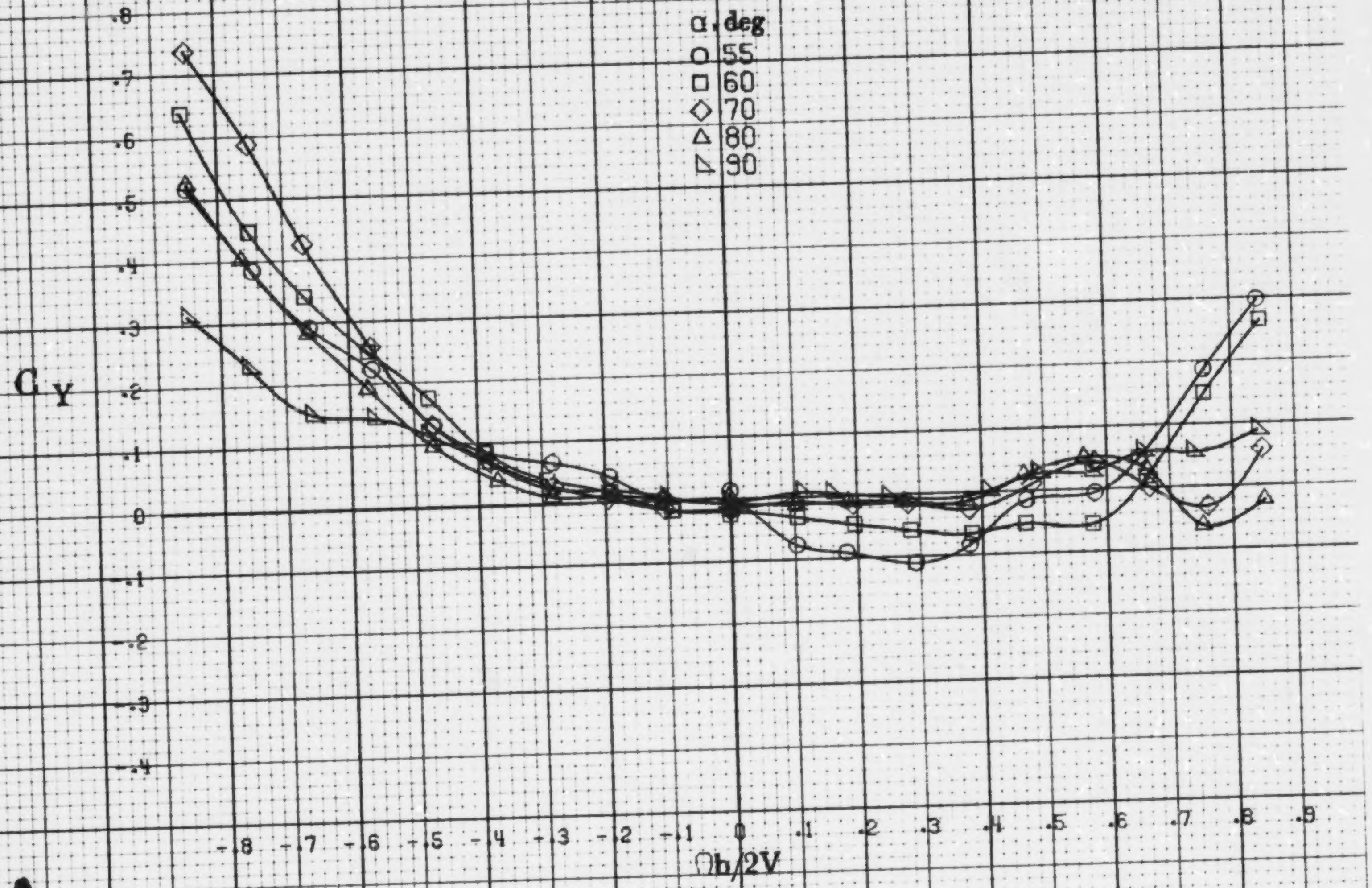

(d) α = 55 to 90 deg, SR = 0.

Figure A17.- Concluded.

A69

A70

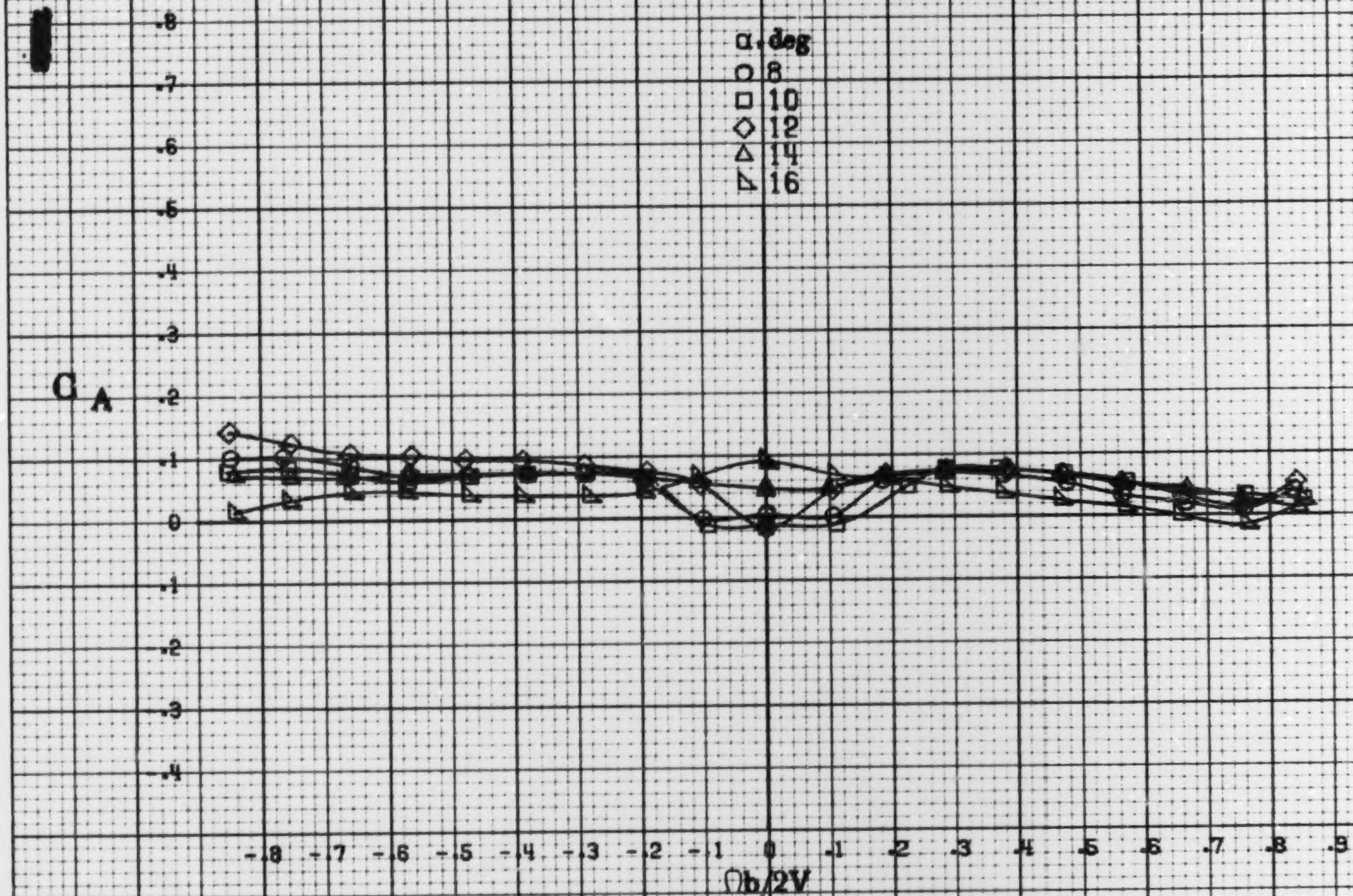

(a) α = 8 to 16 deg, SR = 76 cm (30 in).

Figure A18.- Effect of rotation rate and angle of attack on axial-force coefficient for basic configuration. $\delta_e = 15°$, $\delta_a = 0°$, $\delta_r = -25°$, $\beta = 0°$.

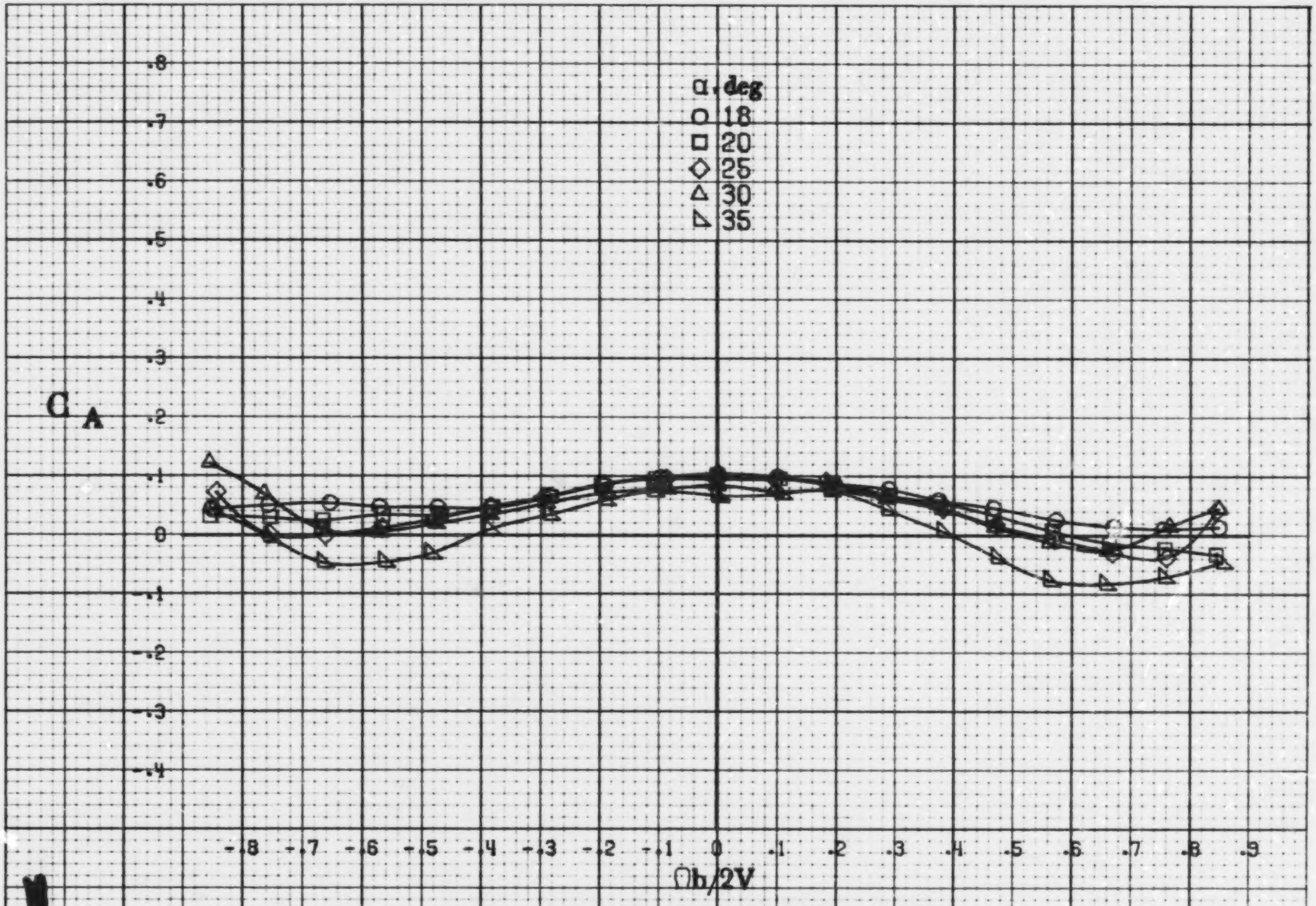

(b) α = 18 to 35 deg, SR = 76 cm (30 in).

Figure A18.-Continued.

A72

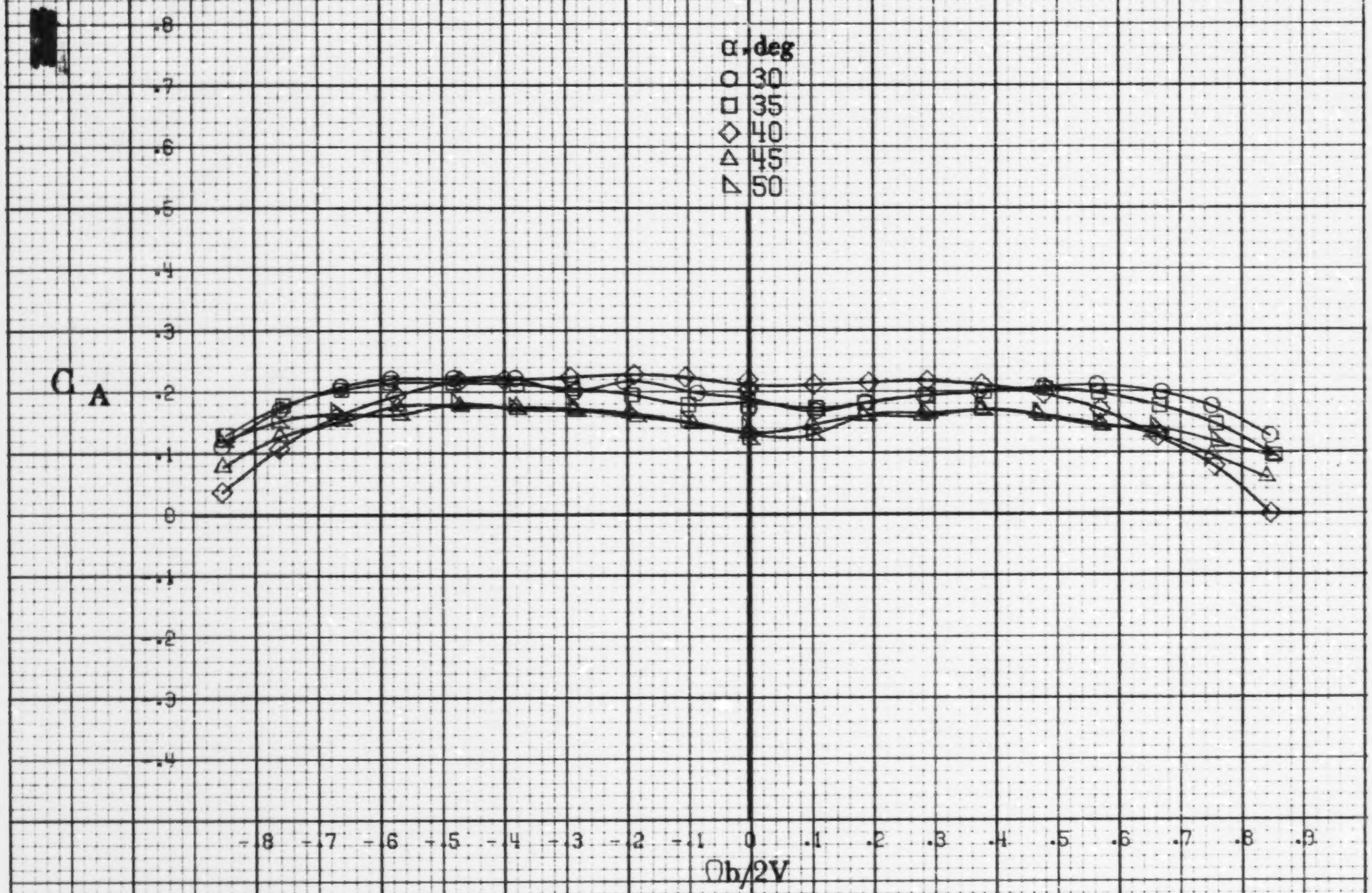

(c) α = 30 to 50 deg, SR = 0.

Figure A18.-Continued.

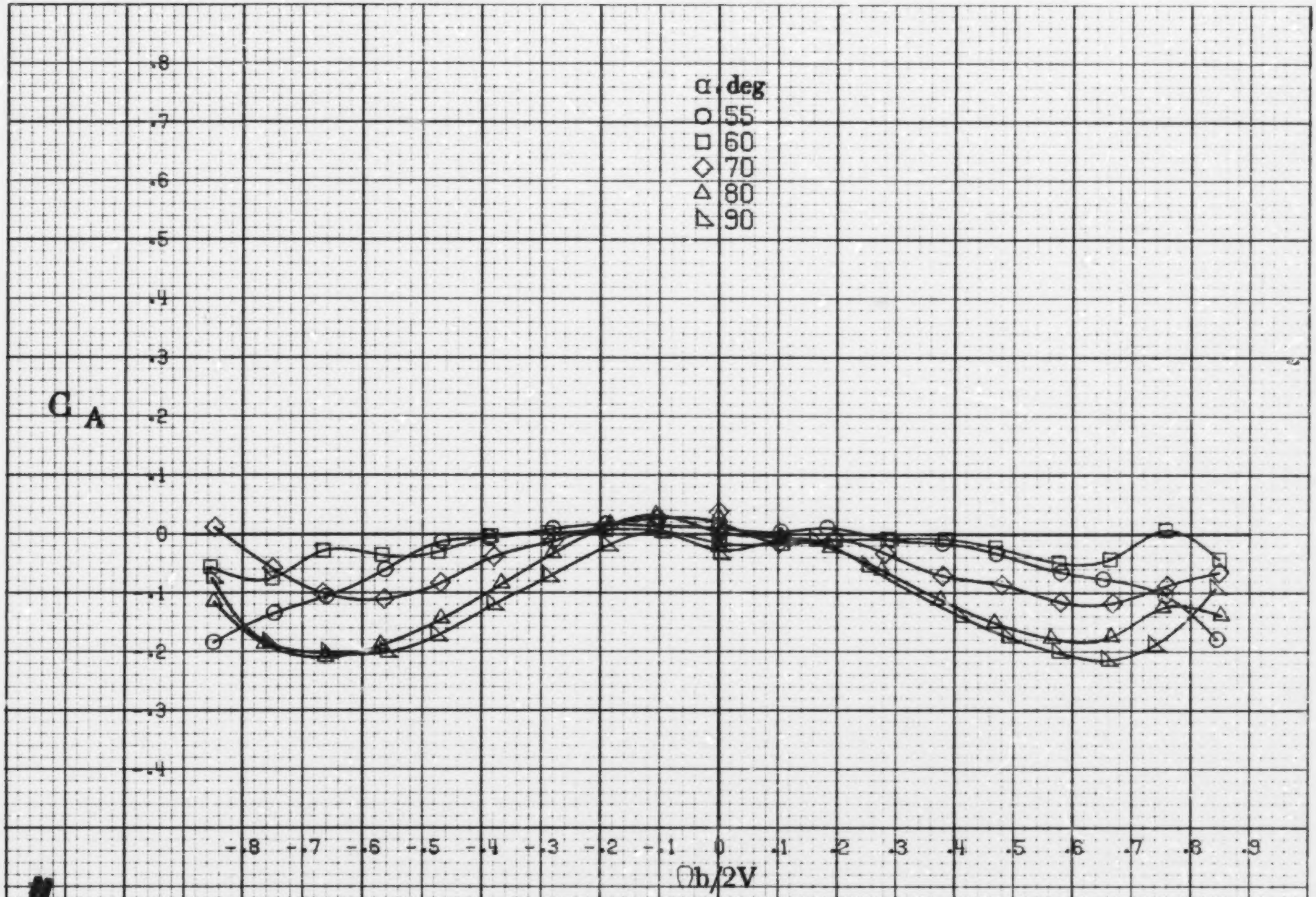

(d) α = 55 to 90 deg, SR = 0.

Figure A18.- Concluded.

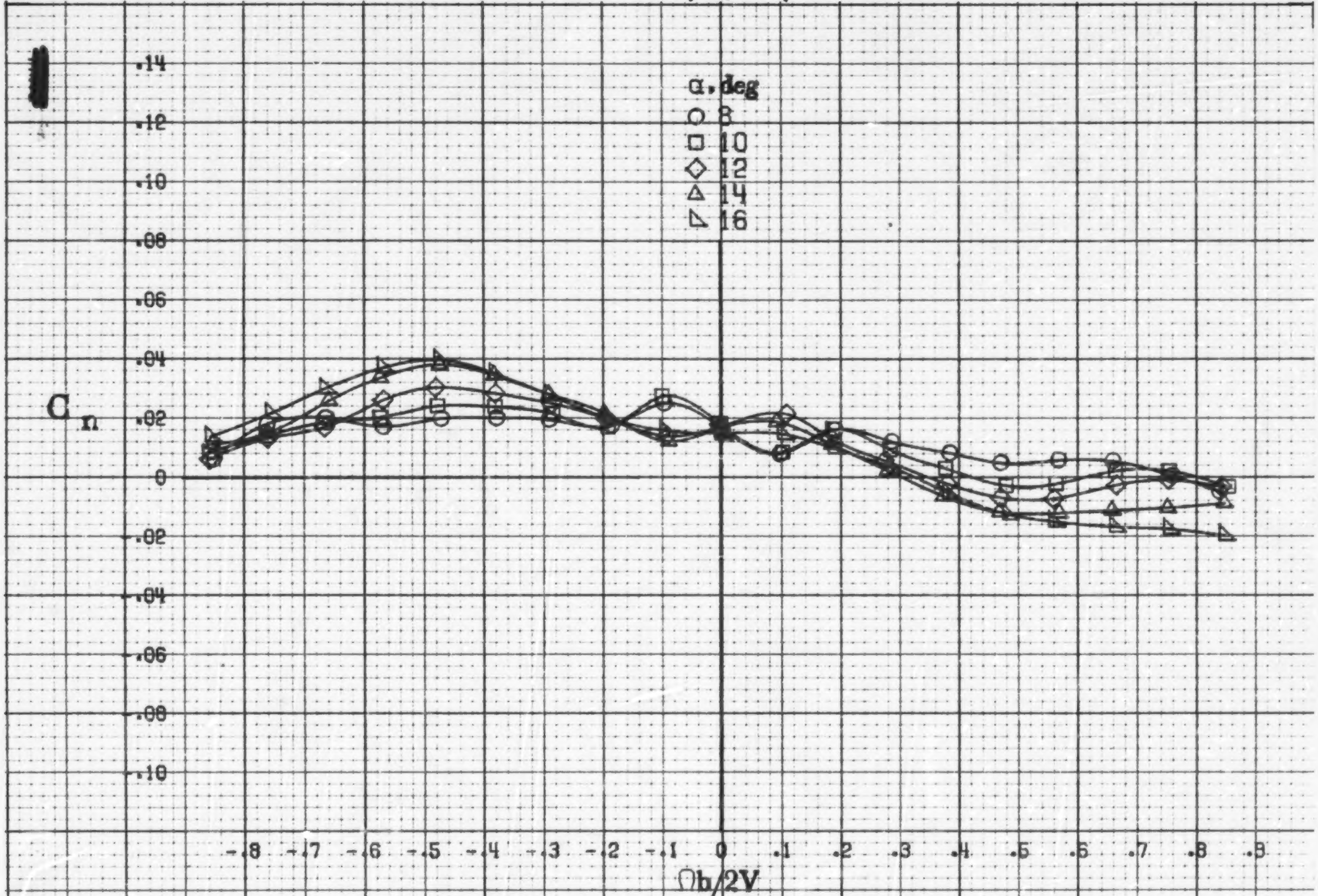

(a) α = 8 to 16 deg, SR = 76 cm (30 in).

Figure A19.-Effect of rotation rate and angle of attack on yawing-moment coefficient for basic configuration. δ_e = -15°, δ_a = 0°, δ_r = -25°, β = 0°.

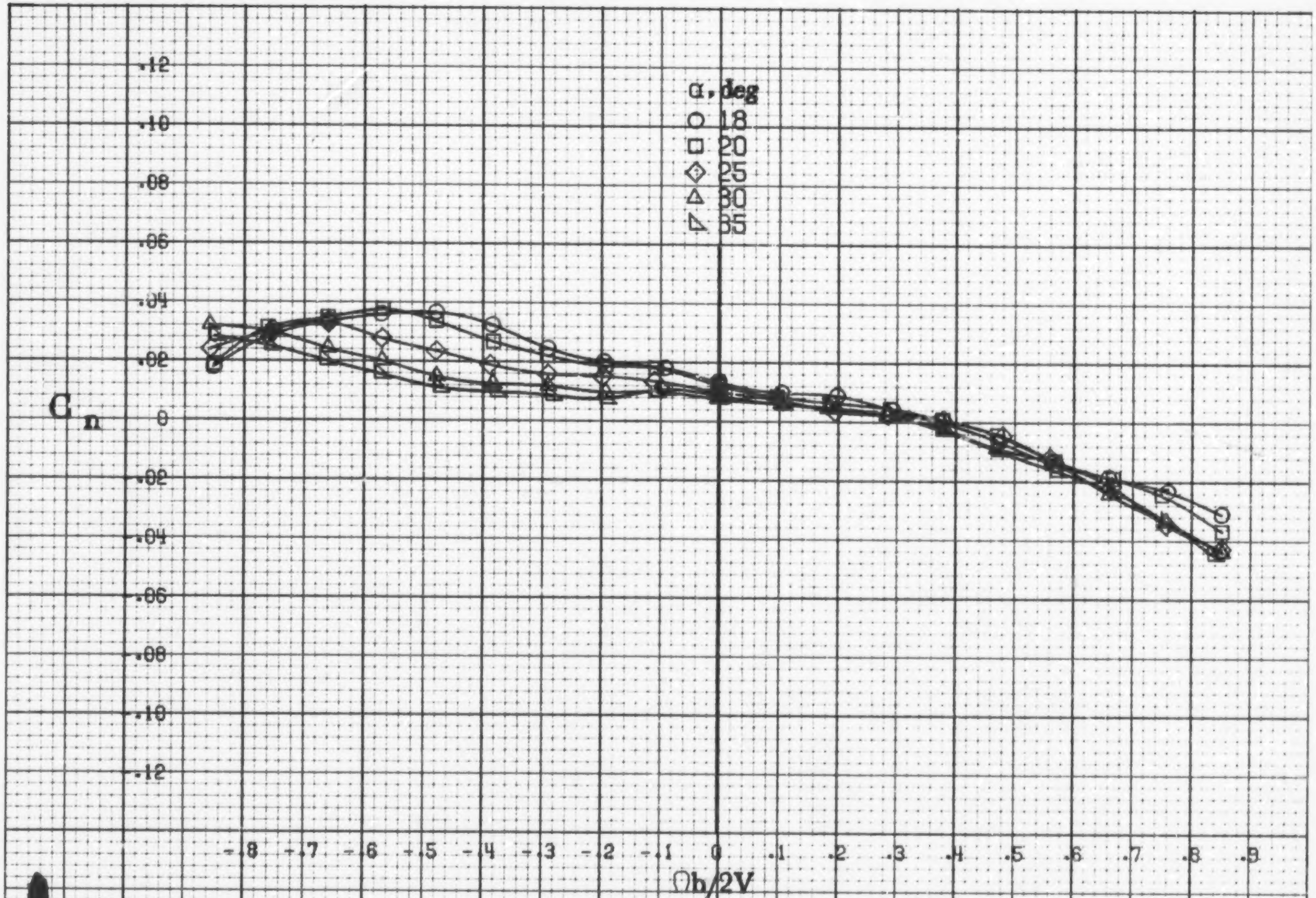

(h) $\alpha = 18$ to 35 deg, SR = 76 cm (30 in).

Figure A19.-Continued.

A76

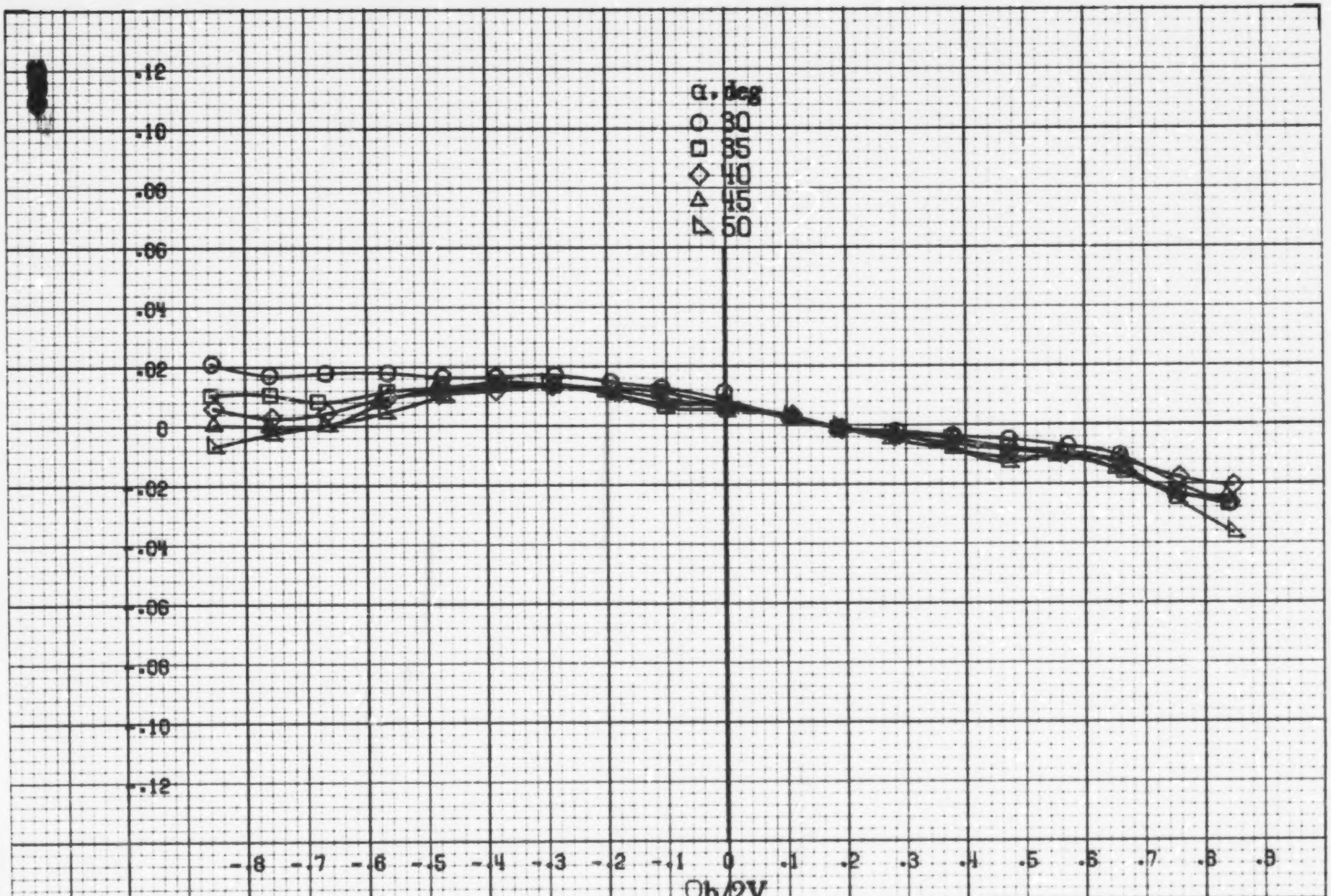

(c) α = 30 to 50 deg, SR = 0.

Figure A19.-Continued.

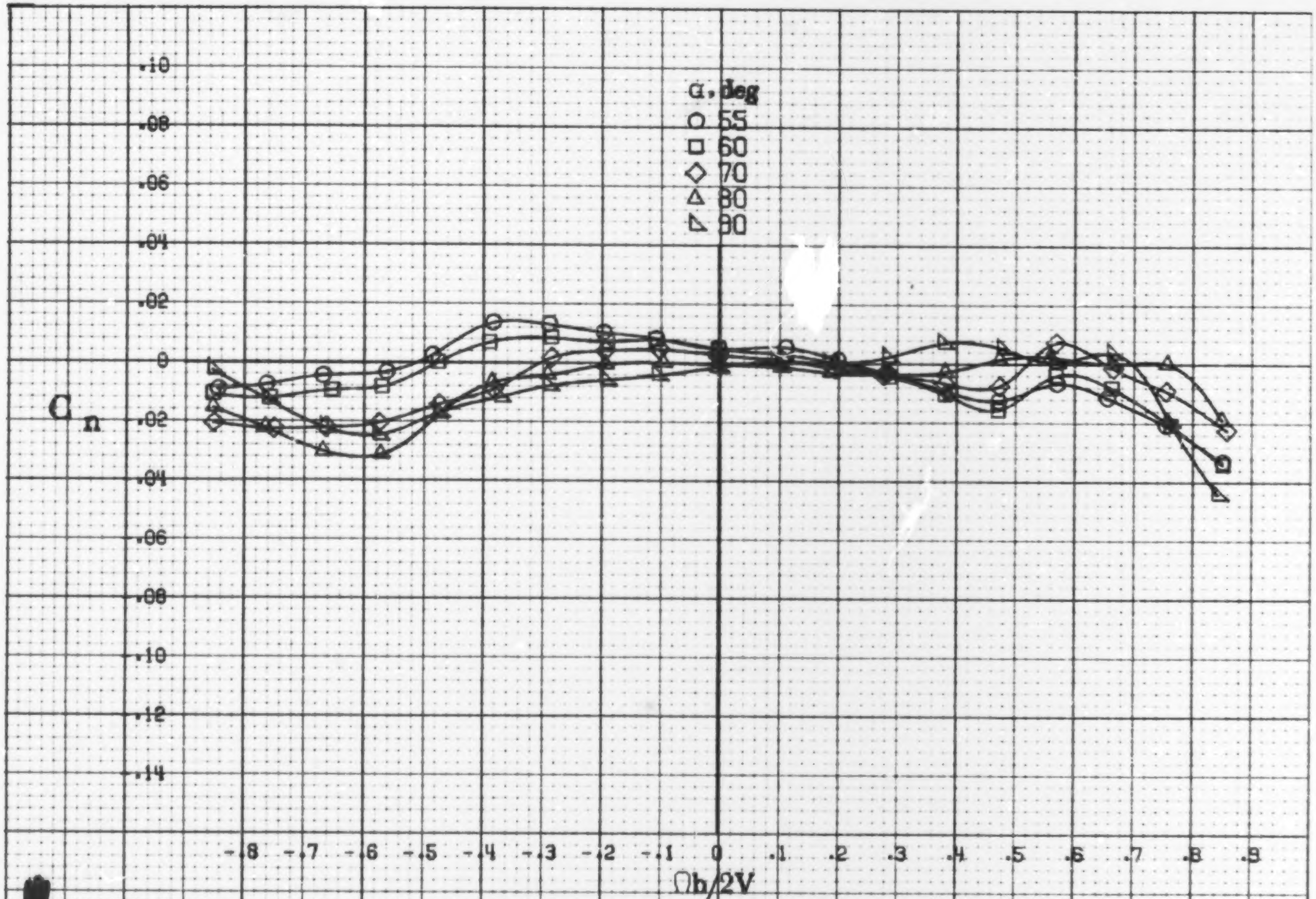

(d) α = 55 to 90 deg, SR = 0.

Figure A19.-Concluded.

A78

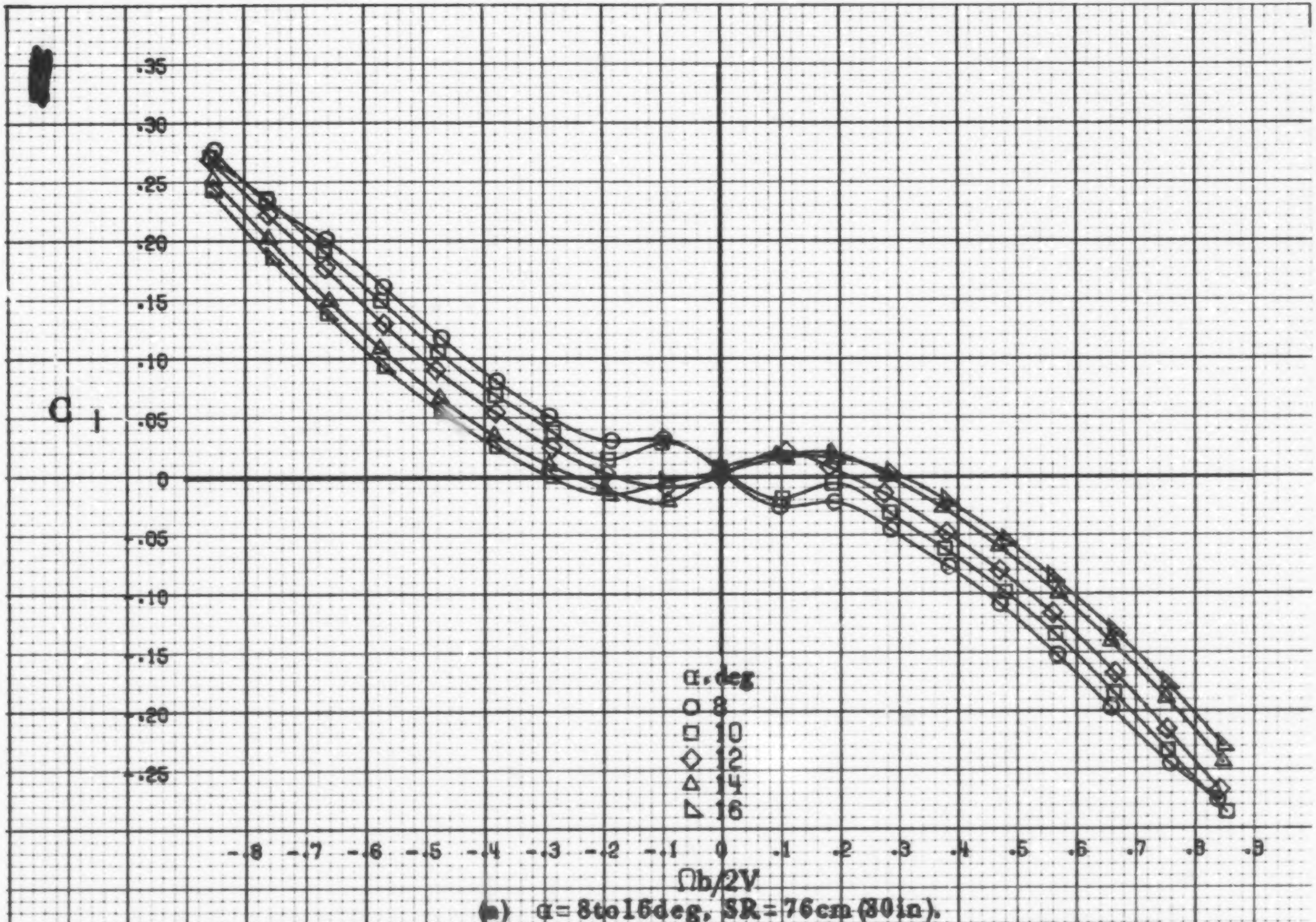

(a) $\alpha = 8$ to 16 deg, SR = 76 cm (30 in).

Figure A20.- Effect of rotation rate and angle of attack on rolling-moment coefficient for basic configuration. $\delta_e = -15°$, $\delta_a = 0°$, $\delta_r = -25°$, $\beta = 0°$.

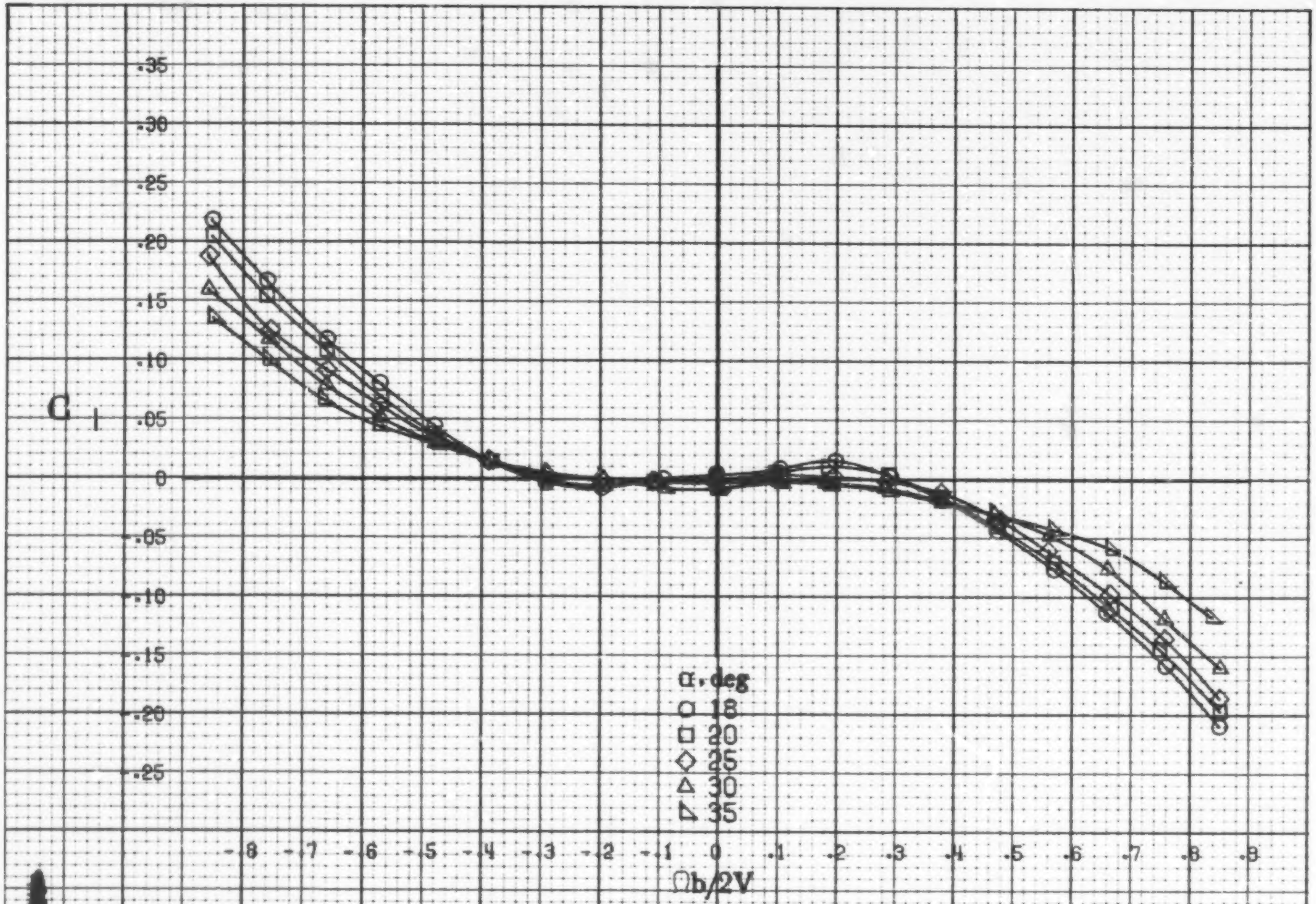

(b) α = 18 to 35 deg. SR = 76 cm (30 in).
Figure A20.-Continued.

A80

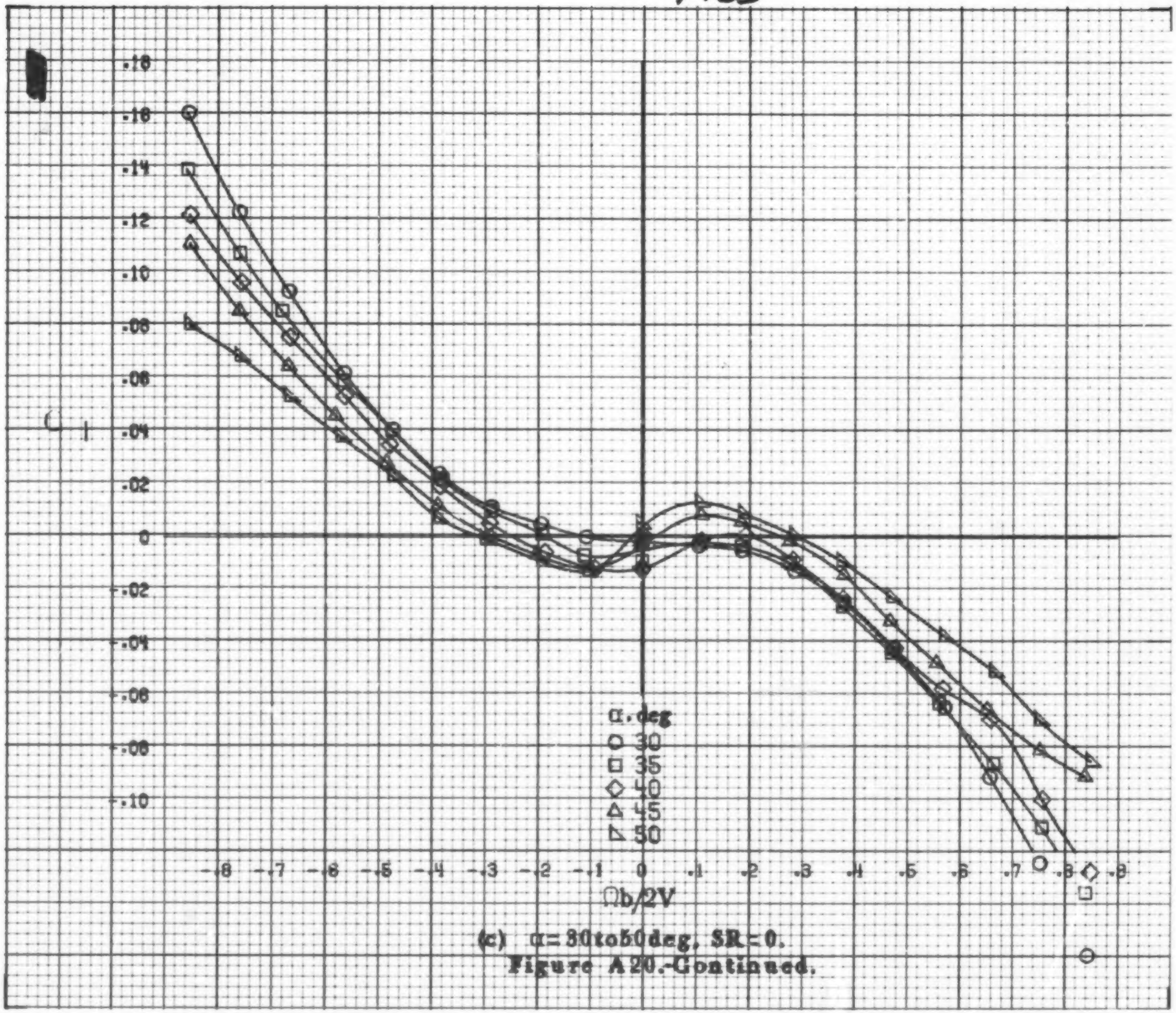

(c) α = 30 to 50 deg, SR = 0.

Figure A20.-Continued.

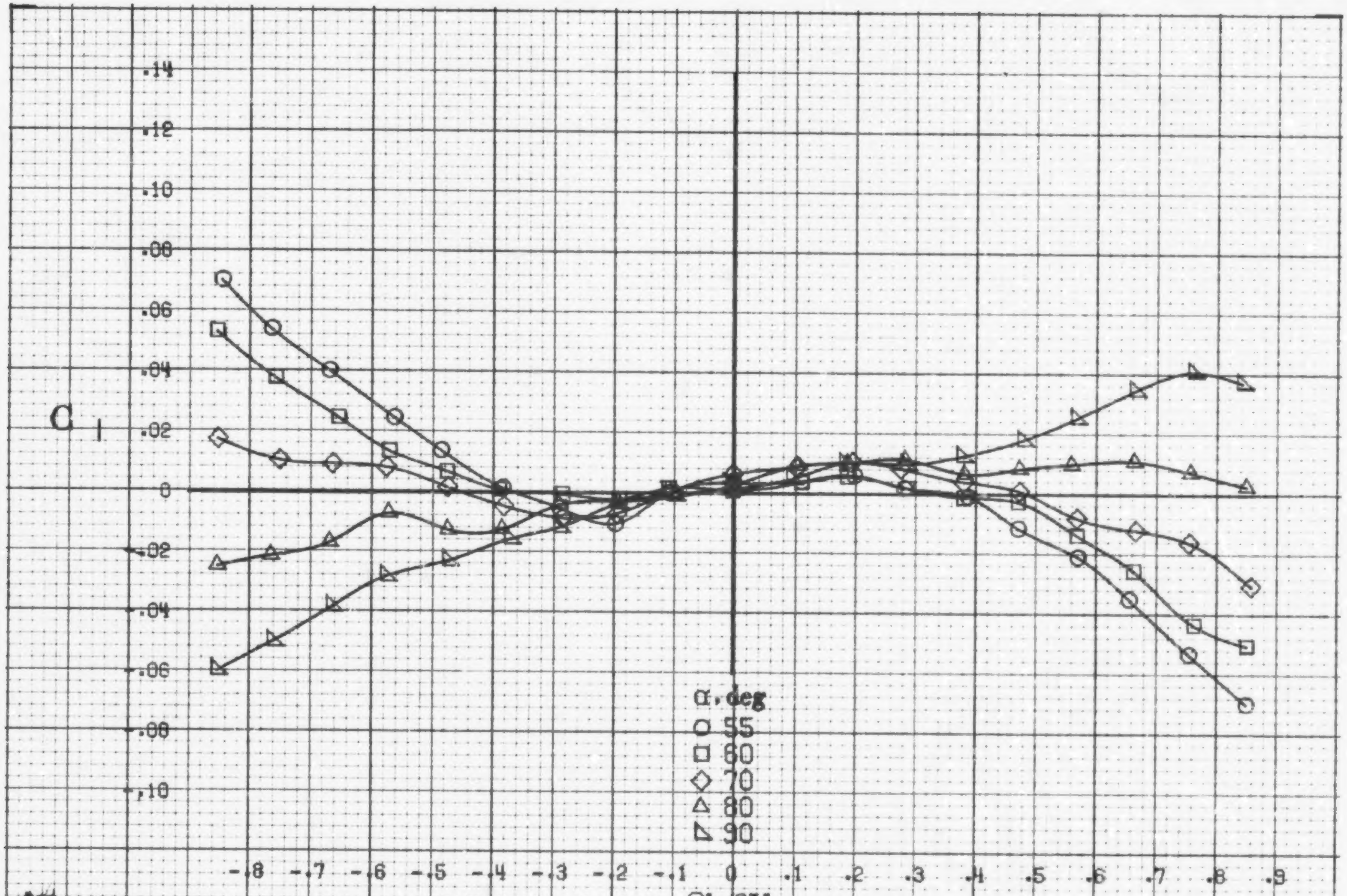

(d) α = 55 to 90 deg, SR = 0.

Figure A20.-Concluded.

A82

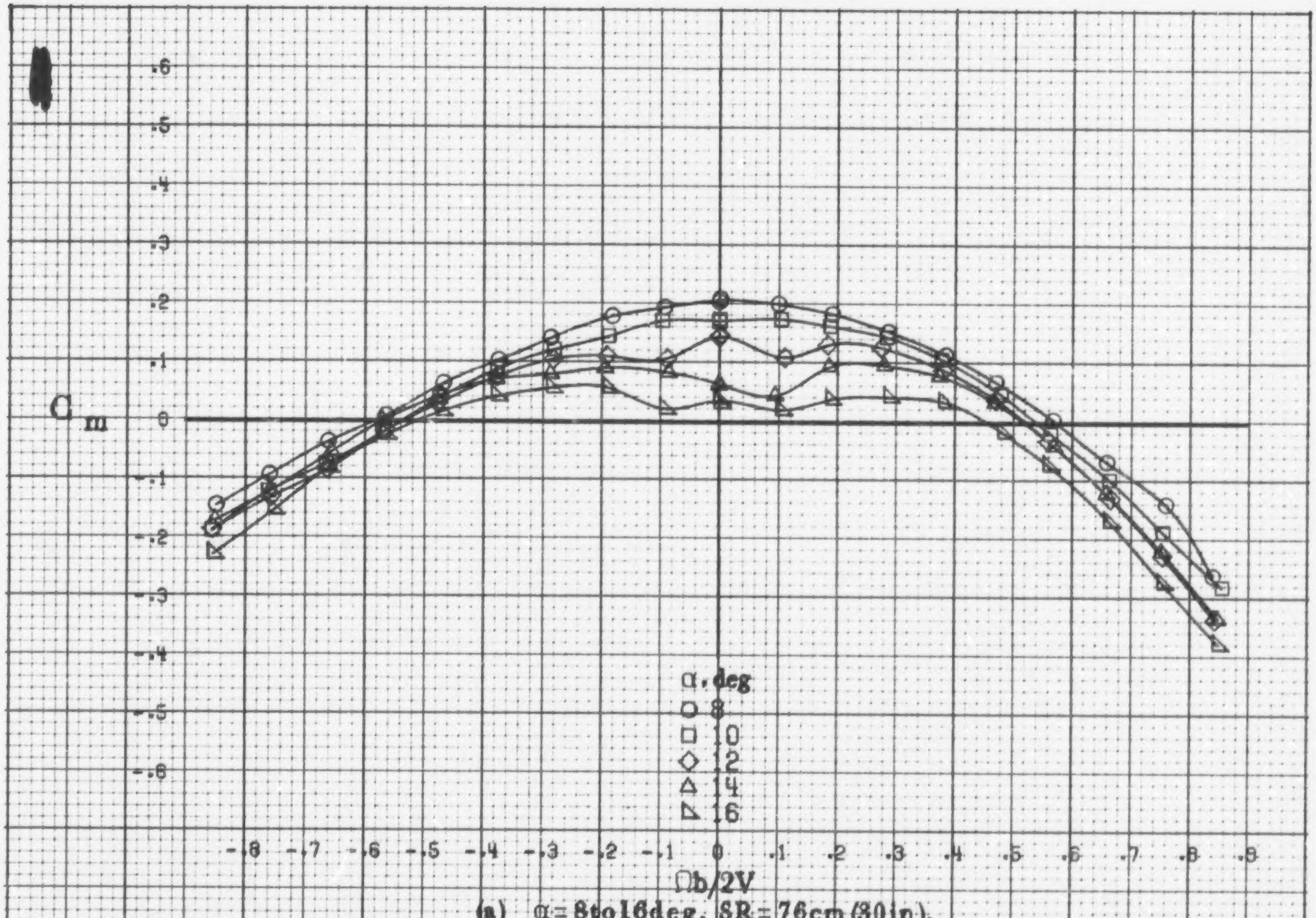

(a) $\alpha = 8$ to 16 deg, SR = 76 cm (30 in).

Figure A21.-Effect of rotation rate and angle of attack on pitching-moment coefficient for basic configuration. $\delta_e = -15°$, $\delta_a = 0°$, $\delta_r = -25°$, $\beta = 0°$.

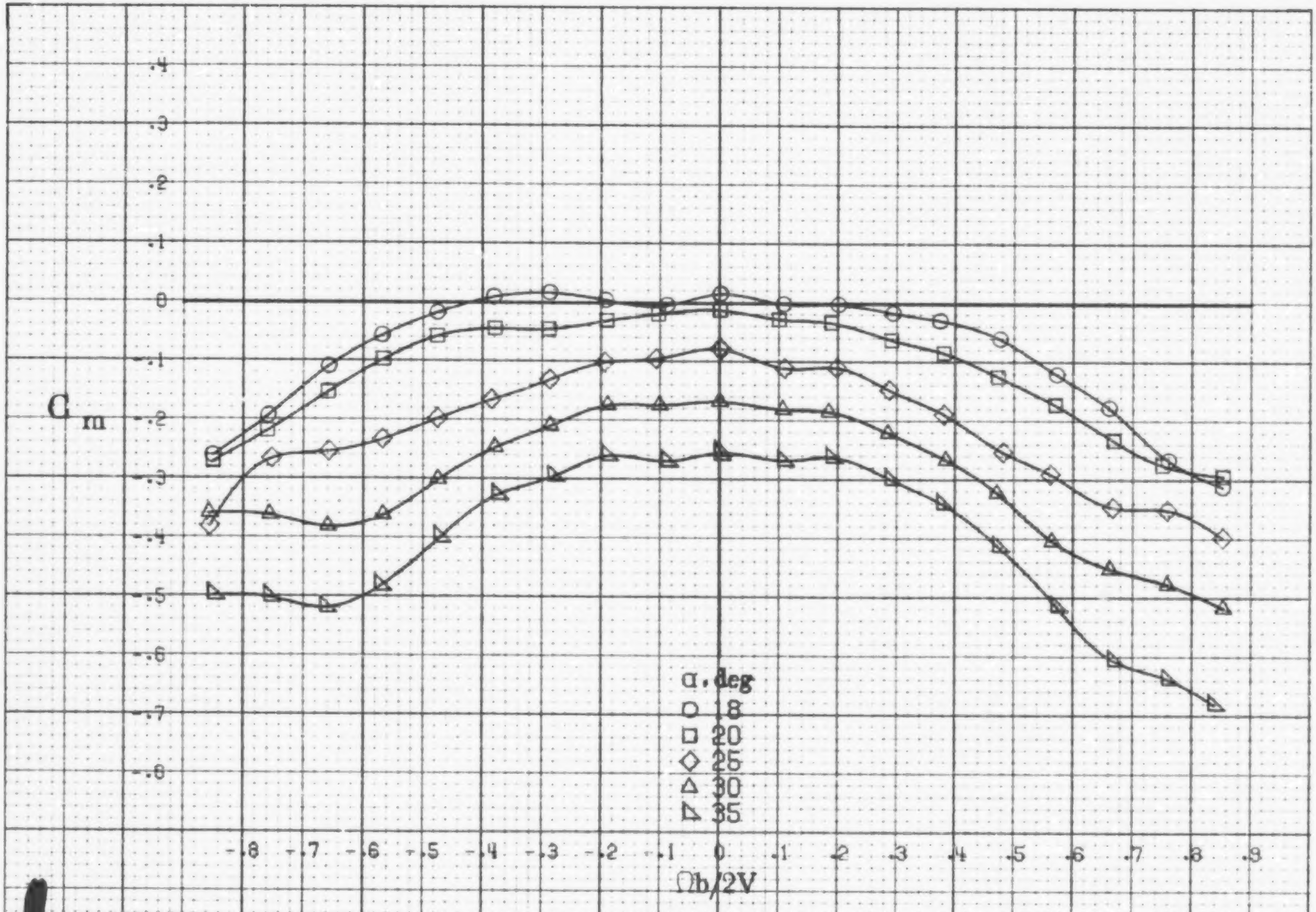

(b) α = 18 to 35 deg, SR = 76 cm (30 in).

Figure A21.-Continued.

A84

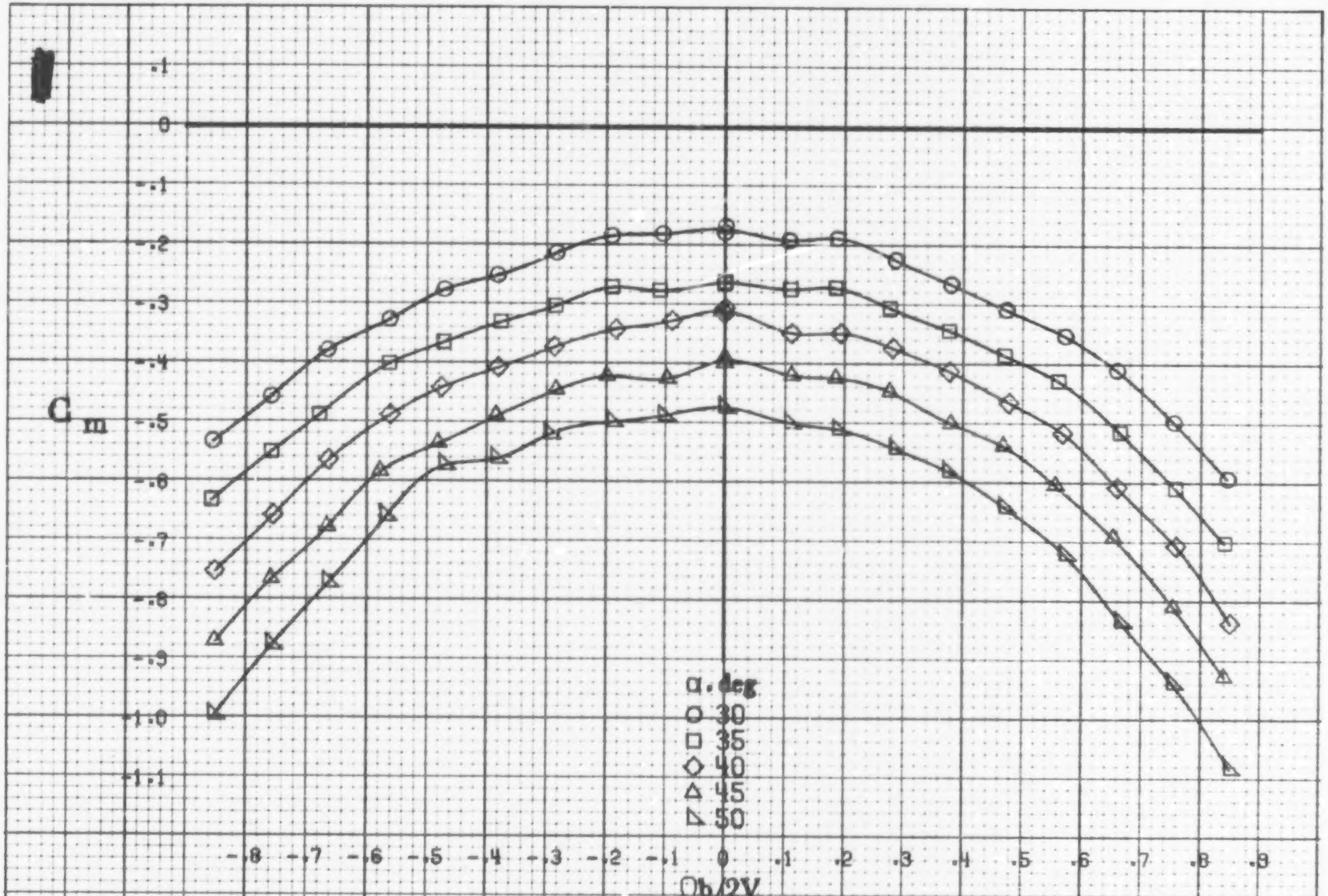

(c) α = 30 to 50 deg, SR = 0.

Figure A21.-Continued.

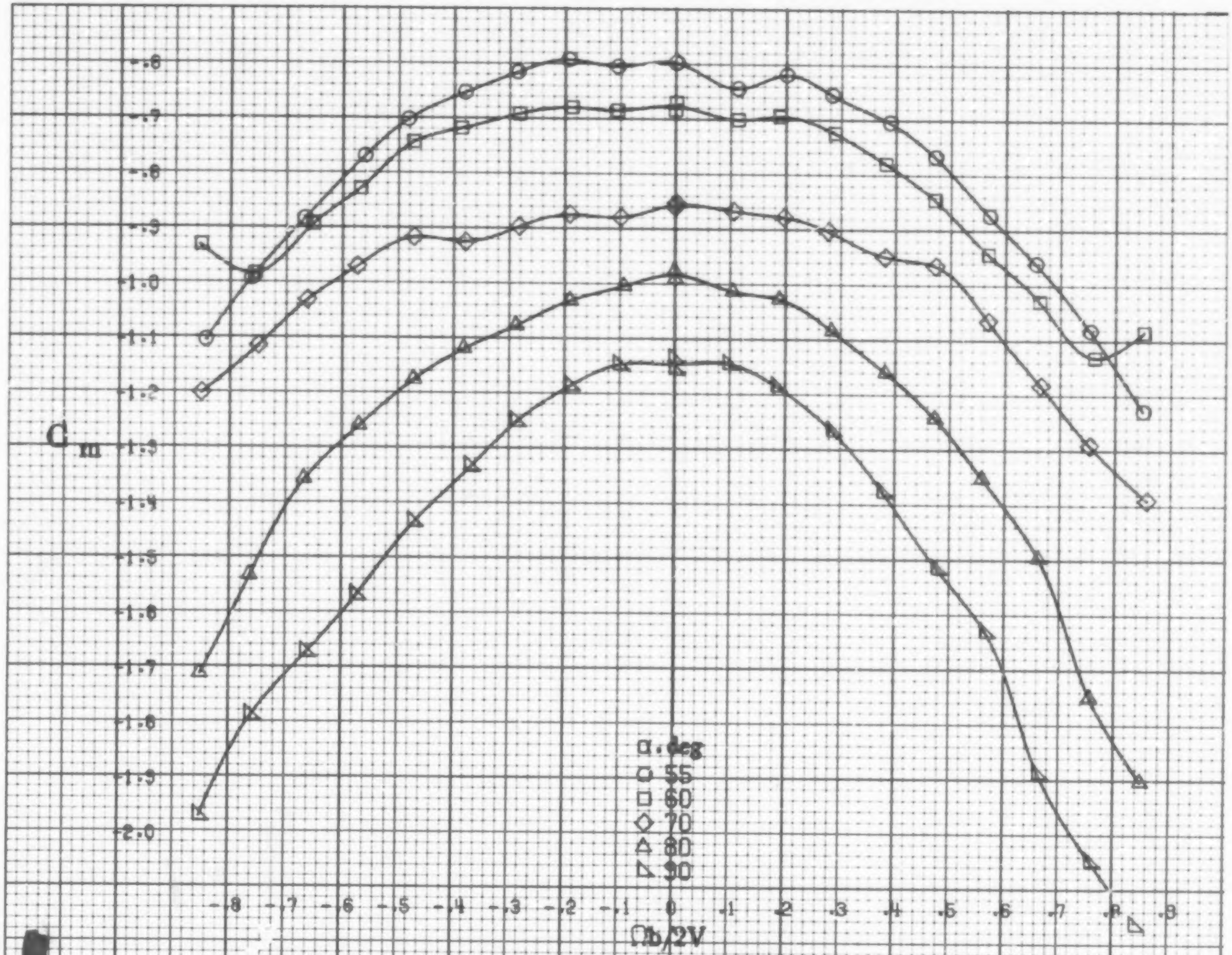

(d) α=55 to 90 deg. SR=0.

Figure A21.-Concluded.

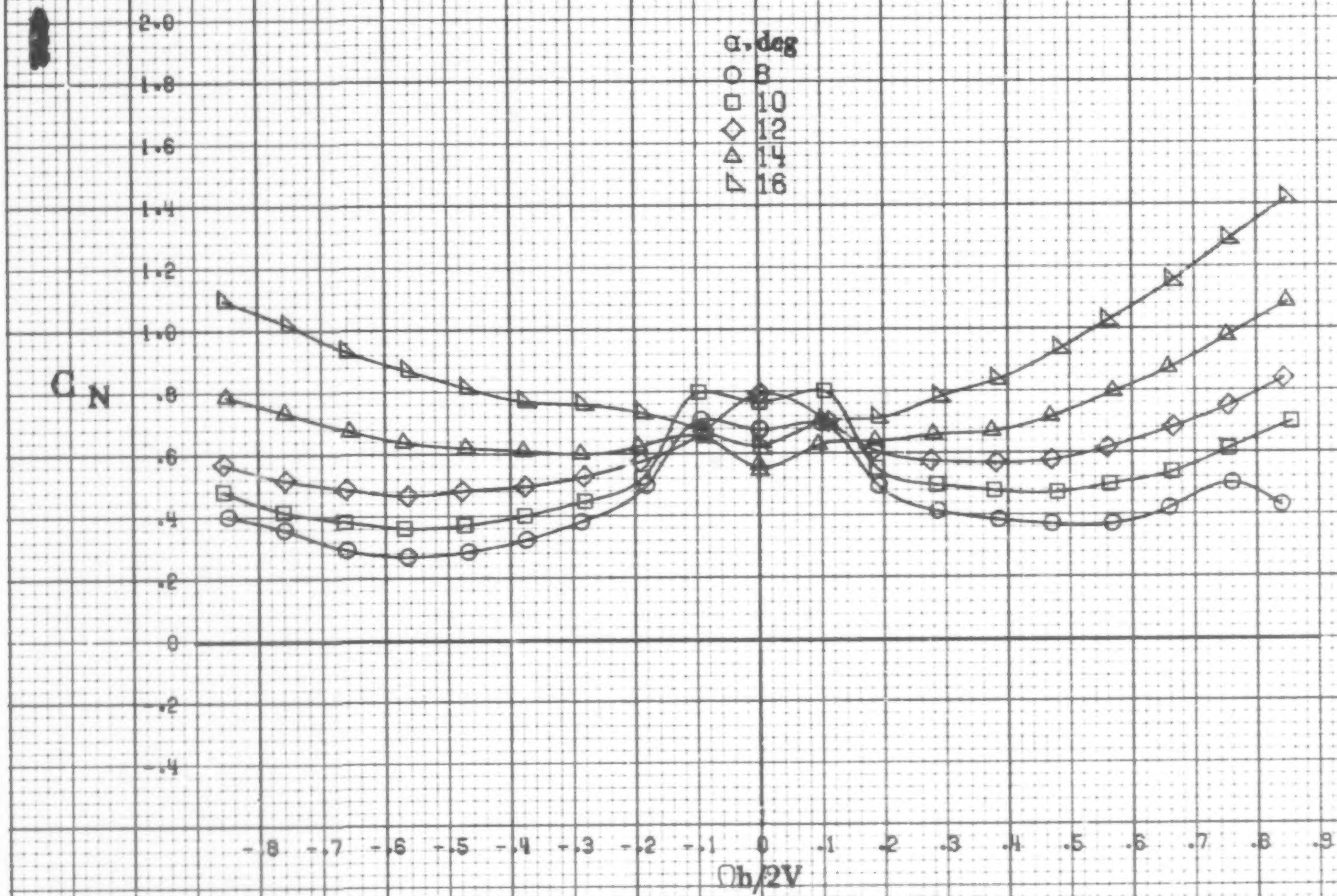

(a) $\alpha = 8$ to 16 deg, SR = 76 cm (30 in).

Figure A22.- Effect of rotation rate and angle of attack on normal-force coefficient for basic configuration. $\delta_e = -15^\circ$, $\delta_a = 0^\circ$, $\delta_r = 25^\circ$, $\beta = 0^\circ$.

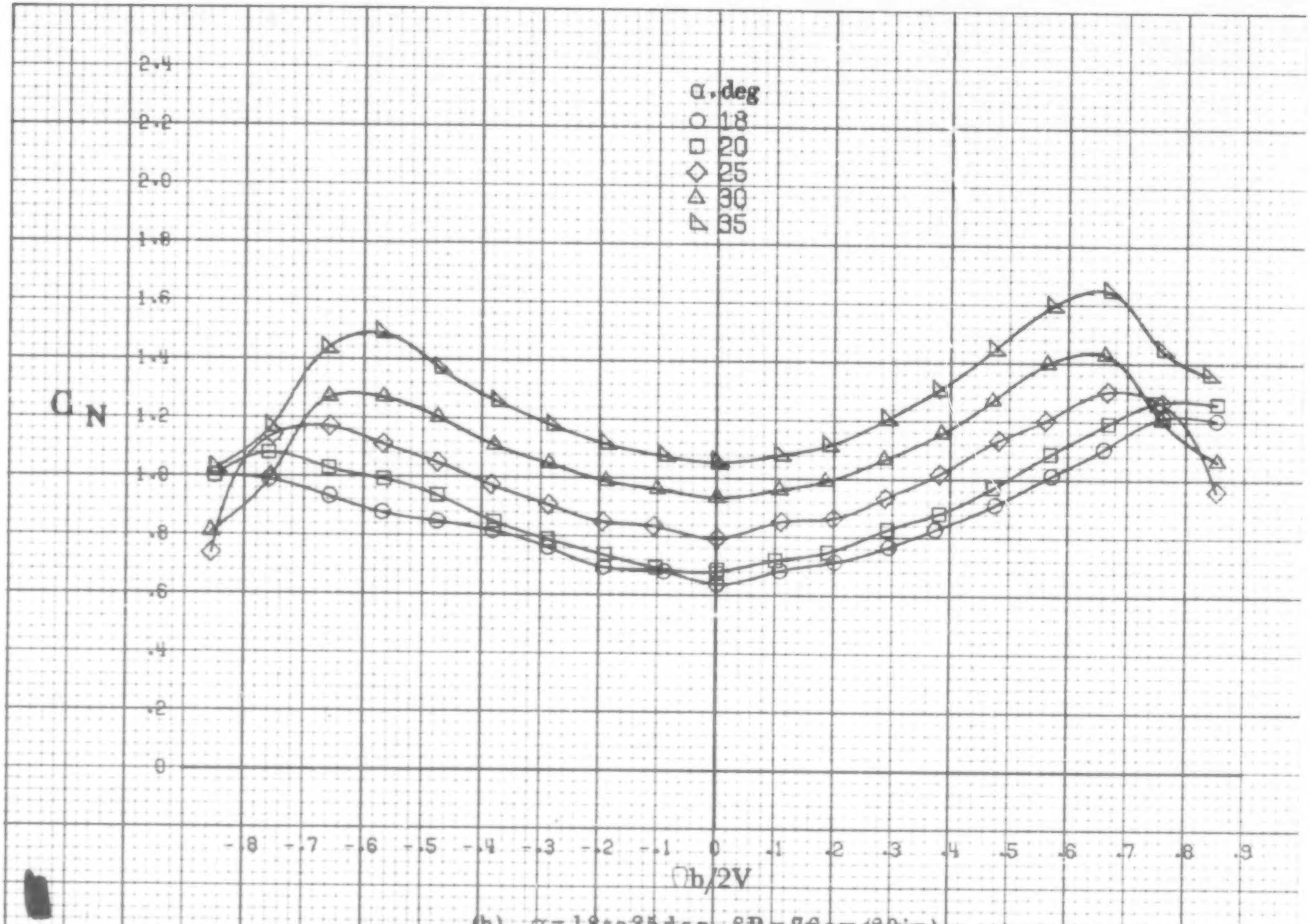

(b) α = 18 to 35 deg, SR = 76 cm (30 in).

Figure A22.-Continued.

A88

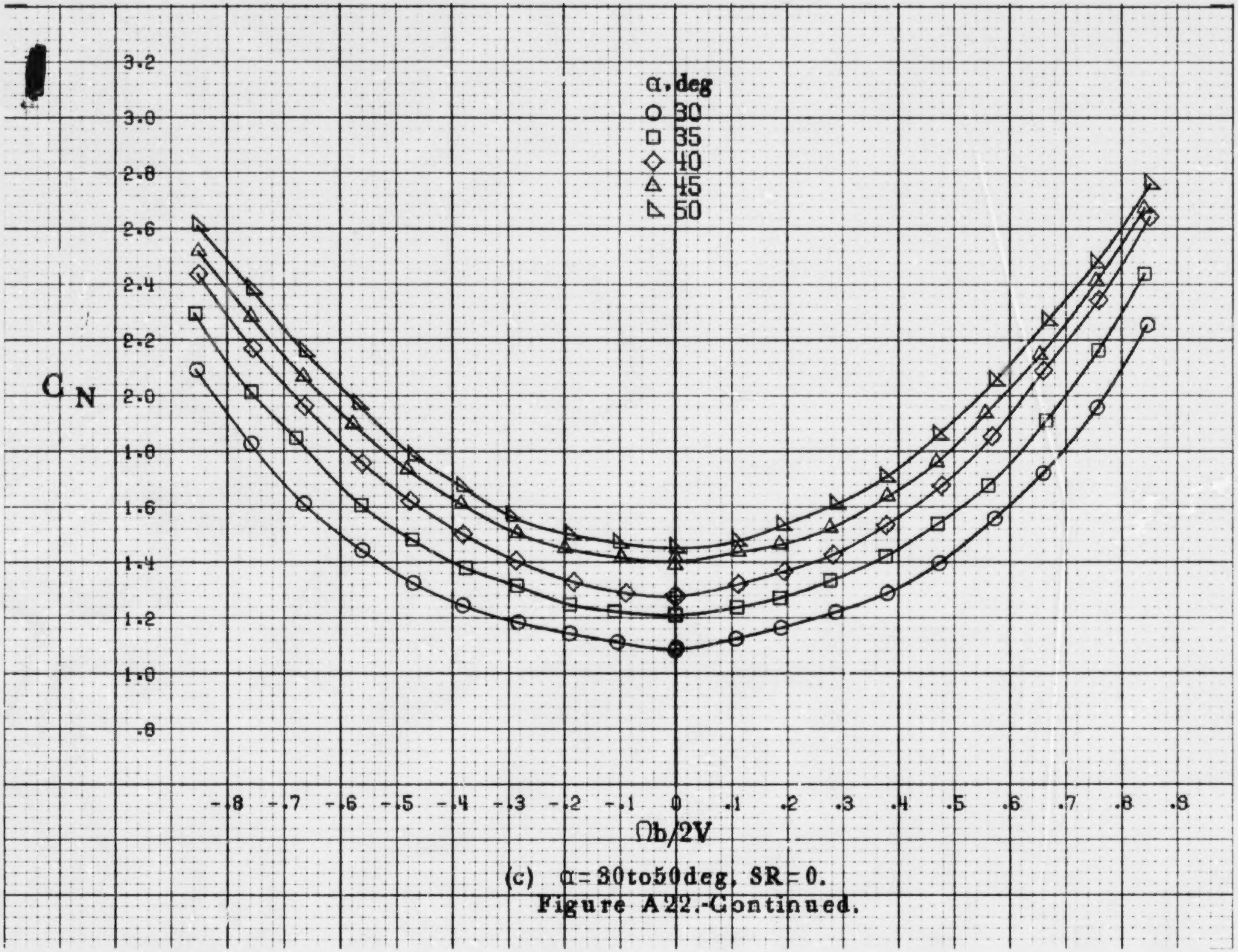

(c) α = 30 to 50 deg, SR = 0.
Figure A22.-Continued.

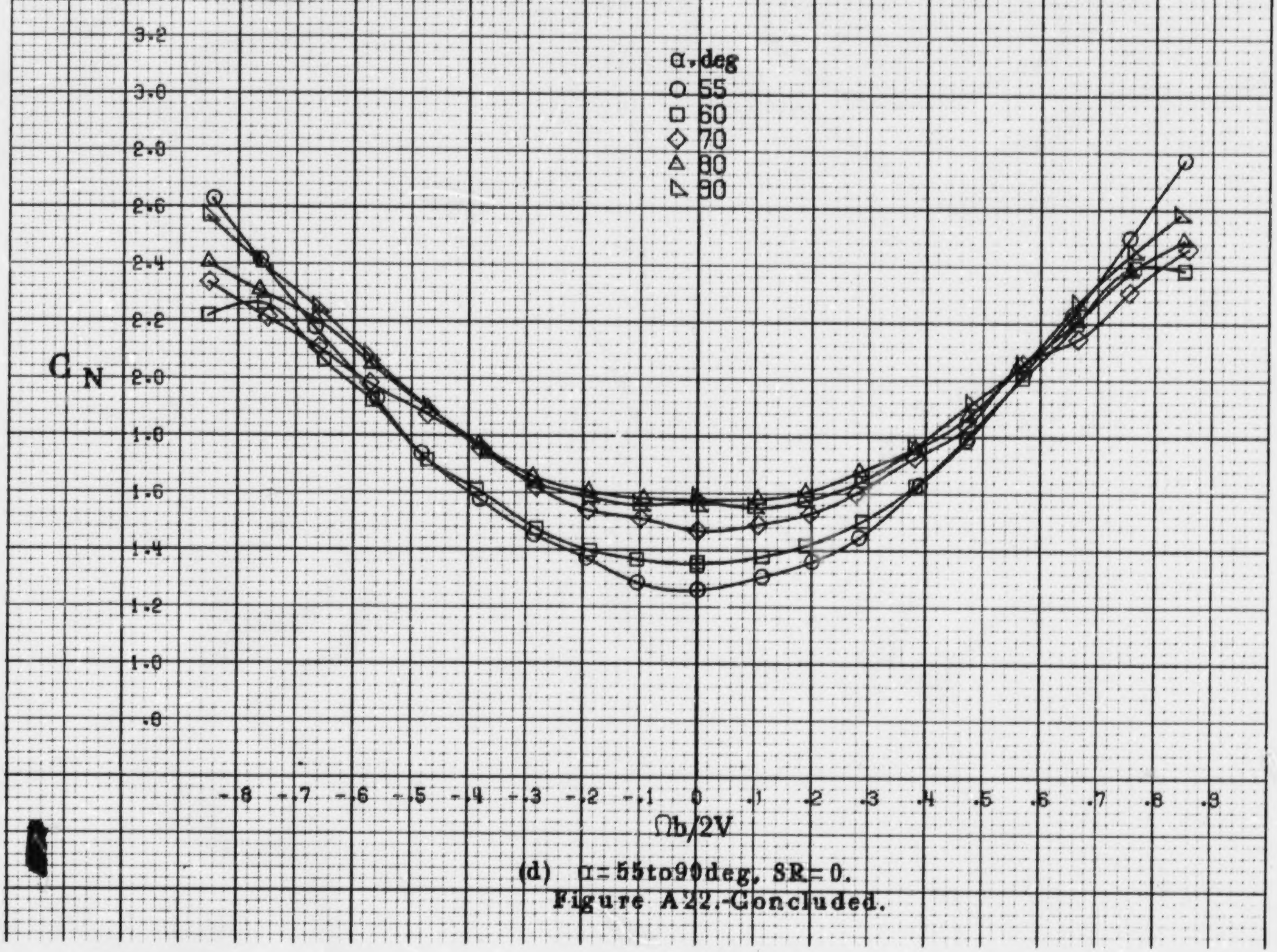

(d) α = 55 to 90 deg, SR = 0.

Figure A22.-Concluded.

A90

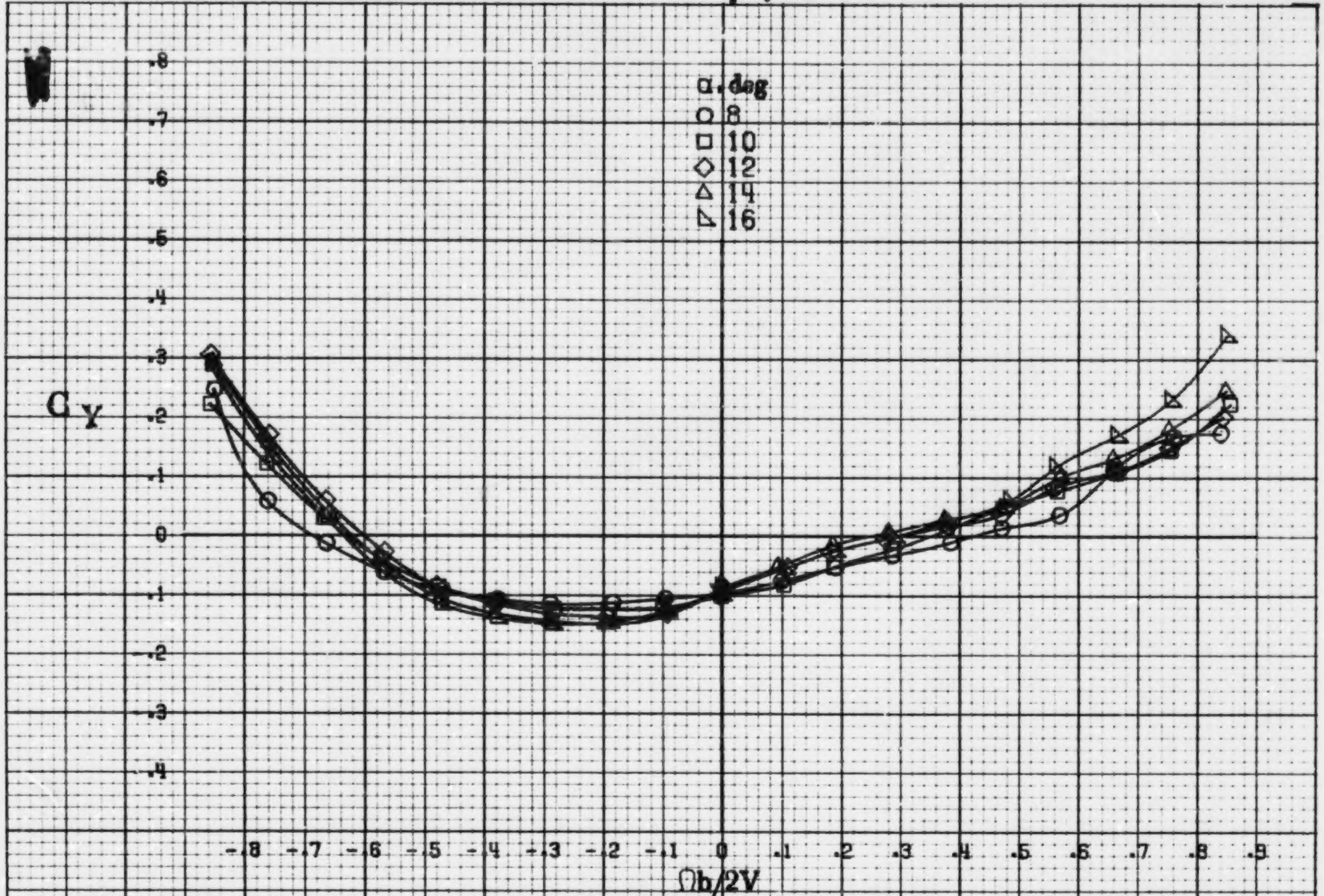

(a) α = 8 to 16 deg, SR = 76 cm (30 in).

Figure A23.- Effect of rotation rate and angle of attack on side-force coefficient for basic configuration. $\delta_e = -15°$, $\delta_a = 0°$, $\delta_r = 25°$, $\beta = 0°$.

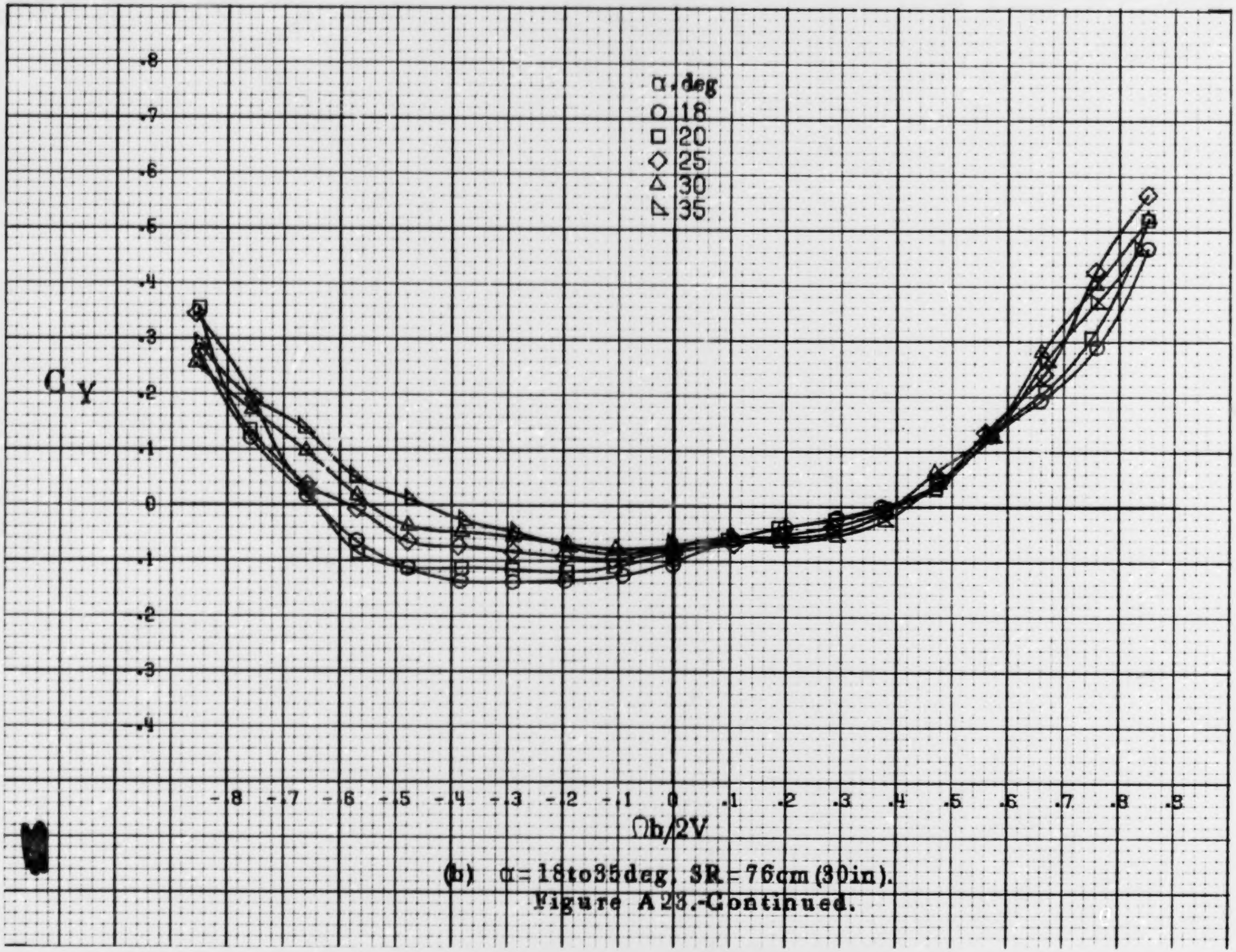

(b) α = 18 to 35 deg, SR = 76 cm (30 in).
Figure A28.-Continued.

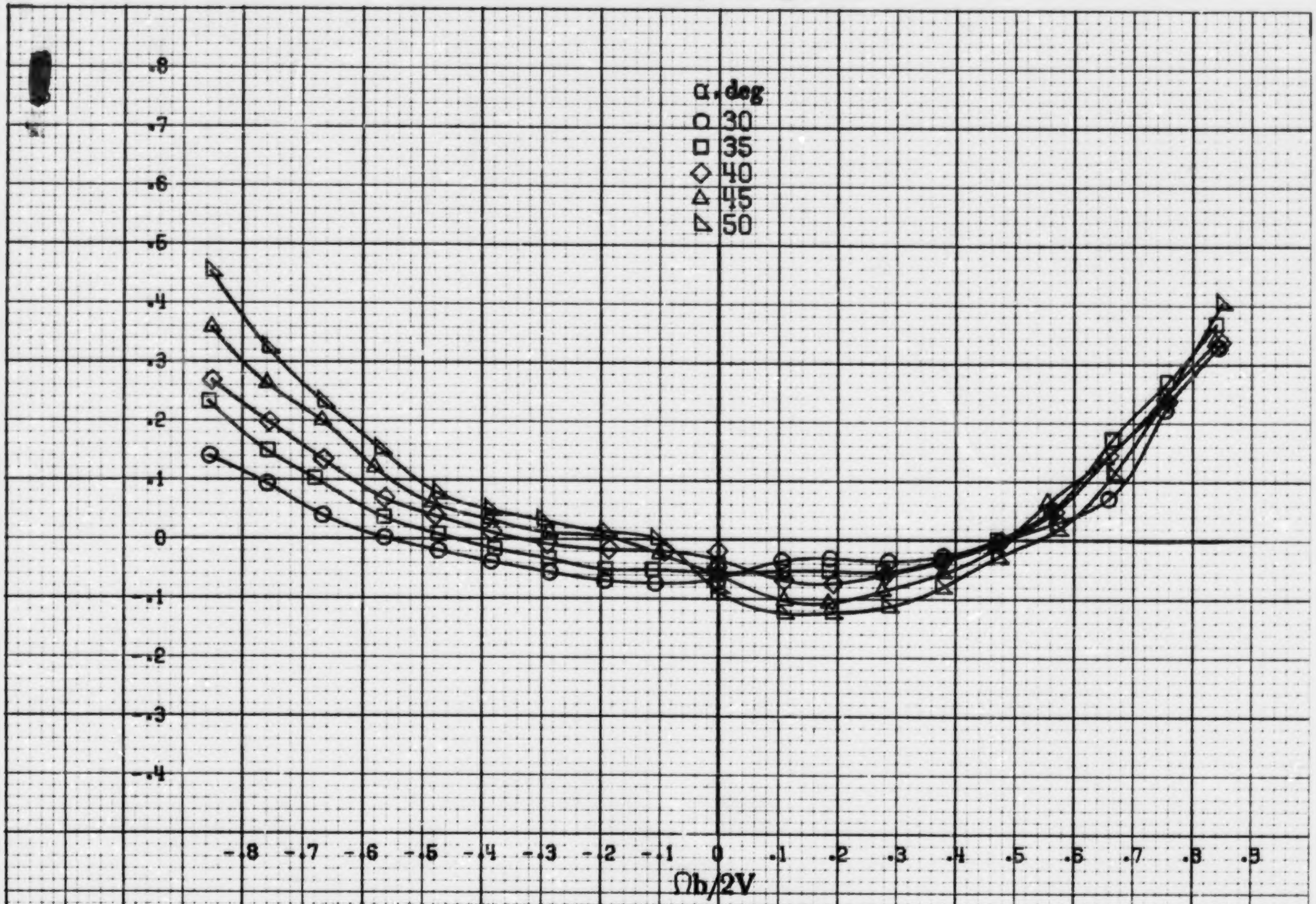

(c) α = 30 to 50 deg, SR = 0.

Figure A23.-Continued.

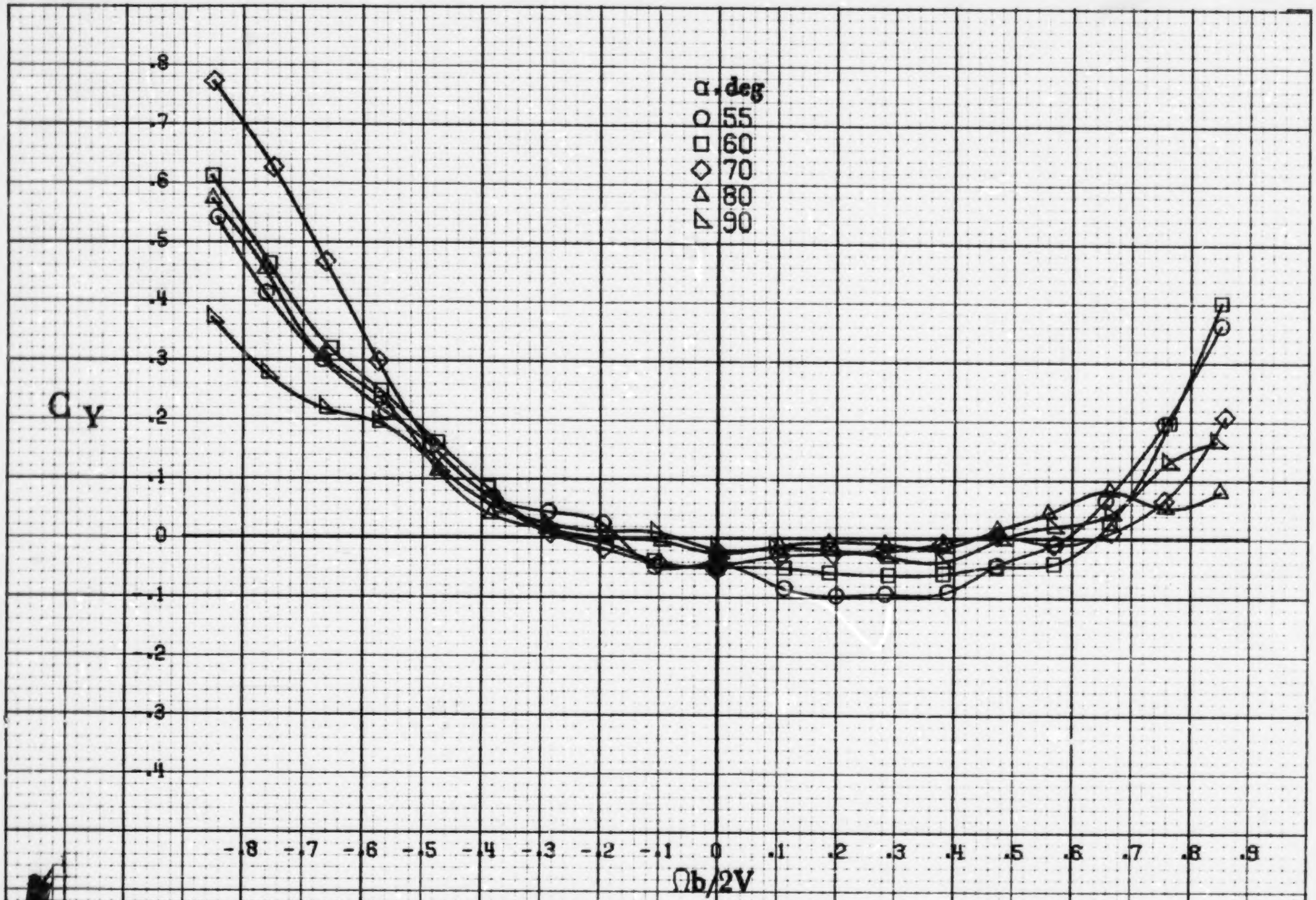

(d) α = 55 to 90 deg, SR = 0.

Figure A23.-Concluded.

A93

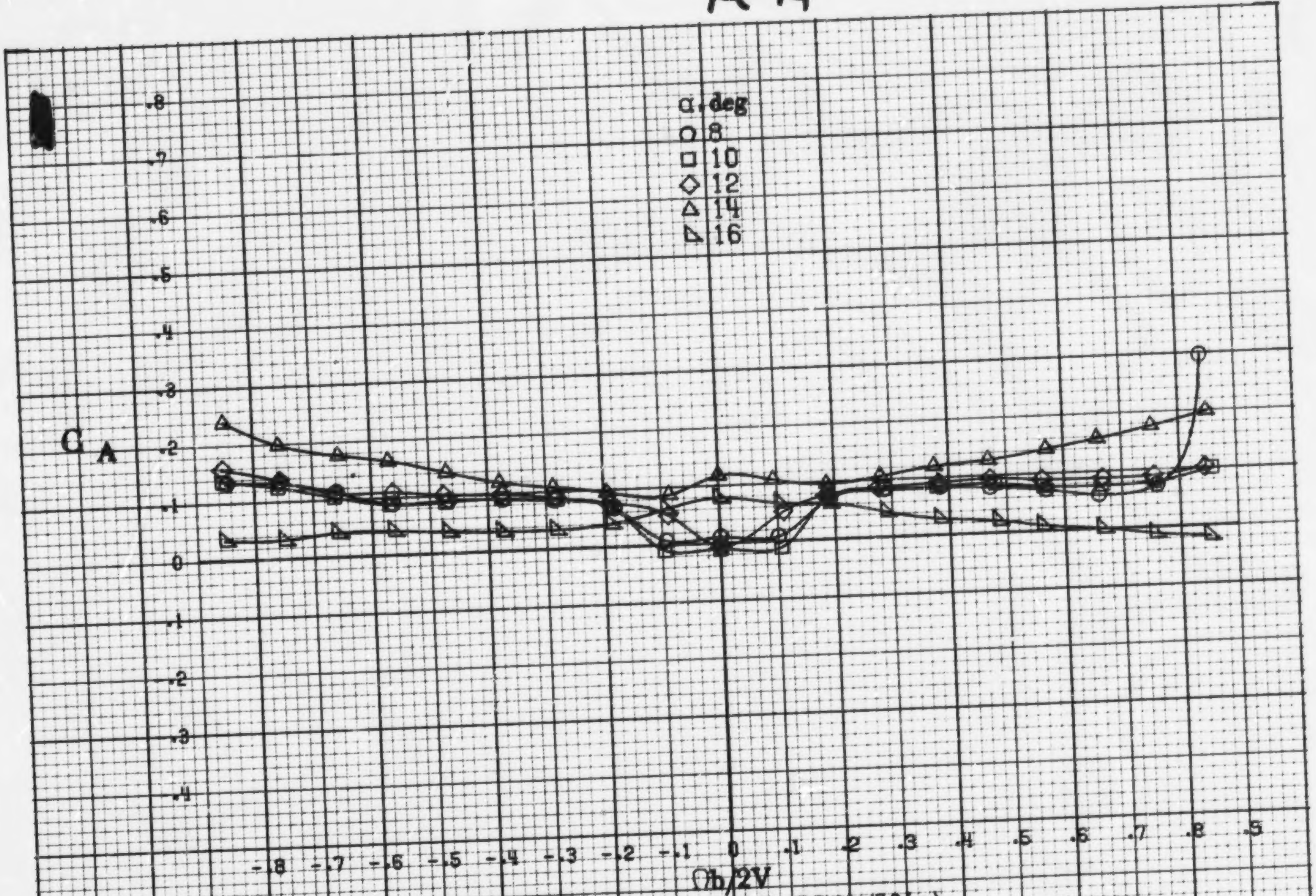

(a) α = 8 to 16 deg, SR = 76 cm (30 in).

Figure A24.- Effect of rotation rate and angle of attack on axial-force coefficient for basic configuration. $\delta_e = -15°$, $\delta_a = 0°$, $\delta_r = -25°$, $\beta = 0°$.

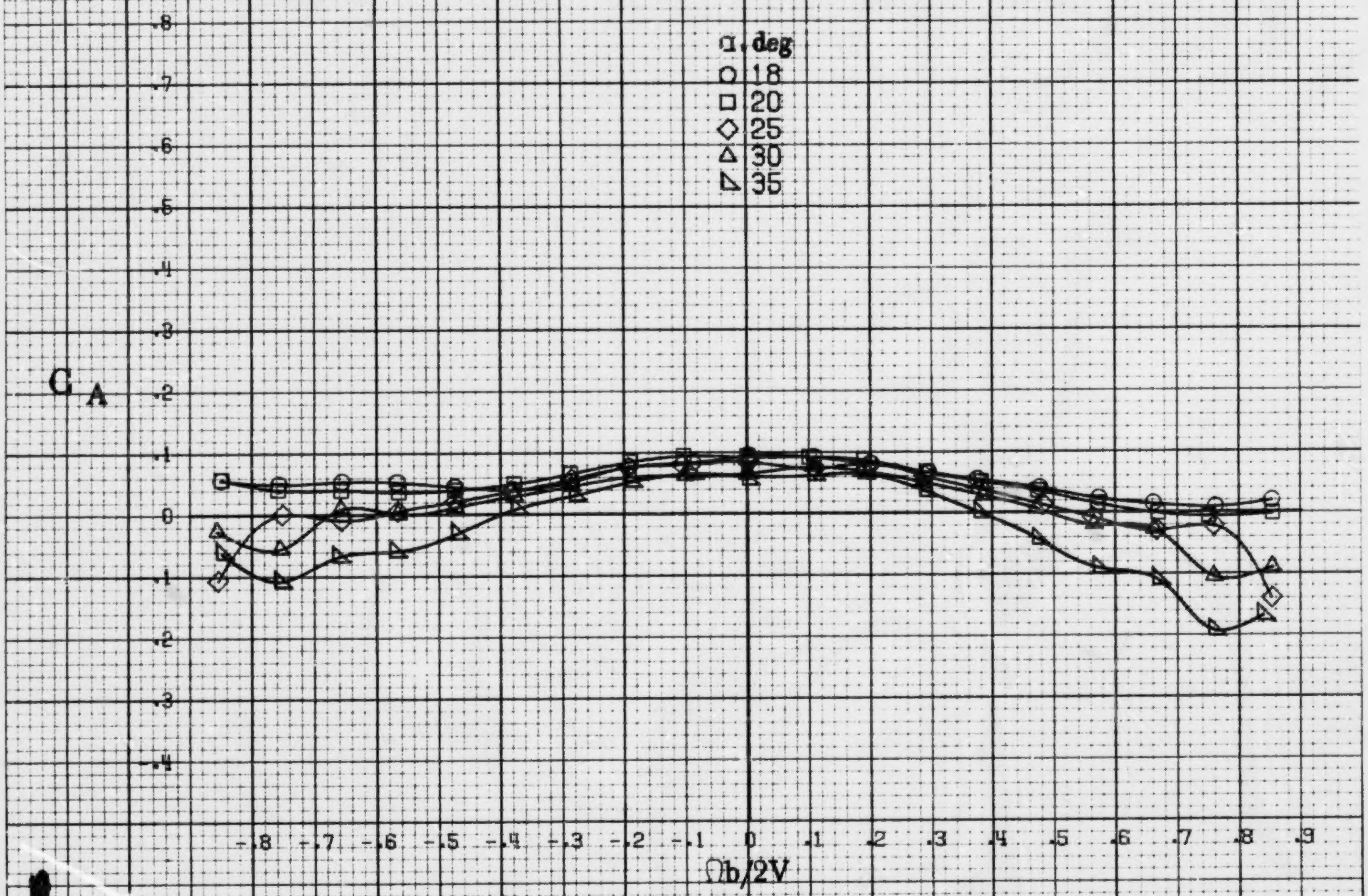

(b) α = 18 to 35 deg, SR = 76 cm (30 in).

Figure A24.-Continued.

A96

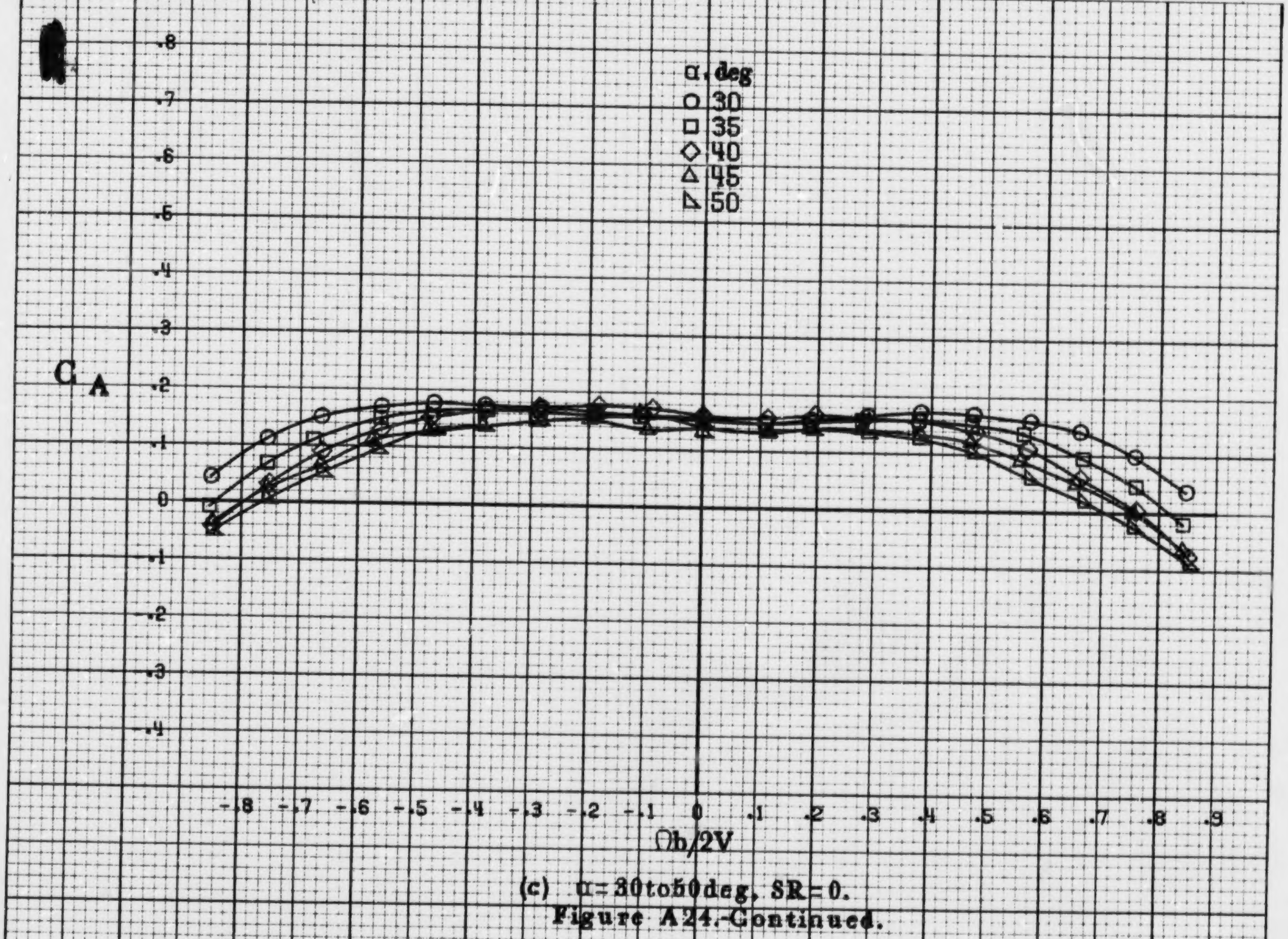

(c) α = 30 to 50 deg, SR = 0.

Figure A24.-Continued.

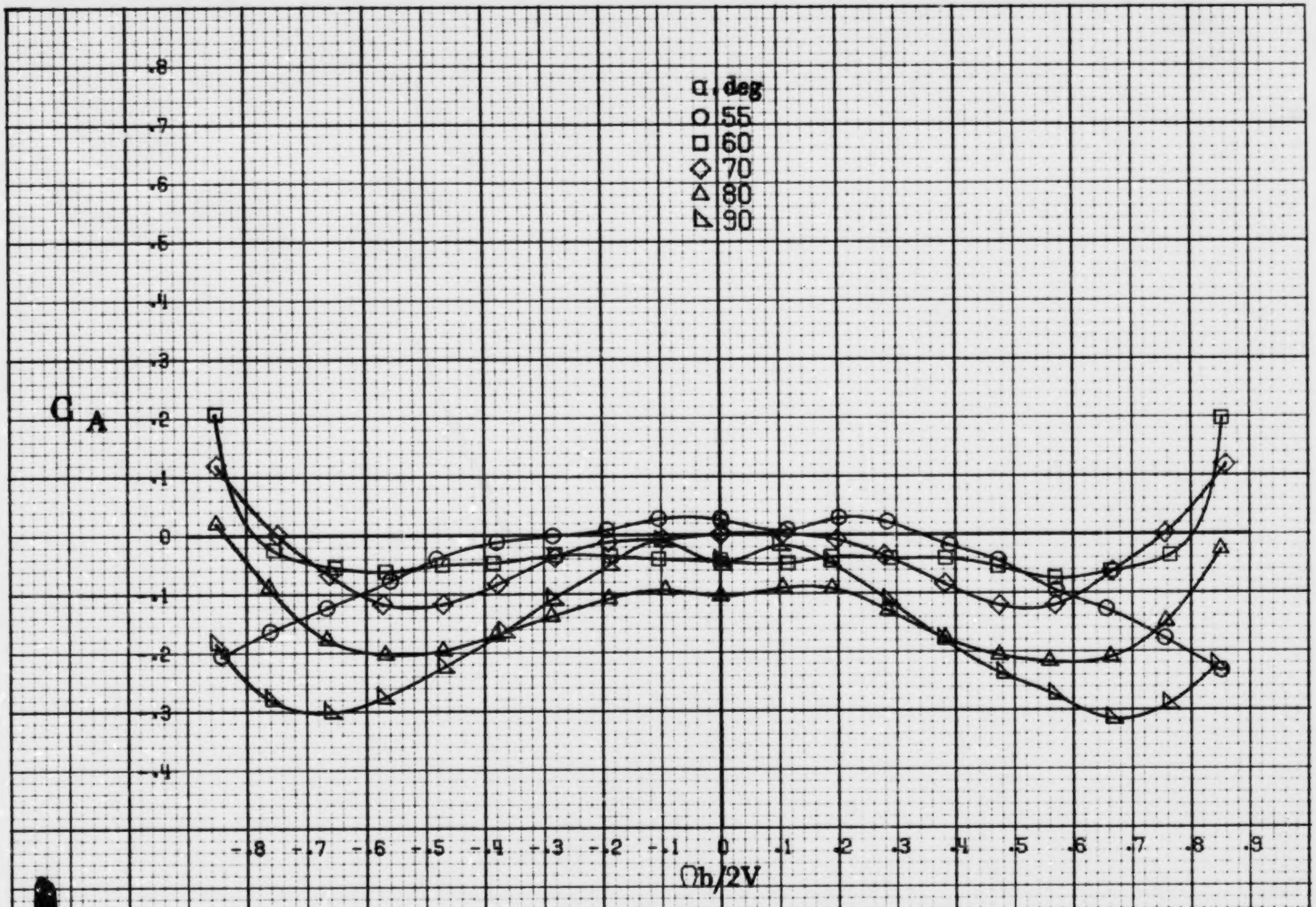

(d) α = 55 to 90 deg, SR = 0.
Figure A24.-Concluded.

A98

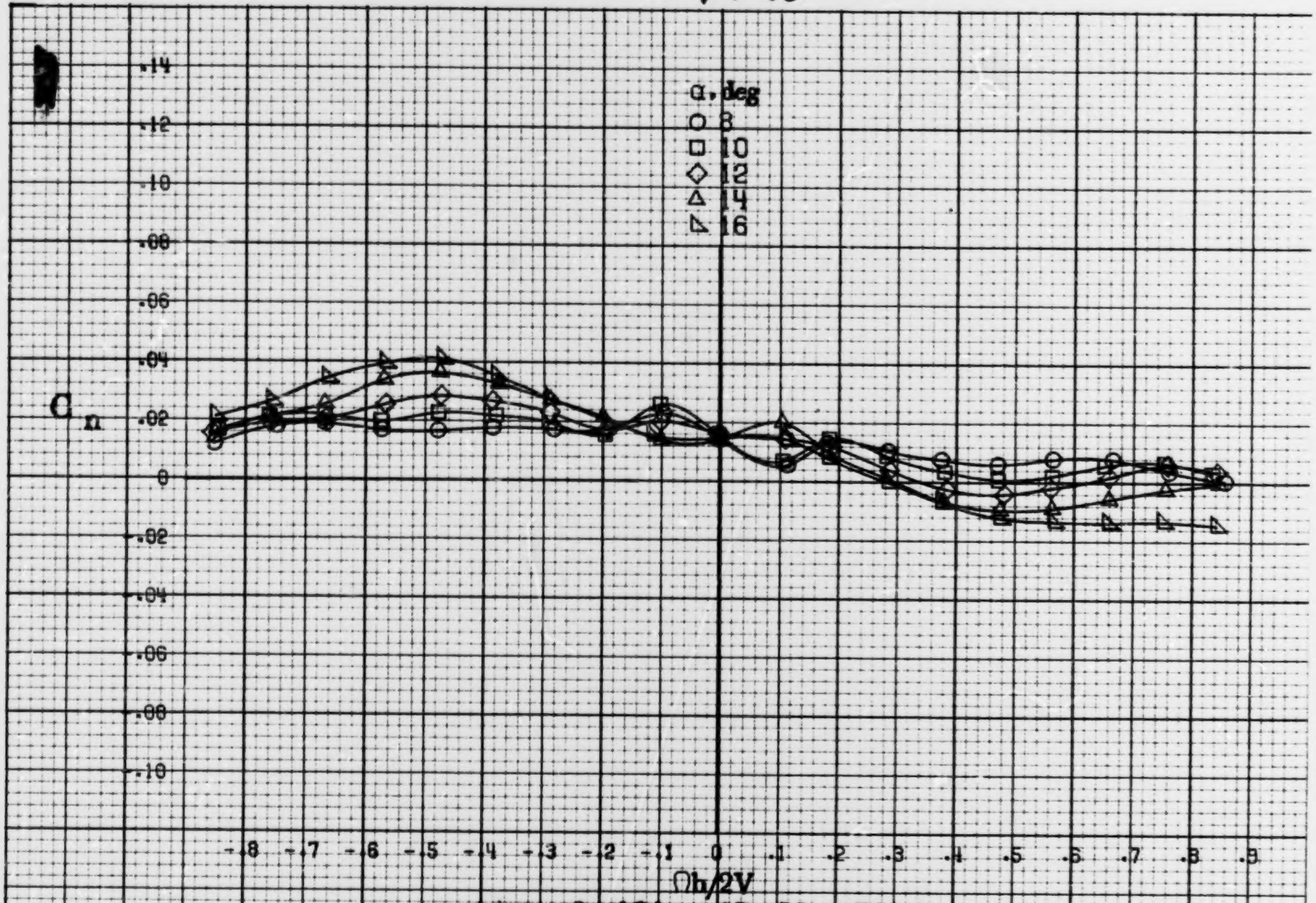

(a) α = 8 to 16 deg, SR = 76 cm (30 in).

Figure A25. Effect of rotation rate and angle of attack on yawing-moment coefficient for basic configuration. $\delta_e = -25°$, $\delta_a = 0°$, $\delta_r = 25°$, $\beta = 0°$.

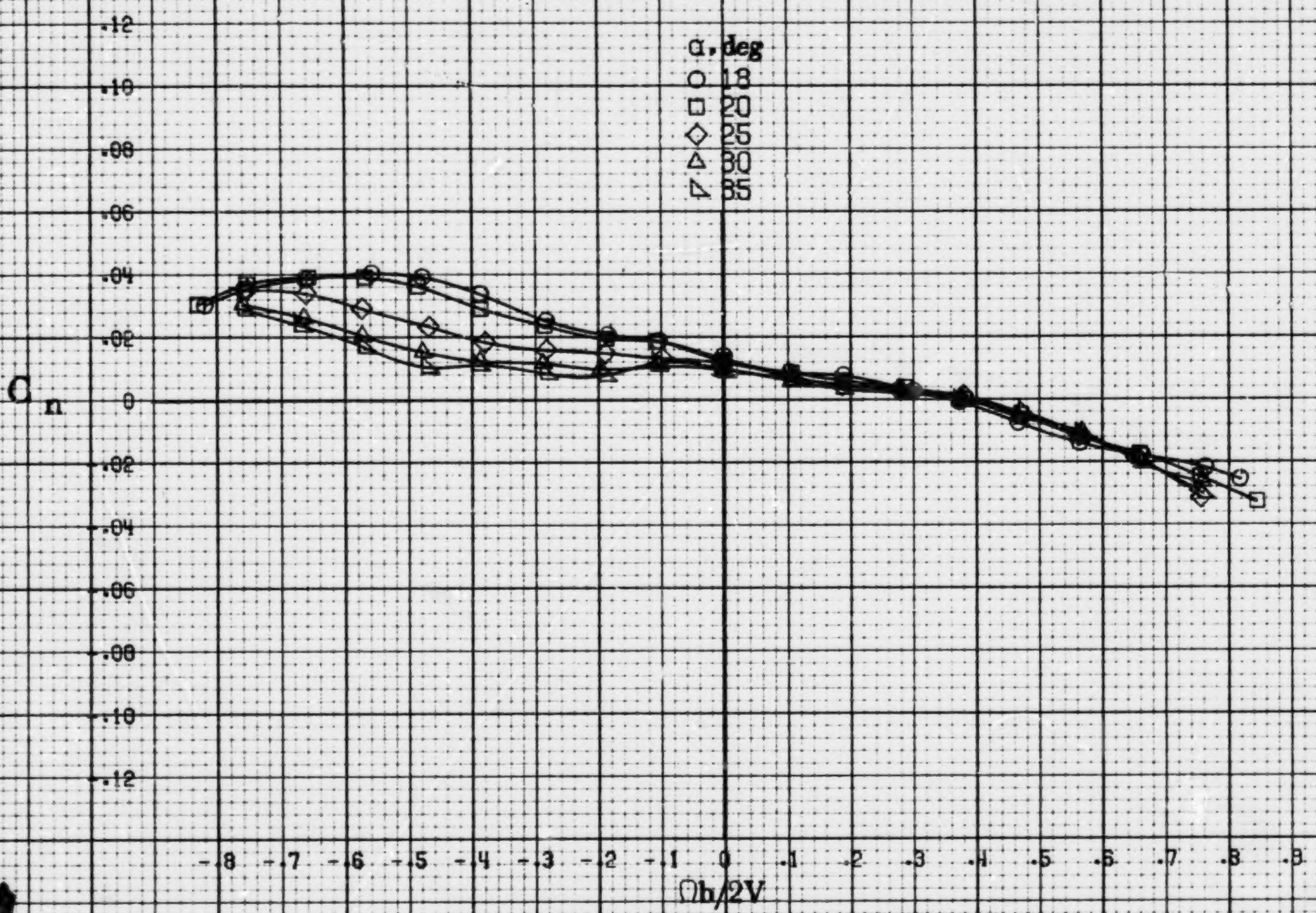

(b) α = 18 to 35 deg, SR = 76 cm (30 in).

Figure A25.-Continued.

A100

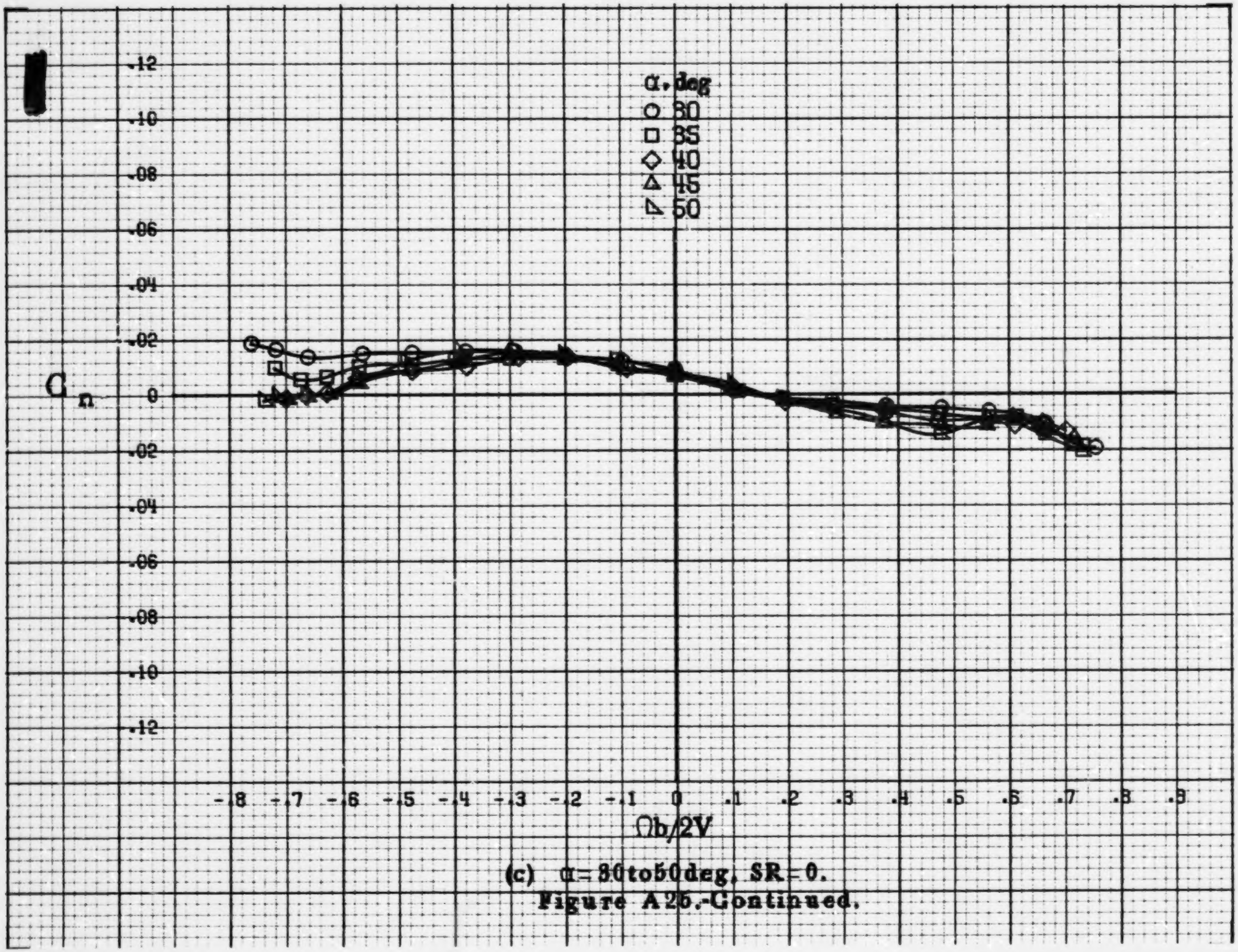

(c) α = 30to50deg, SR = 0.

Figure A25.-Continued.

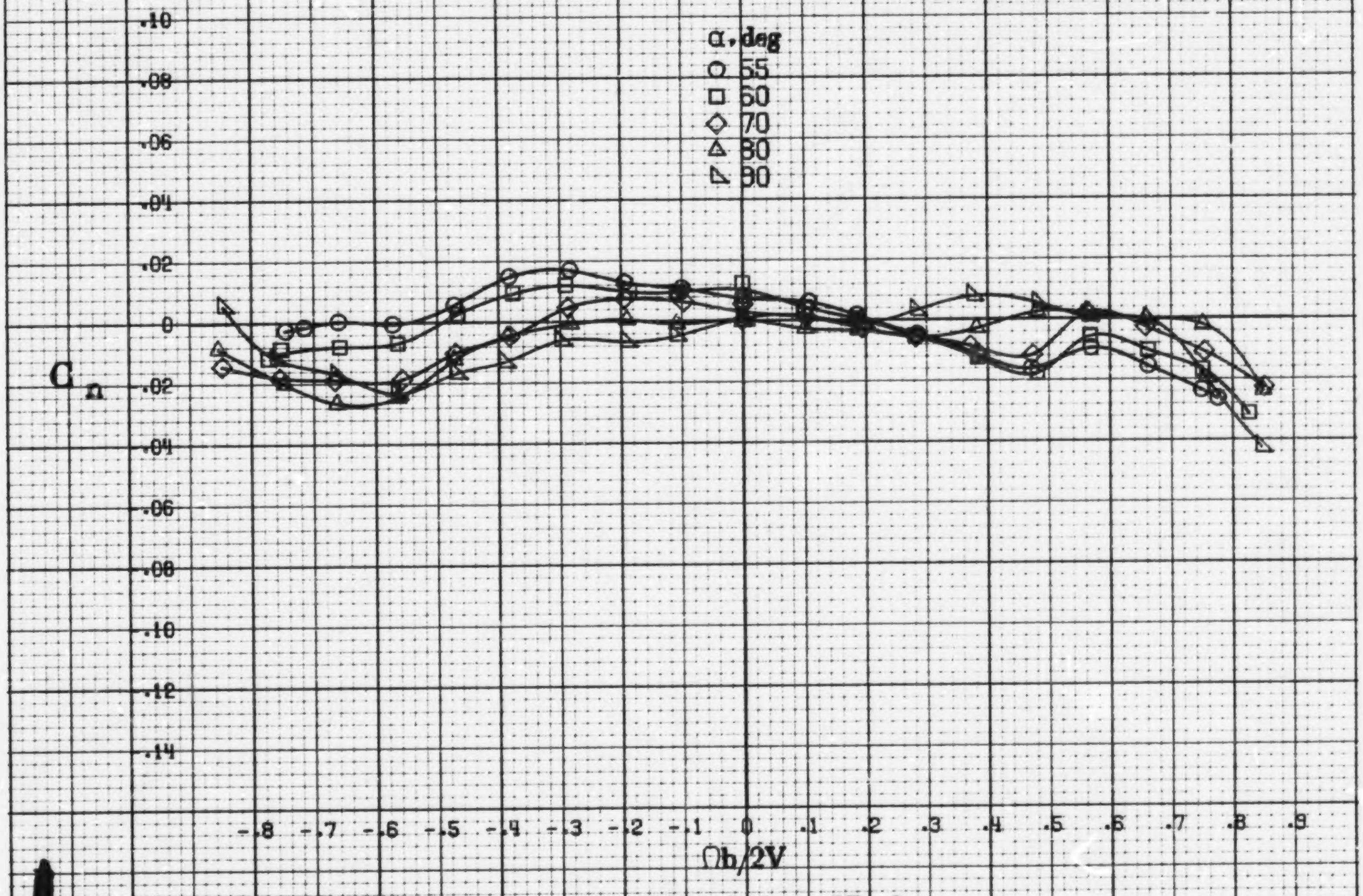

(d) α=55to90deg, SR=0.
Figure A25.-Concluded.

A 107

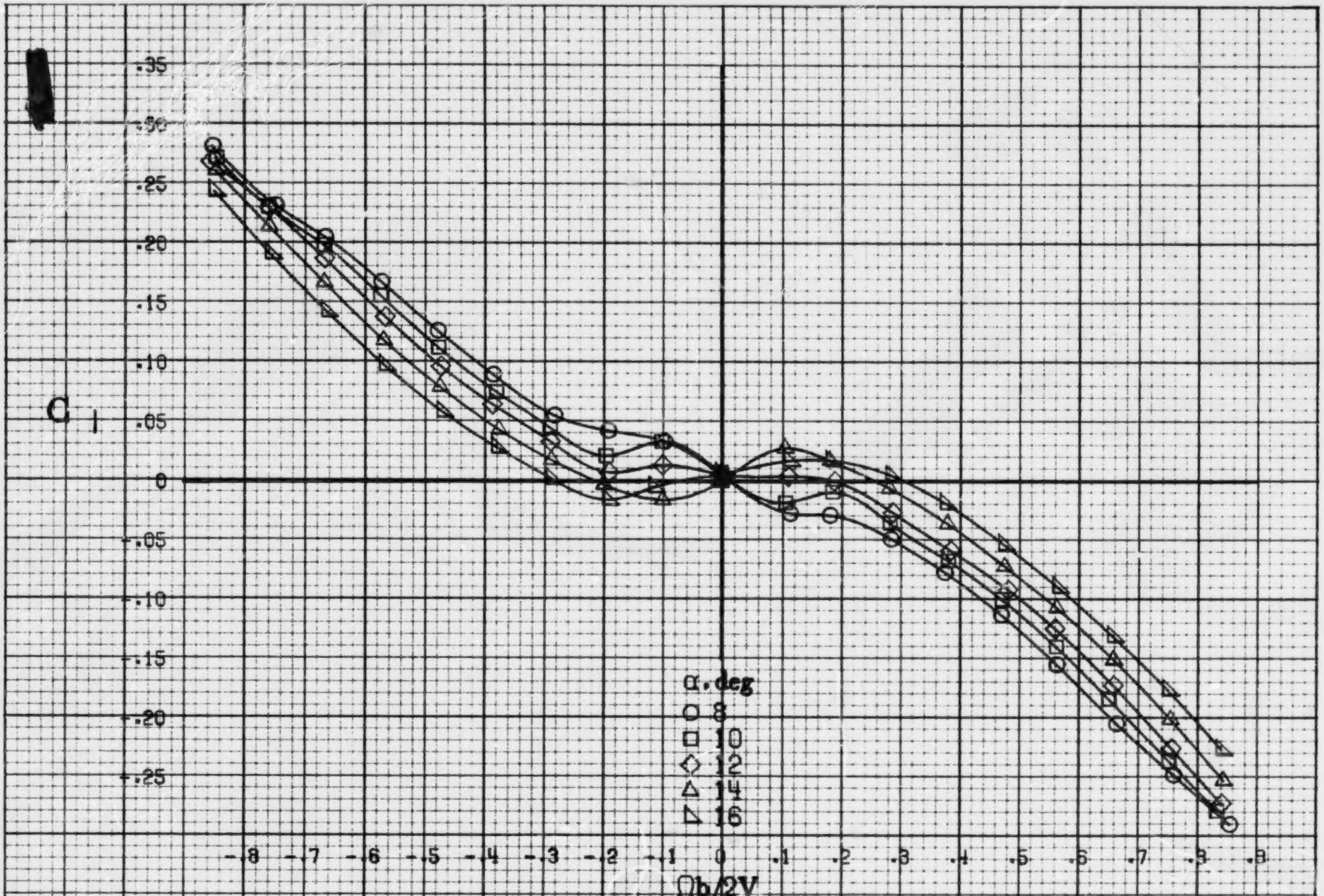

(a) α = 8 to 16 deg, SR = 76 cm (30 in).

Figure A26.-Effect of rotation rate and angle of attack on rolling-moment coefficient for basic configuration. $\delta_e = -25°$. $\delta_a = 0°$. $\delta_r = 25°$. $\beta = 0°$.

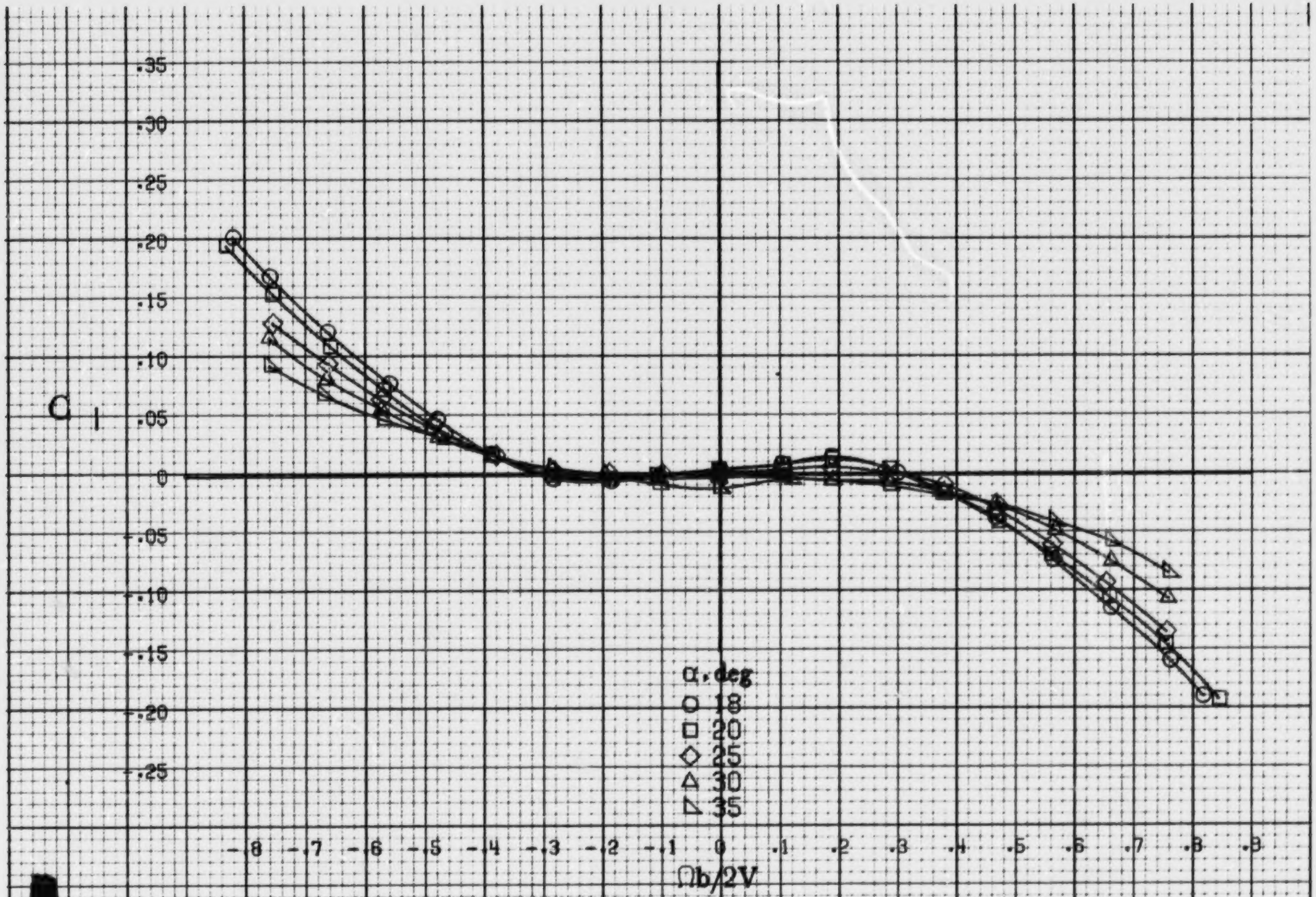

(b) α = 18 to 35 deg, SR = 76 cm (30 in).

Figure A26.-Continued.

A 104

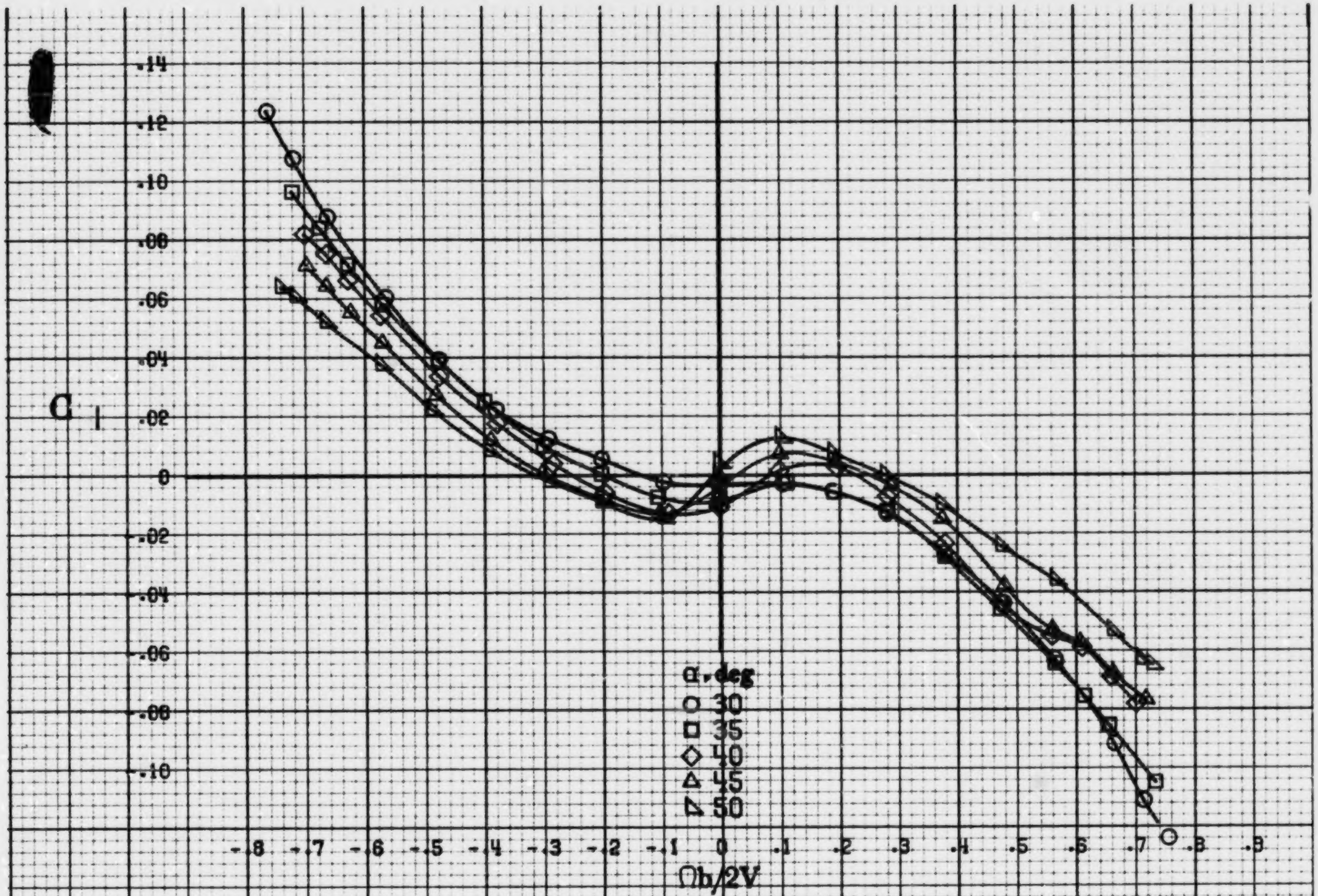

(c) α = 30 to 50 deg, SR = 0.

Figure A26.-Continued.

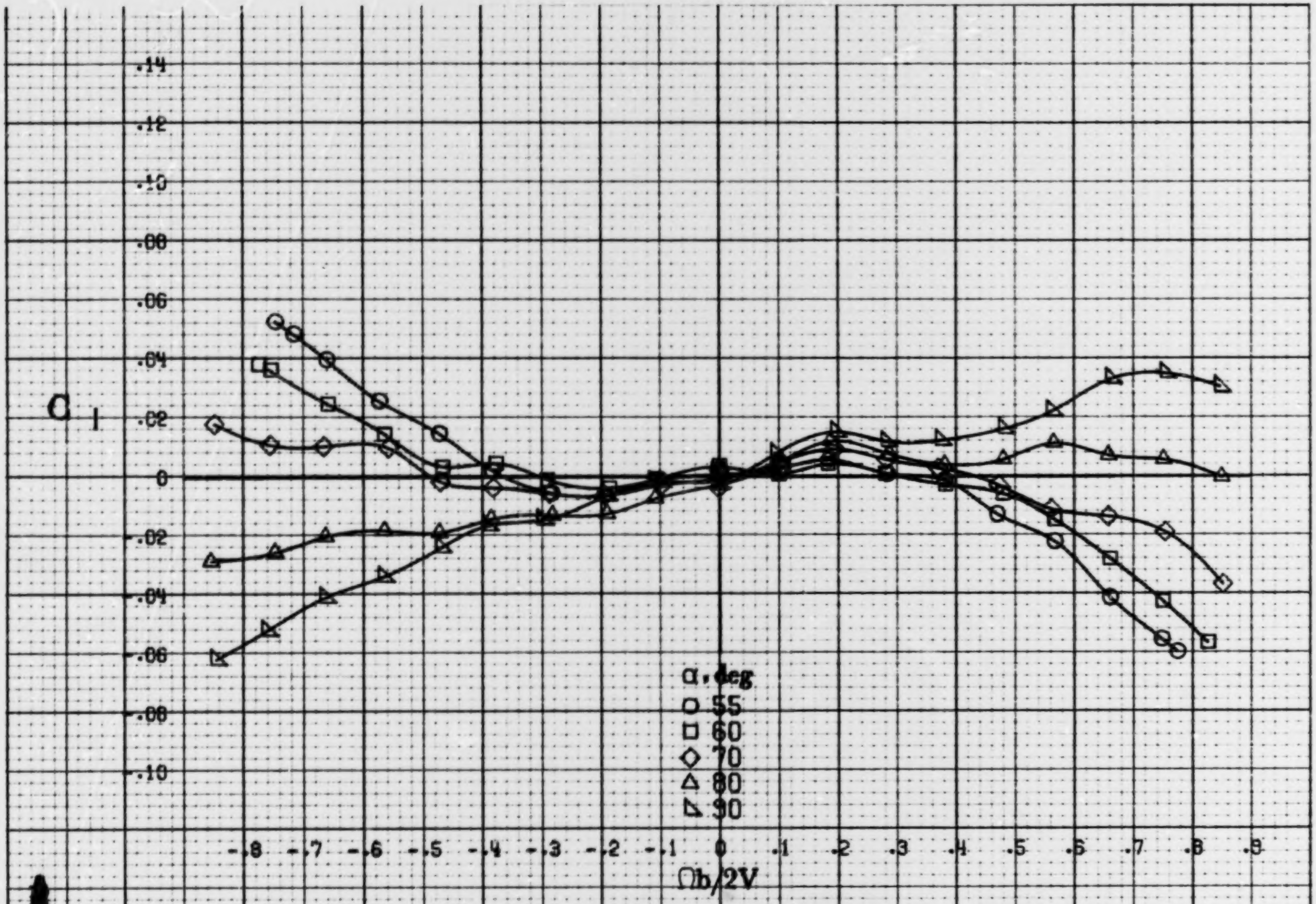

(d) α = 55 to 90 deg, SR = 0.

Figure A26.-Concluded.

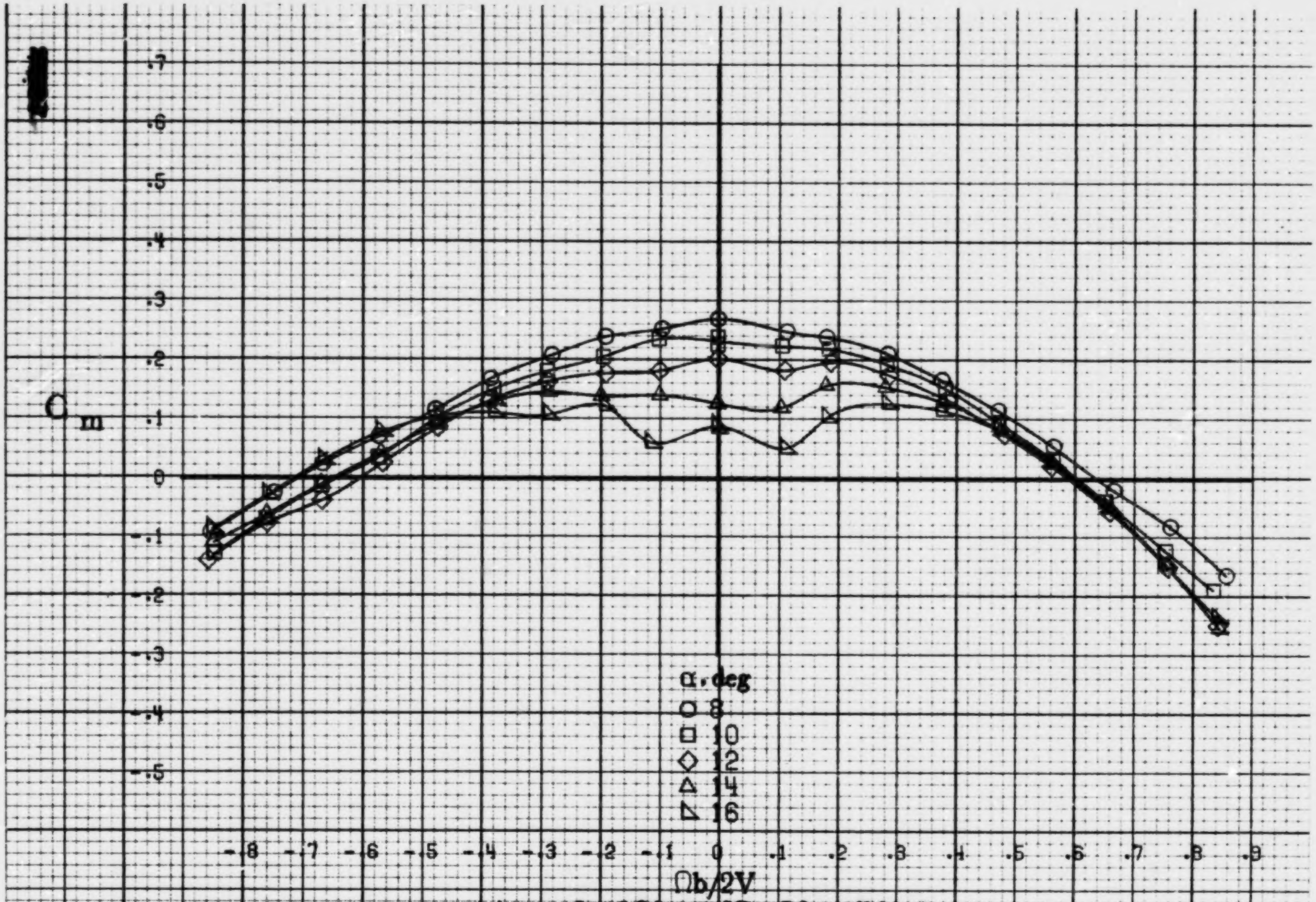

(a) α = 8 to 16 deg, SR = 76 cm (30 in).

Figure A27.- Effect of rotation rate and angle of attack on pitching-moment coefficient for basic configuration. $\delta_e = -25°$, $\delta_a = 0°$, $\delta_r = -25°$, $\beta = 0°$.

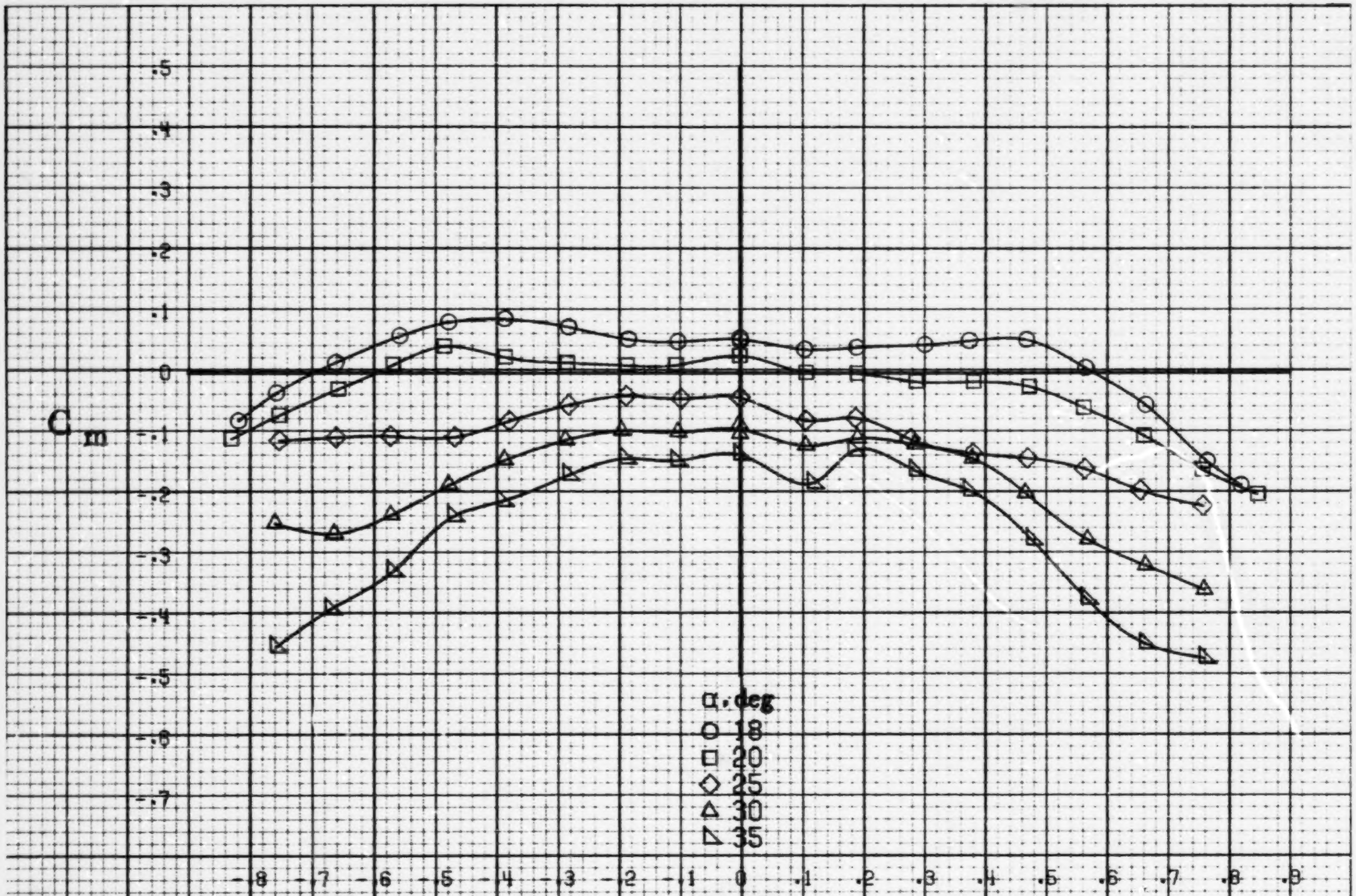

(b) α = 18 to 35 deg, SR = 76 cm (30 in).
Figure A27.-Continued.

A108

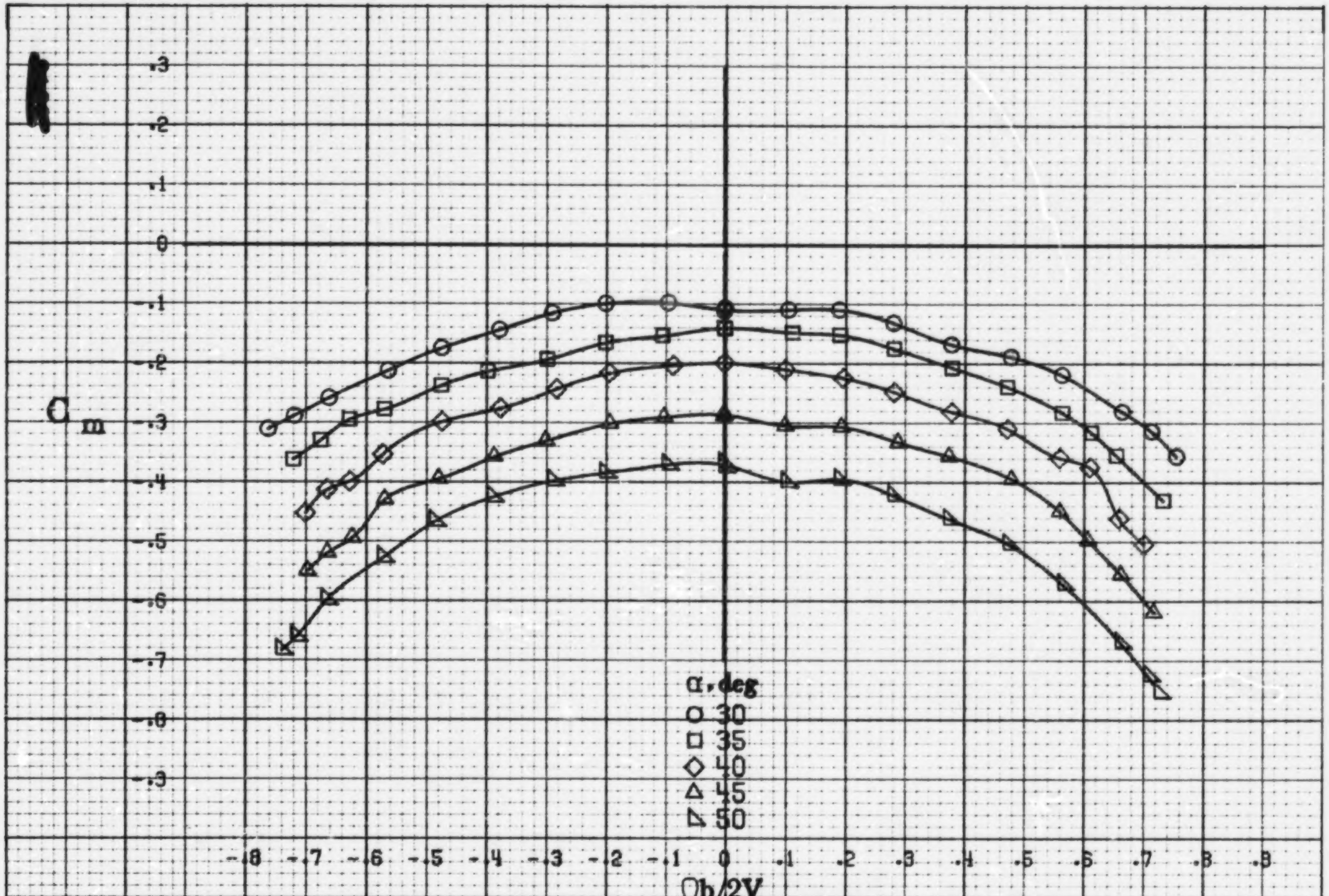

(c) α = 30 to 50 deg, SR = 0.

Figure A27.-Continued.

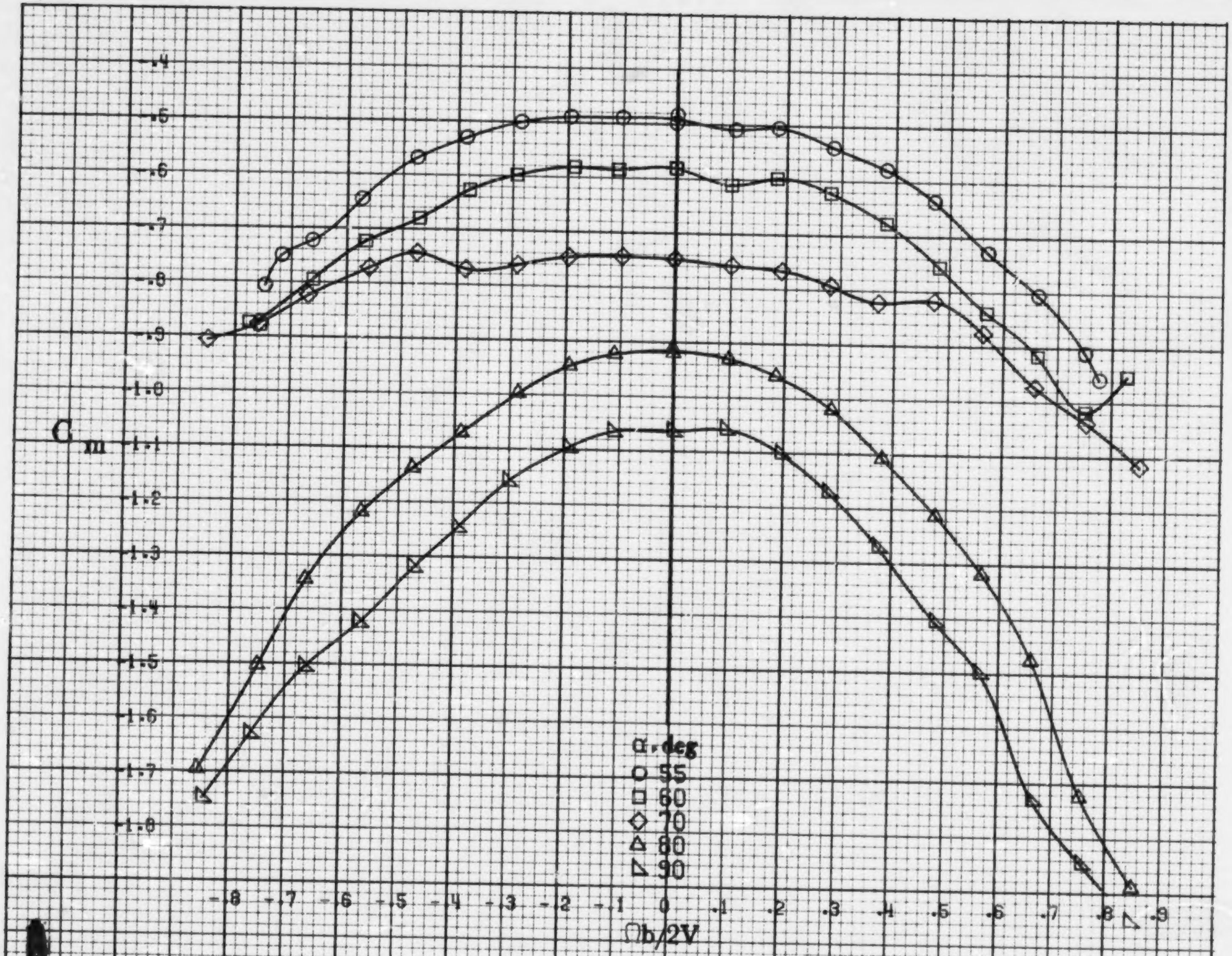

(d) α = 55 to 90 deg, SR = 0.

Figure A27.-Concluded.

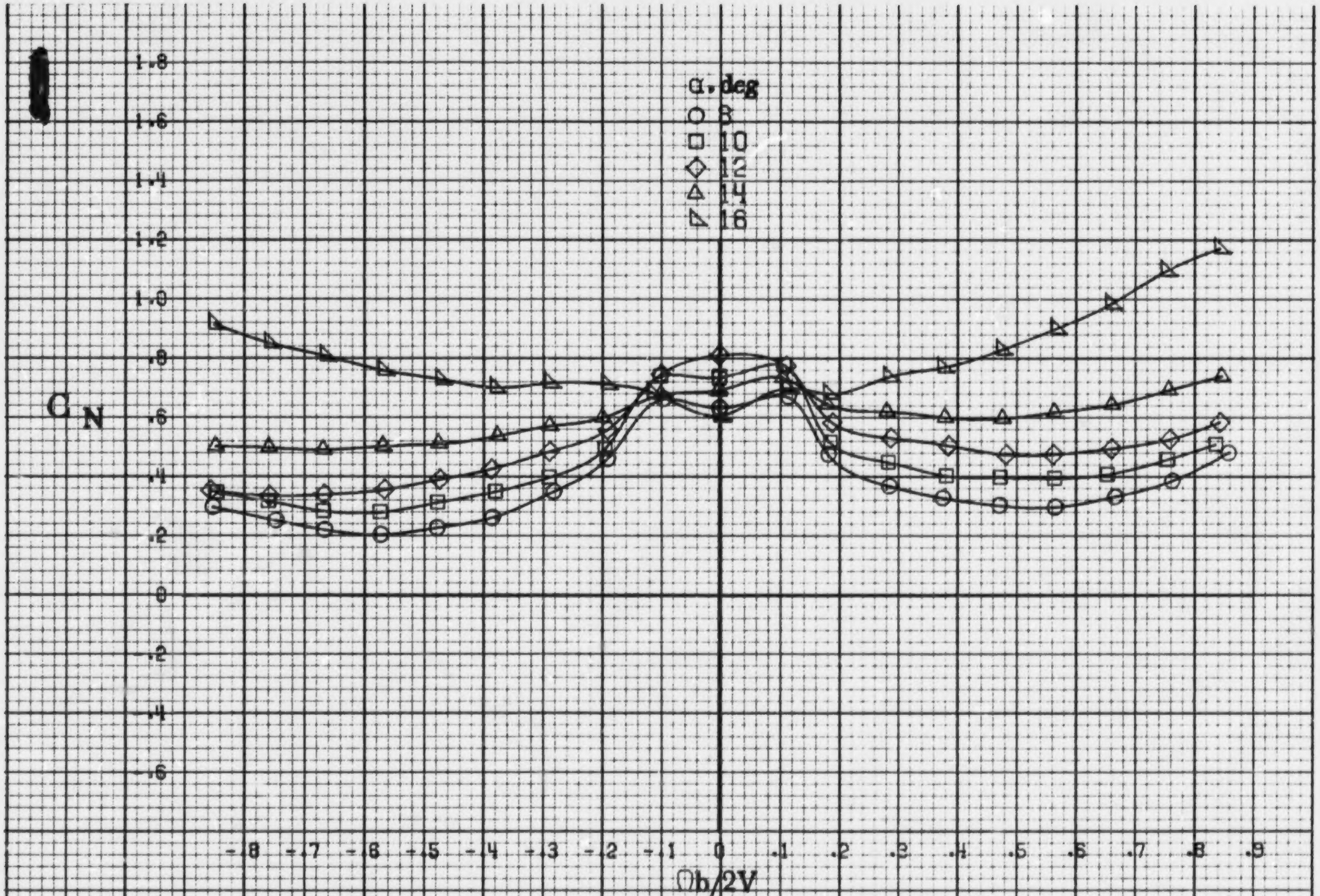

(a) α = 8 to 16 deg, SR = 76 cm (30 in).

Figure A28.-Effect of rotation rate and angle of attack on normal-force coefficient for basic configuration. $\delta_e = -25°$, $\delta_a = 0°$, $\delta_r = 25°$, $\beta = 0°$.

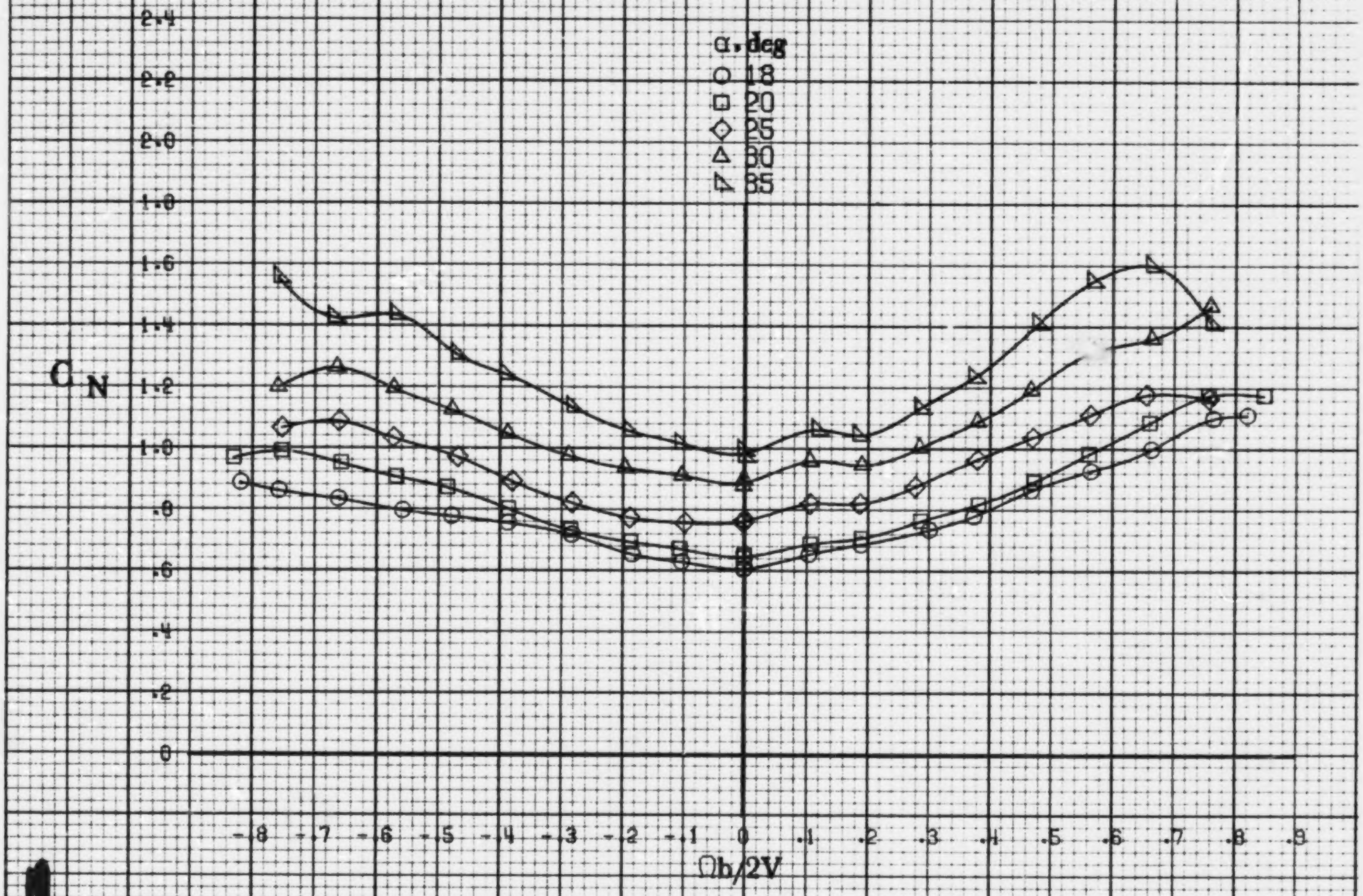

(b) α = 18 to 35 deg, SR = 76 cm (30 in).

Figure A28.-Continued.

A112

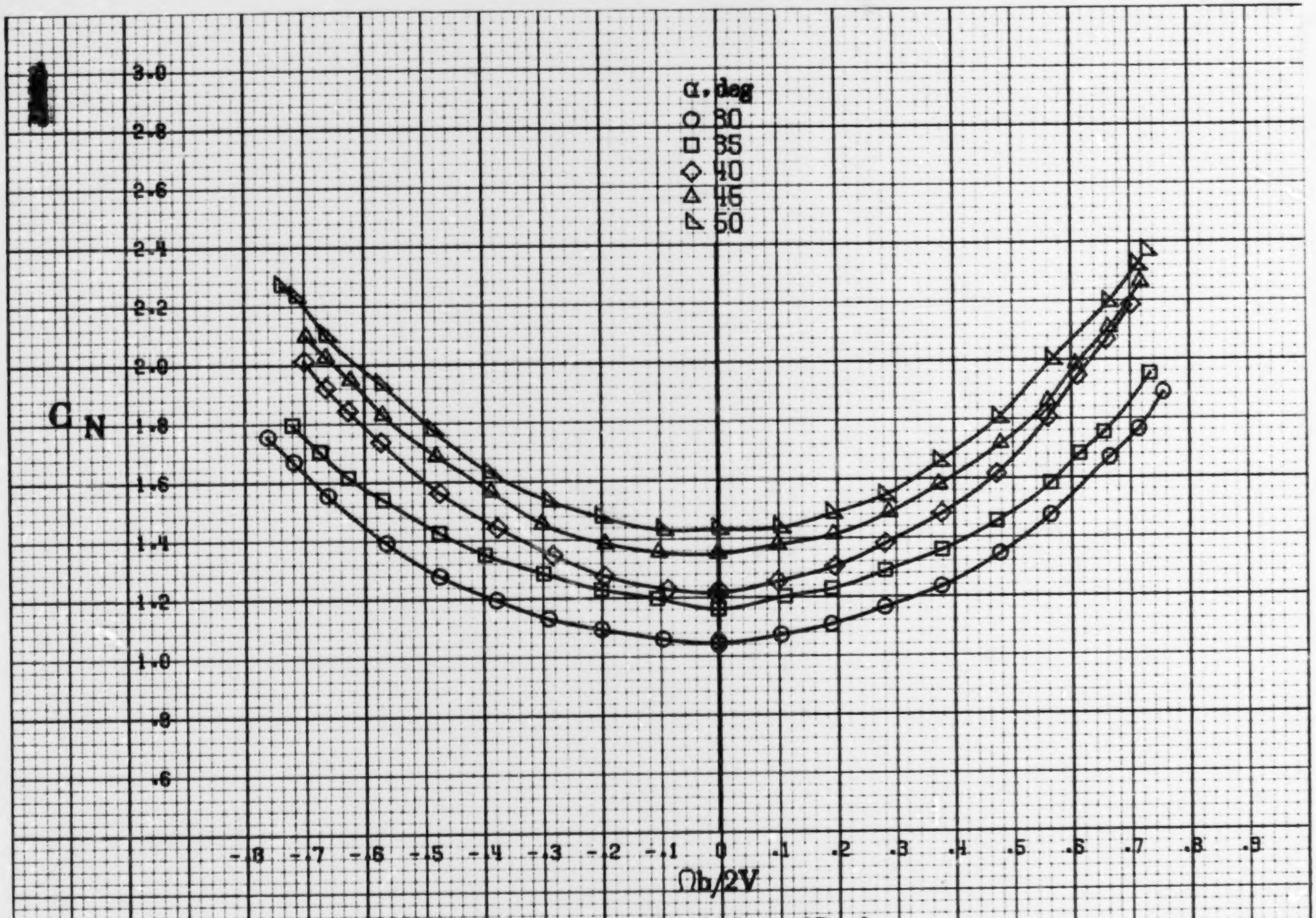

(c) α = 30 to 50 deg, SR = 0.

Figure A28.-Continued.

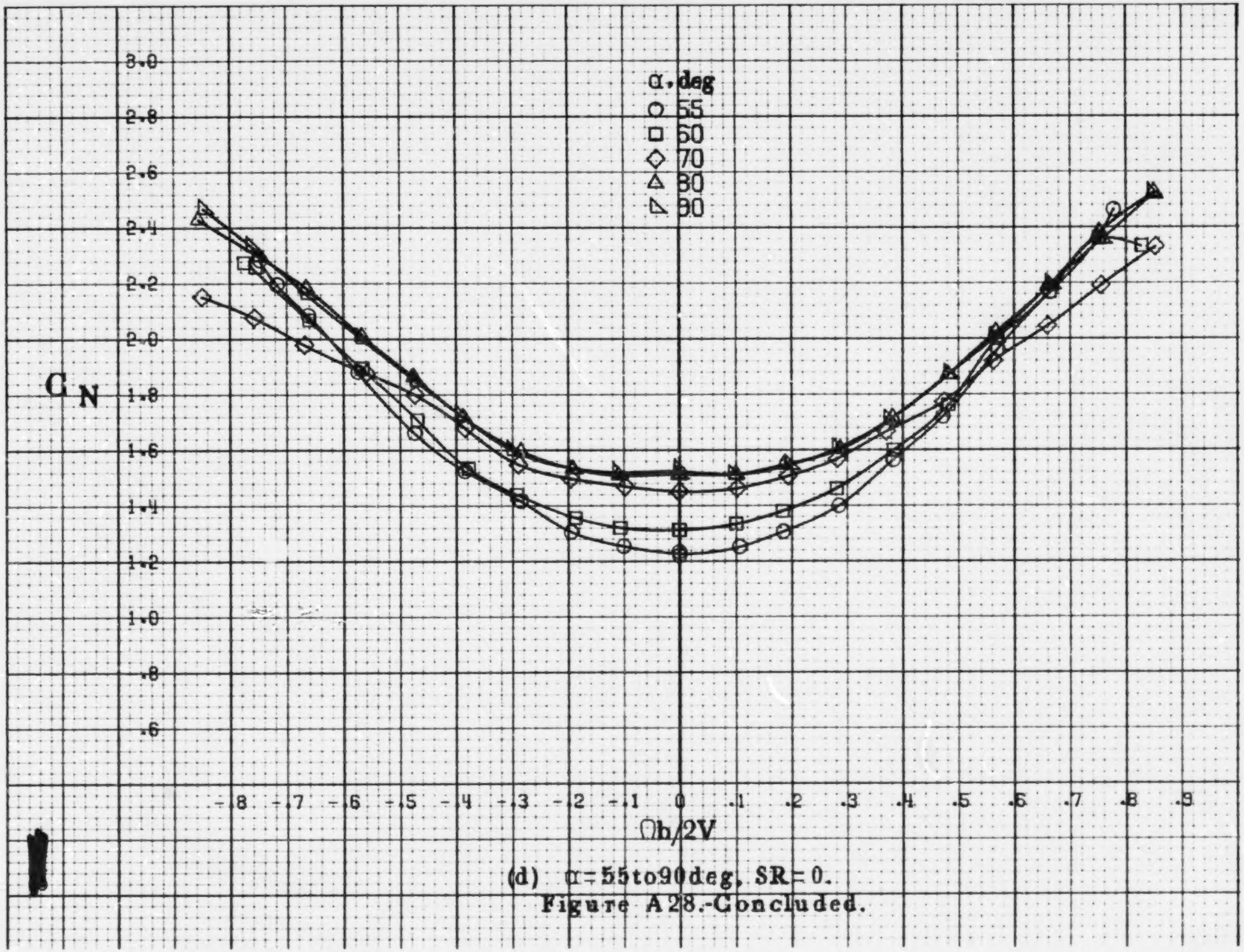

(d) α = 55 to 90 deg, SR = 0.

Figure A28.-Concluded.

A 114

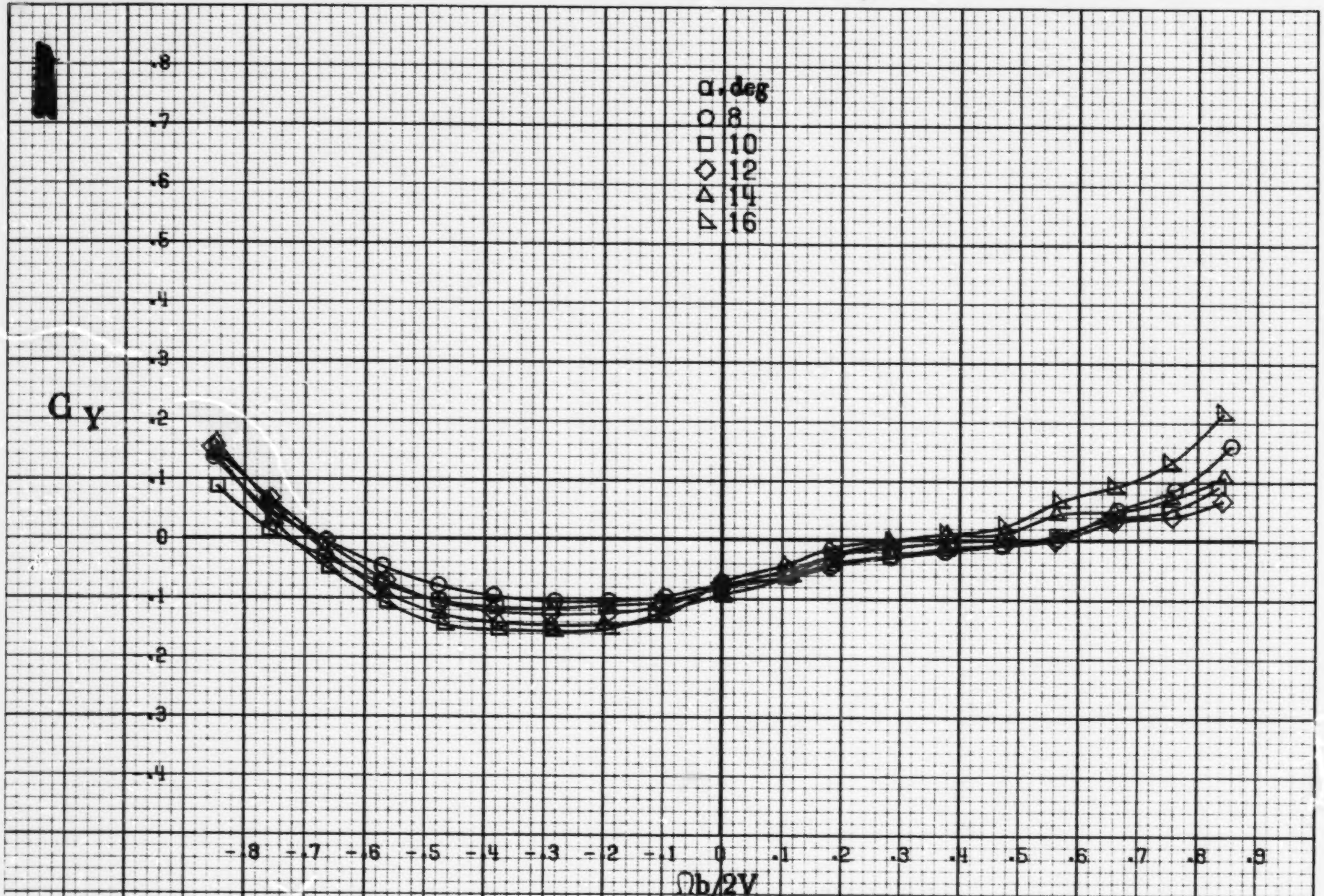

(a) α = 8 to 16 deg, SR = 76 cm (30 in).

Figure A29.- Effect of rotation rate and angle of attack on side-force coefficient for basic configuration. δ_e = -25°, δ_a = 0°, δ_r = 25°, β = 0°.

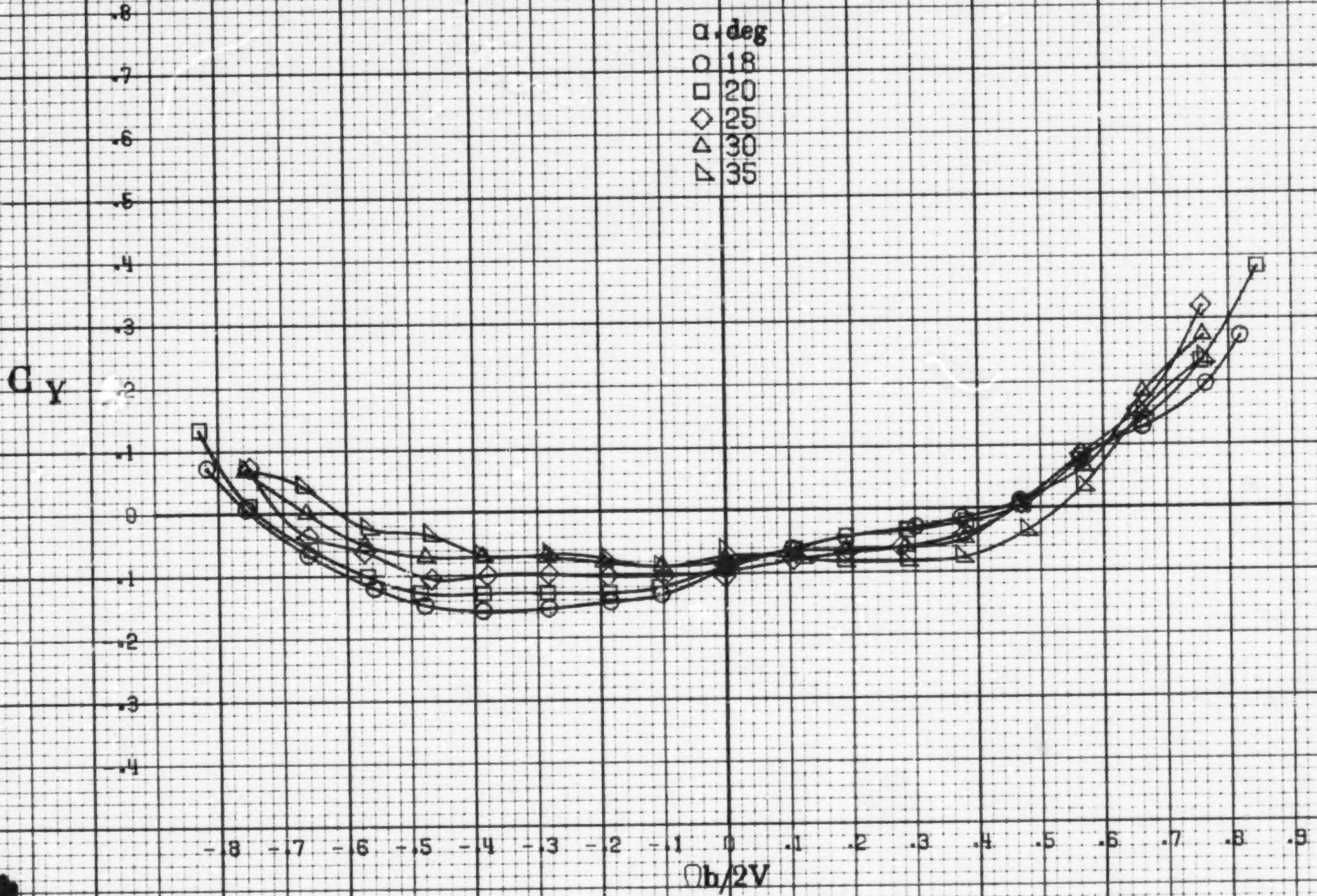

(b) α = 18 to 35 deg, SR = 76 cm (30 in).

Figure A29.-Continued.

A116

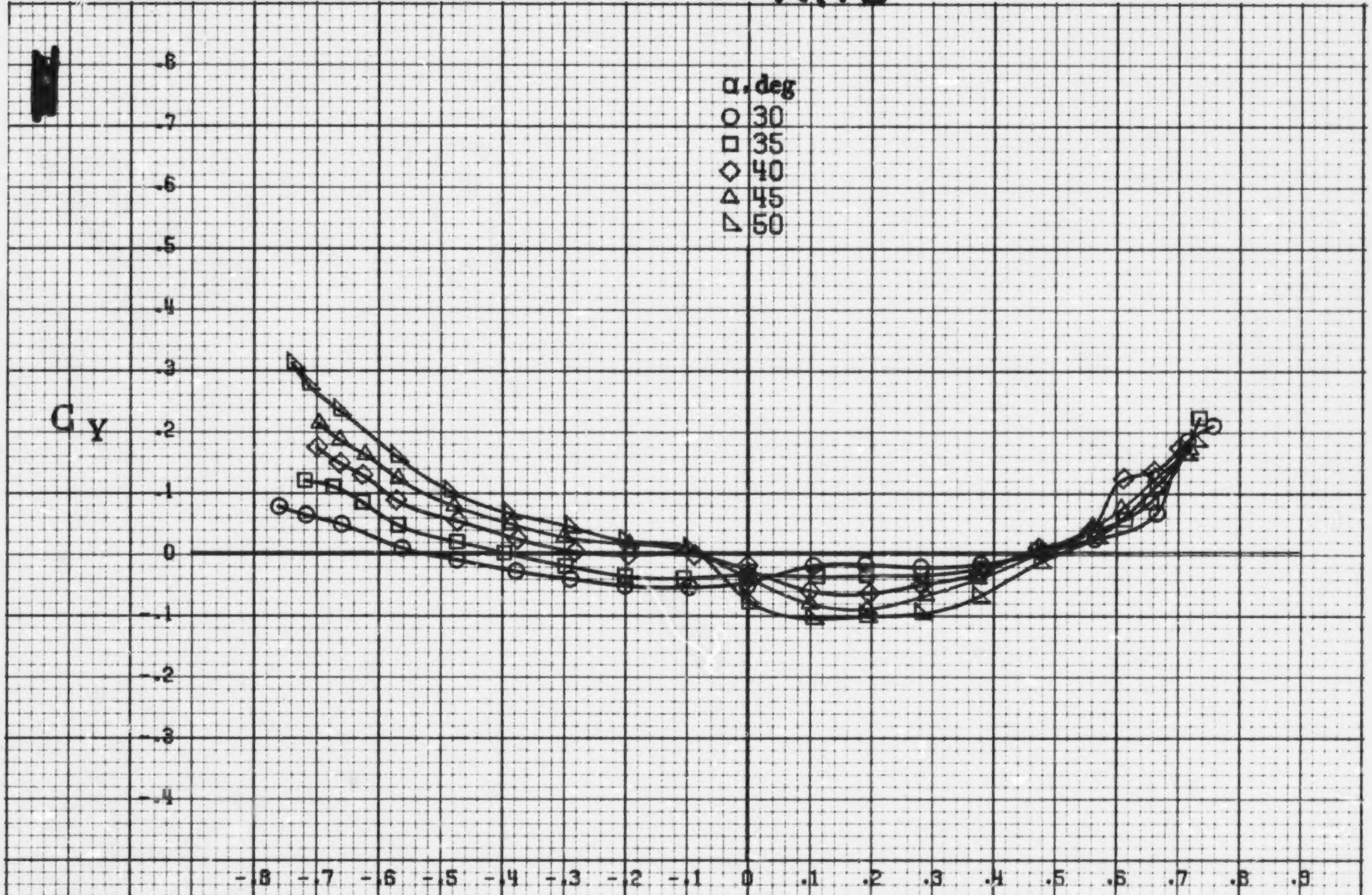

(c) α = 30 to 50 deg, SR = 0.

Figure A29.-Continued.

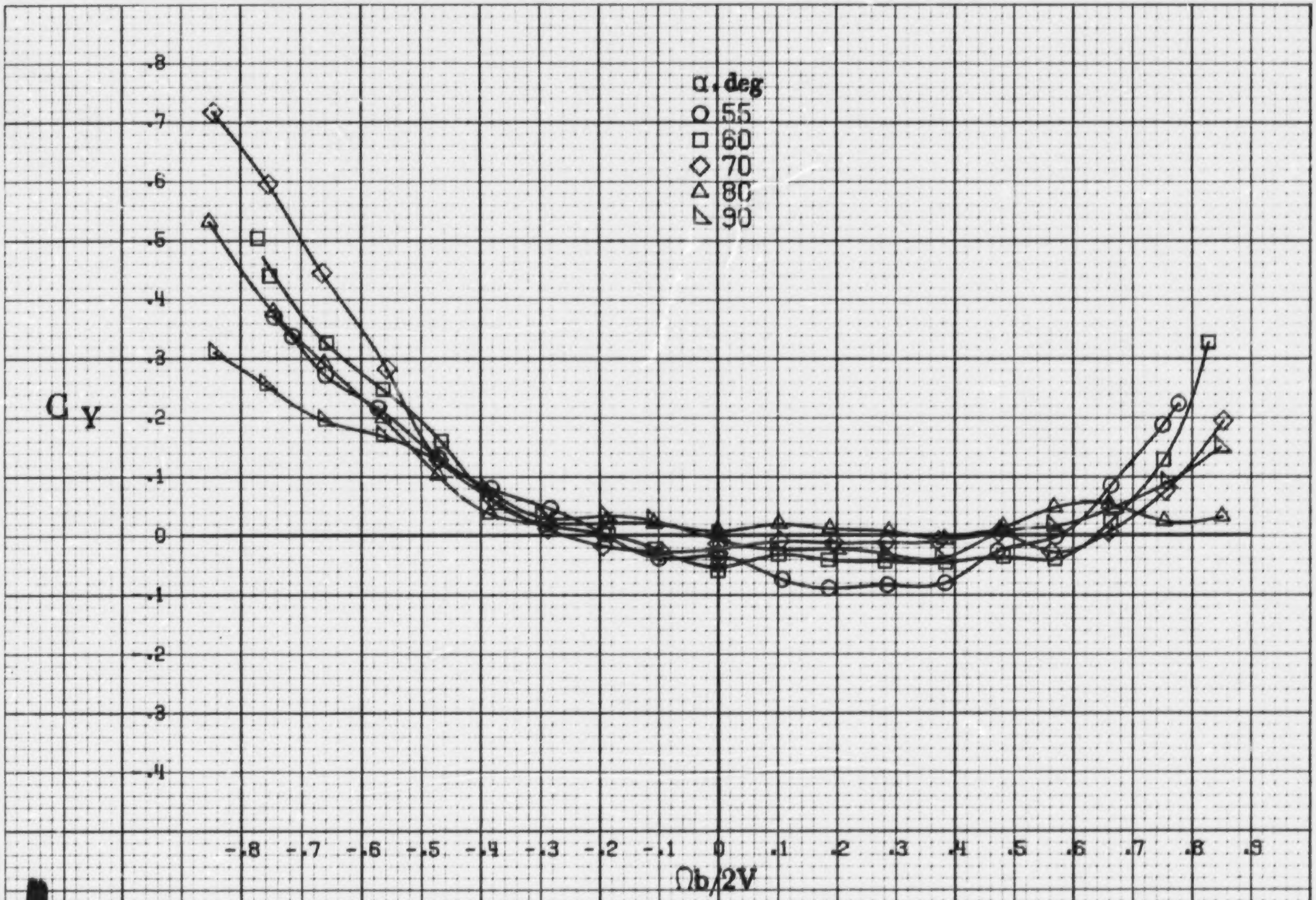

(d) α=55to90deg, SR=0.
Figure A29.-Concluded.

A118

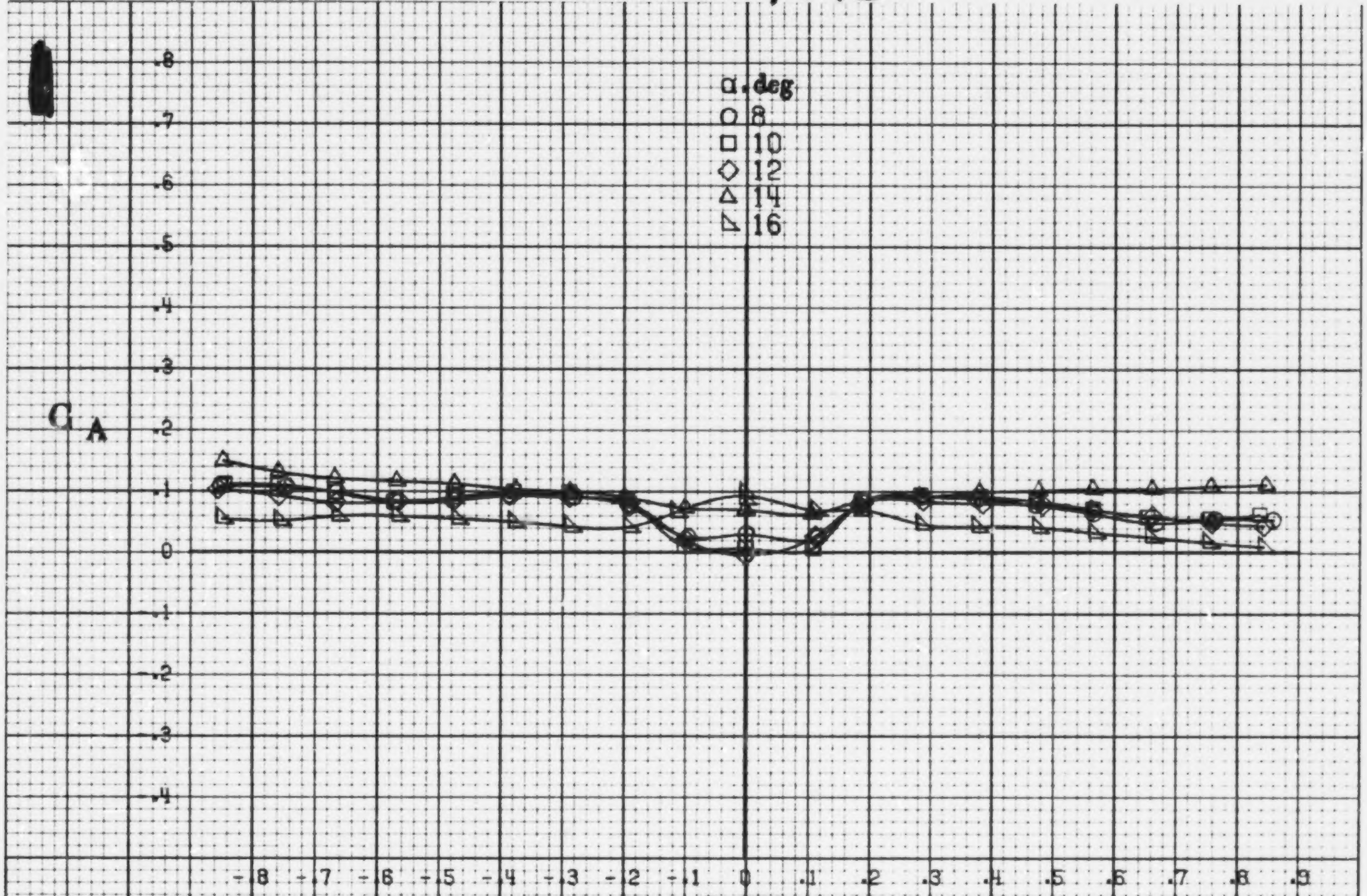

(a) α = 8 to 16 deg, SR = 76 cm (30 in).

Figure A30.- Effect of rotation rate and angle of attack on axial-force coefficient for basic configuration. $\delta_e = -25°$, $\delta_a = 0°$, $\delta_r = -25°$, $\beta = 0°$.

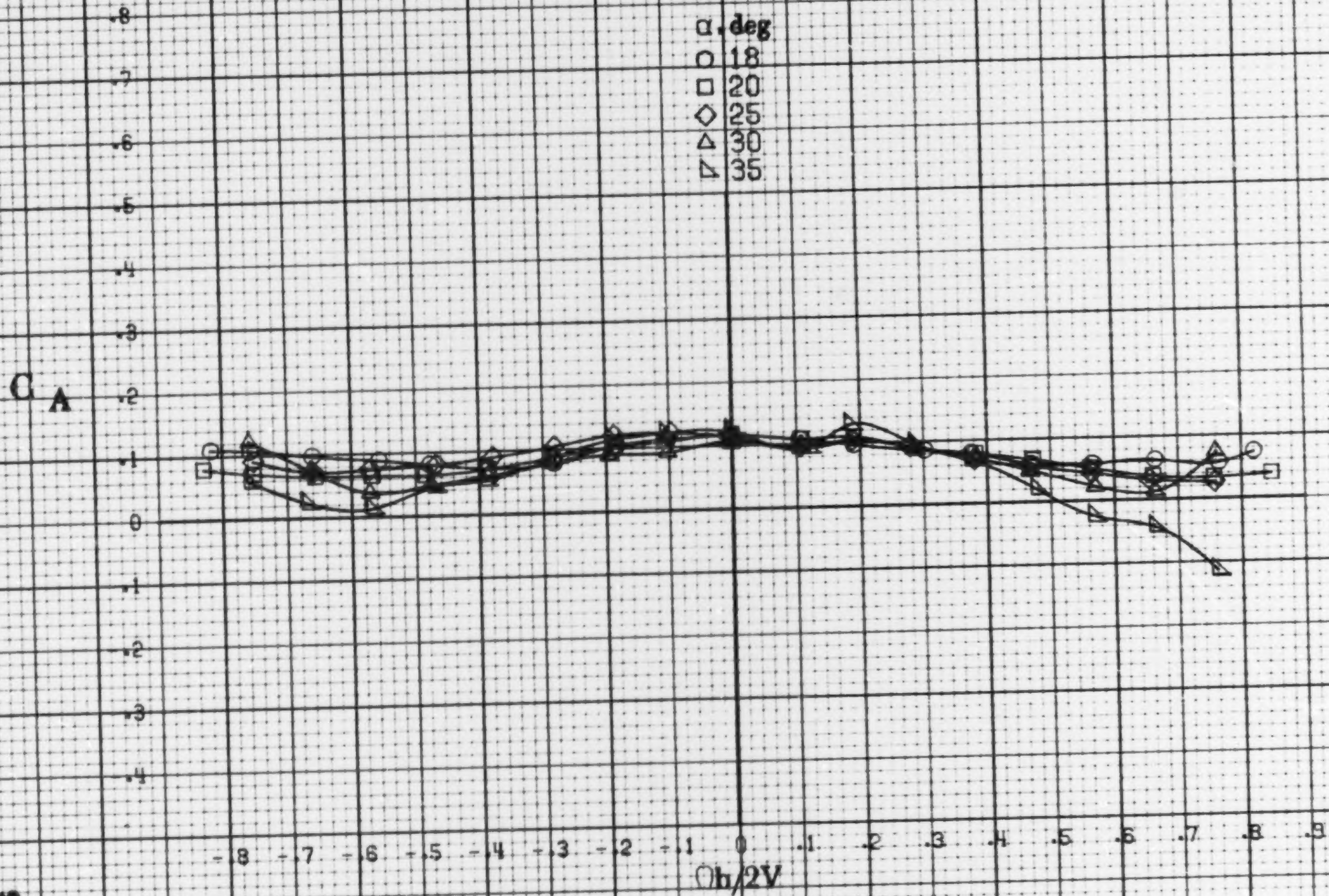

(b) α = 18 to 35 deg. SR = 76 cm (30 in).

Figure A80.-Continued

A119

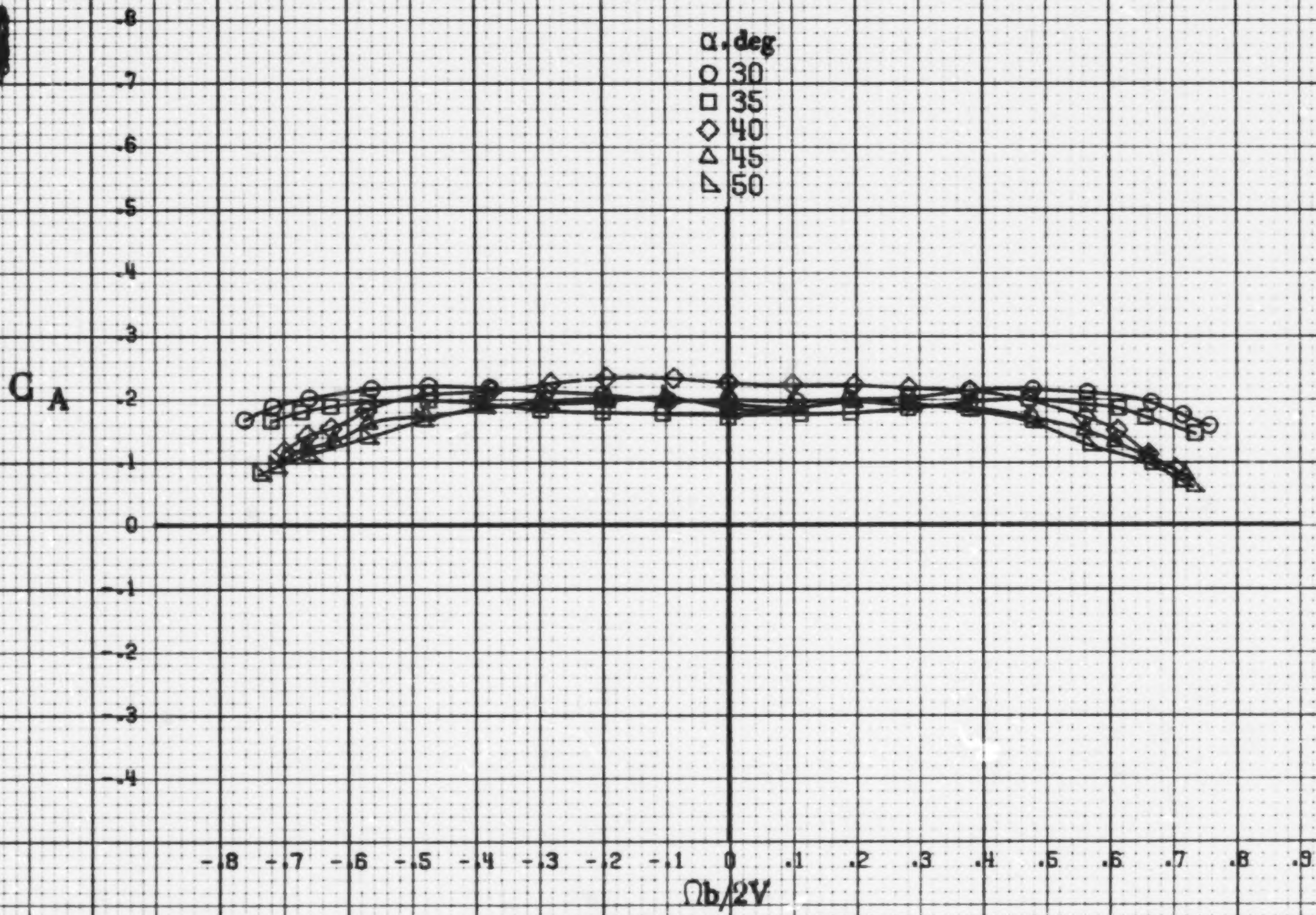

(c) α = 30 to 50 deg, SR = 0.

Figure A30.-Continued.

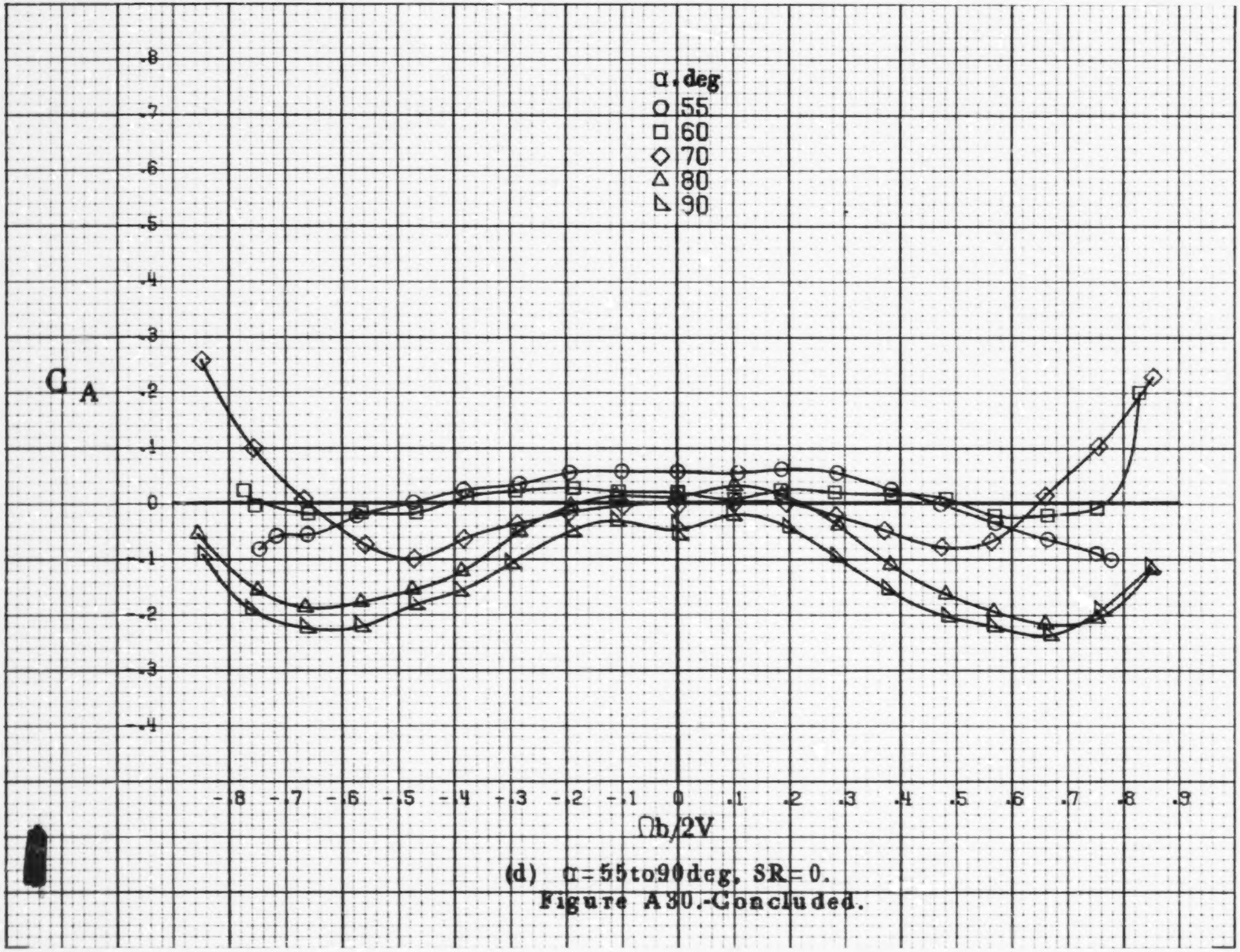

(d) α = 55 to 90 deg, SR = 0.

Figure A30.-Concluded.

A121

A122

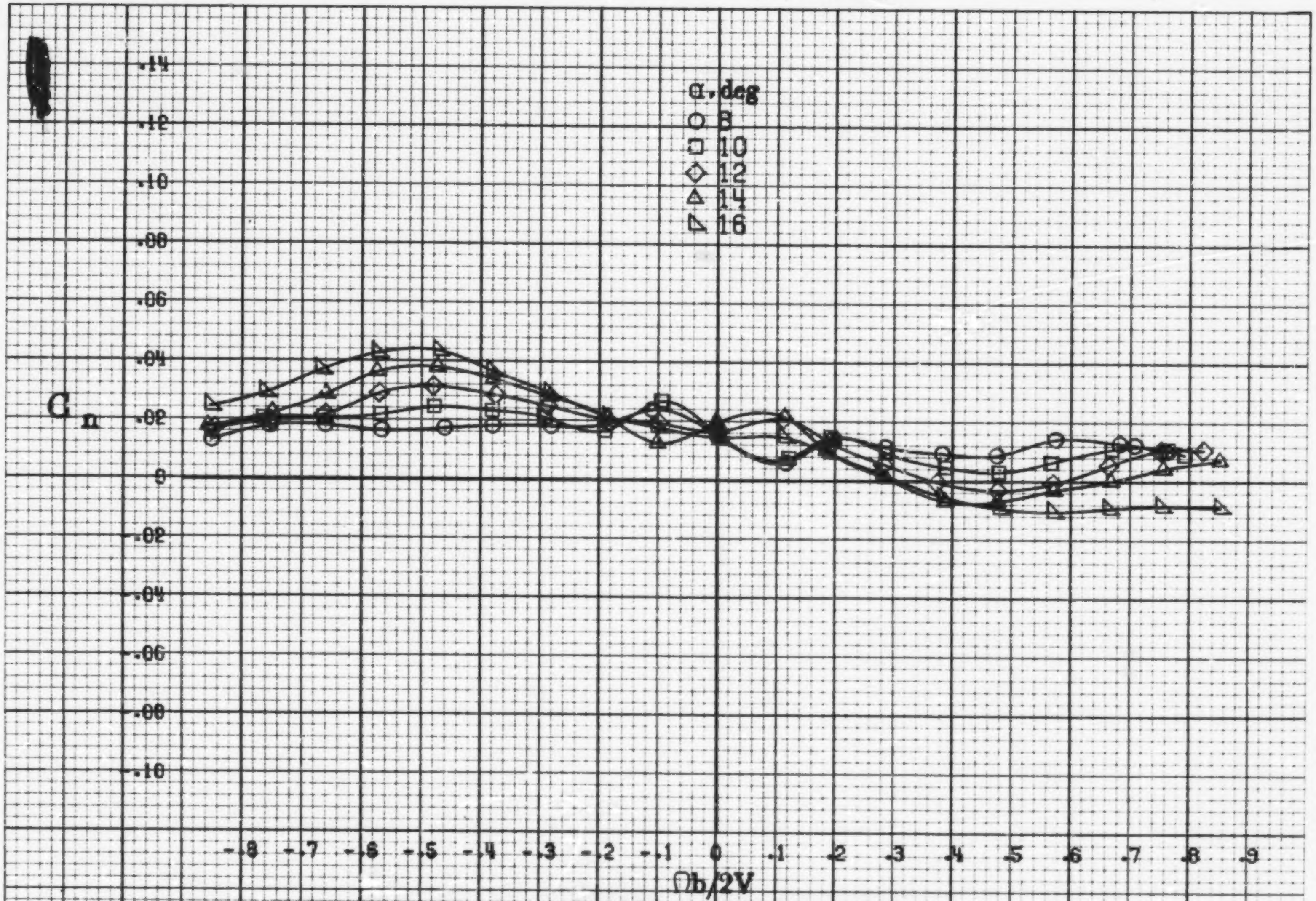

(a) α = 8 to 16 deg, SR = 76 cm (30 in).

Figure A31.- Effect of rotation rate and angle of attack on yawing-moment coefficient for basic configuration. $\delta_e = -25°$, $\delta_a = 22.5°$, $\delta_r = 25°$, $\beta = 0°$.

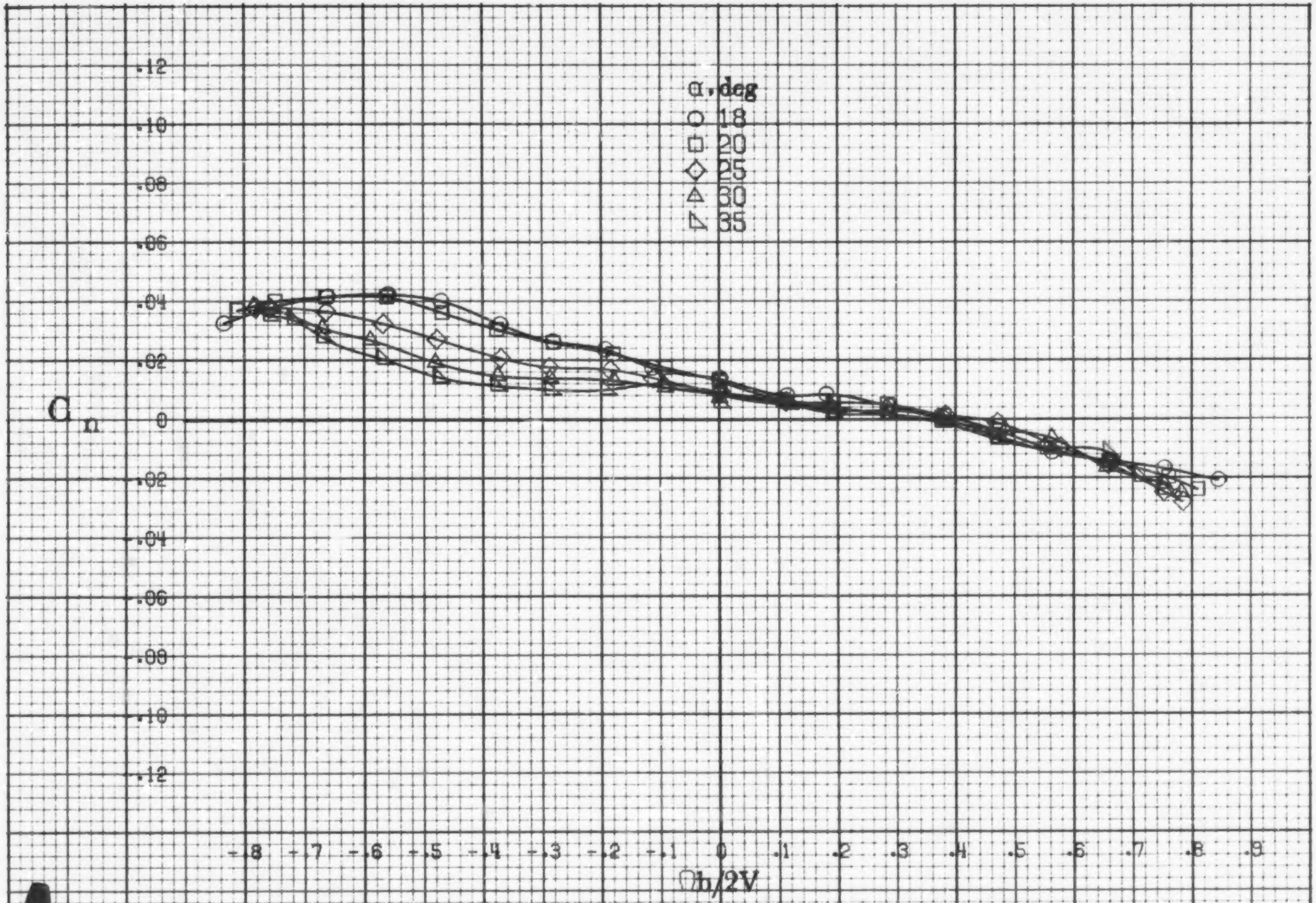

(b) α = 18 to 35 deg, SR = 76 cm (30 in).

Figure A31. Continued.

A124

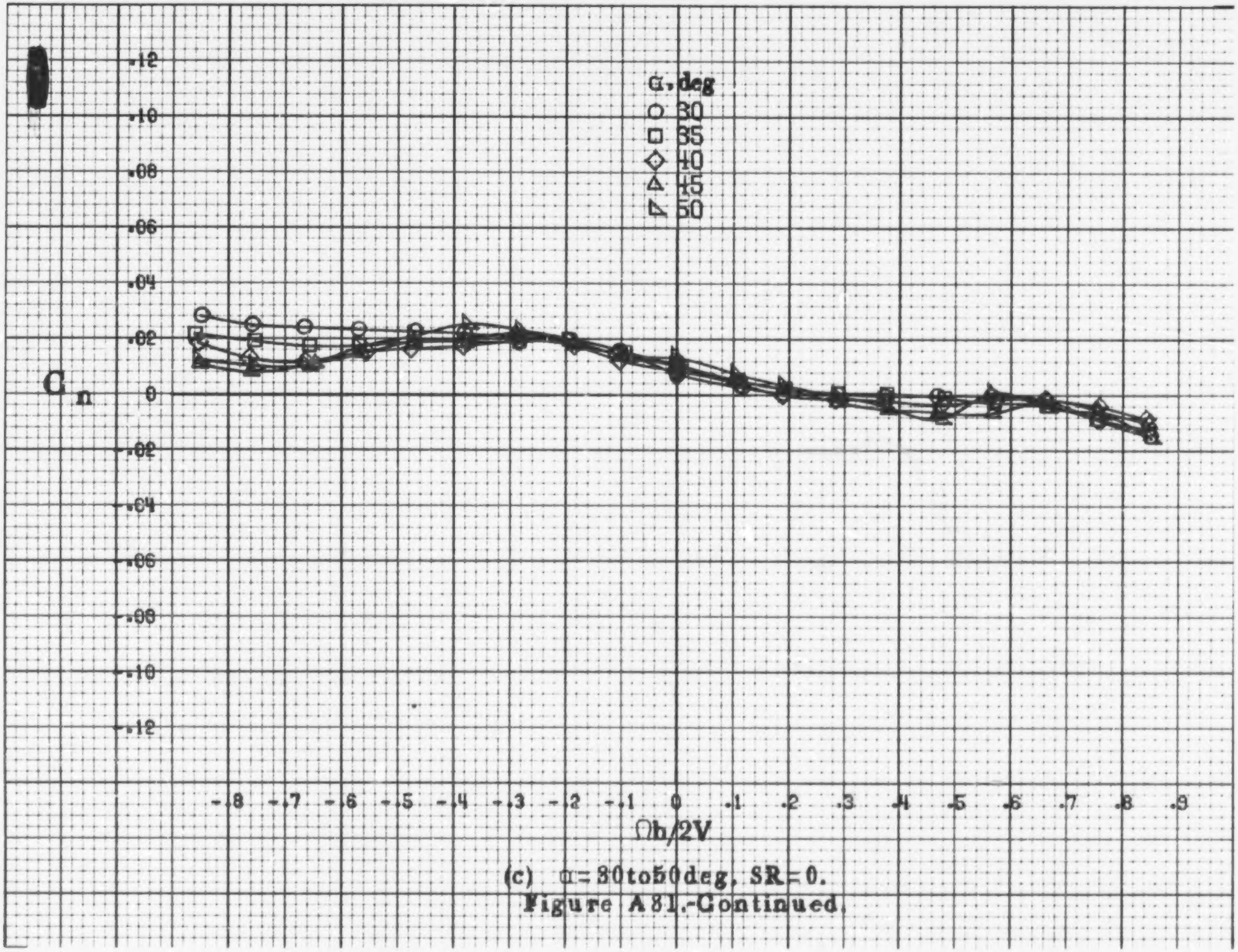

(c) α = 30 to 50 deg, SR = 0.

Figure A81.-Continued.

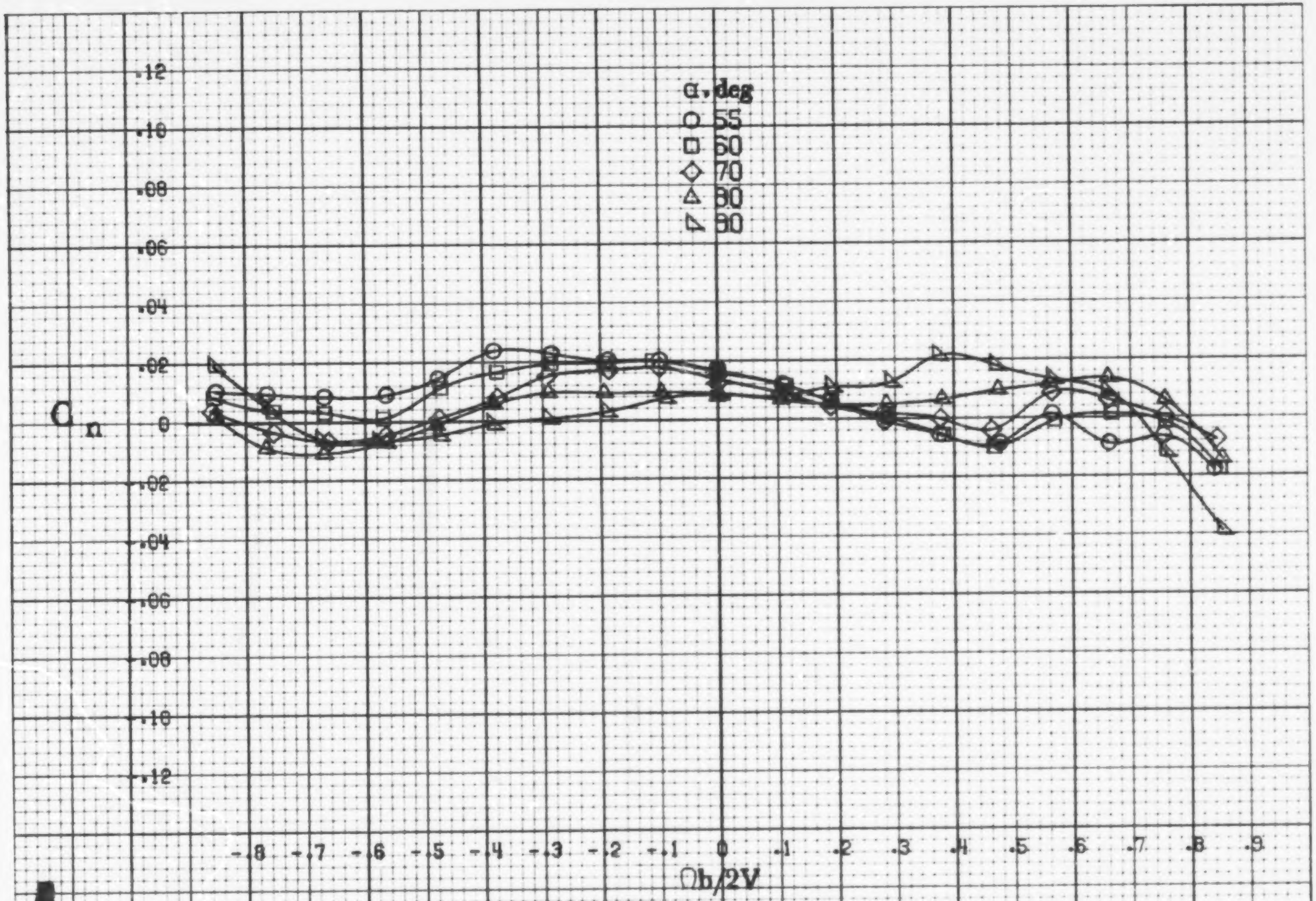

(d) $\alpha = 55$ to 90 deg, $\delta R = 0$.

Figure A81.-Concluded.

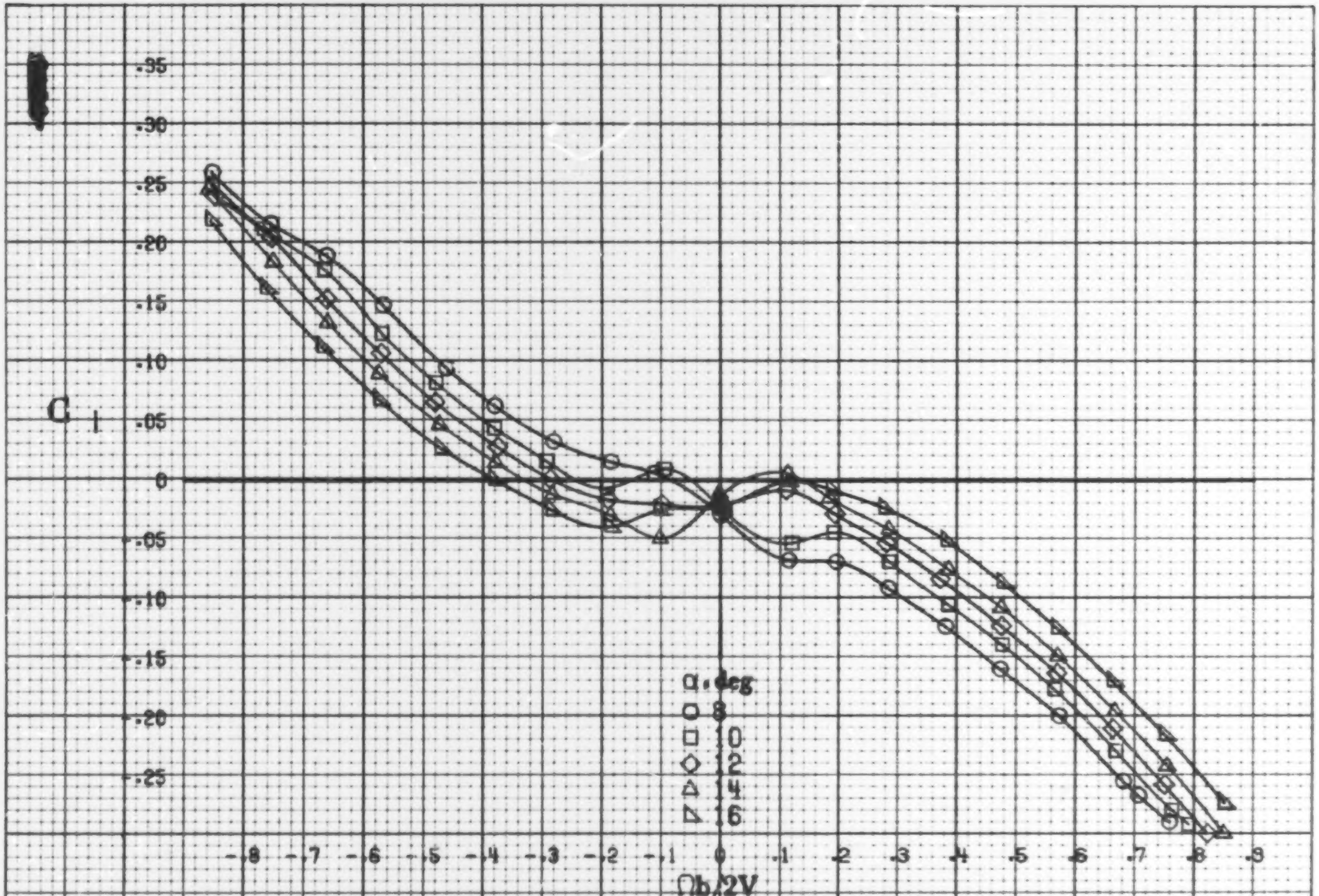

(a) α = 8 to 16 deg, SR = 76 cm (30 in).

Figure A32.-Effect of rotation rate and angle of attack on rolling-moment coefficient for basic configuration. $\delta_e = -25°$, $\delta_a = 22.5°$, $\delta_r = 25°$, $\beta = 0°$.

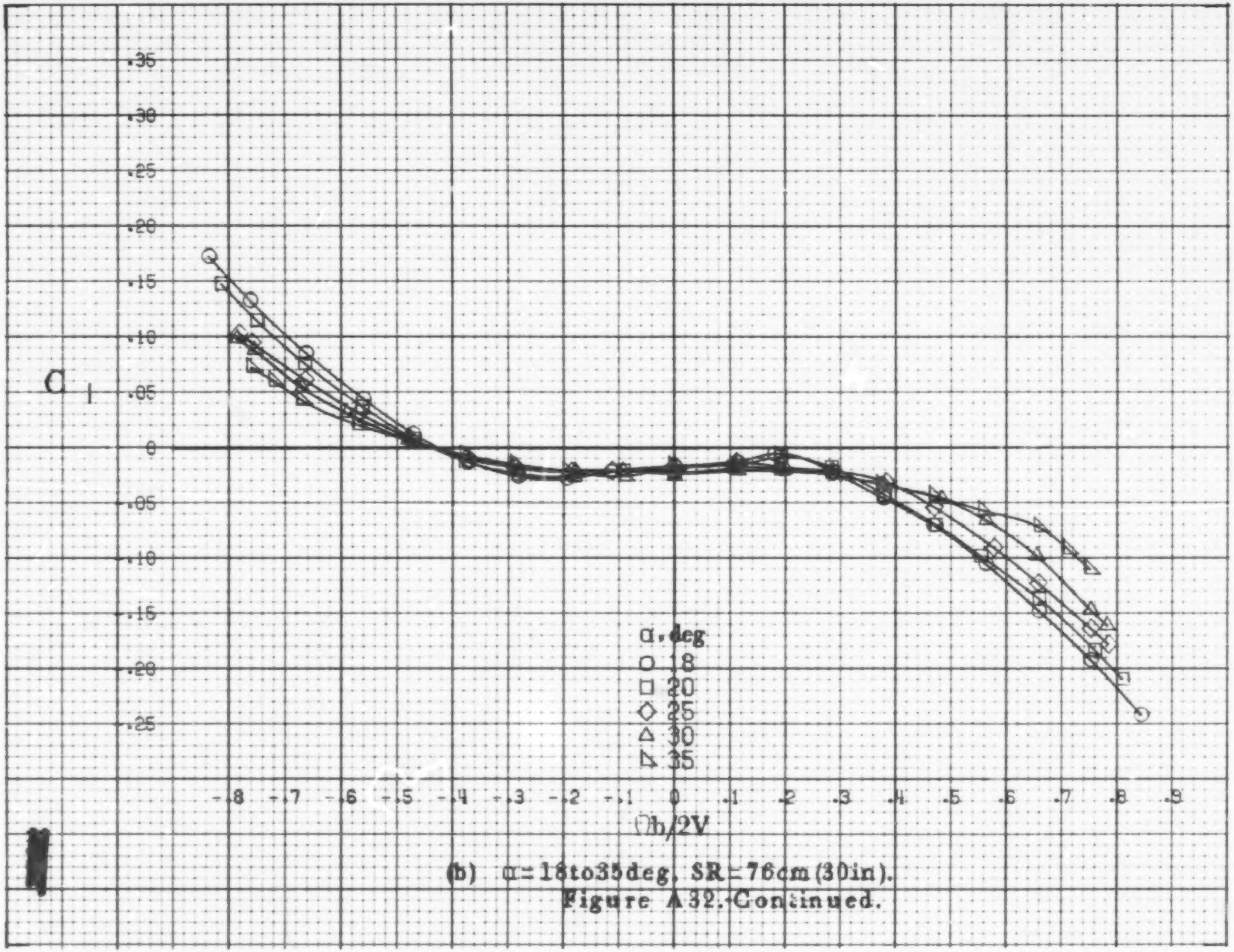

(b) α = 18 to 35 deg, SR = 76 cm (30 in).

Figure A32.- Continued.

A128

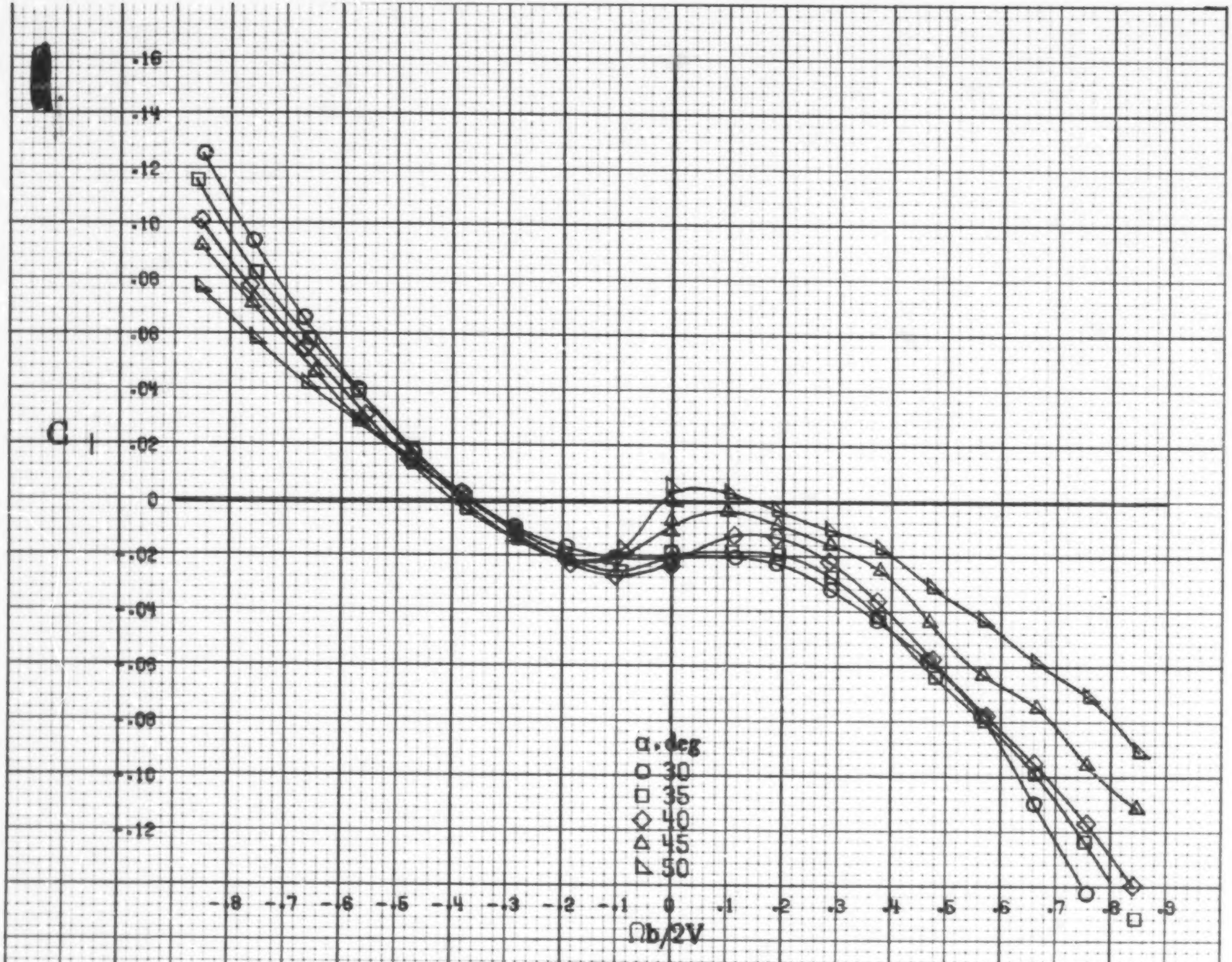

(c) α = 30 to 50 deg, SR = 0.

Figure A32.-Continued.

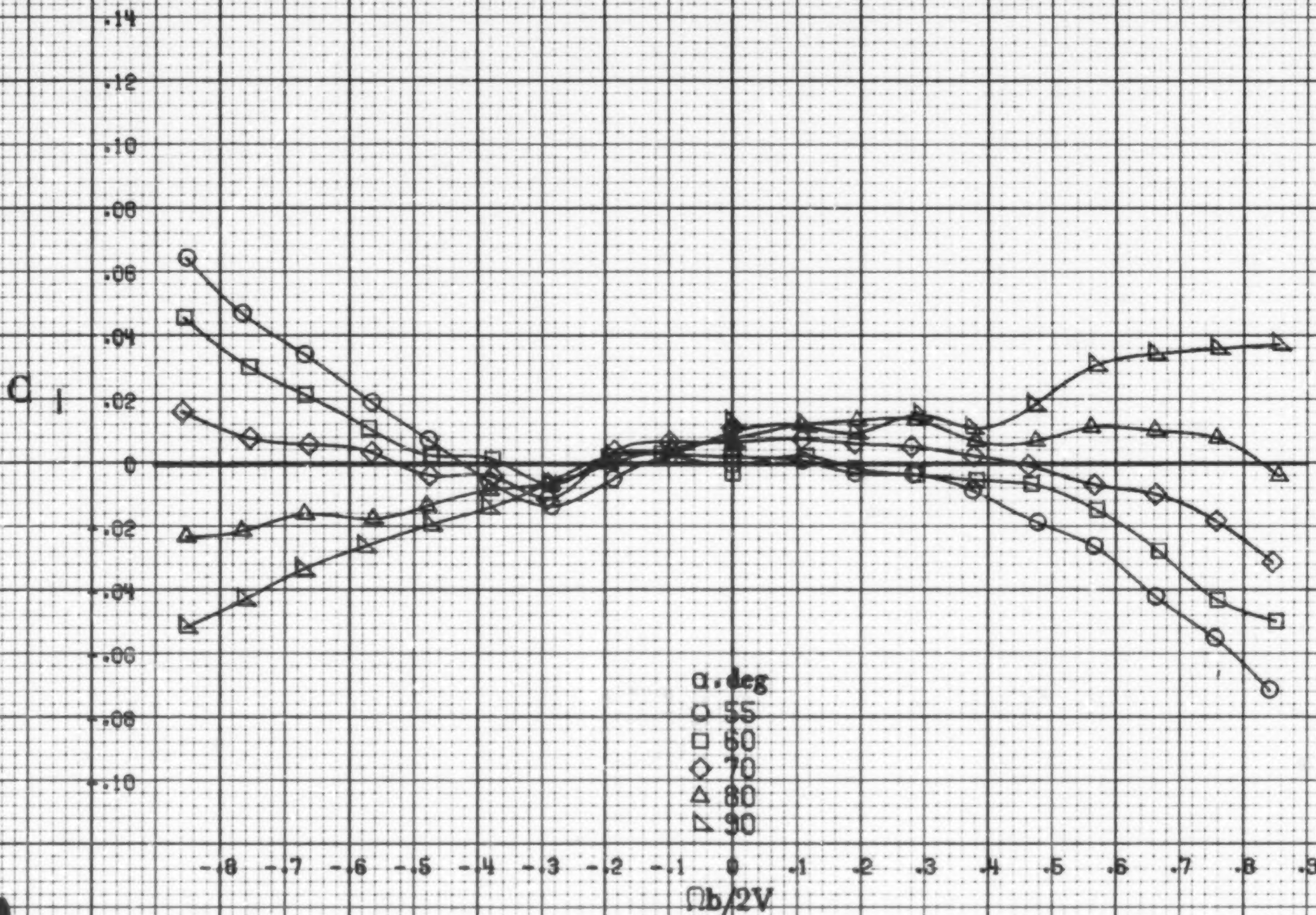

(d) α = 55 to 90 deg, SR = 0.

Figure A82.-Concluded.

A130

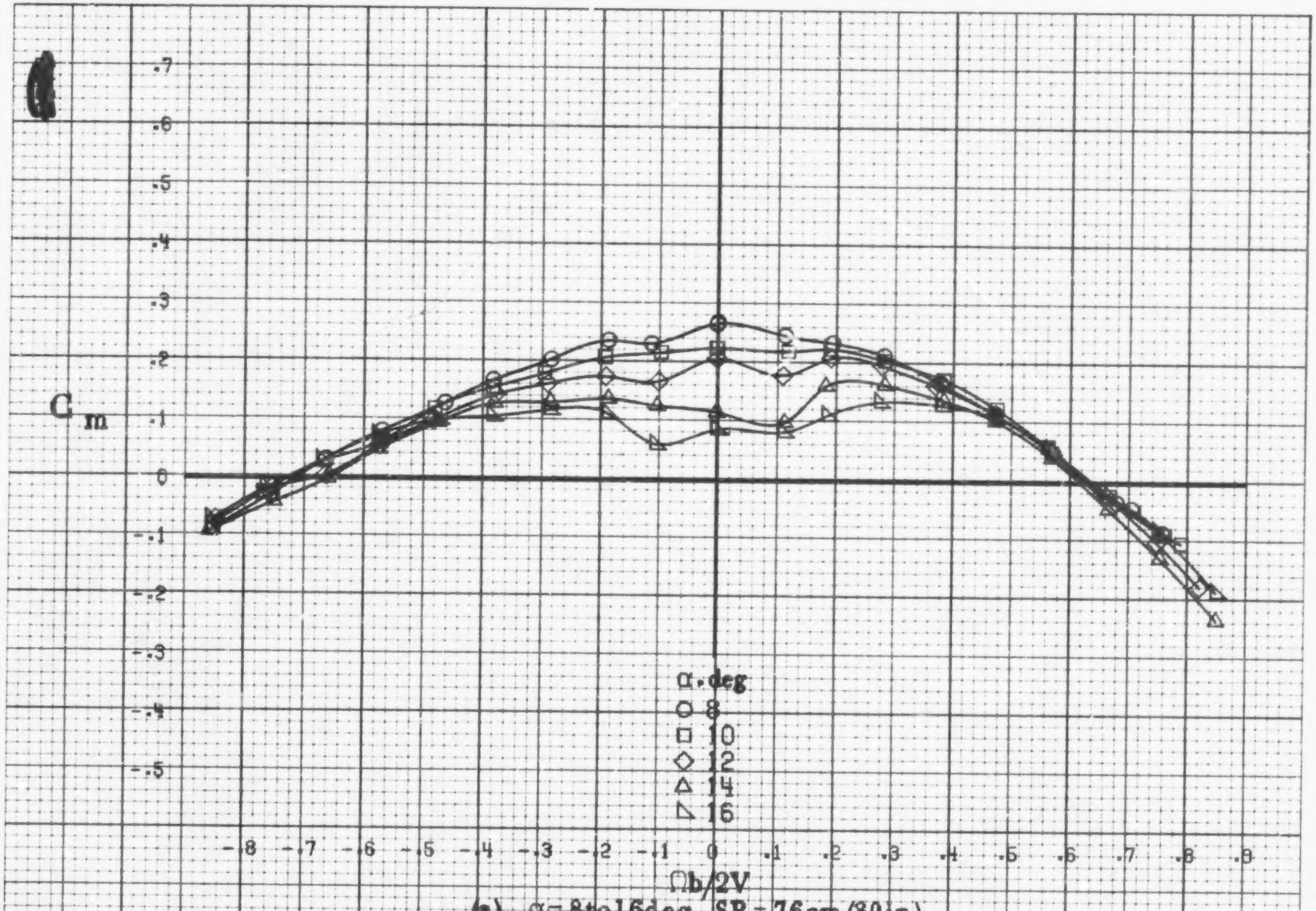

(a) $\alpha = 8$ to 16 deg, SR = 76 cm (30 in).

Figure A38.-Effect of rotation rate and angle of attack on pitching-moment coefficient for basic configuration. $\delta_e = -25°$. $\delta_a = 22.5°$. $\delta_r = 25°$. $\beta = 0°$.

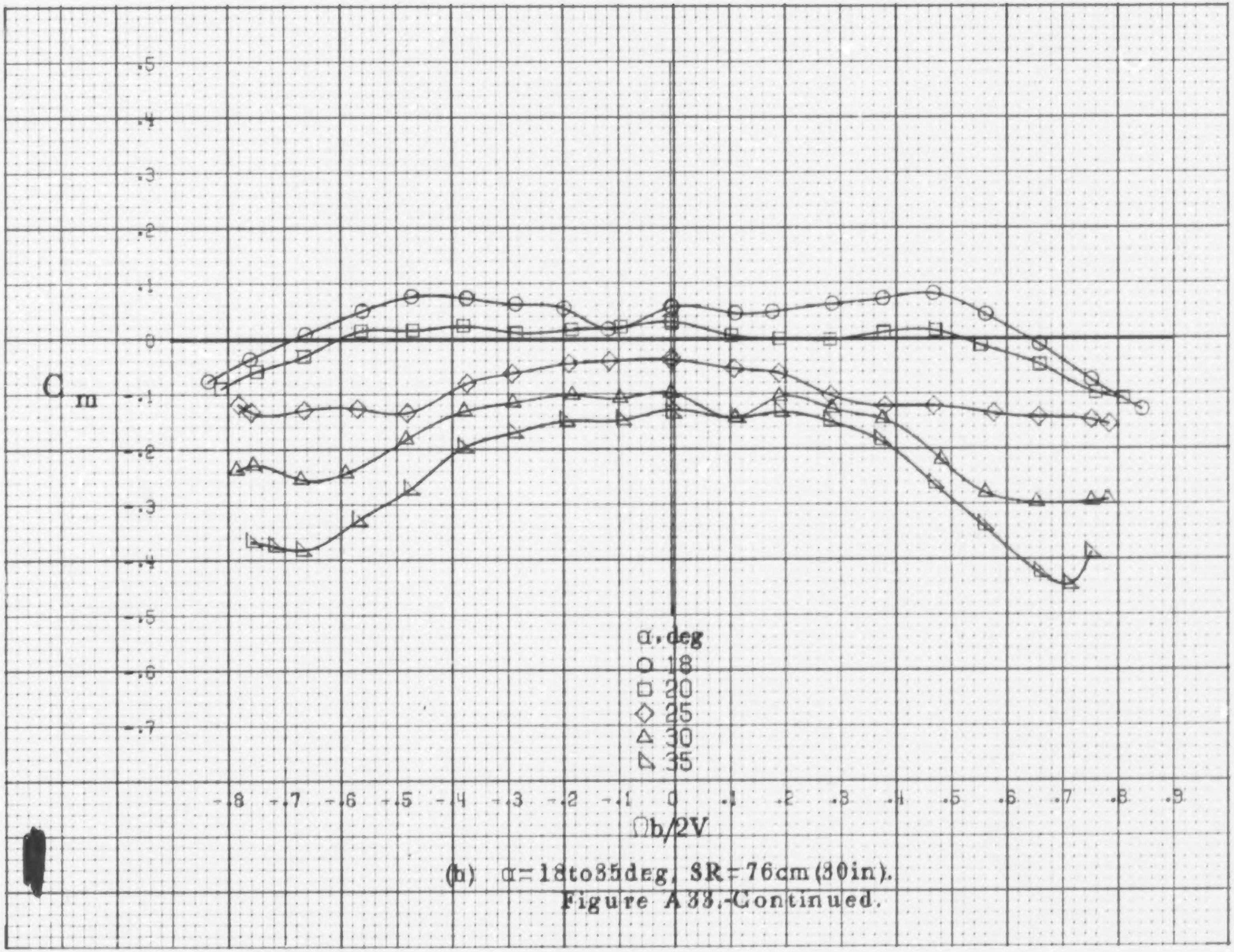

(b) α = 18 to 35 deg, SR = 76 cm (30 in).

Figure A33.- Continued.

A132

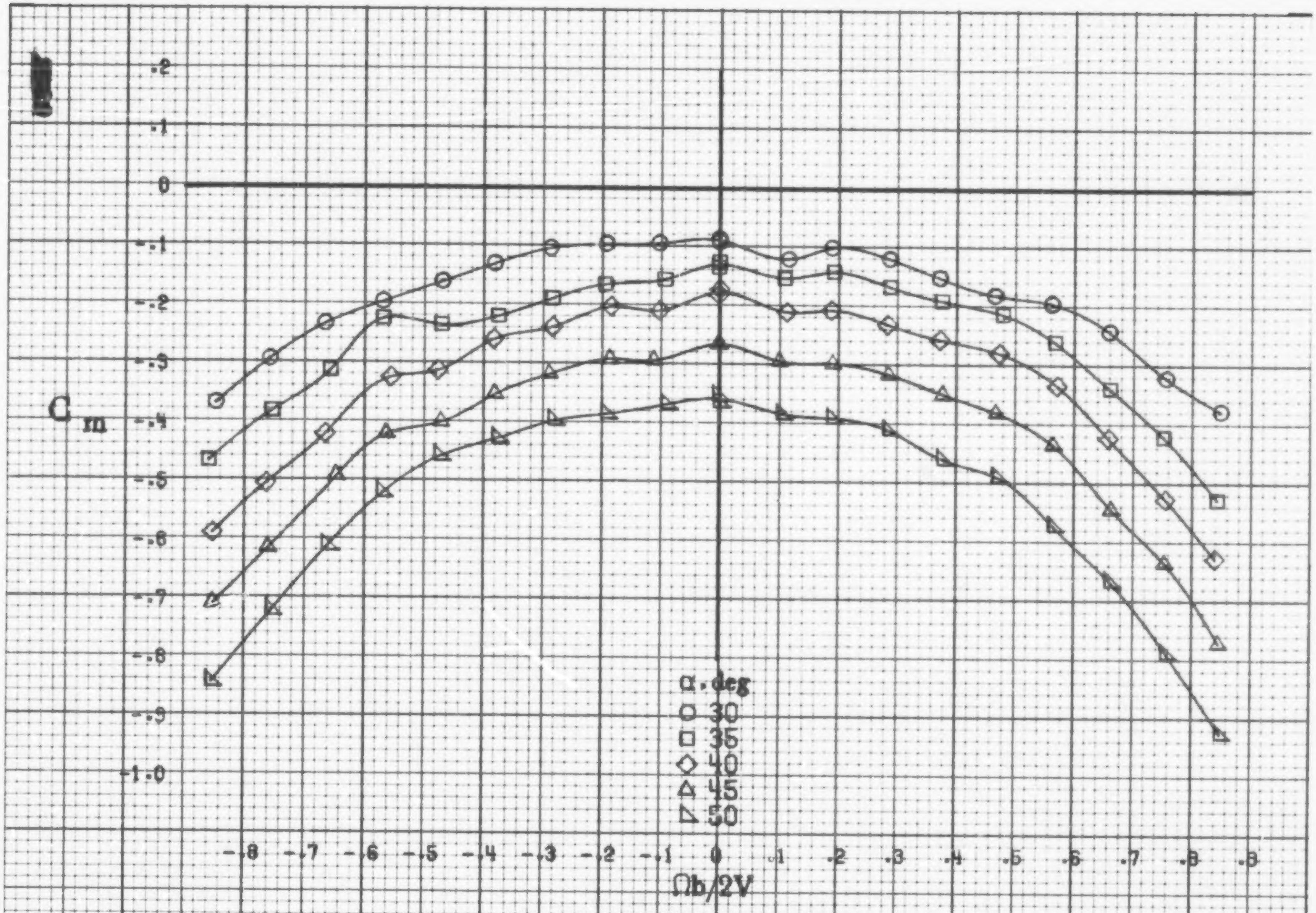

(c) α = 30 to 50 deg, SR = 0.
Figure A33.-Continued.

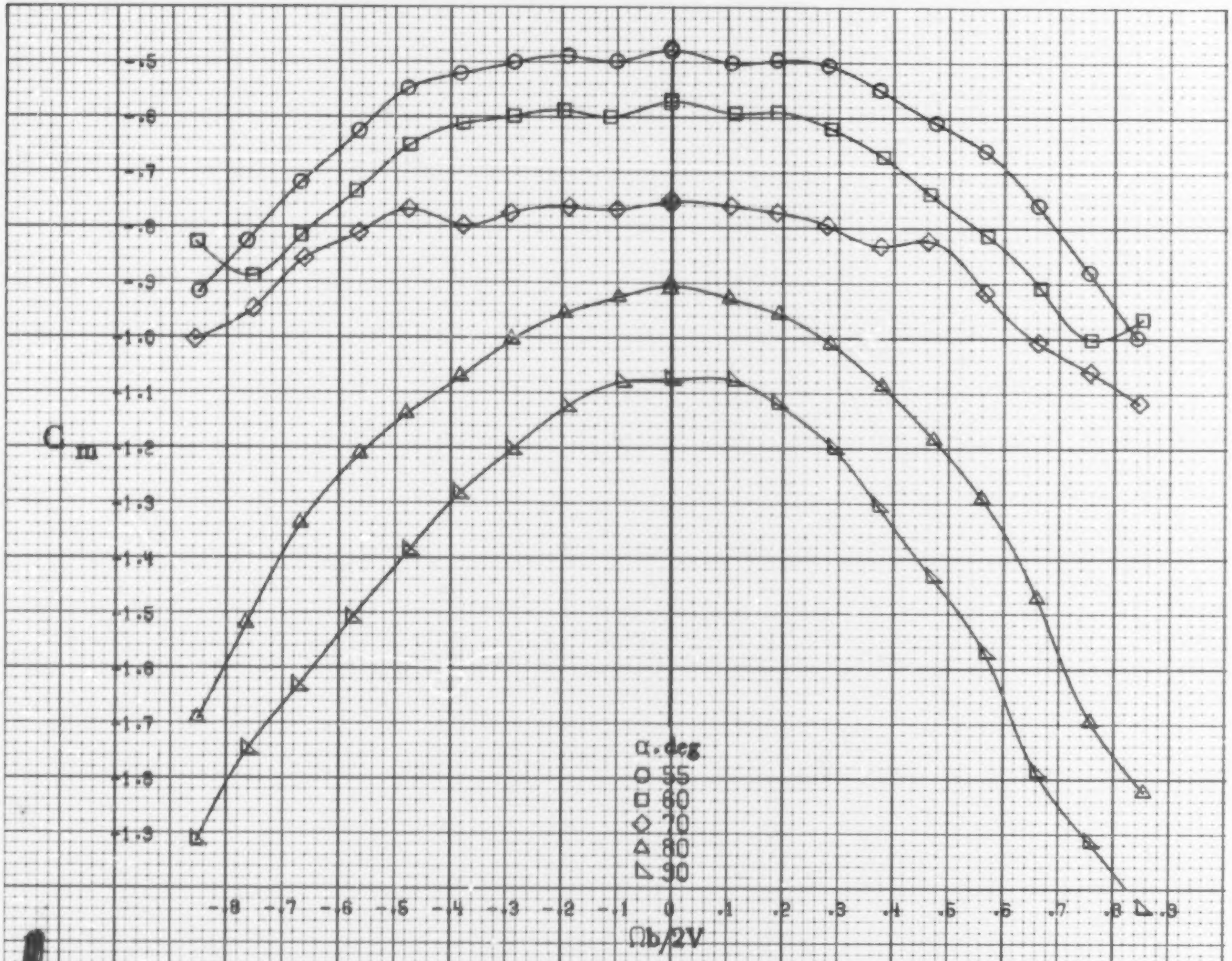

(d) $\alpha = 55$ to 90 deg, SR = 0.

Figure A88.-Concluded.

A134

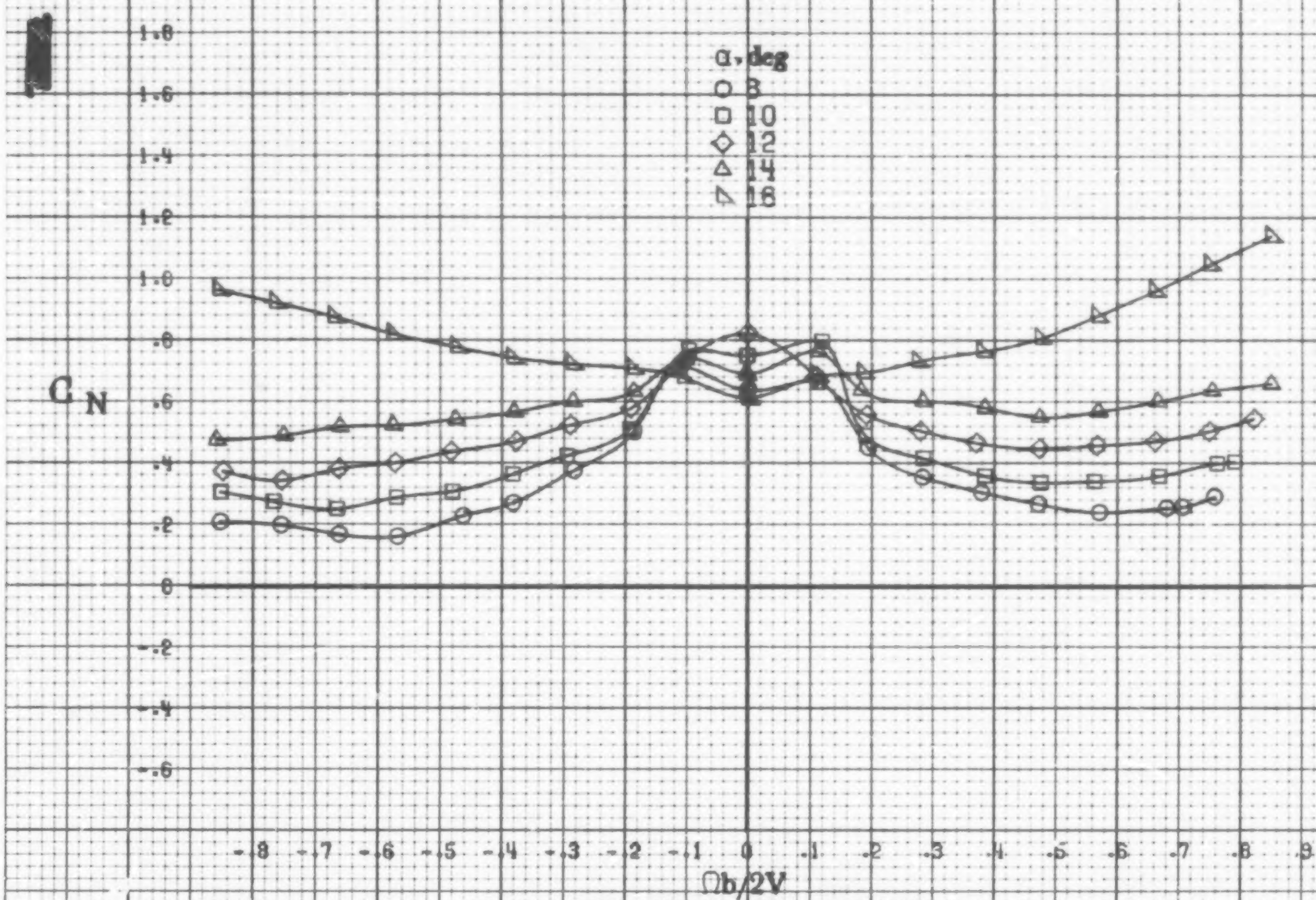

(a) α = 8 to 16 deg, SR = 76 cm (30 in).

Figure A34.- Effect of rotation rate and angle of attack on normal-force coefficient for basic configuration. $\delta_e = -25°$, $\delta_a = 22.5°$, $\delta_r = 25°$, $\beta = 0°$.

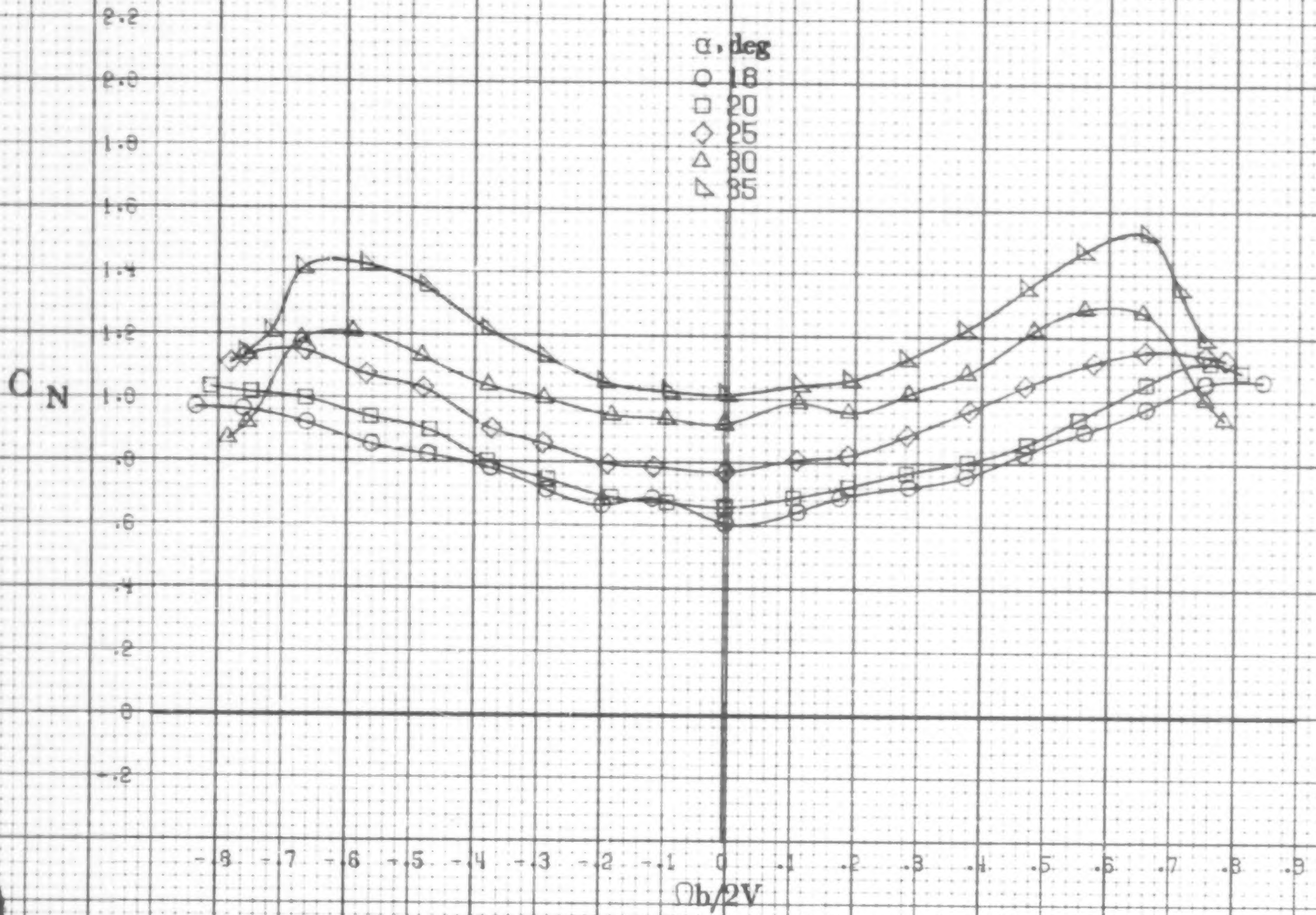

(b) α = 18 to 35 deg, SR = 76 cm (30 in).
Figure A34.- Continued.

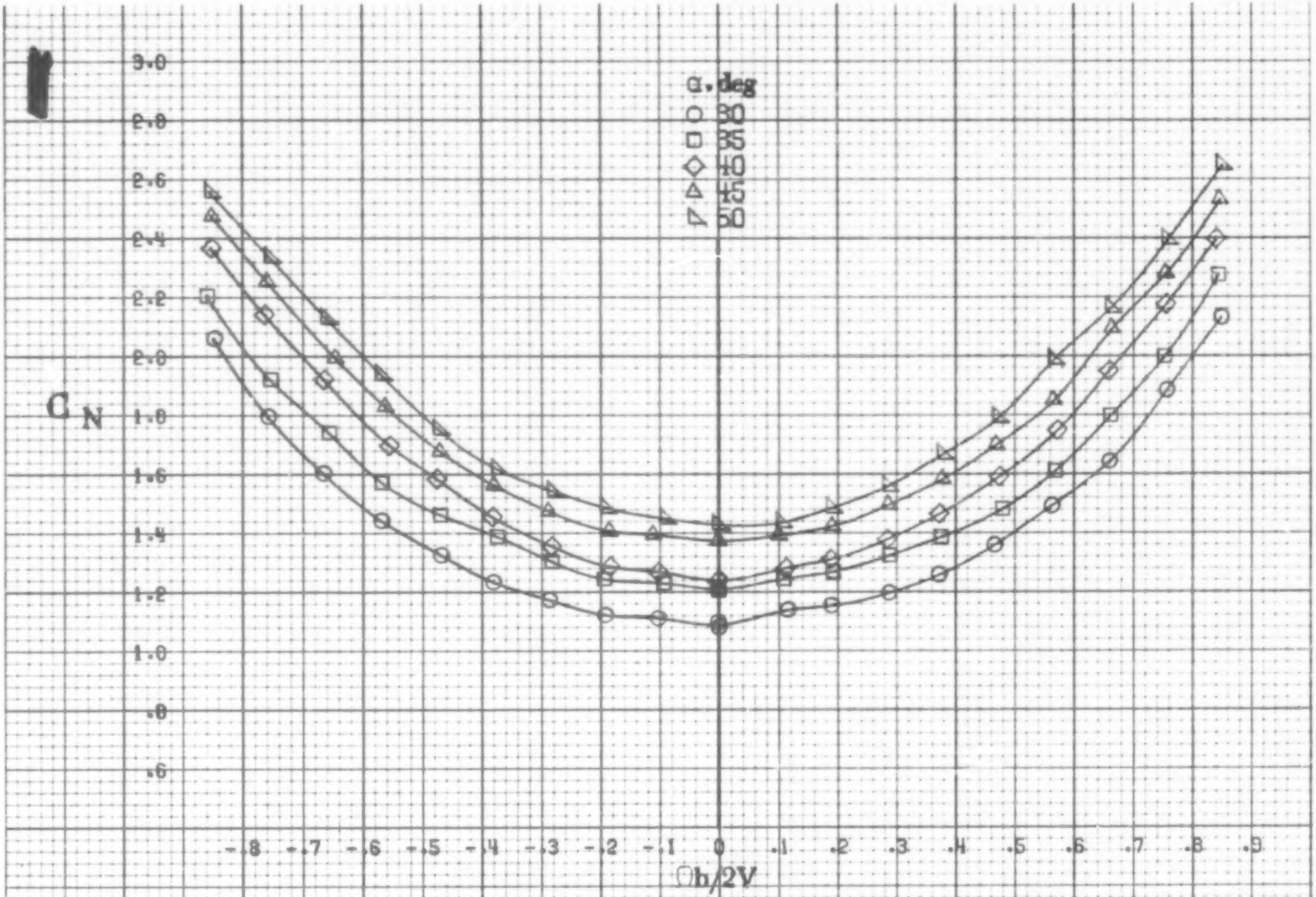

(c) α = 30 to 50 deg, SR = 0.
Figure A84.-Continued.

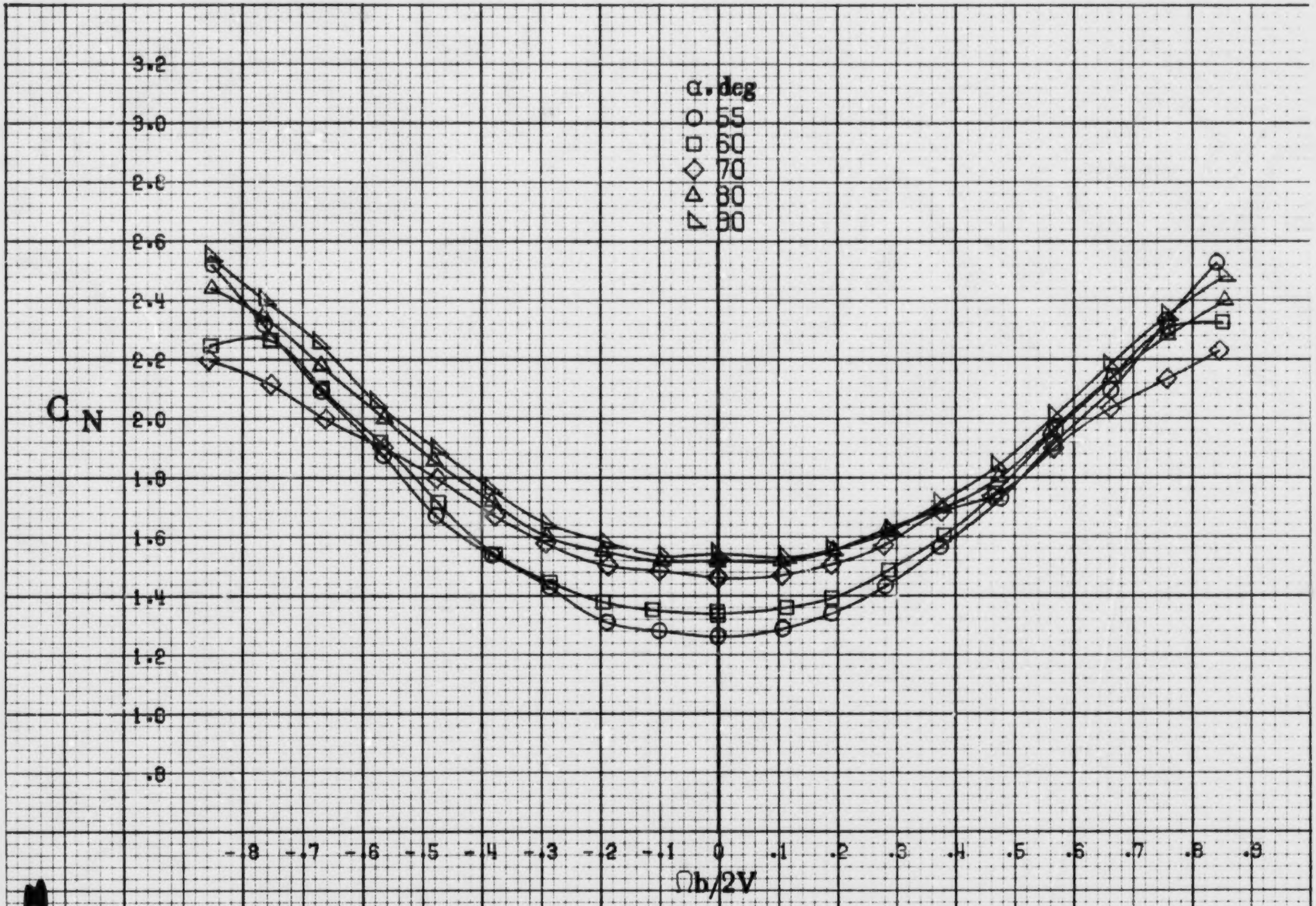

(d) α = 55 to 90 deg, SR = 0.

Figure A84.-Concluded.

A 138

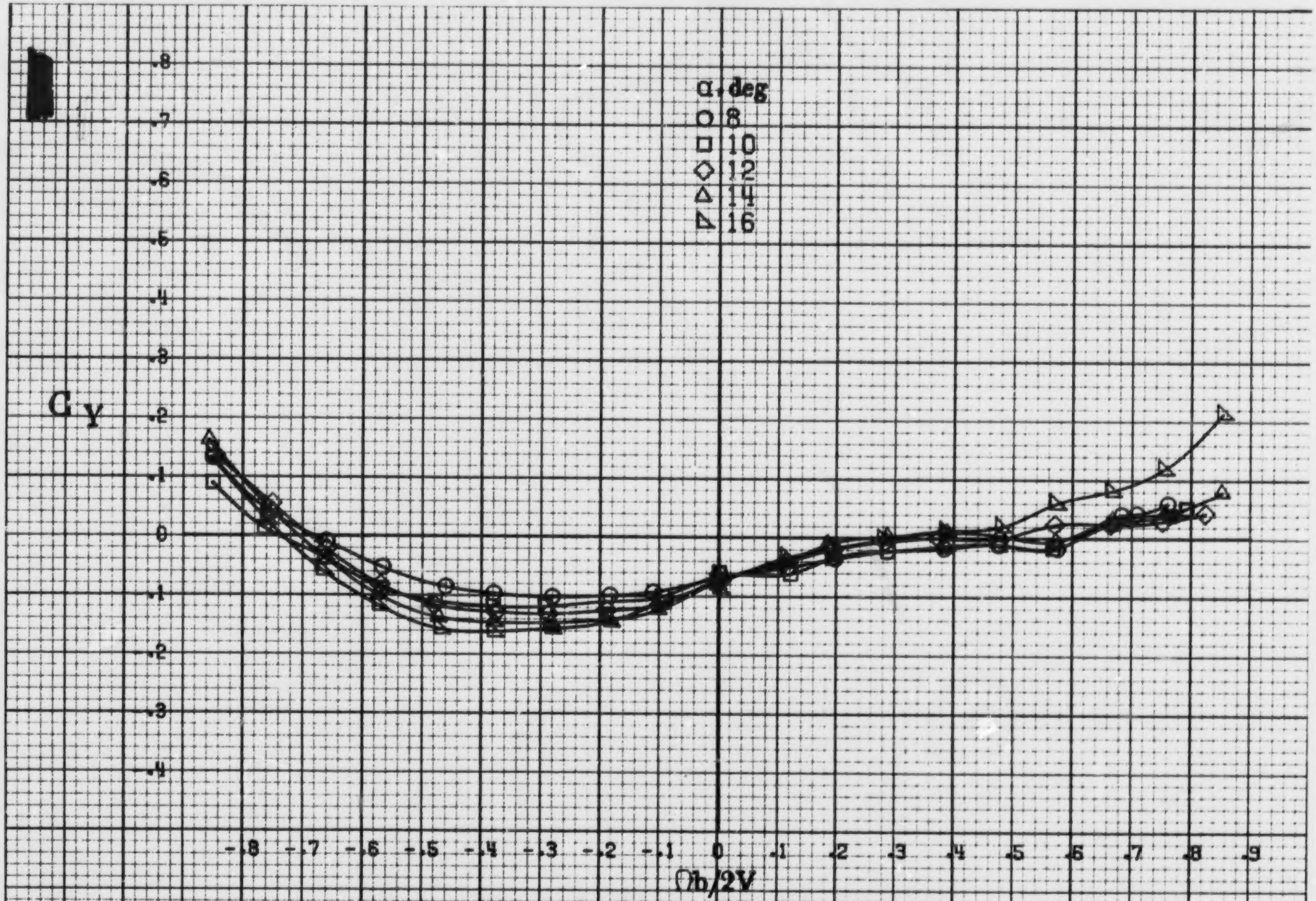

(a) α = 8 to 16 deg, SR = 76 cm (30 in).

Figure A35.-Effect of rotation rate and angle of attack on side-force coefficient for basic configuration. $\delta_e = -25°$, $\delta_a = 22.5°$, $\delta_r = 25°$, $\beta = 0°$.

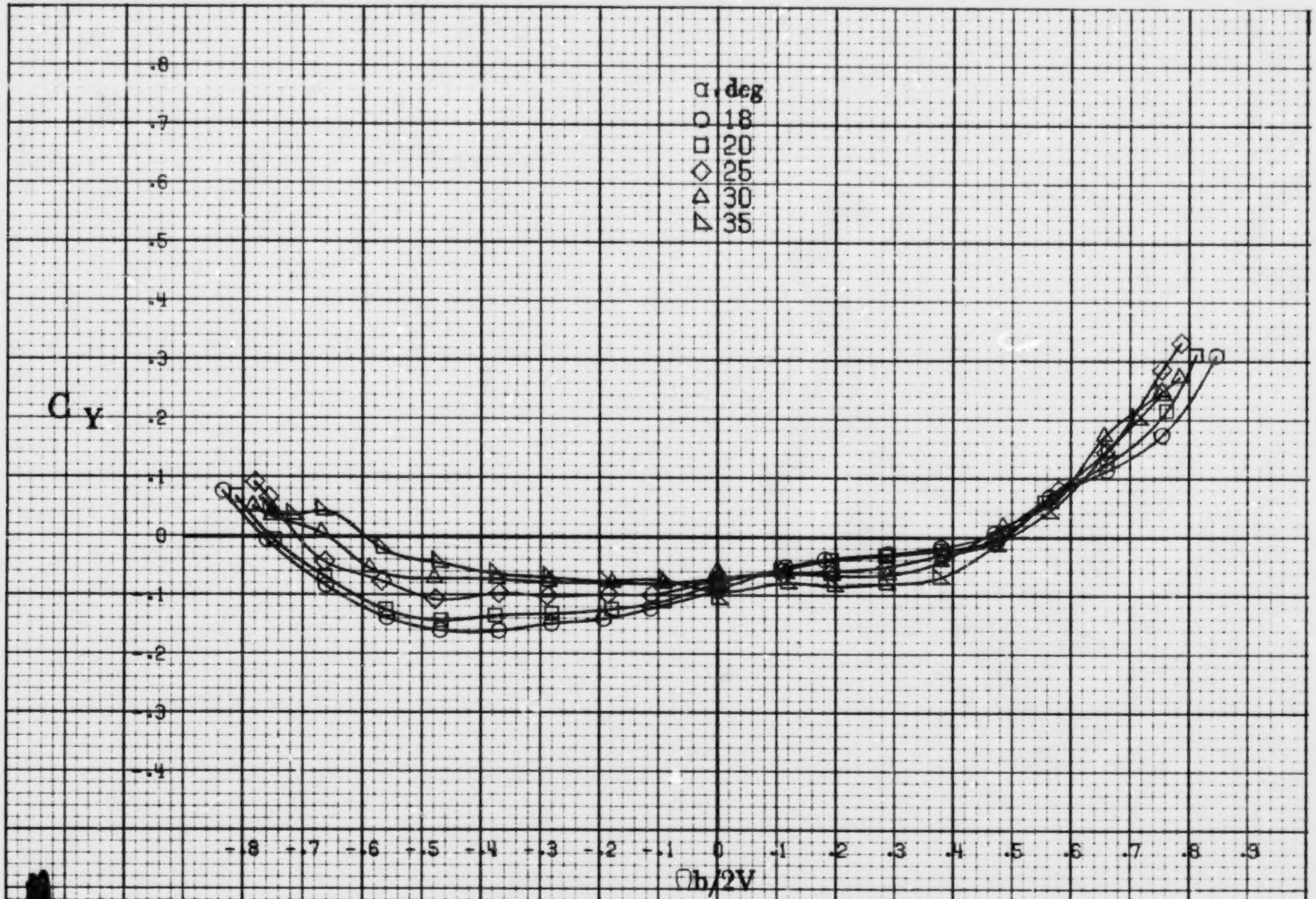

(b) α = 18 to 35 deg, SR = 76 cm (30 in).

Figure A35.- Continued.

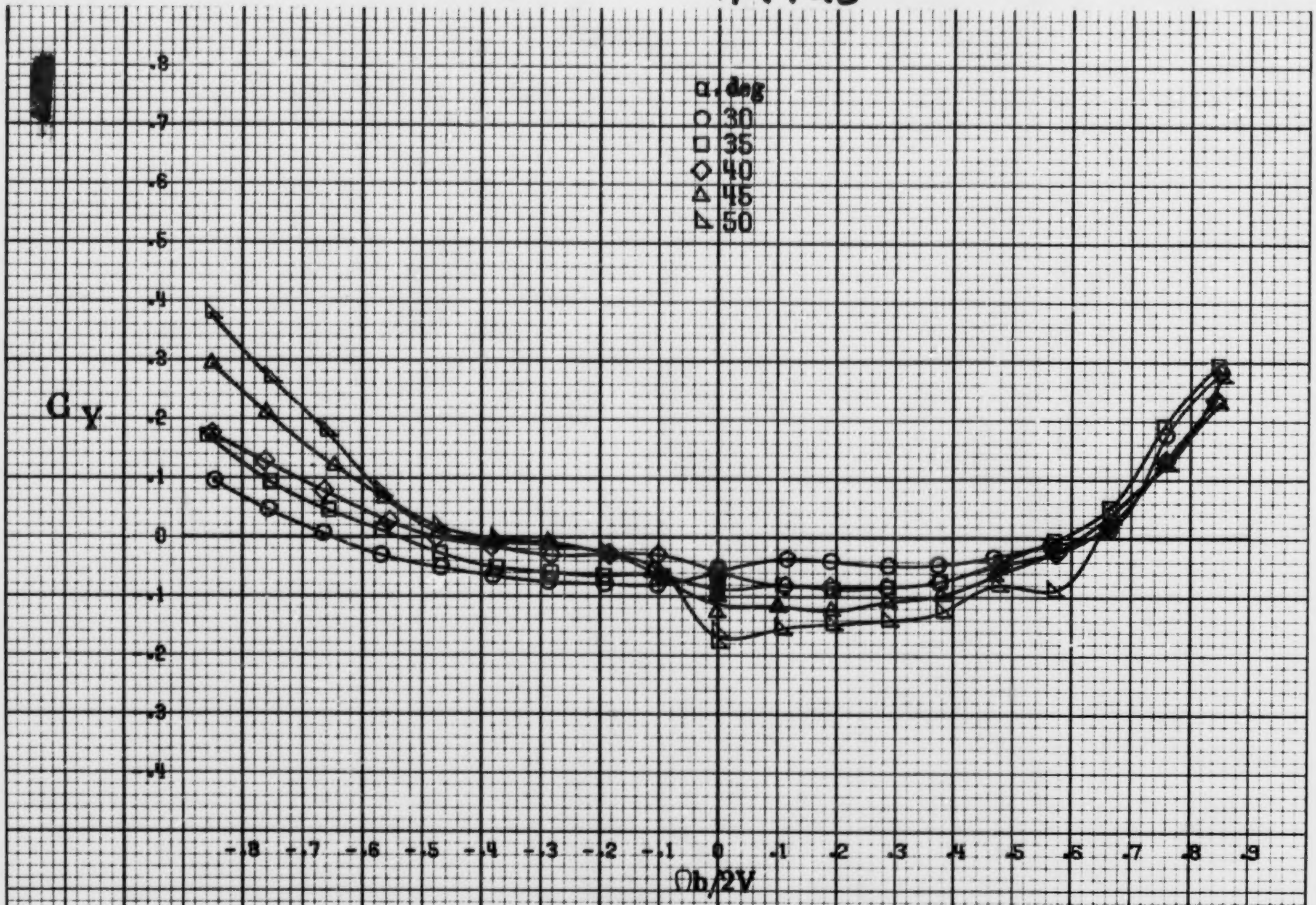

(c) $\alpha = 30$ to 50 deg, $\delta R = 0$.
Figure A85.-Continued.

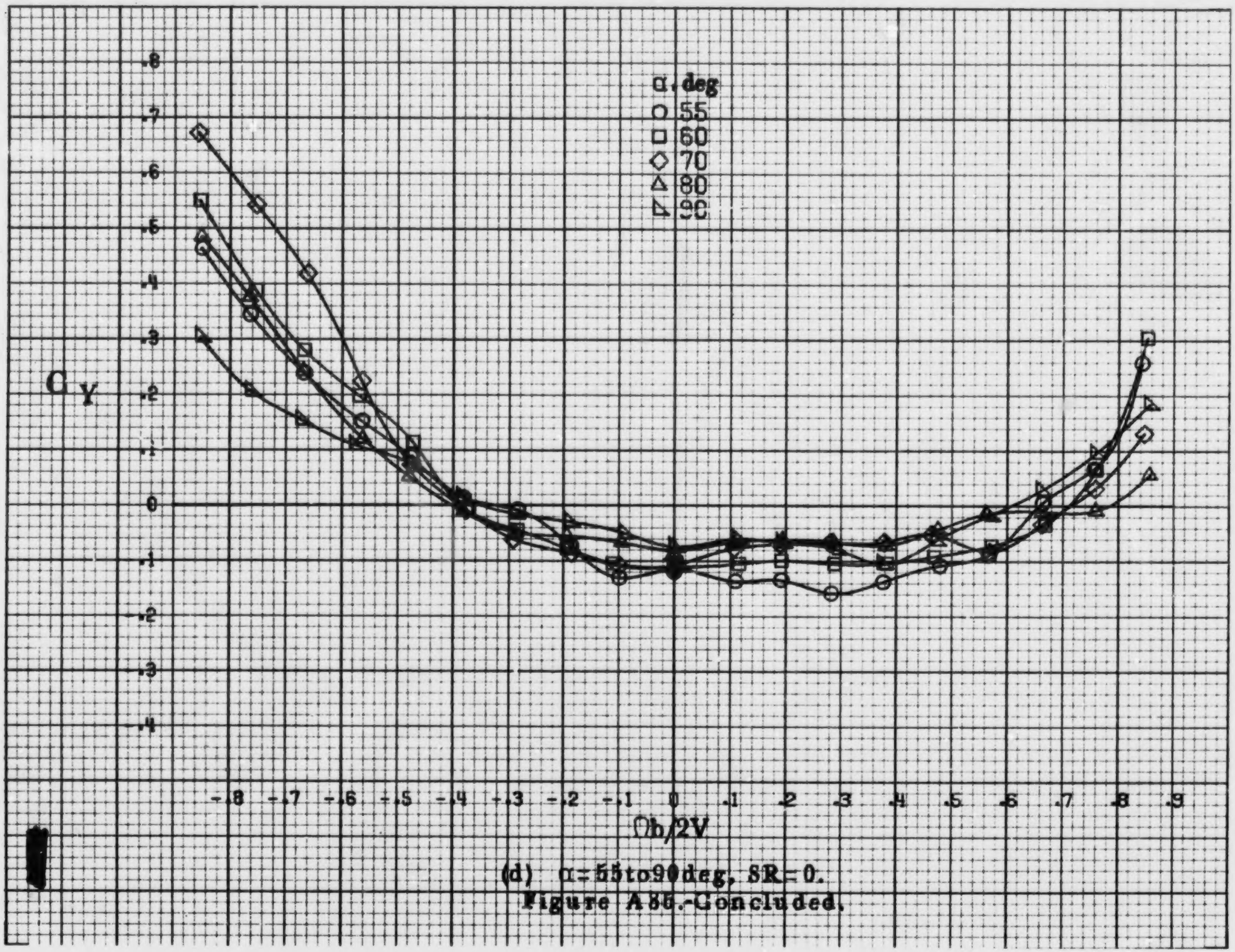

(d) α = 55 to 90 deg, SR = 0.

Figure A35.-Concluded.

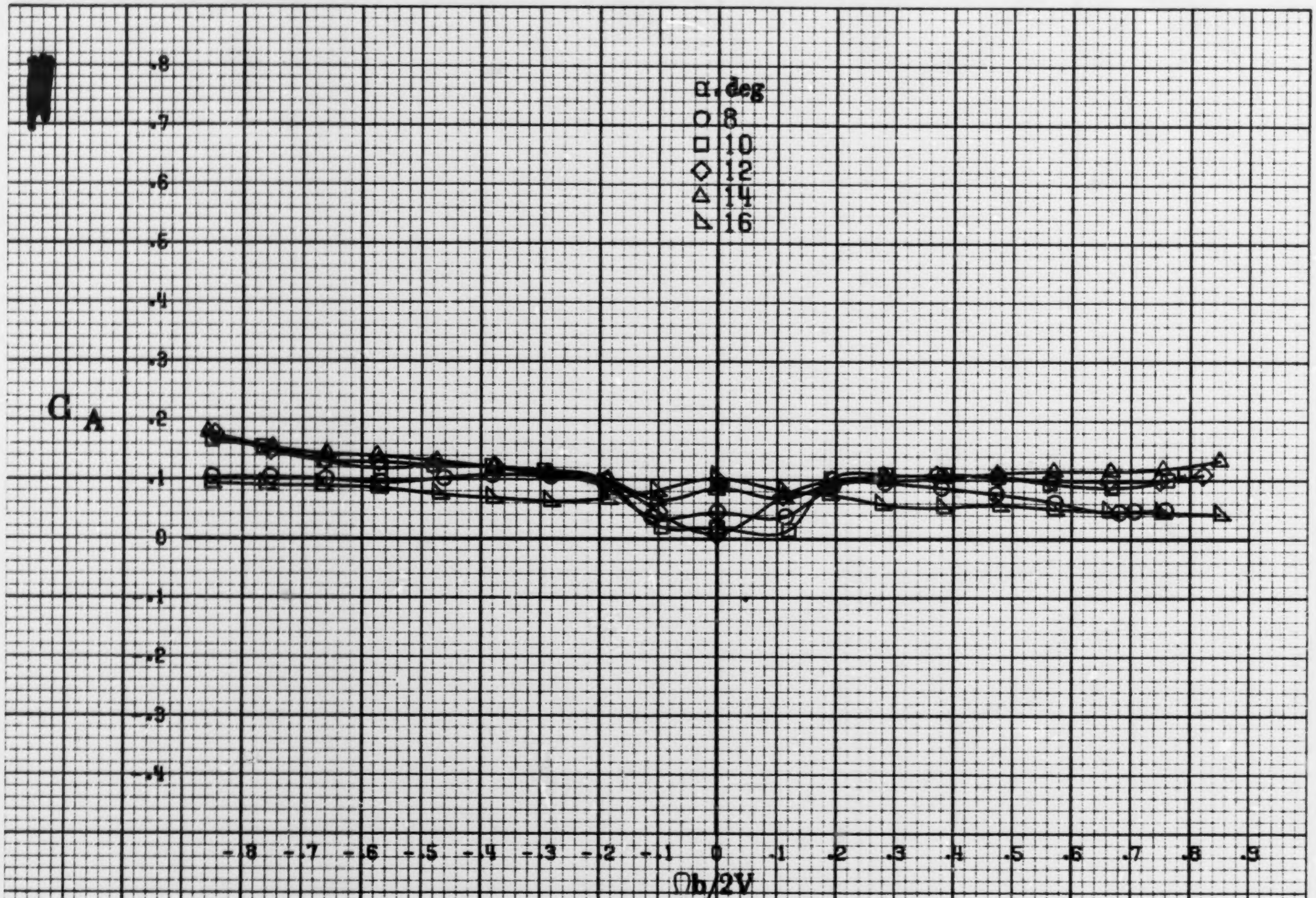

(a) $\alpha = 8$ to 16 deg, SR = 76 cm (30 in).

Figure A36.-Effect of rotation rate and angle of attack on axial-force coefficient for basic configuration. $\delta_e = -25°$, $\delta_a = 22.5°$, $\delta_r = -25°$, $\beta = 0°$.

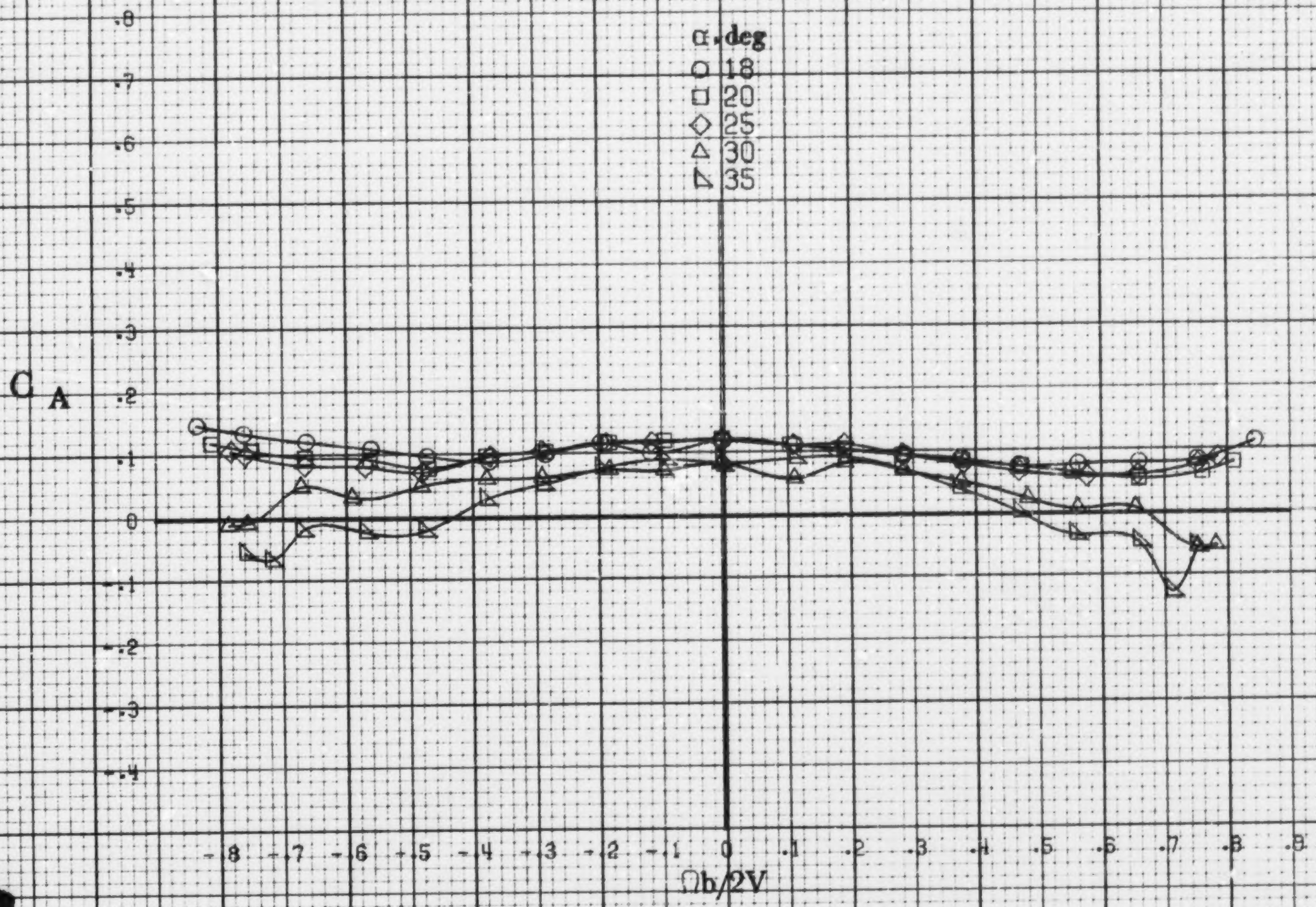

(b) α = 18 to 35 deg, SR = 76 cm (30 in).

Figure A36.-Continued.

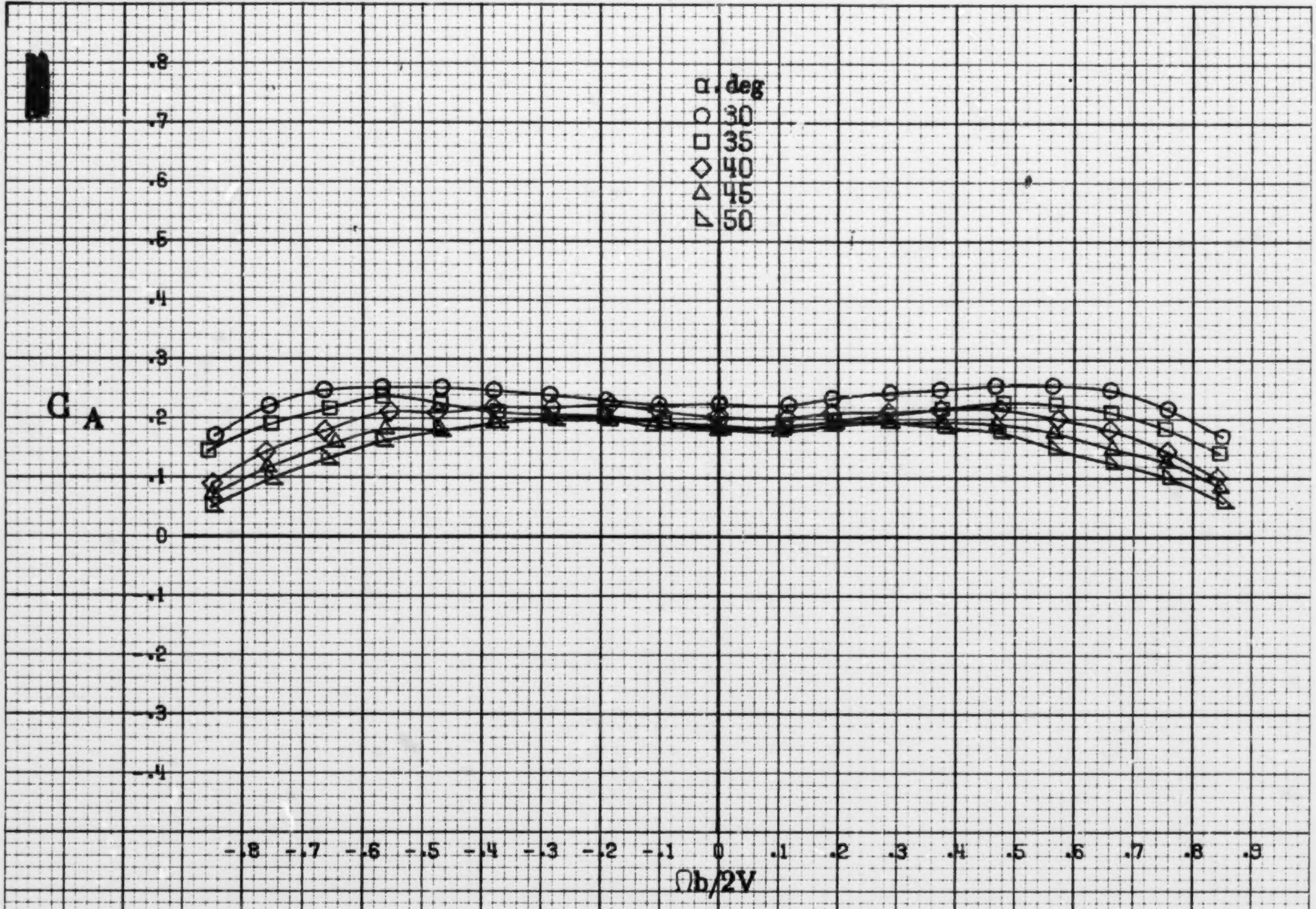

(c) α = 30 to 50 deg, SR = 0.

Figure A86.-Continued.

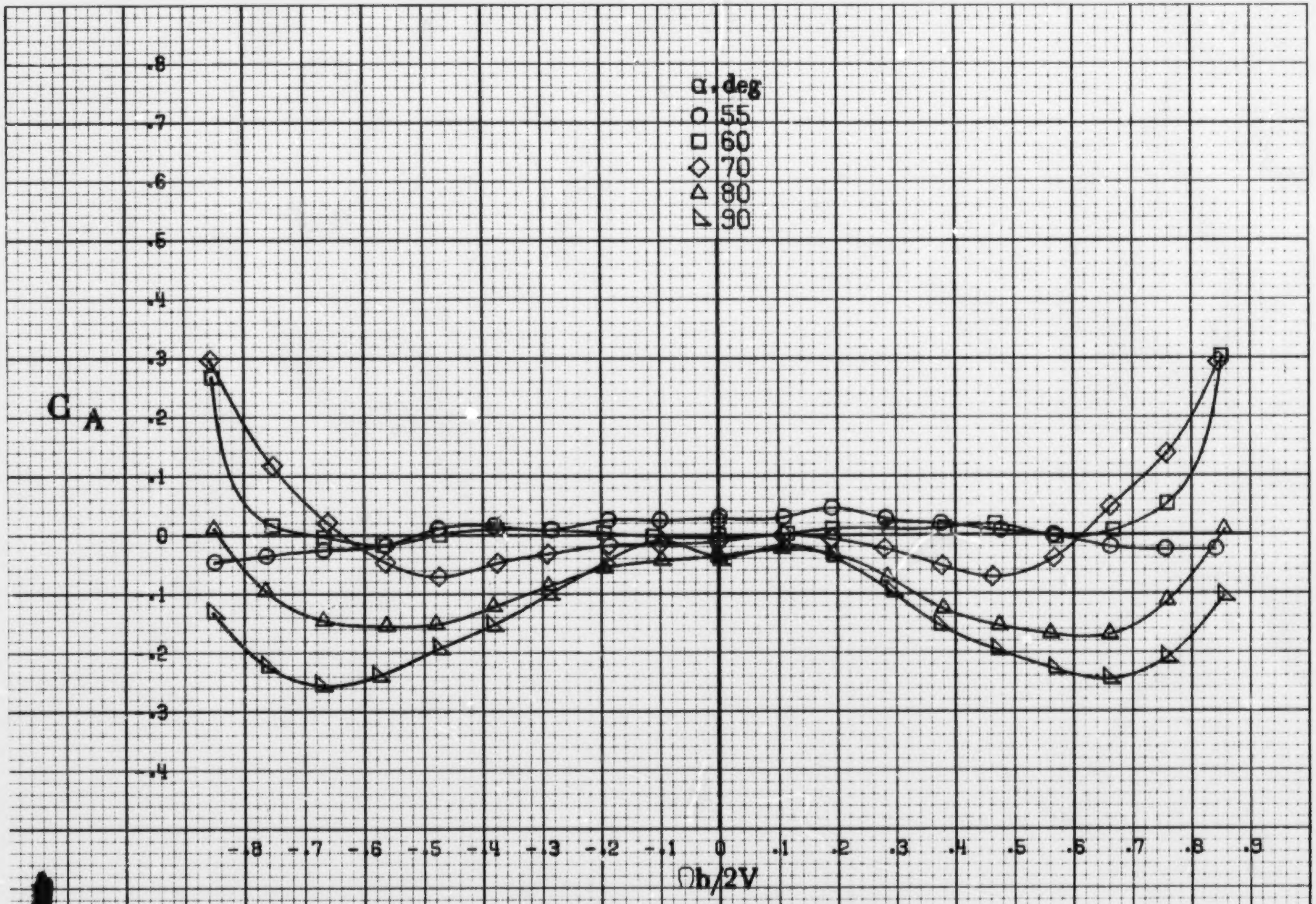

(d) α = 55 to 90 deg, SR = 0.

Figure A86.-Concluded.

A146

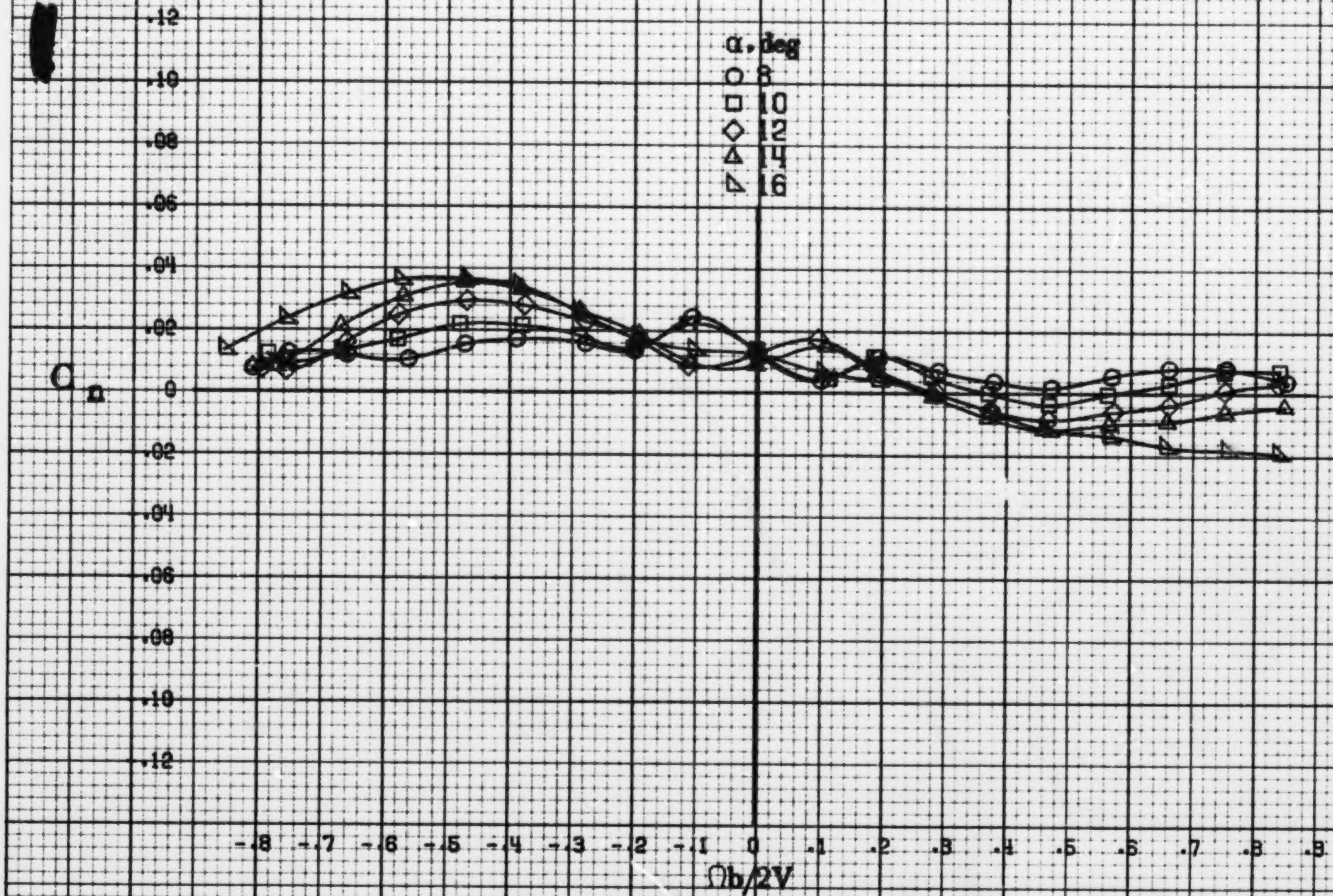

(a) α = 8 to 16 deg, SR = 76 cm (30 in).

Figure A37.- Effect of rotation rate and angle of attack on yawing-moment coefficient for basic configuration. $\delta_e = -25°$, $\delta_a = -22.5°$, $\delta_r = 25°$, $\beta = 0°$.

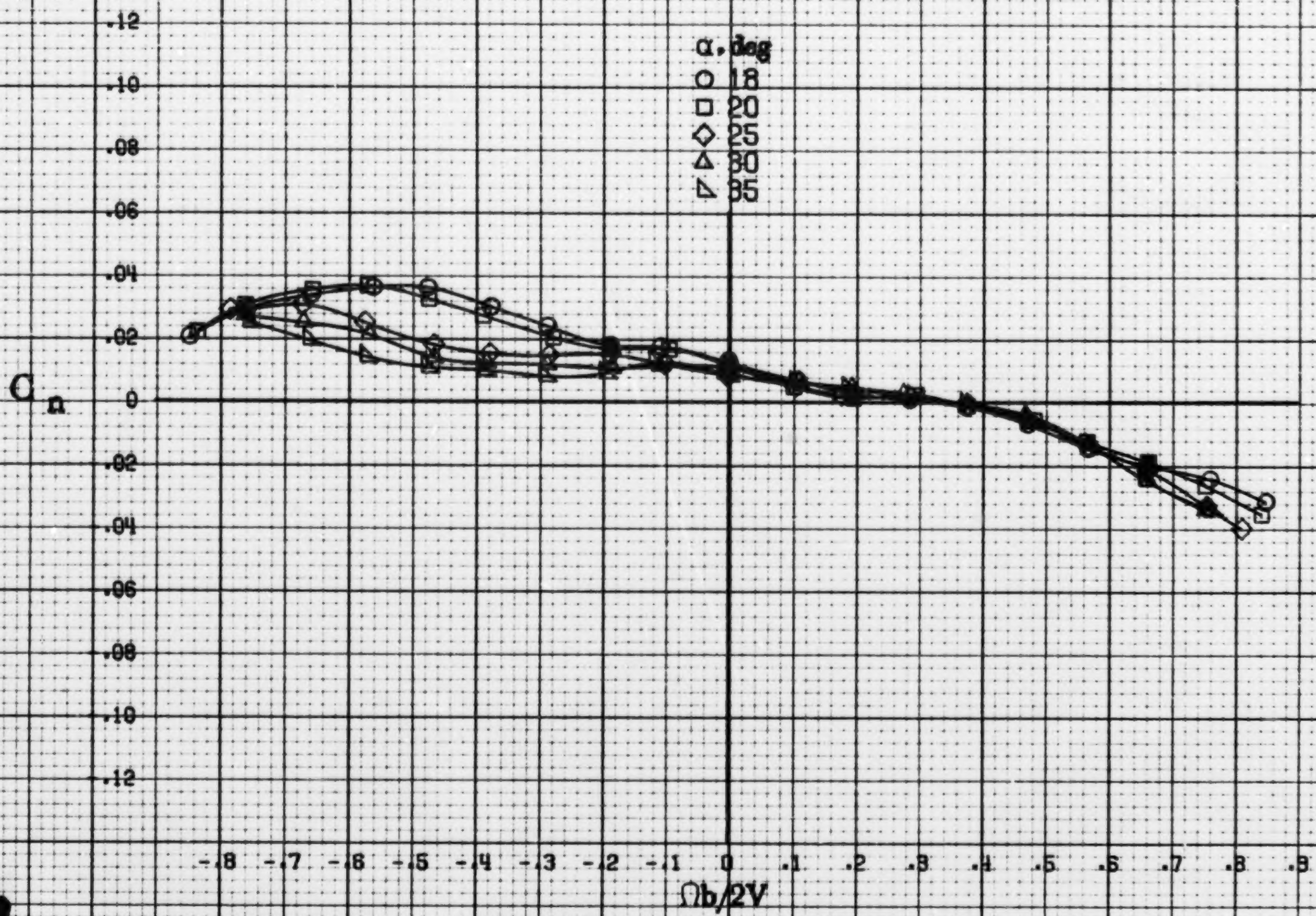

(b) α = 18 to 35 deg, SR = 76 cm (30 in).

Figure A87.-Continued.

A148

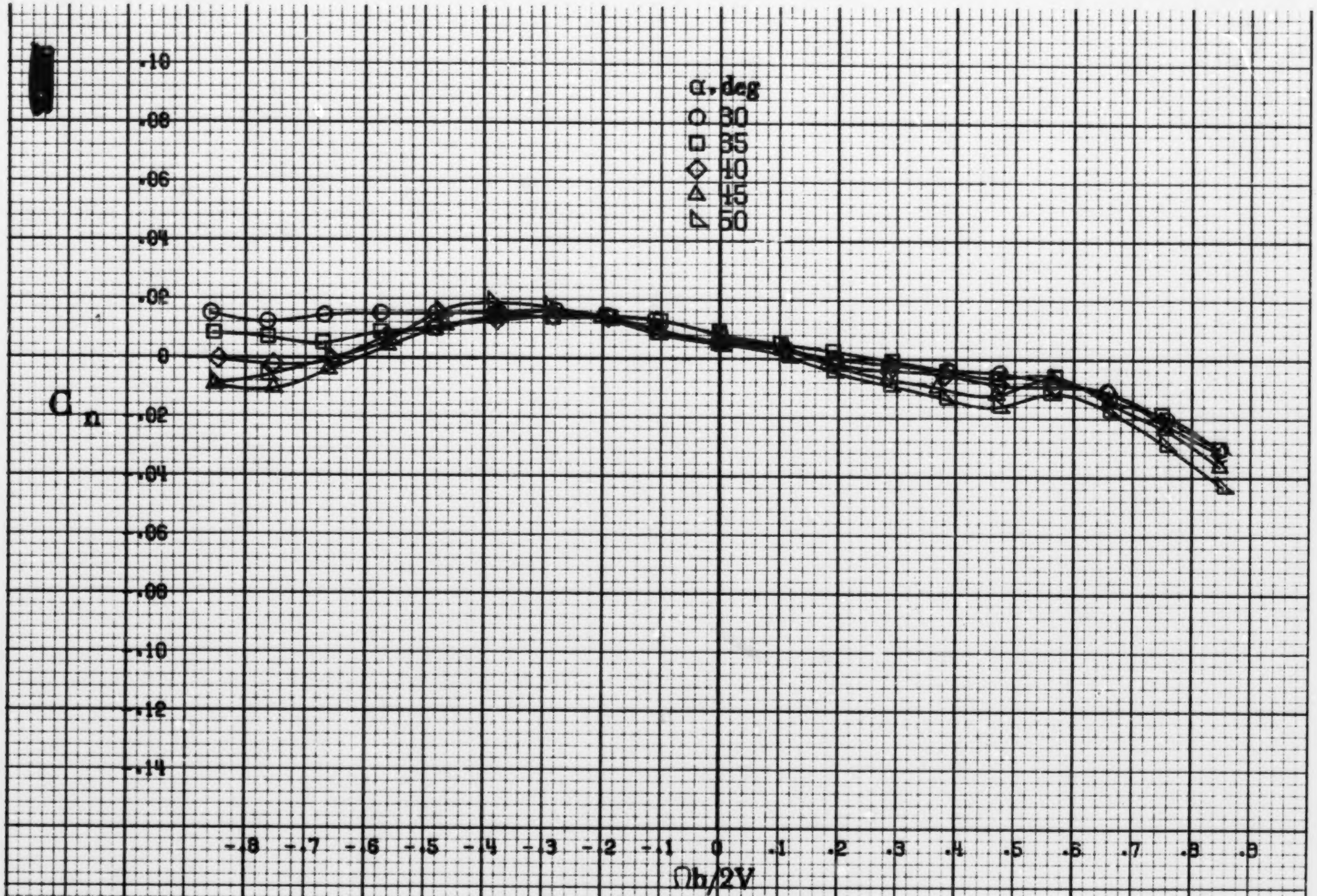

(c) α = 30 to 50 deg, SR = 0.

Figure A87.-Continued.

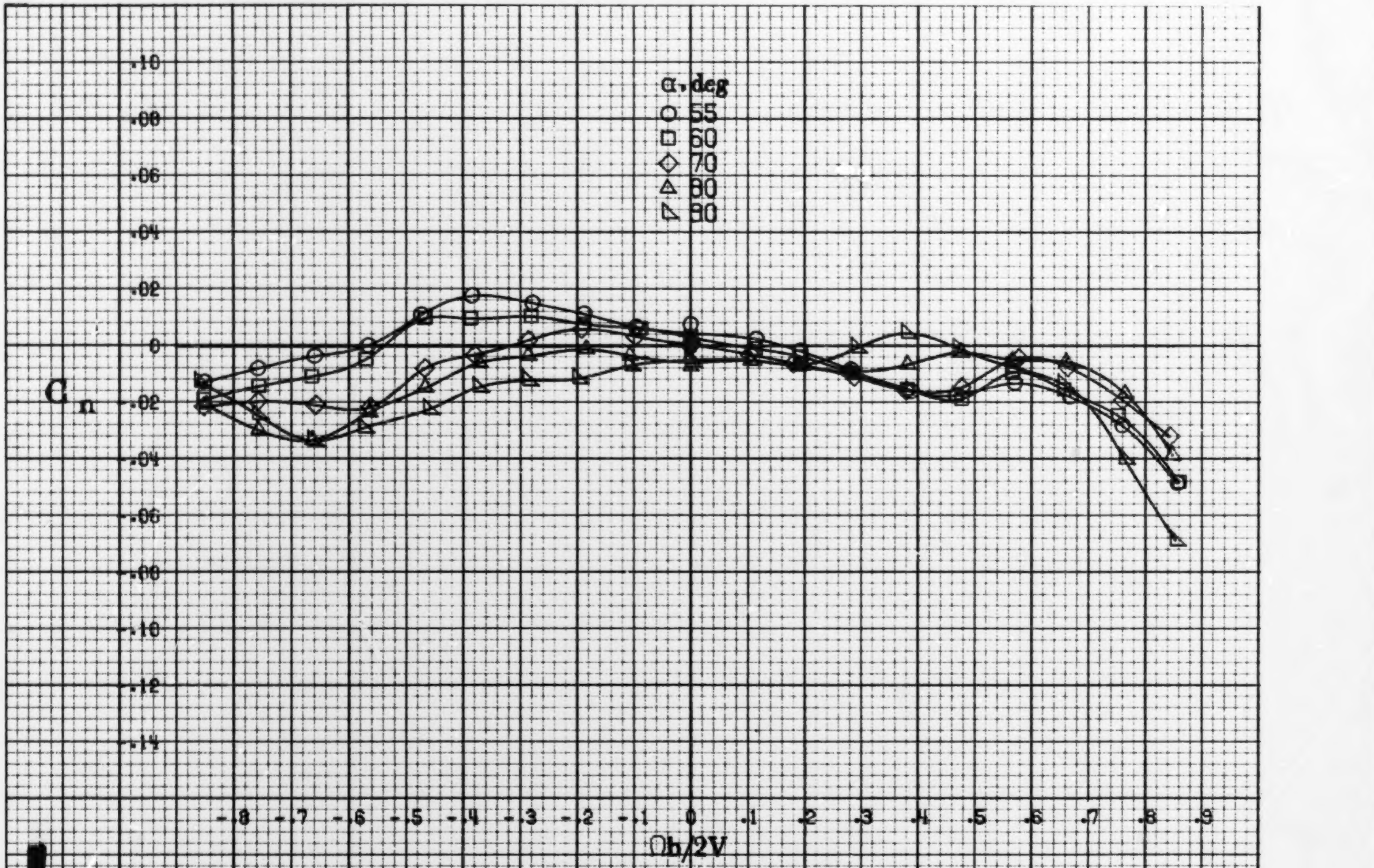

(d) α = 55 to 90 deg, SR = 0.

Figure A87.-Concluded.

A150

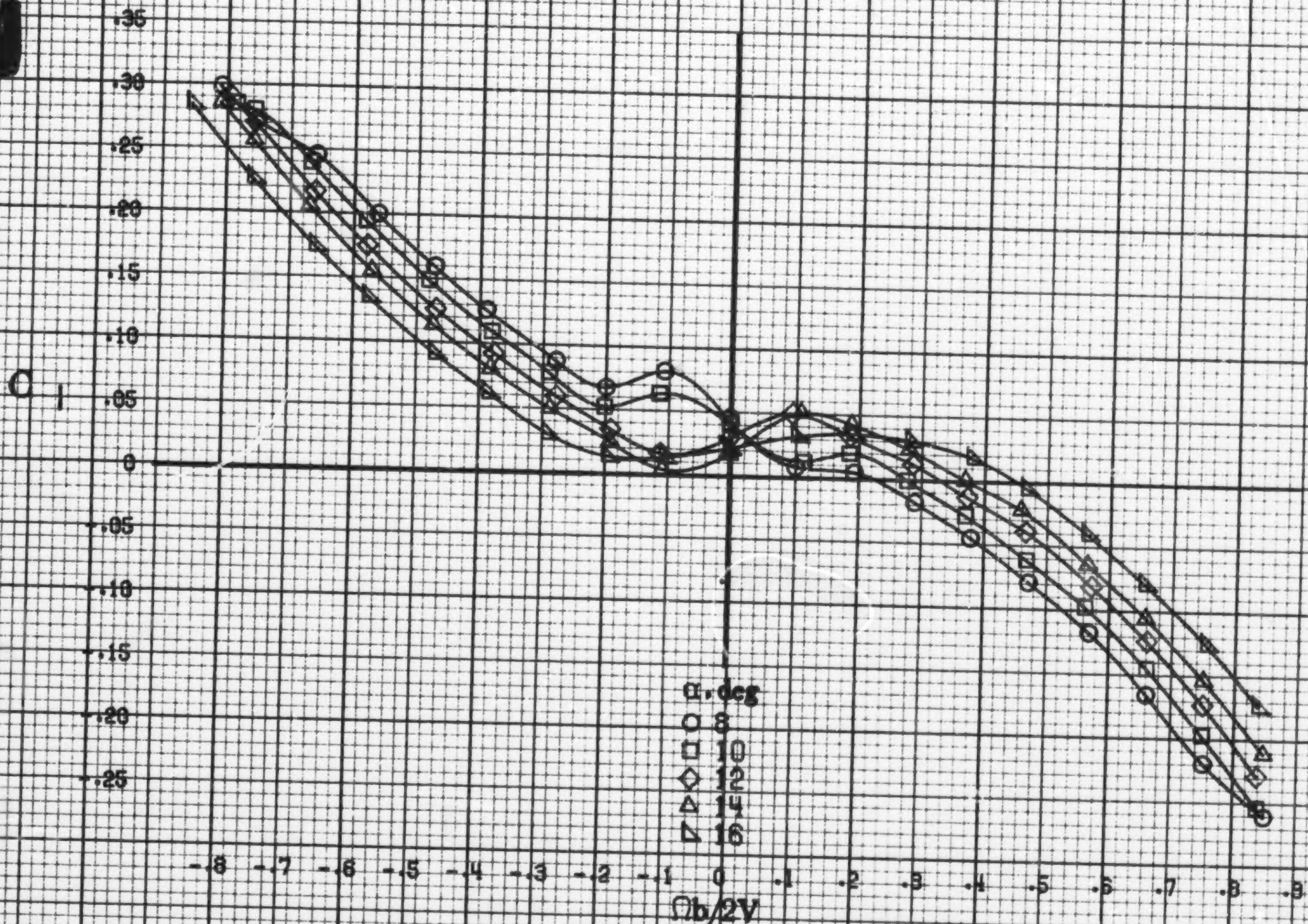

(a) $\alpha = 8$ to 16 deg, SR = 76 cm (30 in).

Figure A38.-Effect of rotation rate and angle of attack on rolling-moment coefficient for basic configuration. $\delta_e = -25°$, $\delta_a = -22.5°$, $\delta_r = 25°$, $\beta = 0°$.

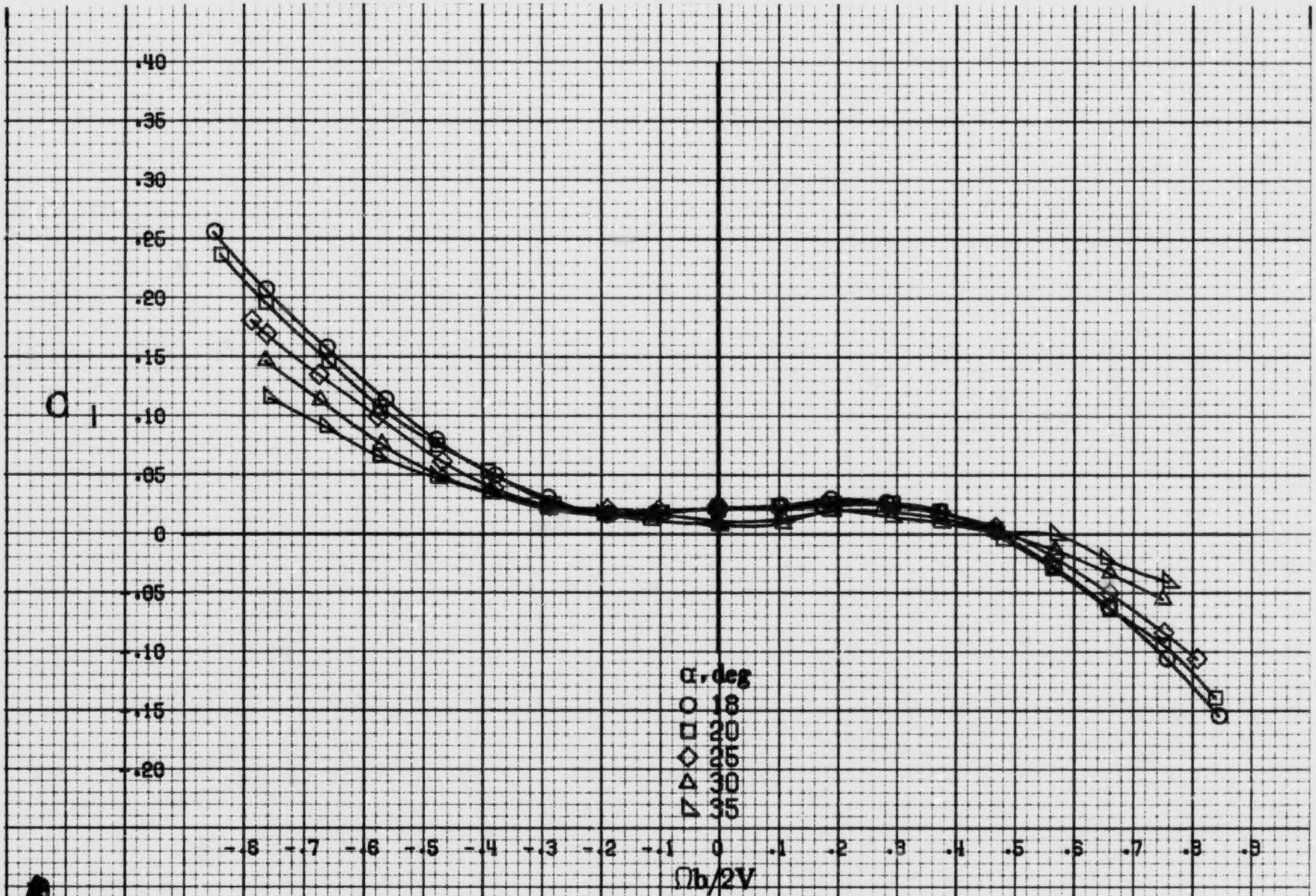

(b) α = 18 to 35 deg, SR = 76 cm (30 in).

Figure A33.-Continued.

A152

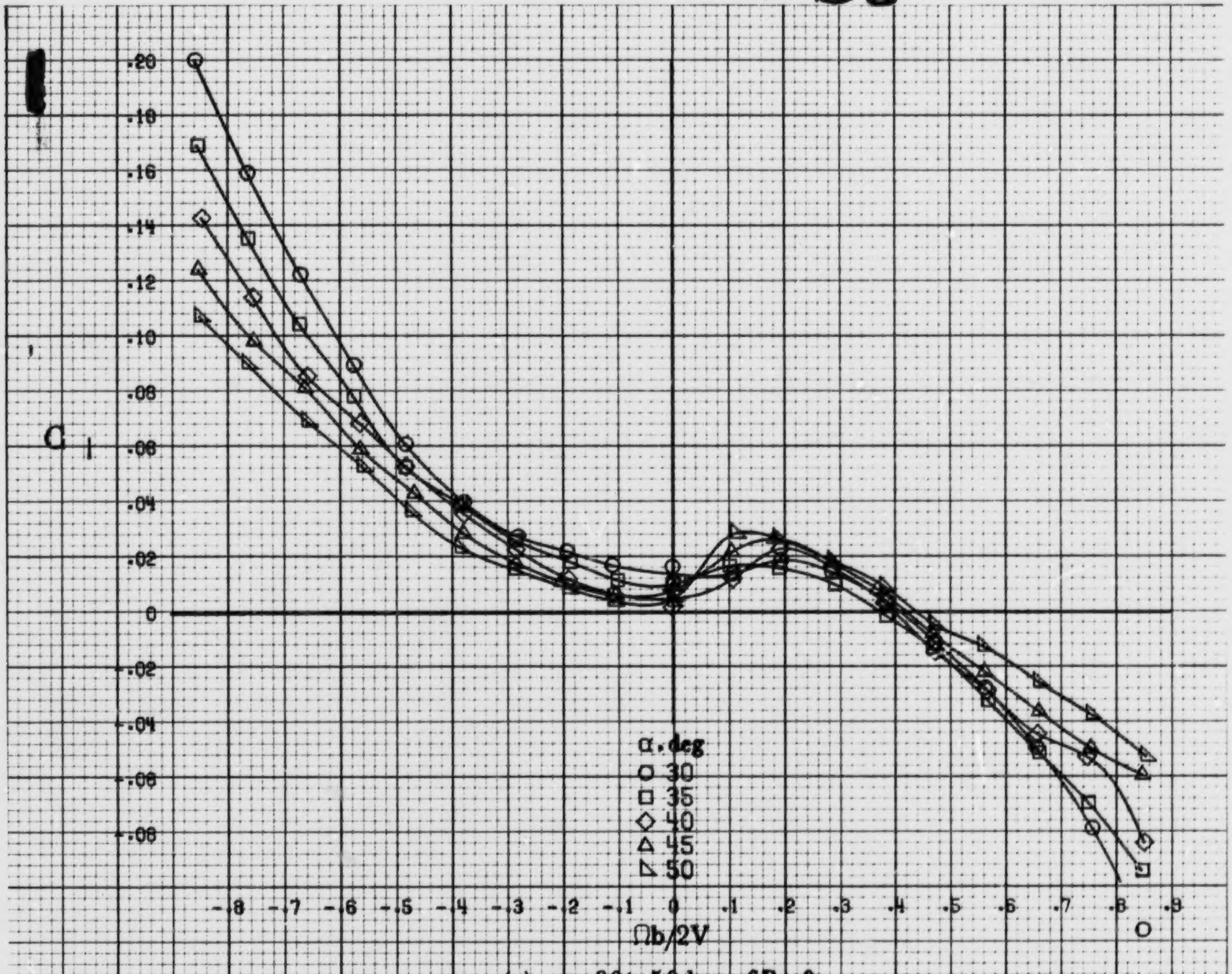

(c) α = 30 to 50 deg, SR = 0.

Figure A88.-Continued.

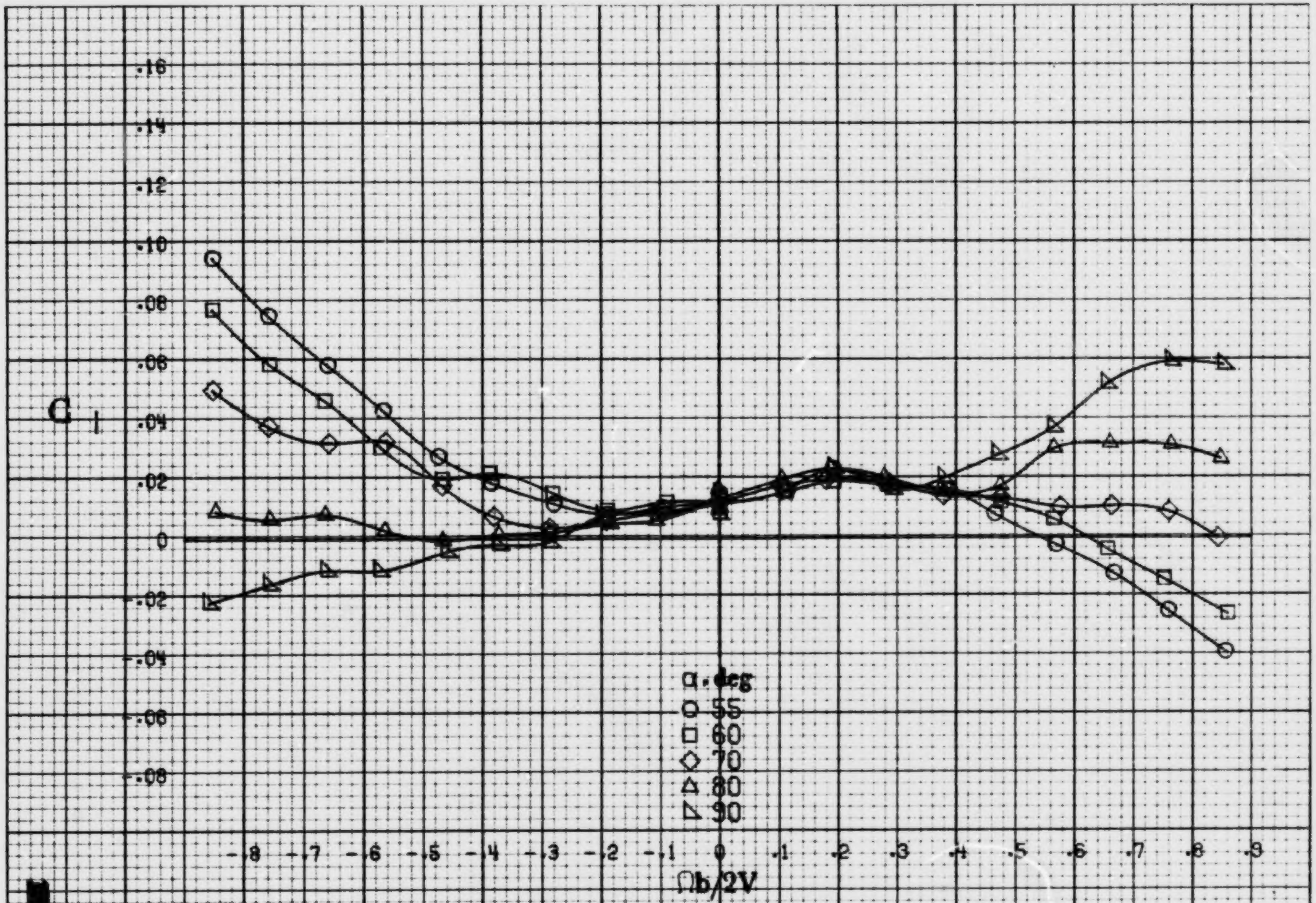

(d) α=55to90deg, SR=0.

Figure A88.-Concluded.

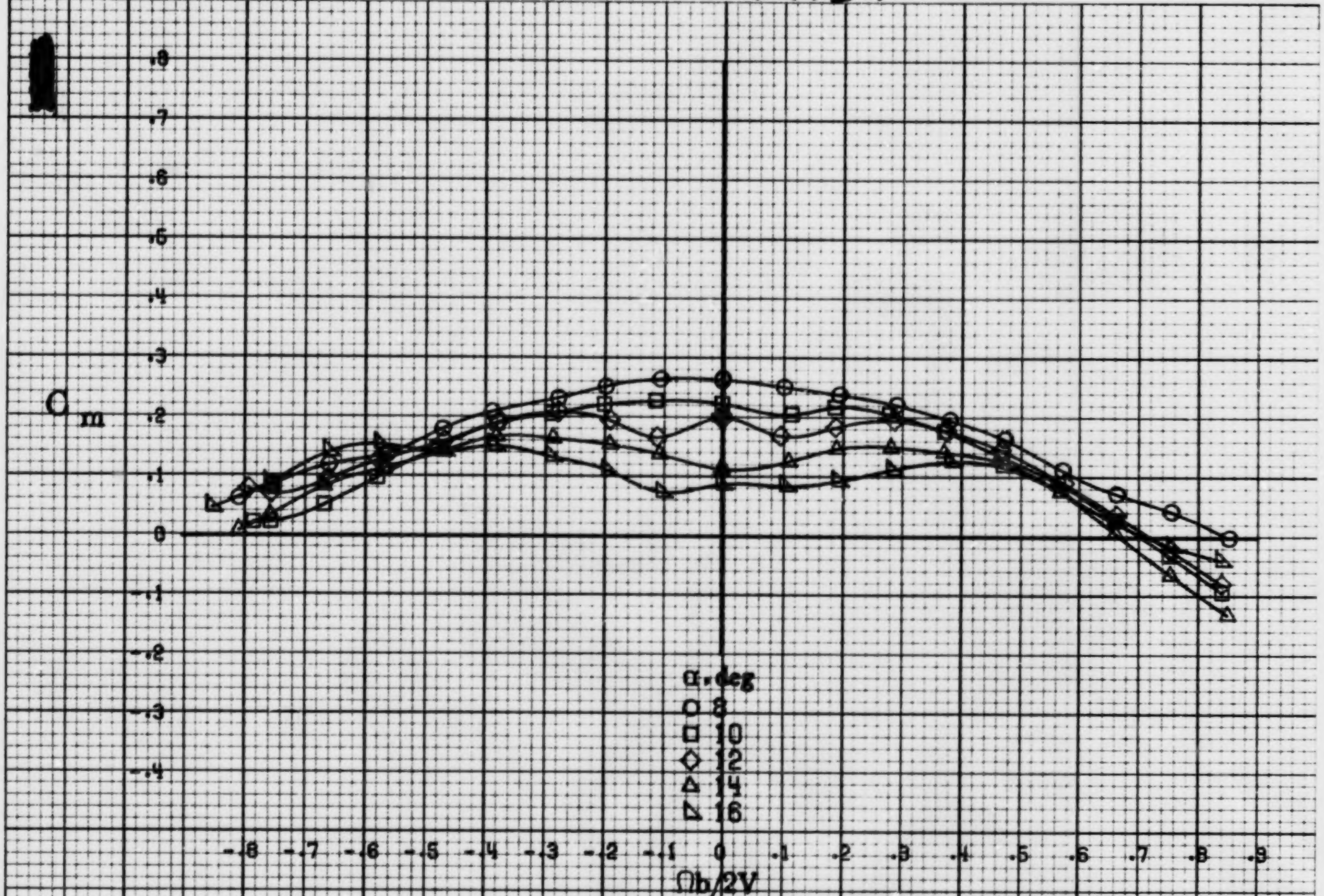

(a) $\alpha = 8$ to 16 deg, SR = 76 cm (30 in).

Figure A39.-Effect of rotation rate and angle of attack on pitching-moment coefficient for basic configuration. $\delta_e = -25°$, $\delta_a = -22.5°$, $\delta_r = 25°$, $\beta = 0°$.

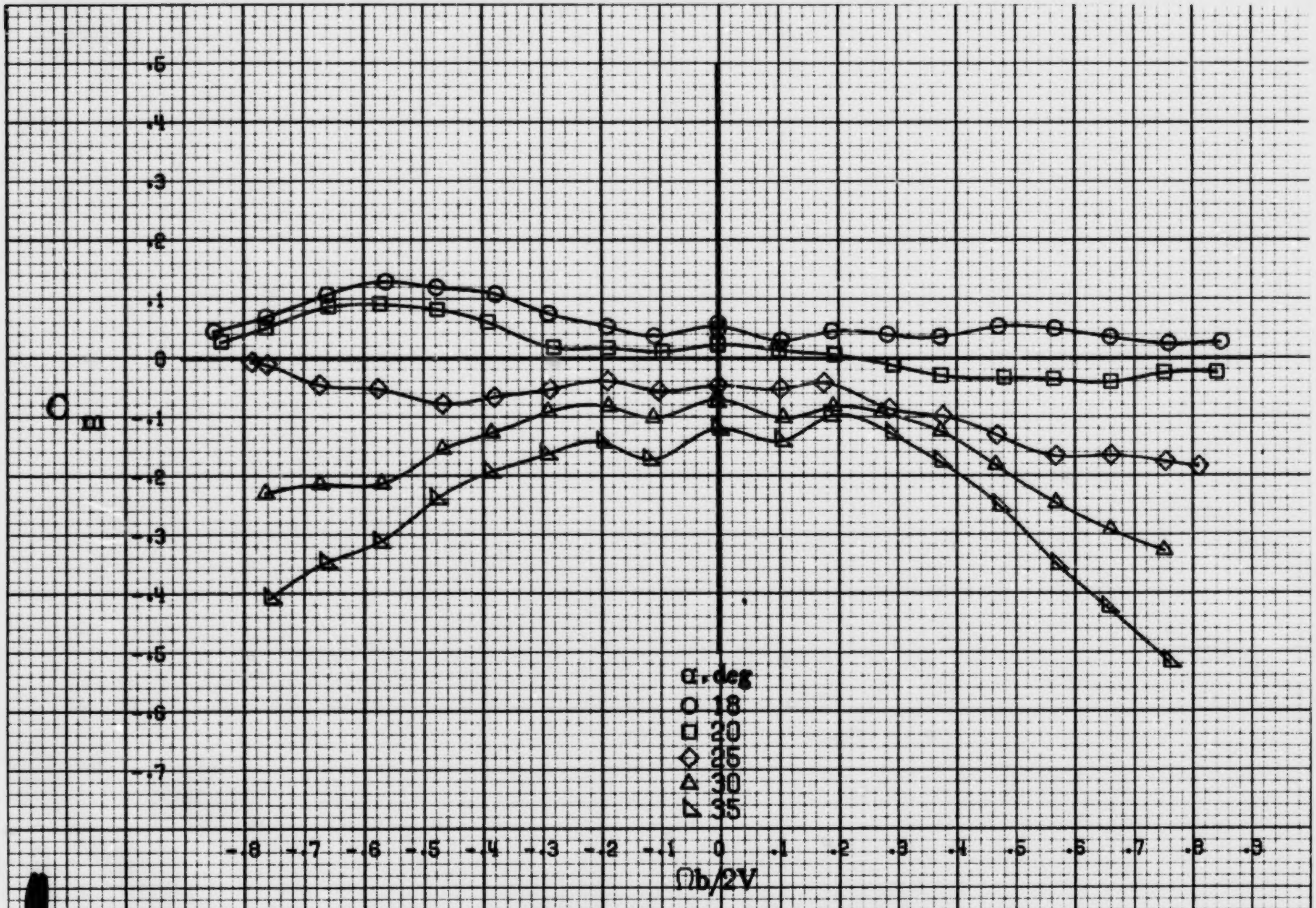

(b) α = 18 to 35 deg, SR = 76 cm (30 in).

Figure A39.-Continued.

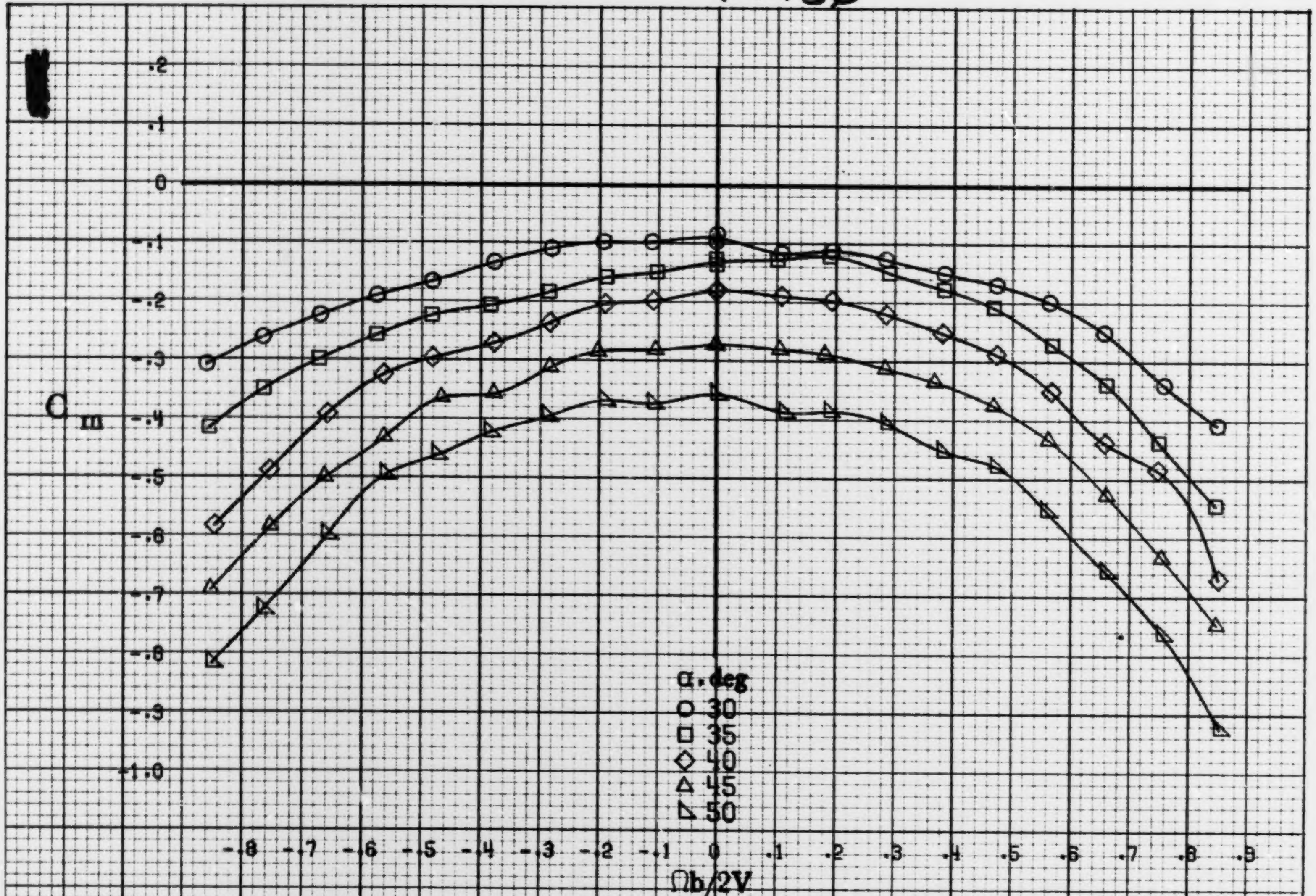

(c) α = 30 to 50 deg, SR = 0.
Figure A39.-Continued.

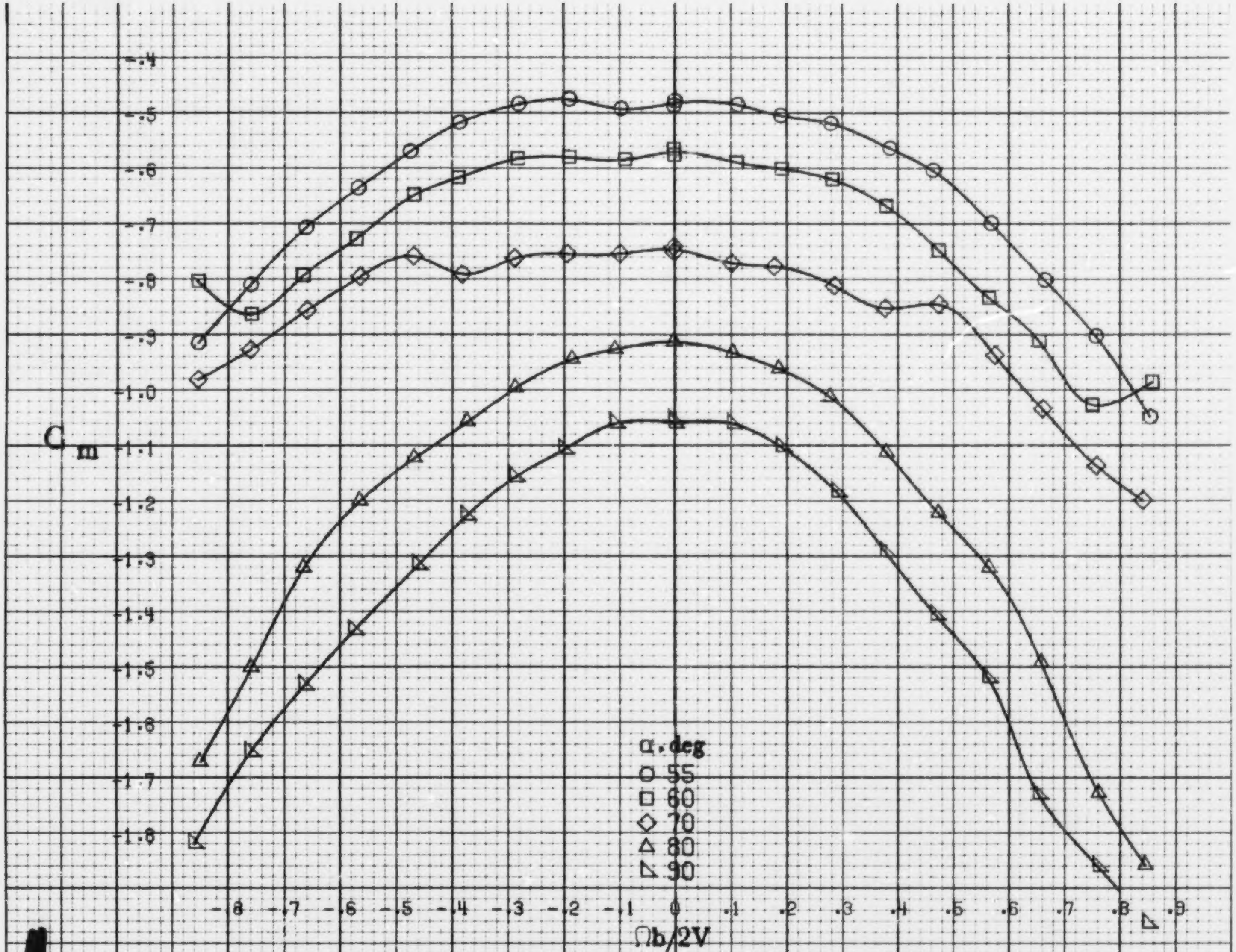

(d) α = 55 to 90 deg, SR = 0.
Figure A39.-Concluded.

A157

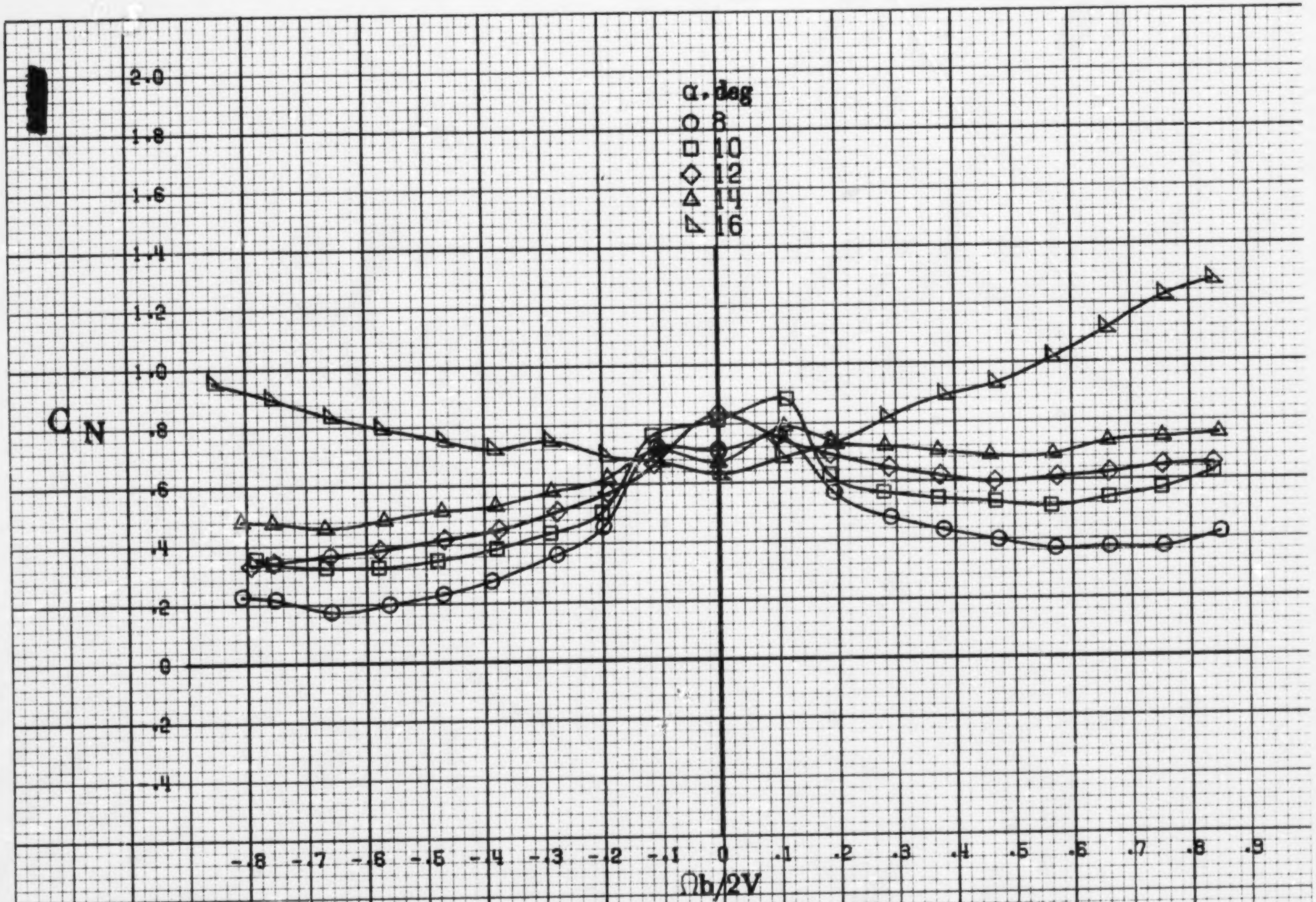

(a) α = 8 to 16 deg, SR = 76 cm (30 in).

Figure A40.-Effect of rotation rate and angle of attack on normal-force coefficient for basic configuration. $\delta_e = -25°$, $\delta_a = -22.5°$, $\delta_r = 25°$, $\beta = 0°$.

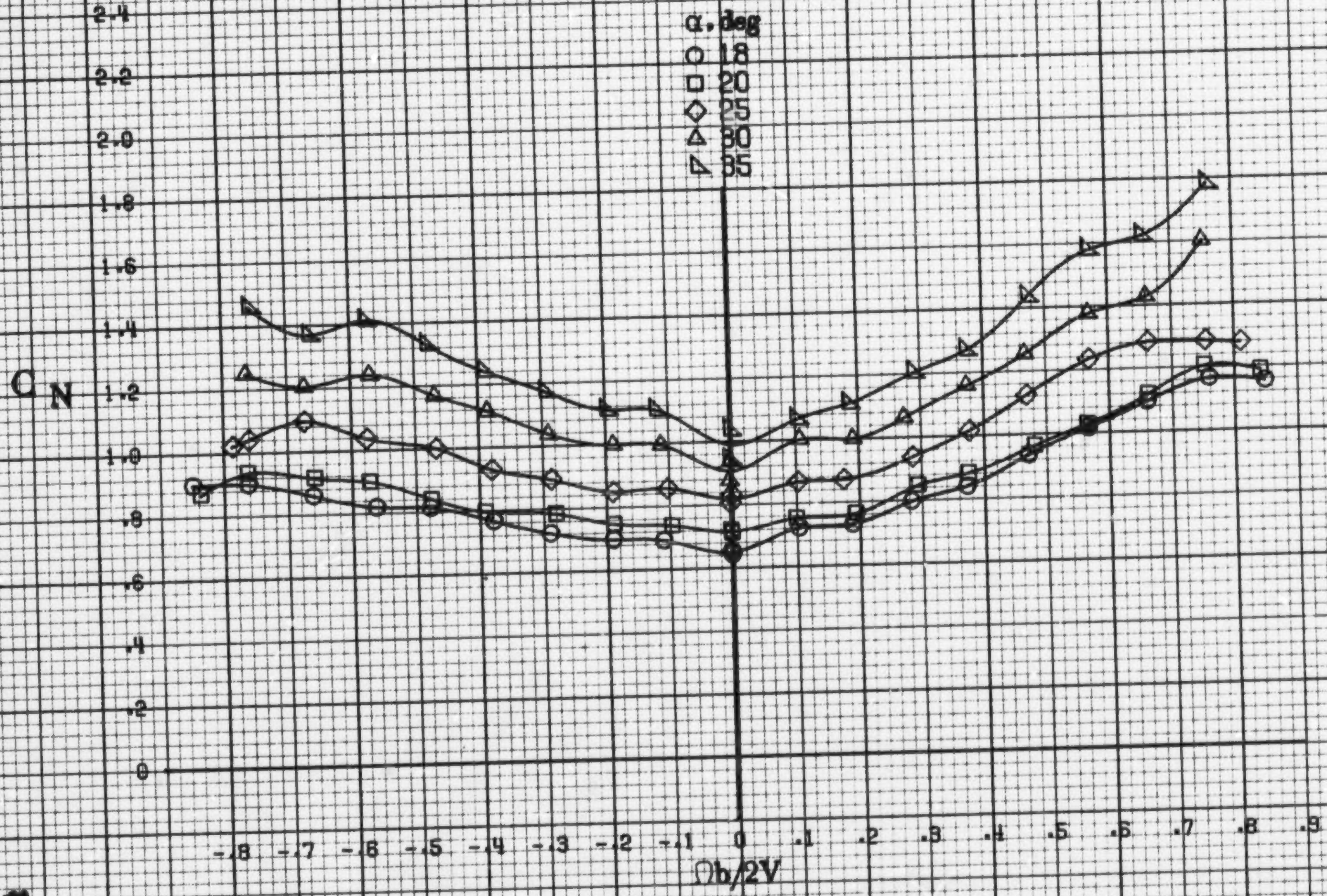

(b) α = 18 to 35 deg, SR = 76 cm (30 in).

Figure A40.-Continued.

A159

A160

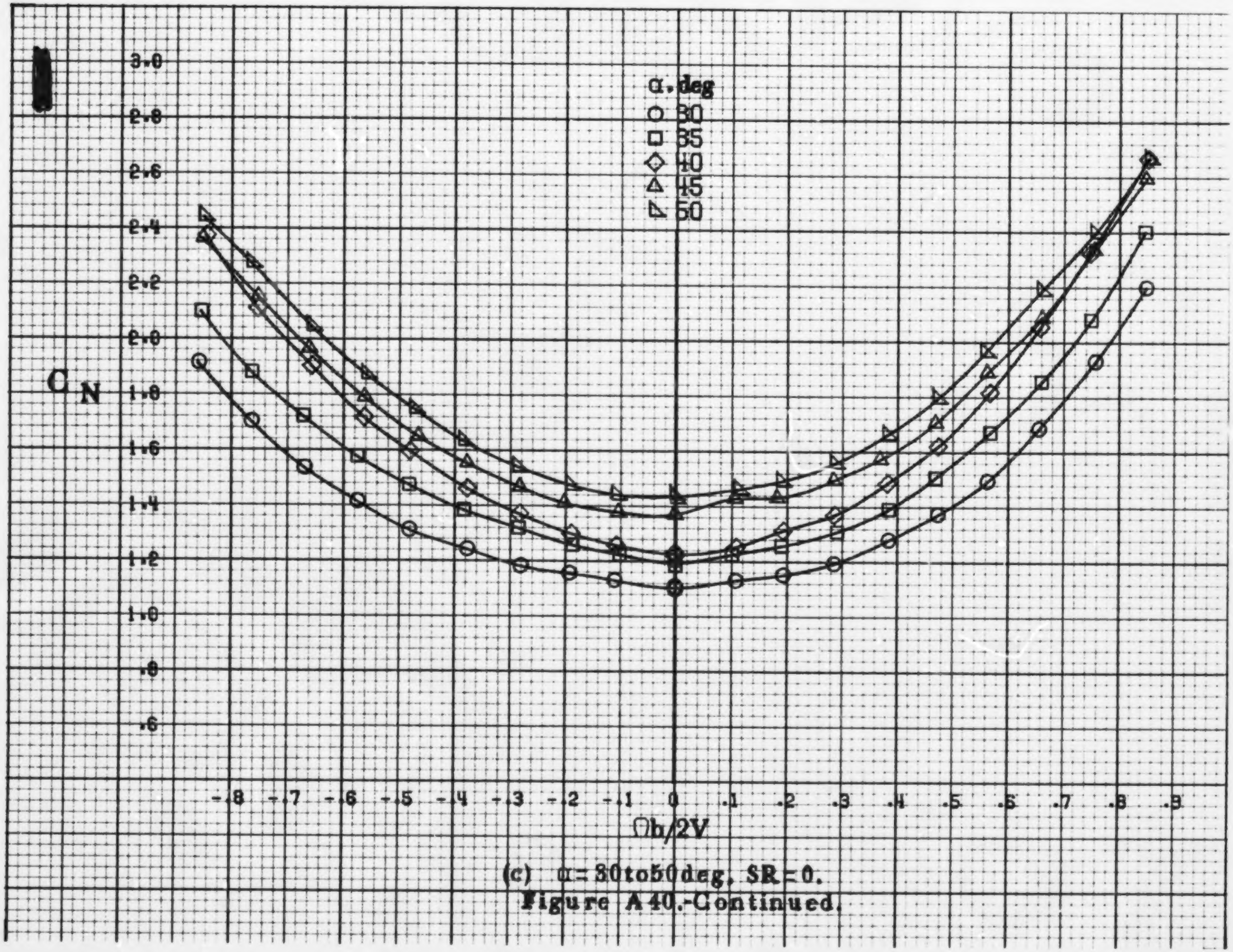

(c) α = 30 to 50 deg, SR = 0.

Figure A40.-Continued.

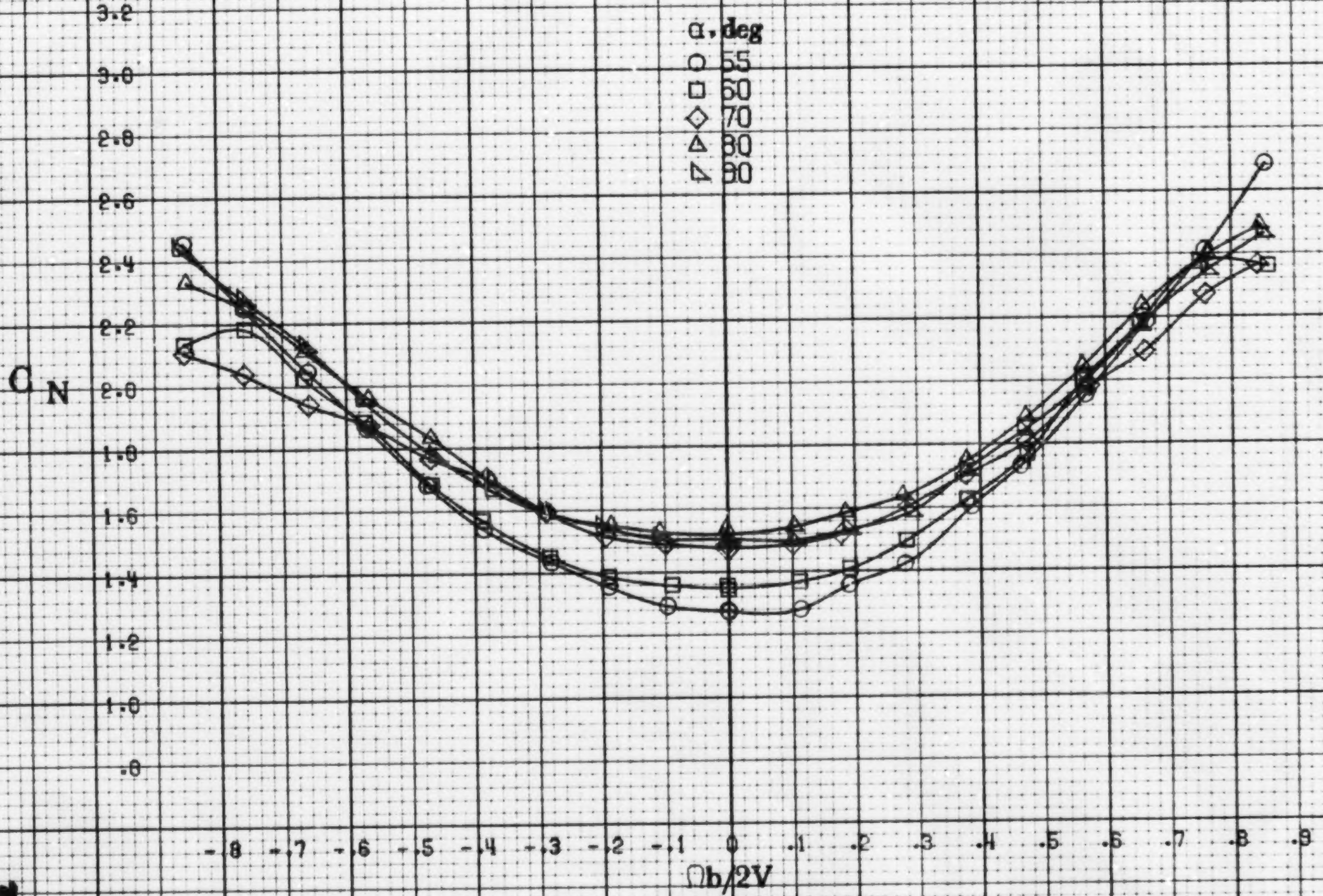

(d) $\alpha = 55$ to 90 deg, SR = 0.

Figure A40.-Concluded.

A161

A162

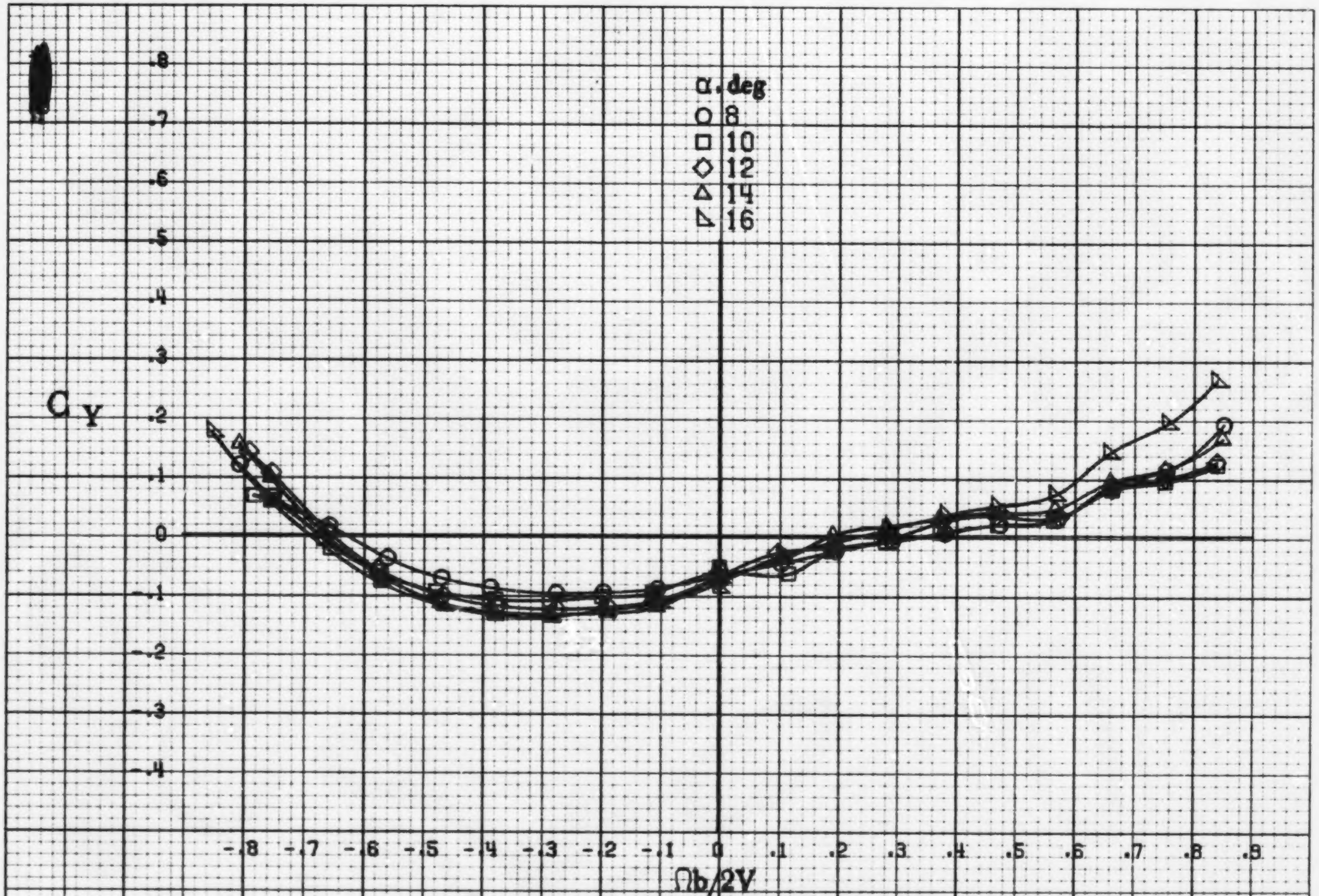

(a) $\alpha = 8$ to 16 deg, SR = 76 cm (30 in).

Figure A41.-Effect of rotation rate and angle of attack on side-force coefficient for basic configuration. $\delta_e = -25°$, $\delta_a = -22.5°$, $\delta_r = -25°$, $\beta = 0°$.

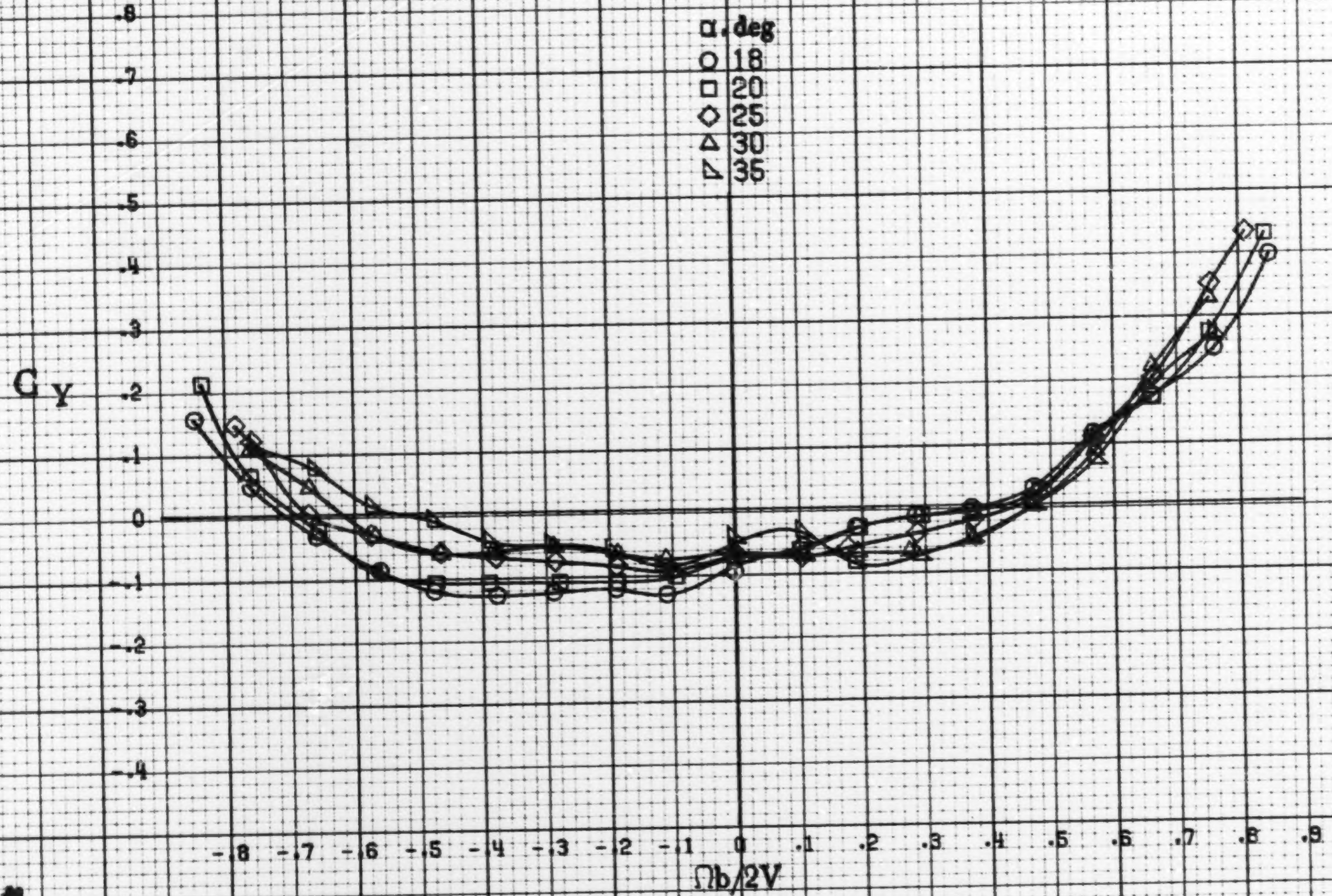

(b) α = 18 to 35 deg, SR = 76 cm (30 in).

Figure A41.-Continued.

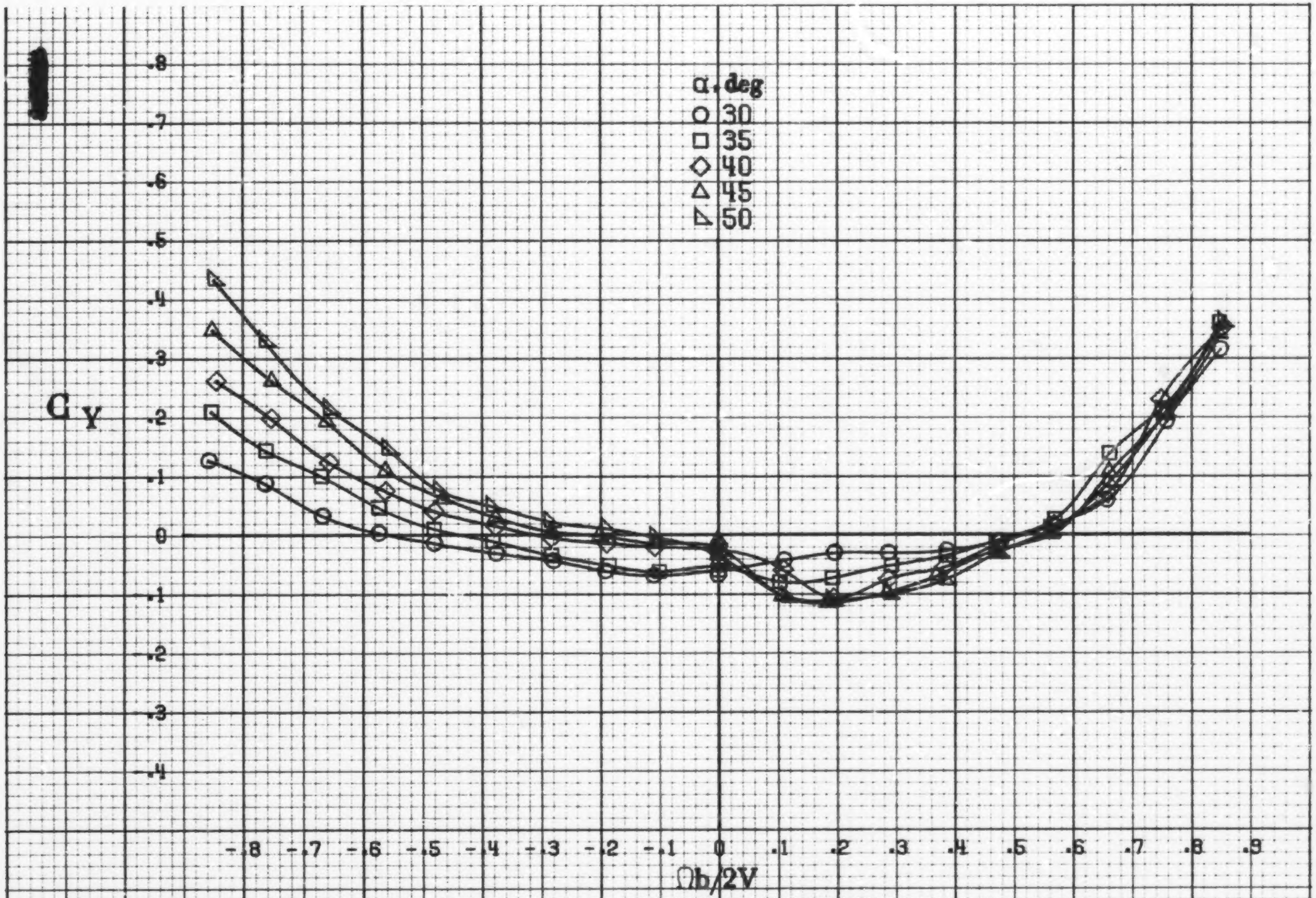

(c) $\alpha = 30$ to 50 deg, SR = 0.

Figure A41.-Continued.

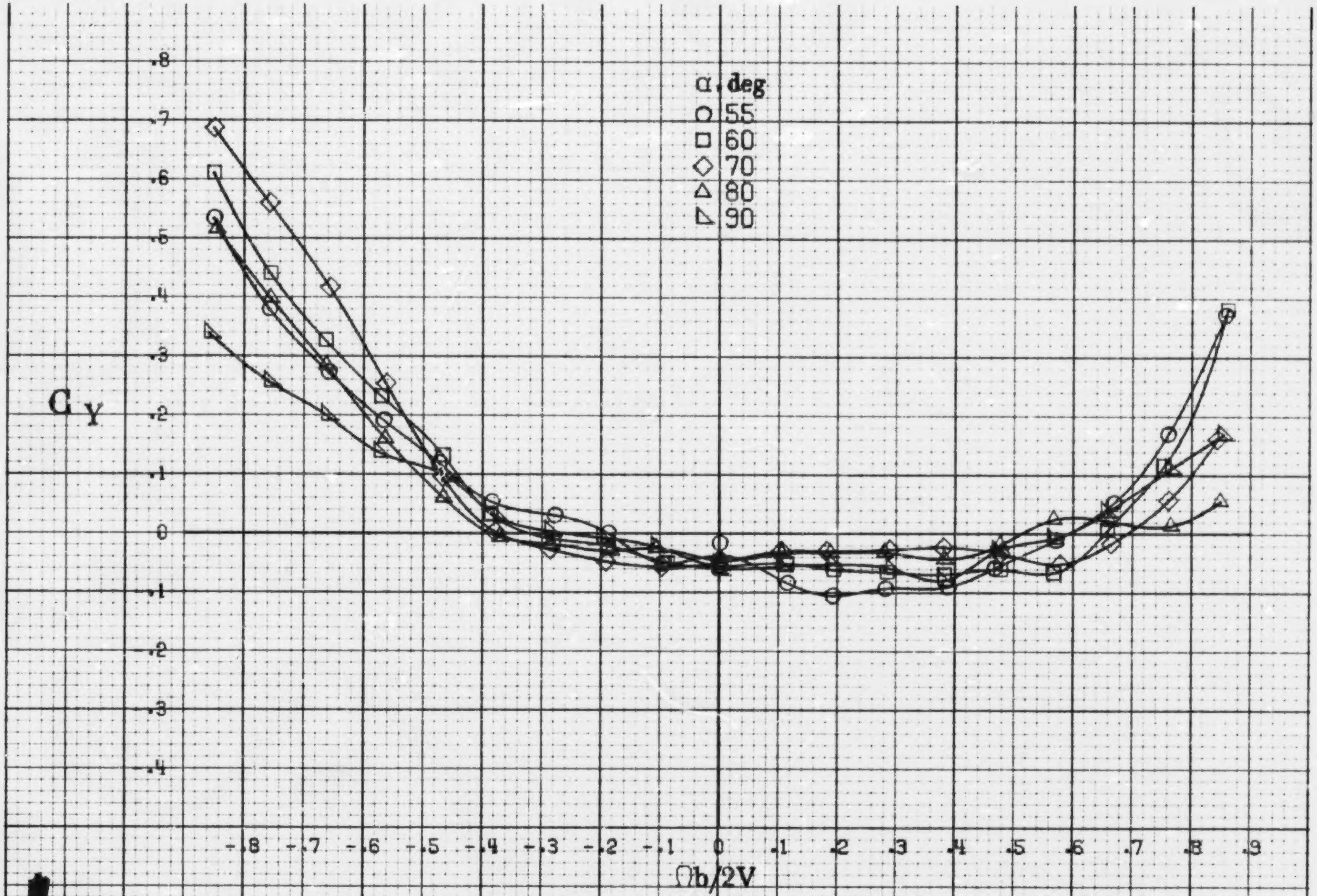

(d) α = 55 to 90 deg, SR = 0.

Figure A41.-Concluded.

A 165

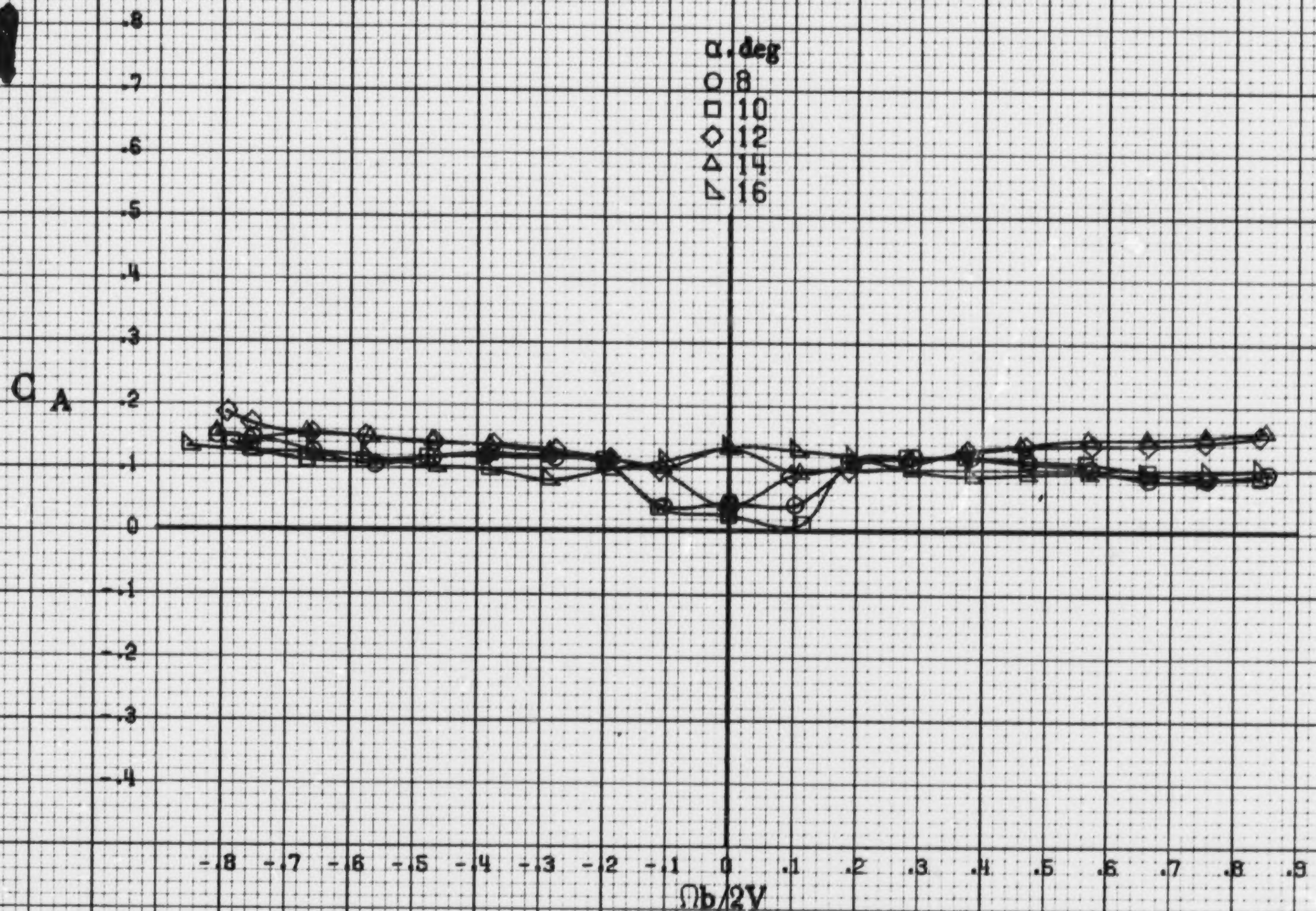

(a) $\alpha = 8$ to 16 deg, SR = 76 cm (30 in).

Figure A42.- Effect of rotation rate and angle of attack on axial-force coefficient for basic configuration. $\delta_e = -25°$, $\delta_a = -22.5°$, $\delta_r = -25°$, $\beta = 0°$.

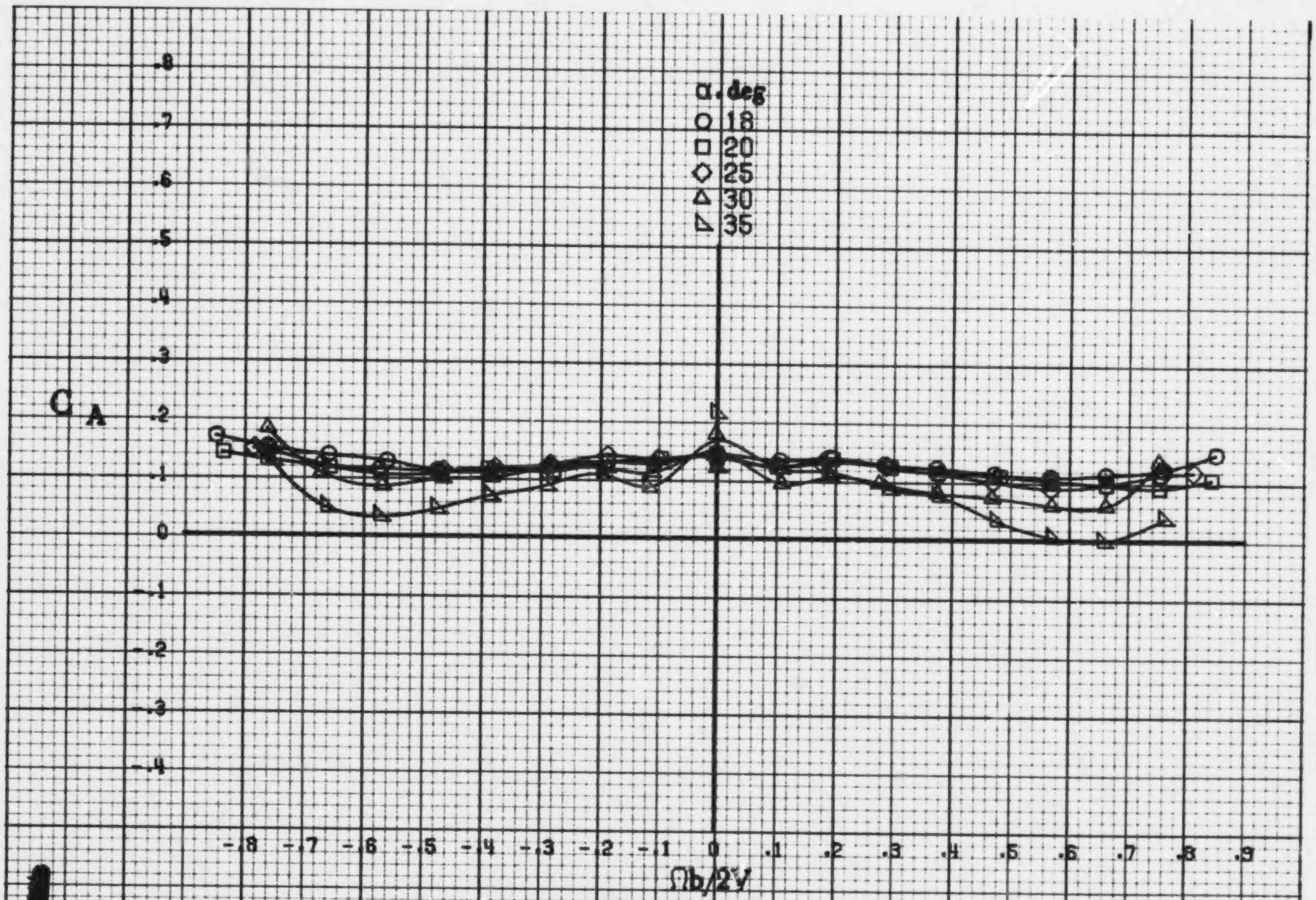

(b) $\alpha = 18$ to 35 deg. SR = 76cm (30in).

Figure A42.-Continued.

A168

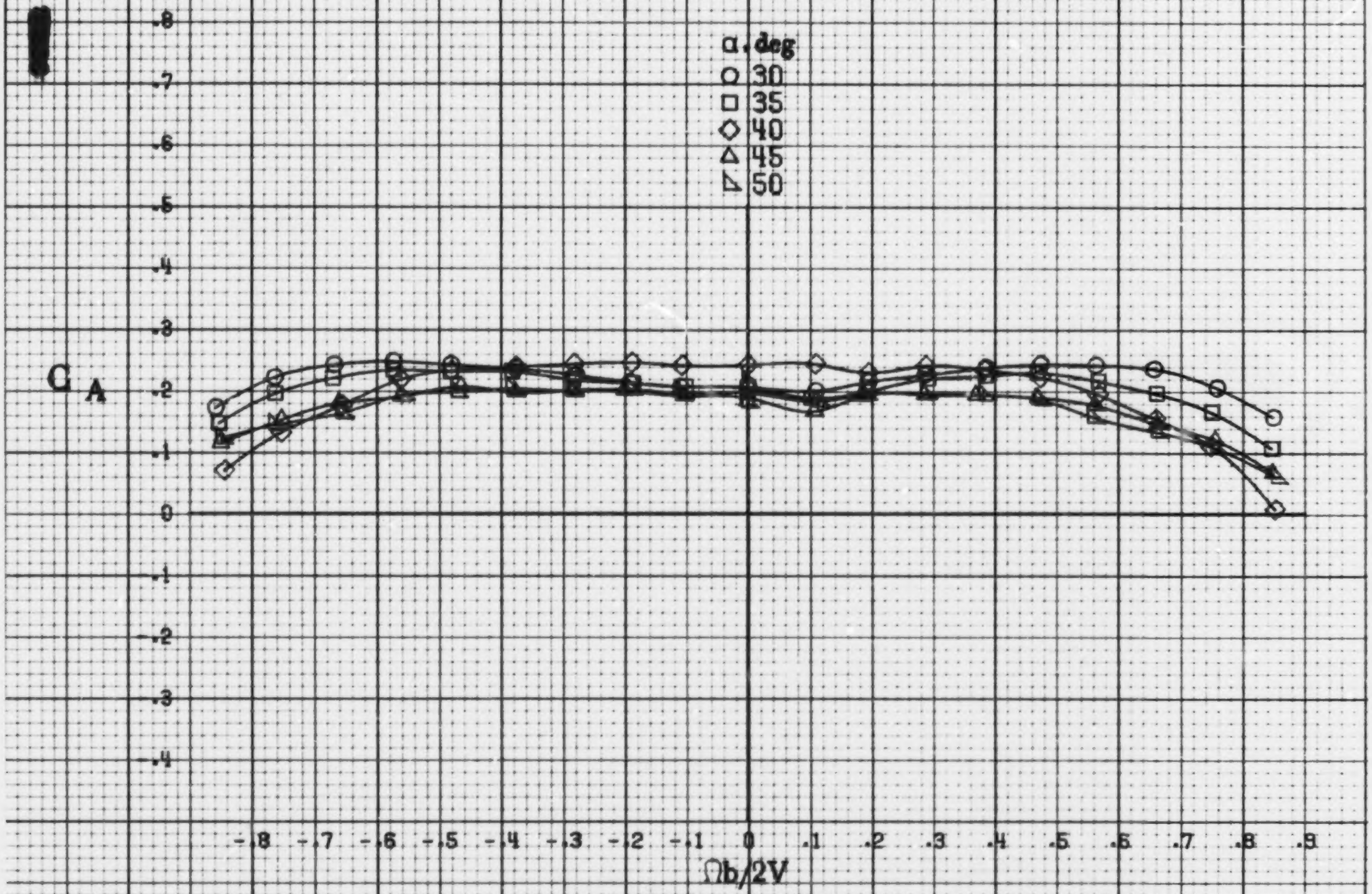

(c) α = 30 to 50 deg, SR = 0.

Figure A42.-Continued.

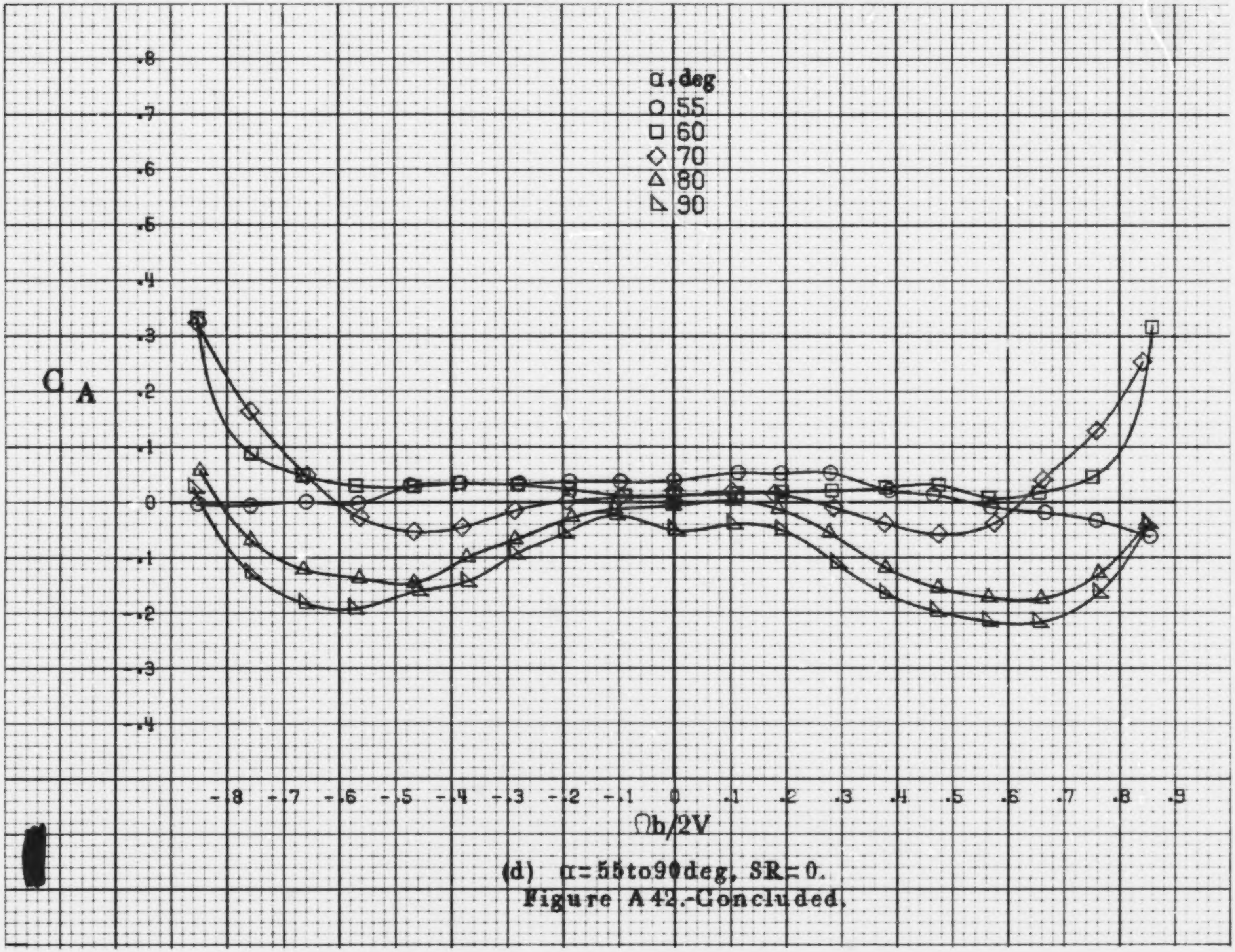

(d) α = 55 to 90 deg, SR = 0.

Figure A42.-Concluded.

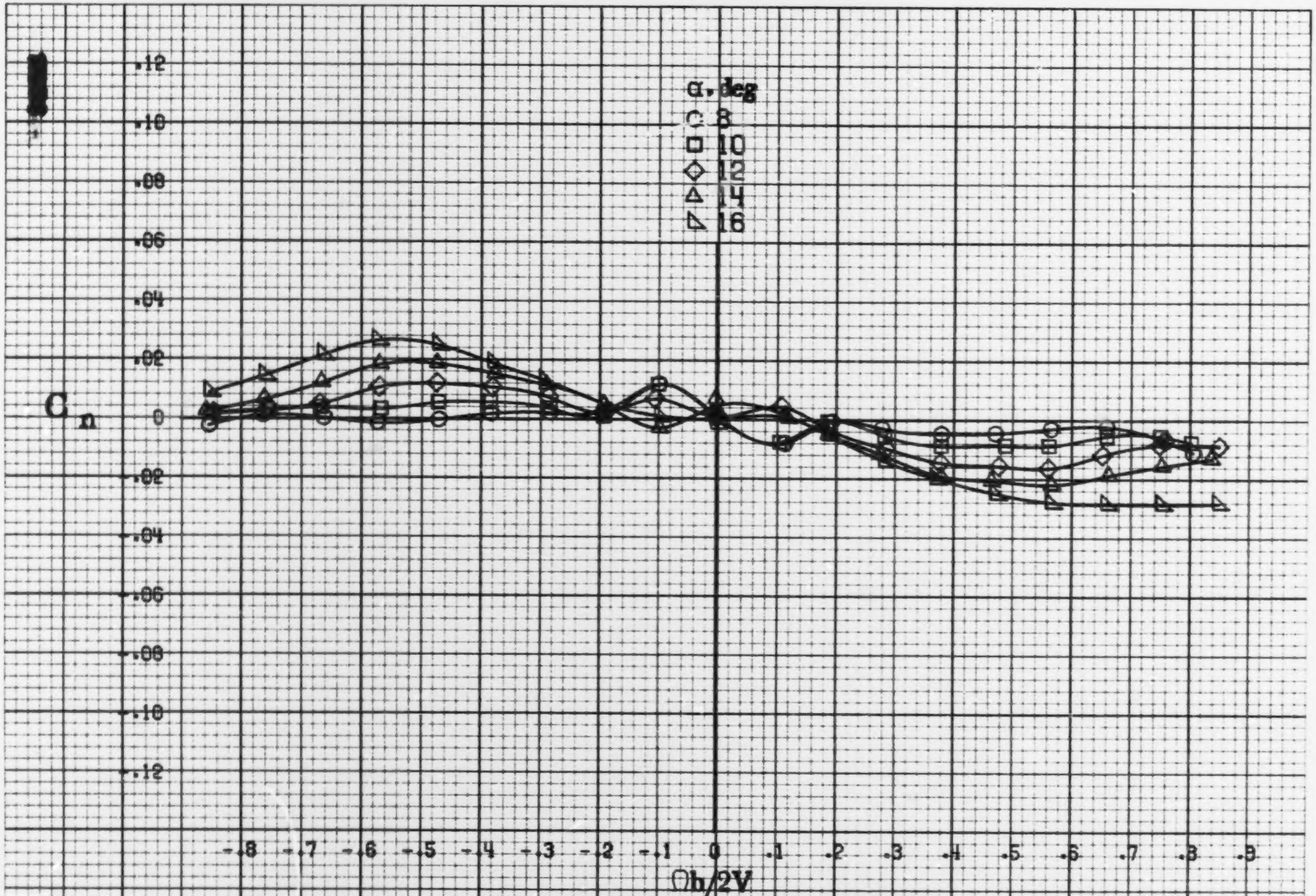

(a) α = 8 to 16 deg, SR = 76 cm (30 in).

Figure A43. Effect of rotation rate and angle of attack on yawing-moment coefficient for basic configuration. $\delta_e = -25°$, $\delta_a = 22.5°$, $\delta_r = 0°$. $\beta = 0°$.

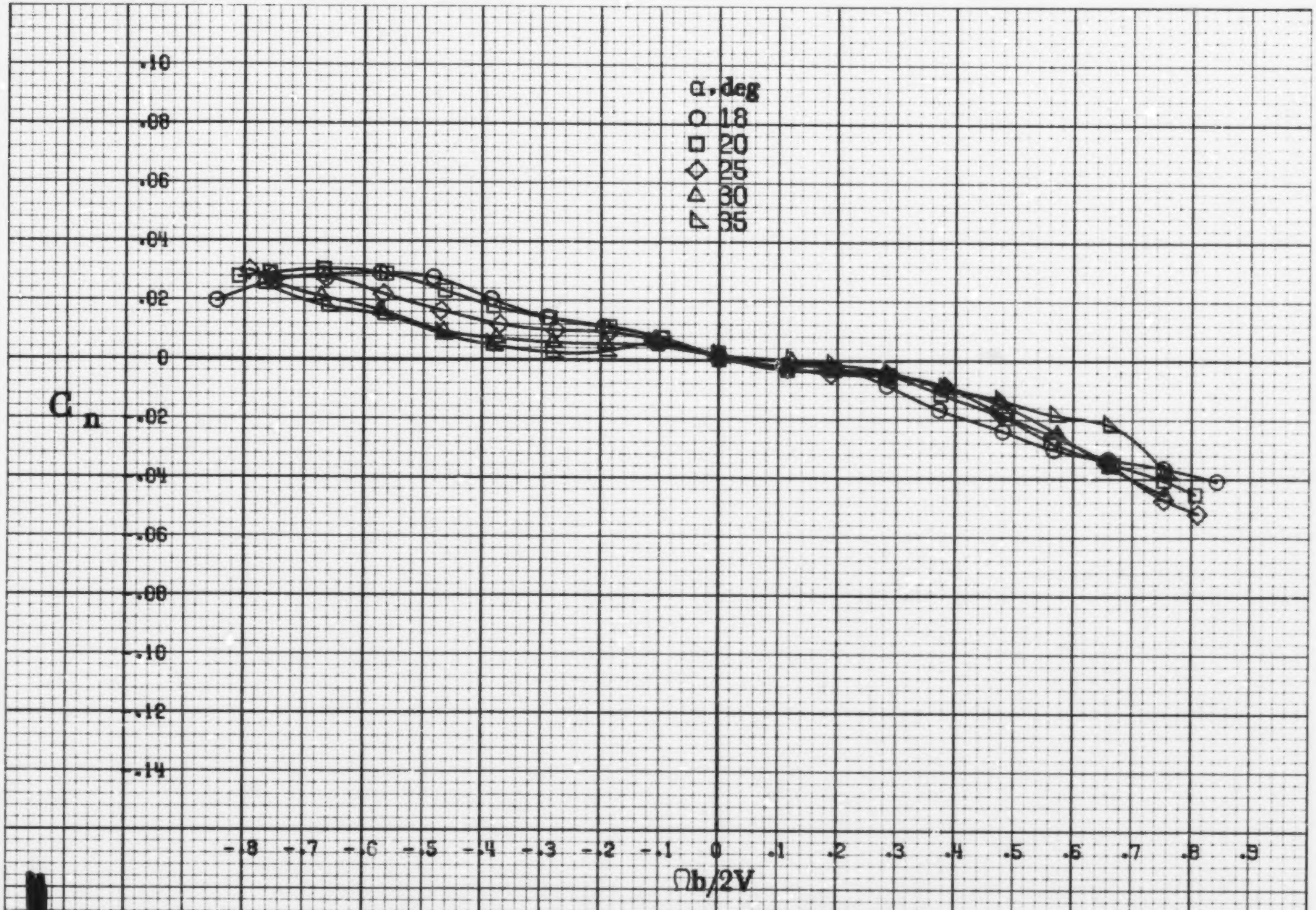

(b) α = 18 to 35 deg, SR = 76 cm (30 in).
Figure A43.-Continued.

A171

A172

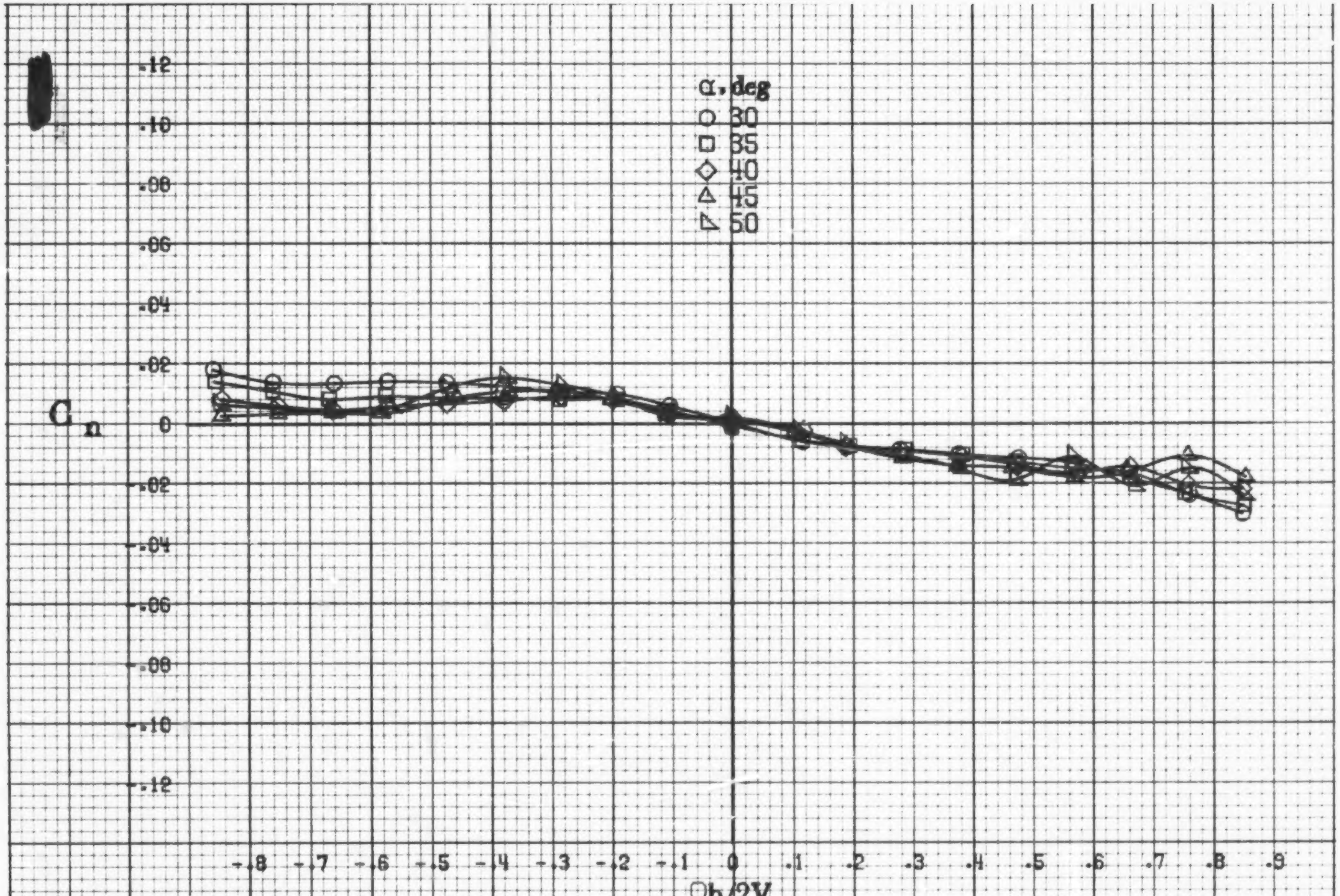

(c) α = 30 to 50 deg, SR = 0.

Figure A43.-Continued.

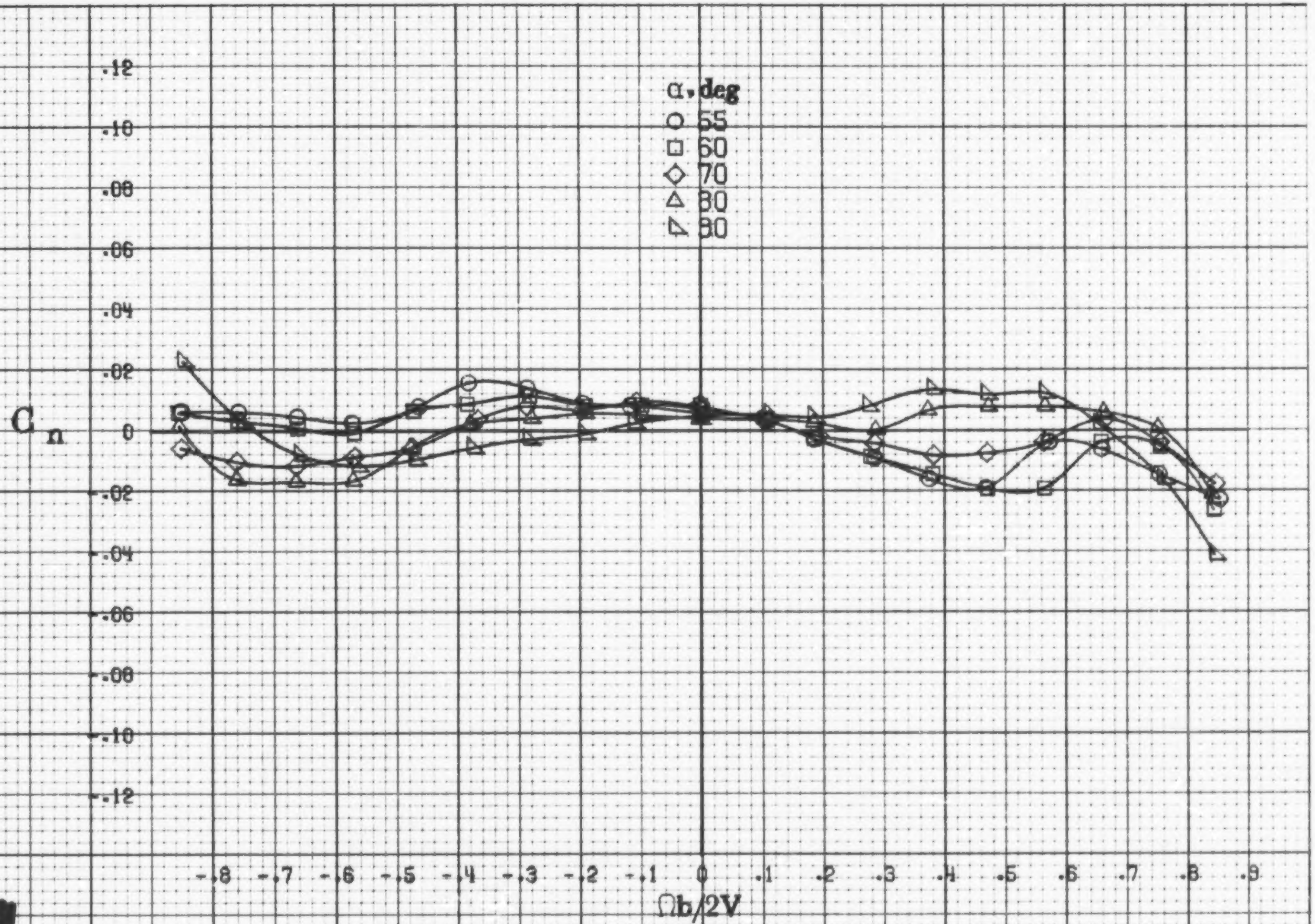

(d) α = 55 to 90 deg, SR = 0.

Figure A43.-Concluded.

A 174

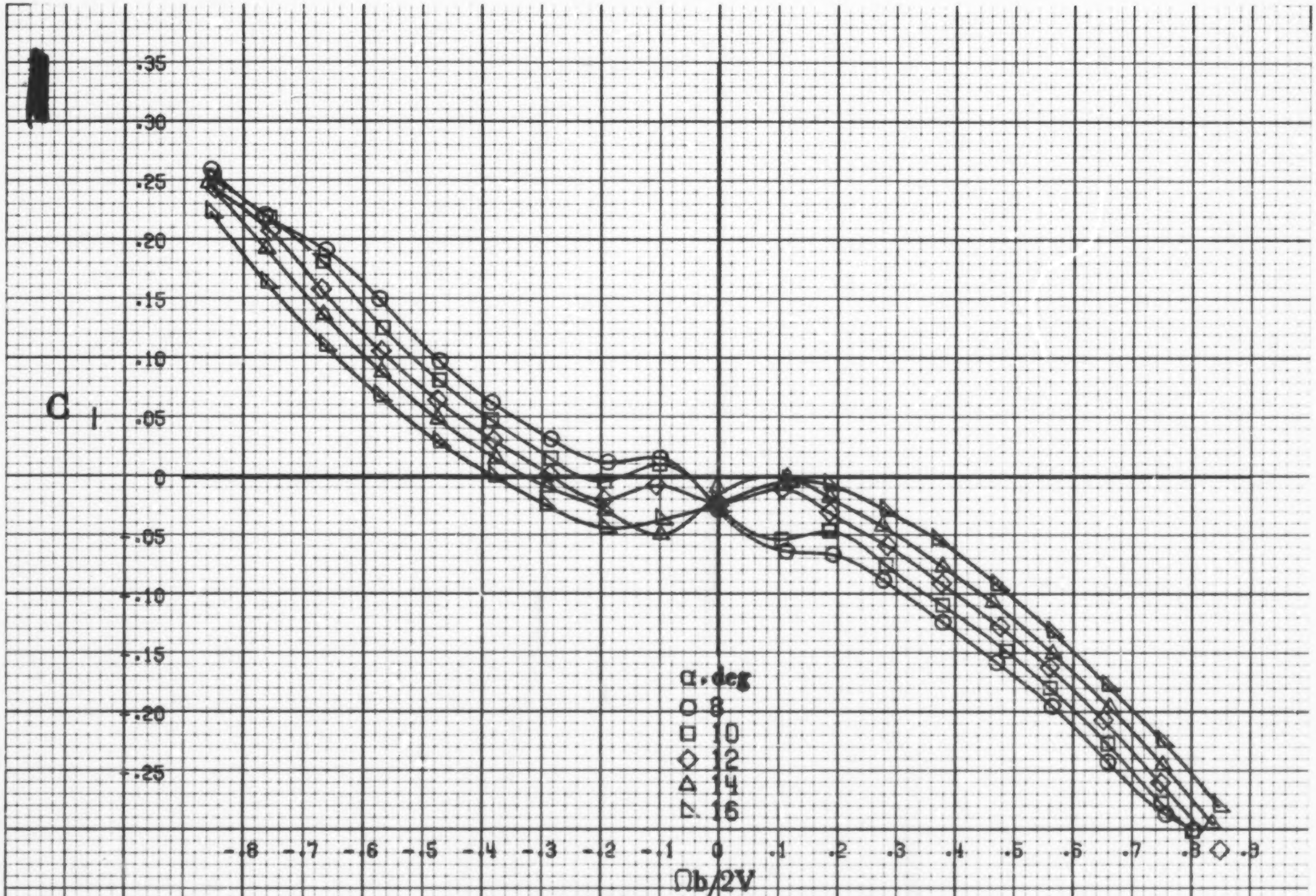

(a) α = 8 to 16 deg. SR = 76 cm (30 in).

Figure A44.-Effect of rotation rate and angle of attack on rolling-moment coefficient for basic configuration. $\delta_e = -25°$. $\delta_a = 22.5°$. $\delta_r = 0°$. $\beta = 0°$.

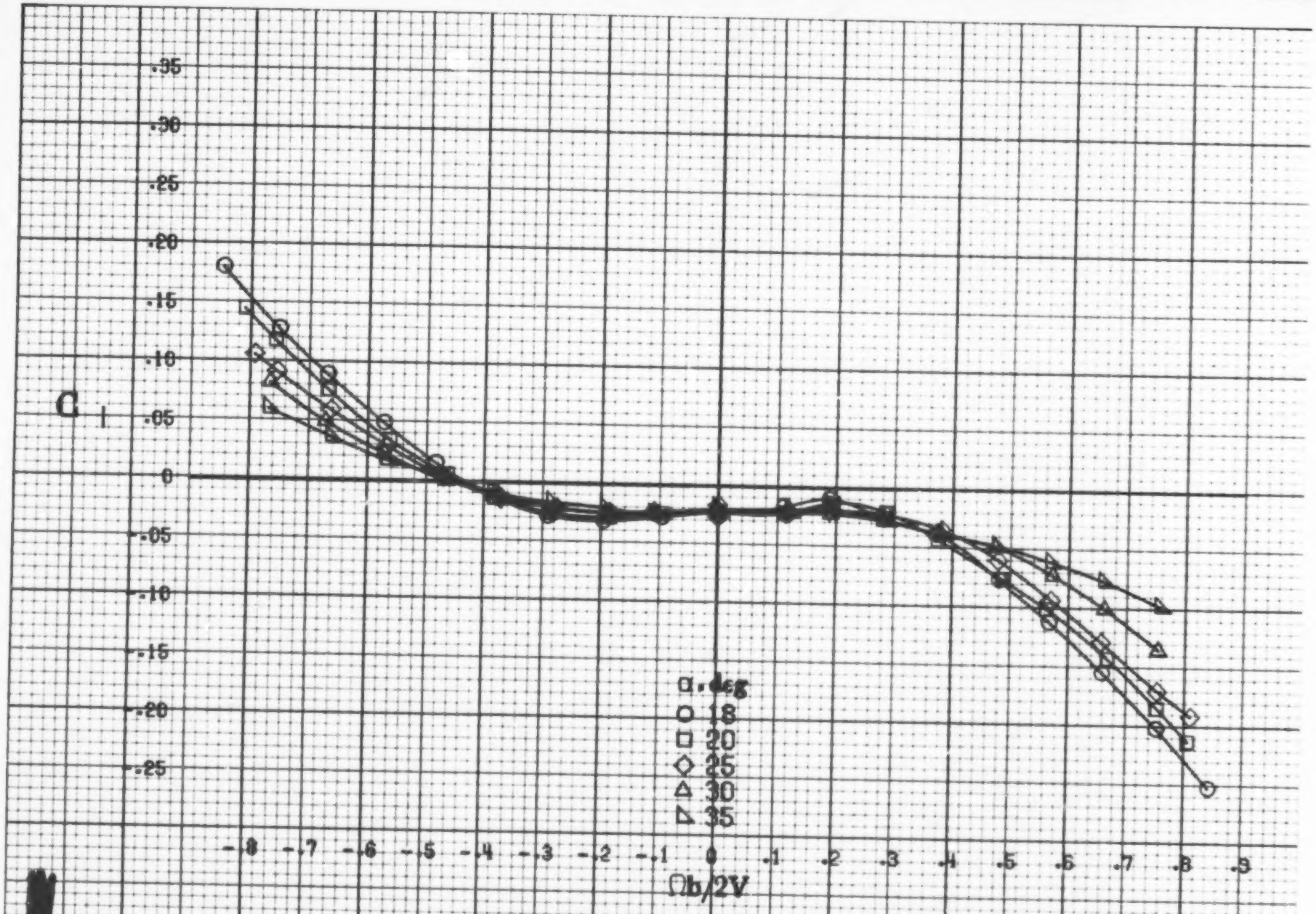

(b) α = 18 to 35 deg, SR = 76 cm (30 in).

Figure A44.-Continued.

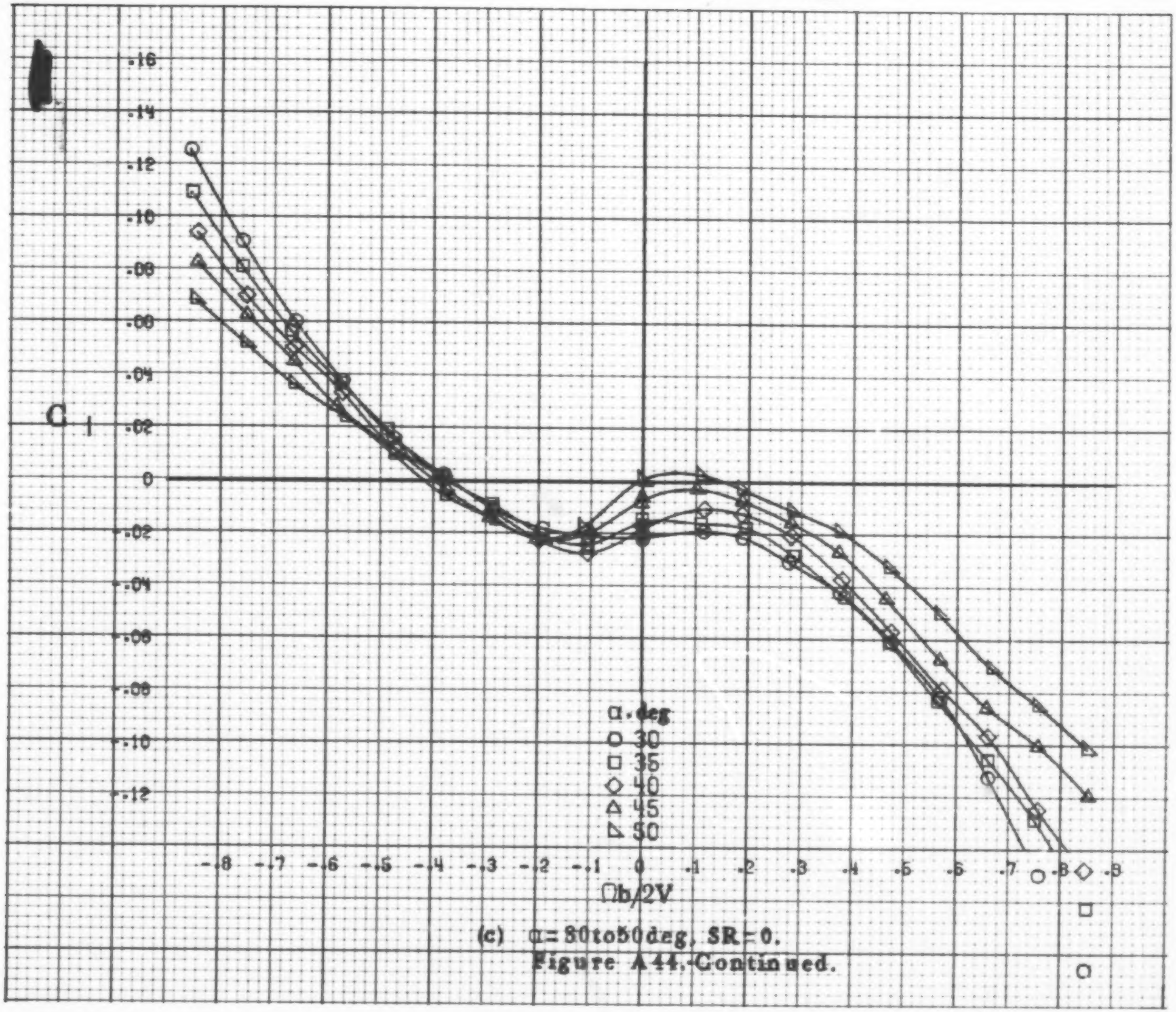

(c) α = 30 to 50 deg, SR = 0.

Figure A44.-Continued.

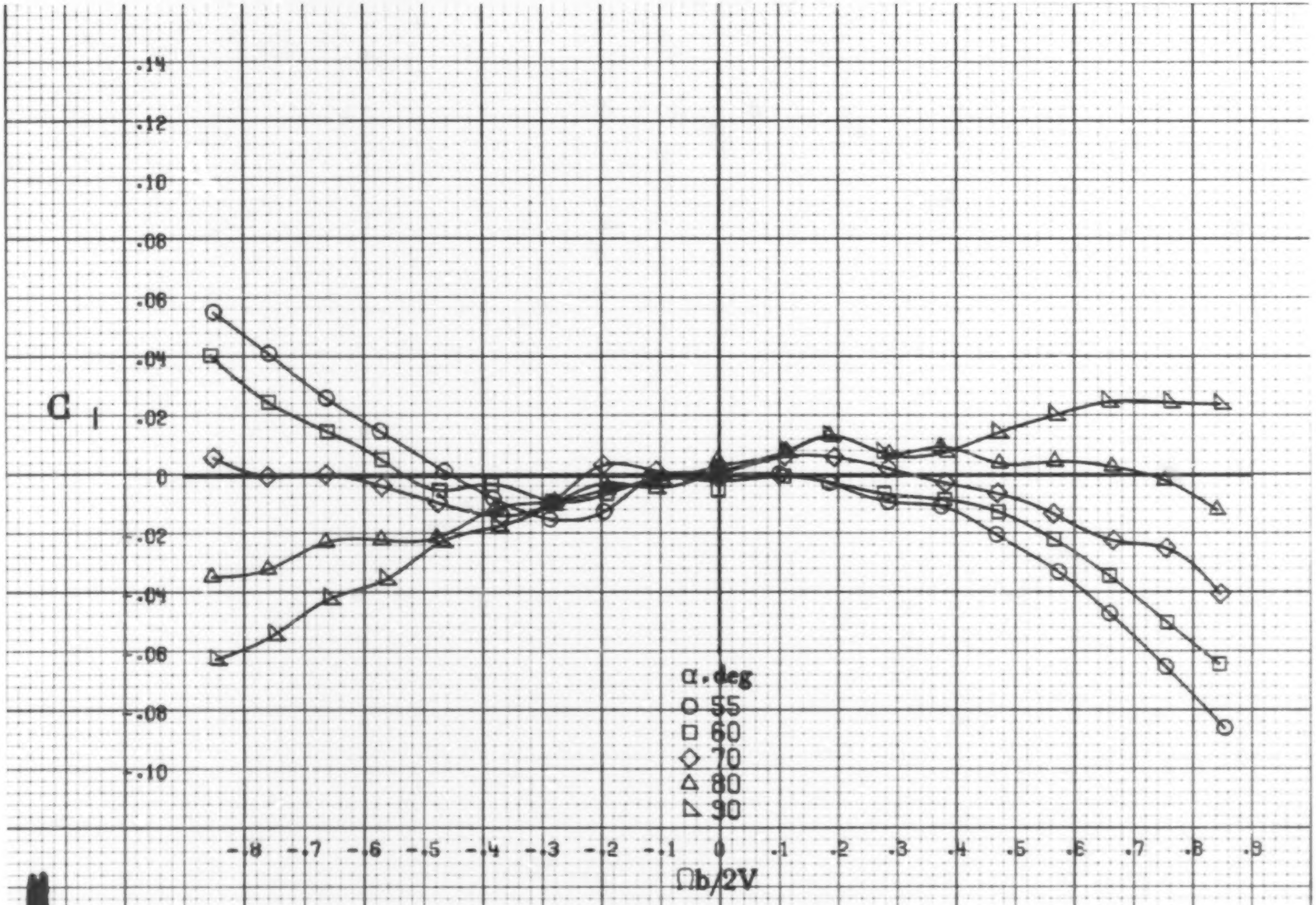

(d) $\alpha = 55$ to 90 deg, SR = 0.
Figure A44.-Concluded.

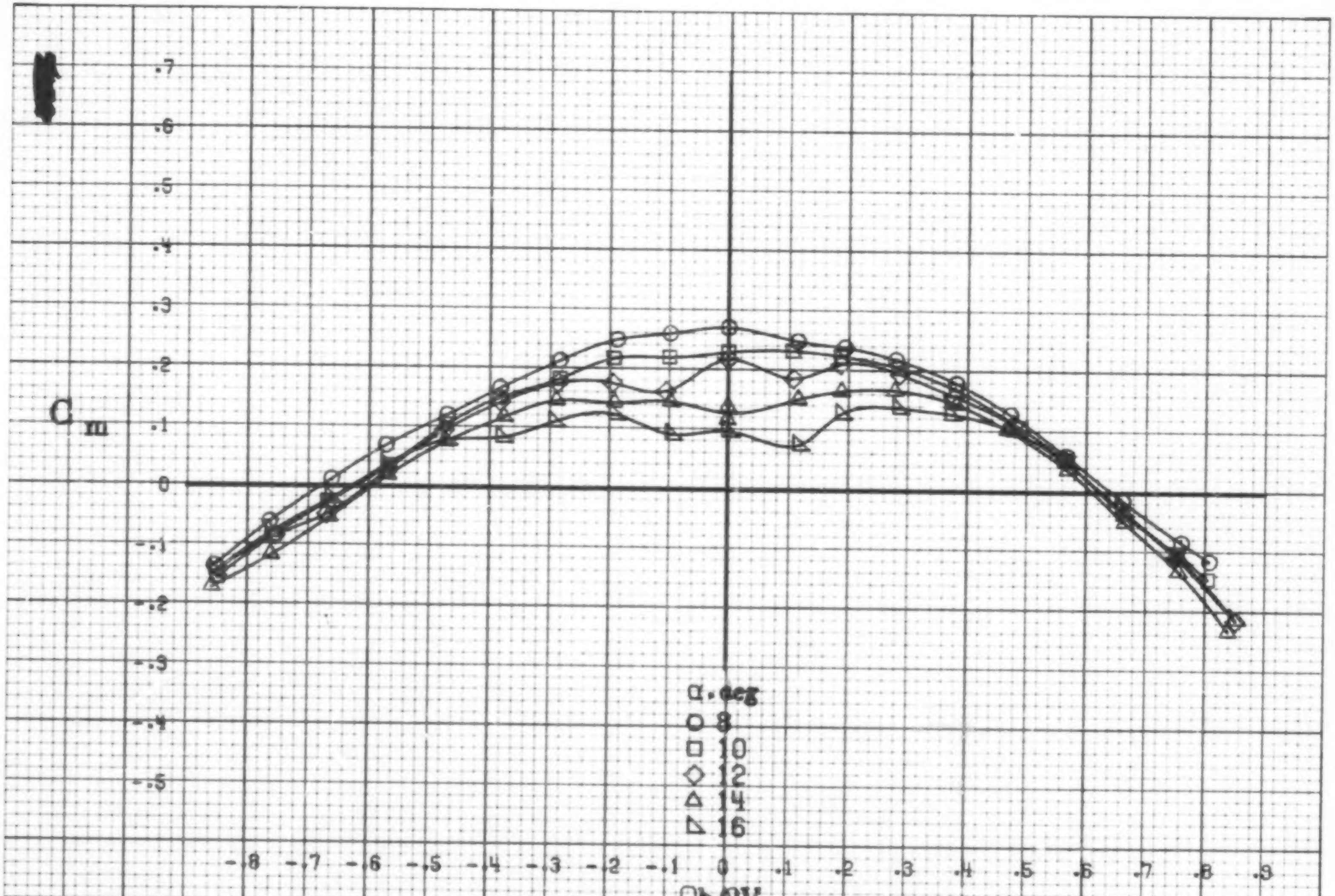

(a) $\alpha = 8$ to 16 deg, SR = 76 cm (30 in).

Figure A45.-Effect of rotation rate and angle of attack on pitching-moment coefficient for basic configuration. $\delta_e = -25°$, $\delta_a = 22.5°$, $\delta_r = 0°$, $\beta = 0°$.

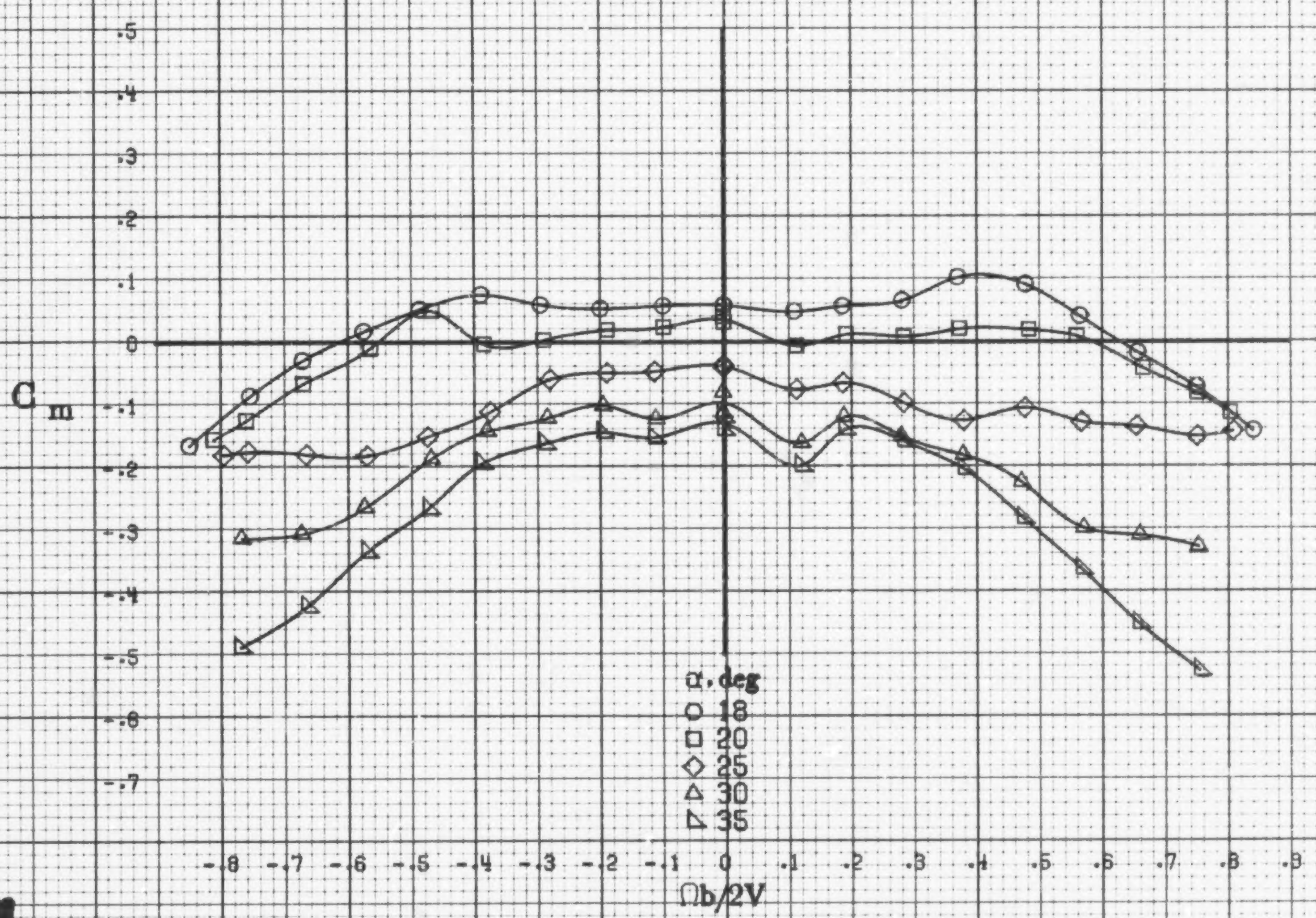

(b) α = 18 to 35 deg, SR = 76 cm (30 in).
Figure A45.-Continued.

A180

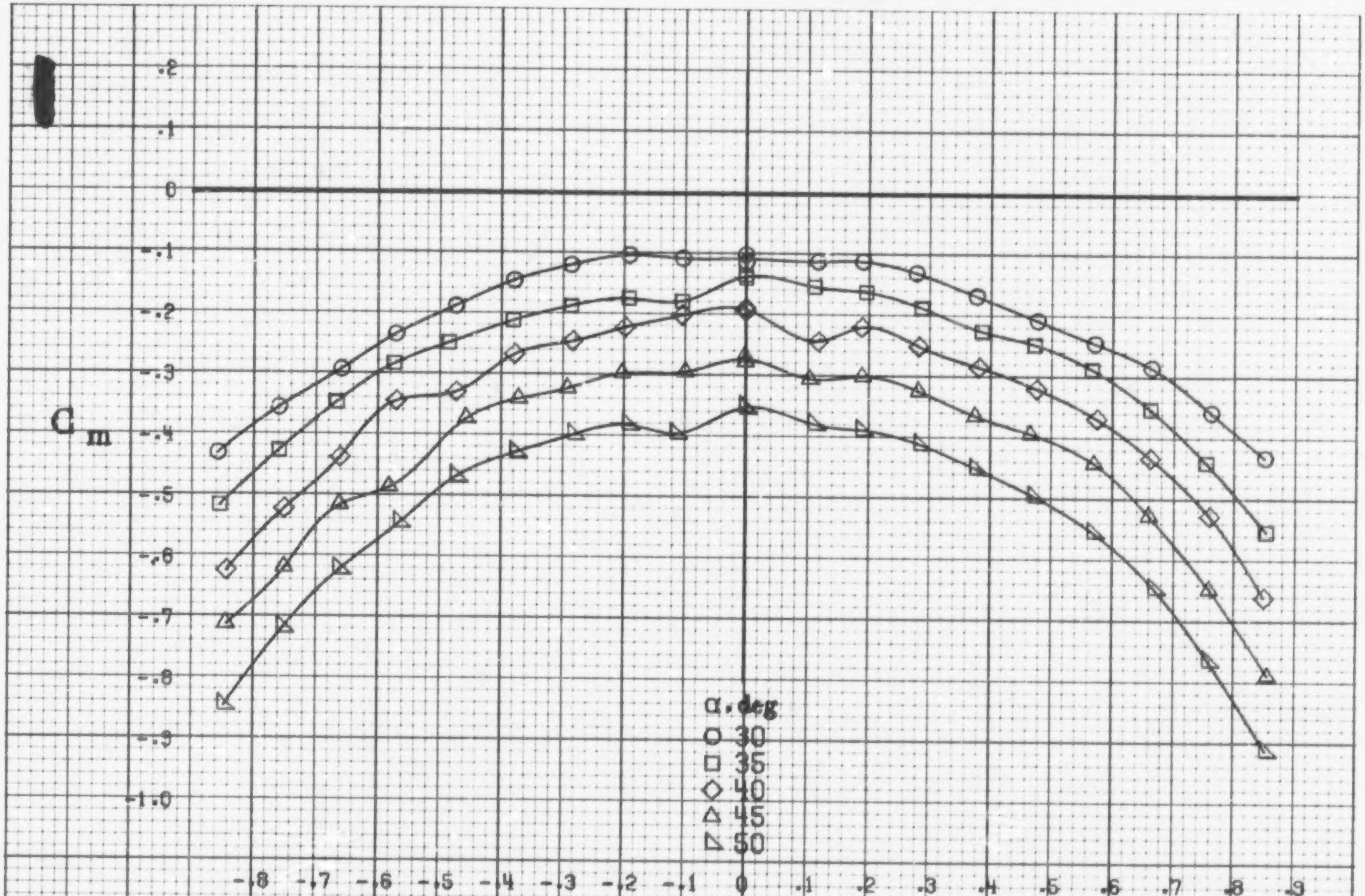

(c) α = 30to50deg, SR = 0.

Figure A45.-Continued.

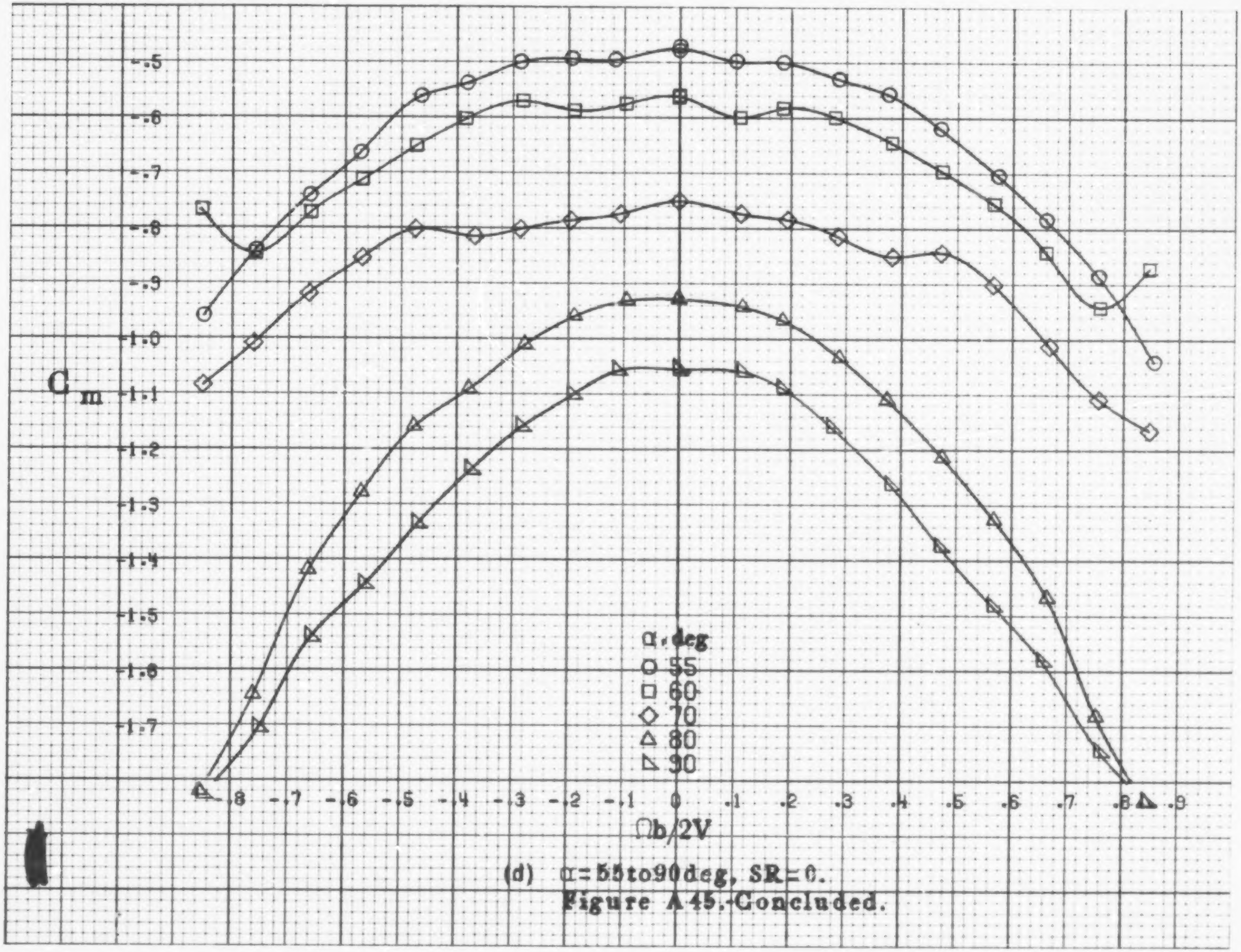

(d) α=55to90deg, SR=0.

Figure A45.-Concluded.

A152

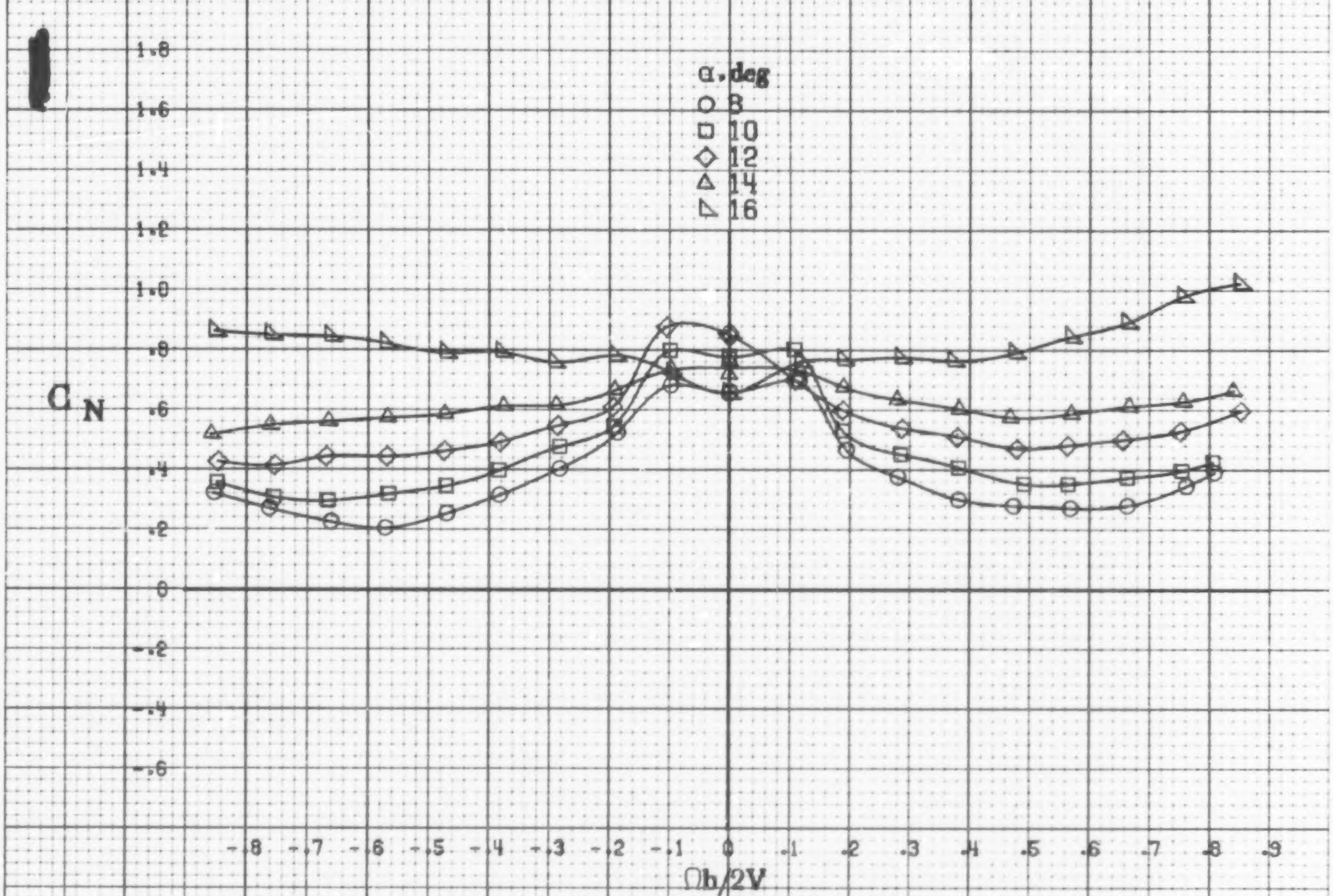

(a) $\alpha = 8$ to 16 deg, SR = 76 cm (30 in).

Figure A46.-Effect of rotation rate and angle of attack on normal-force coefficient for basic configuration. $\delta_e = -25°$, $\delta_a = 22.5°$, $\delta_r = 0°$, $\beta = 0°$.

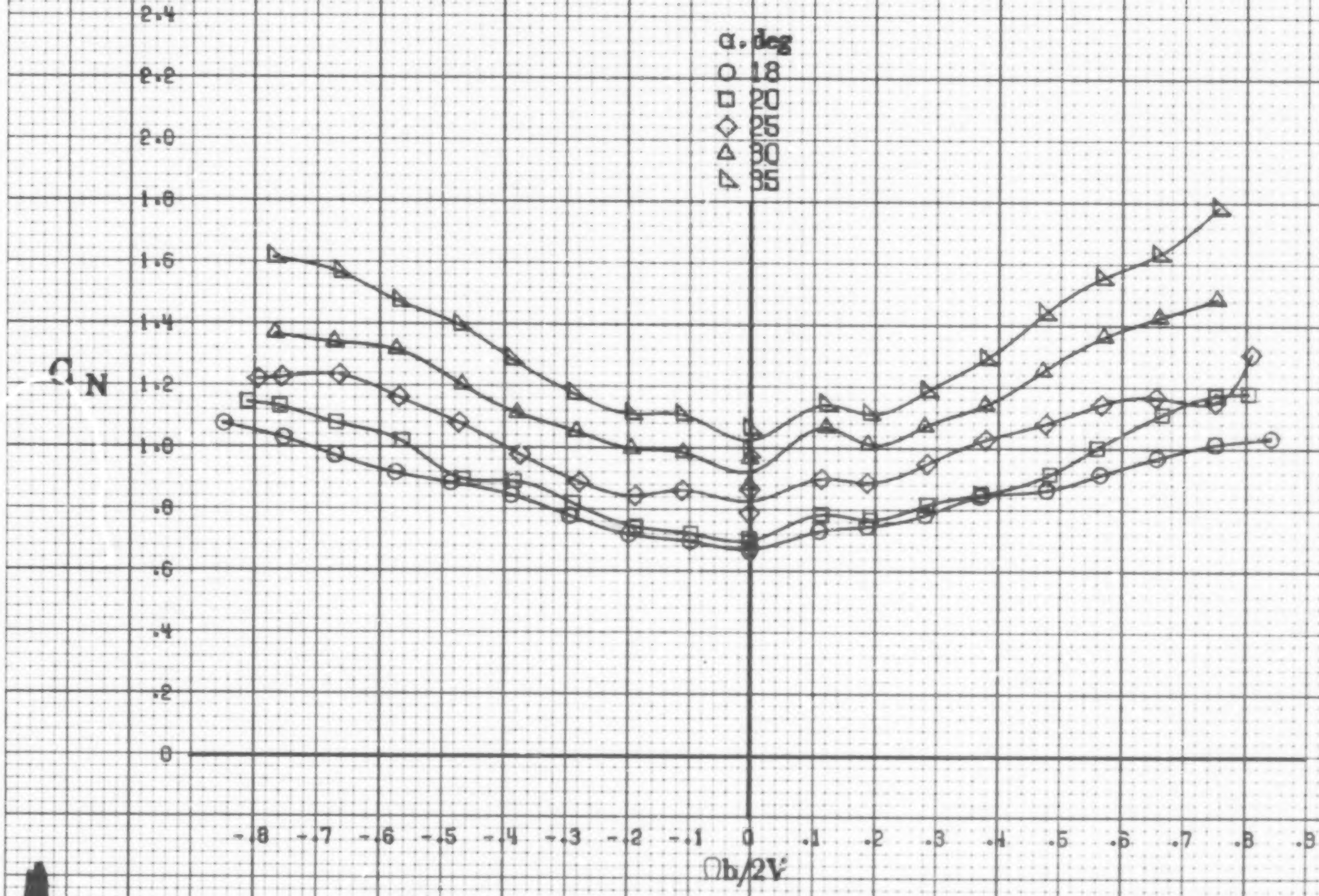

(h) α = 18 to 35 deg, SR = 76 cm (30 in).

Figure A46.-Continued.

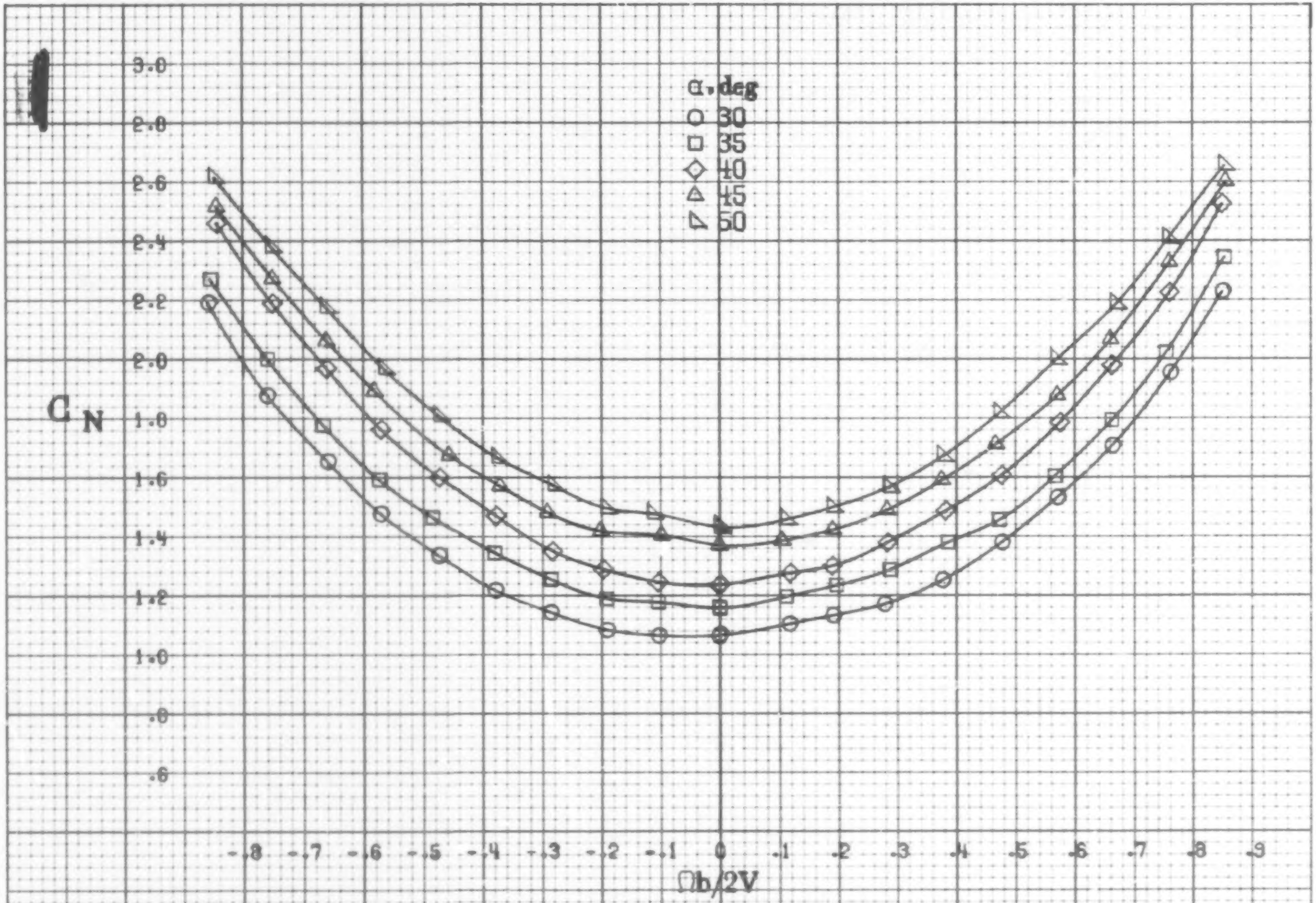

(c) α = 30 to 50 deg, SR = 0.

Figure A46.-Continued.

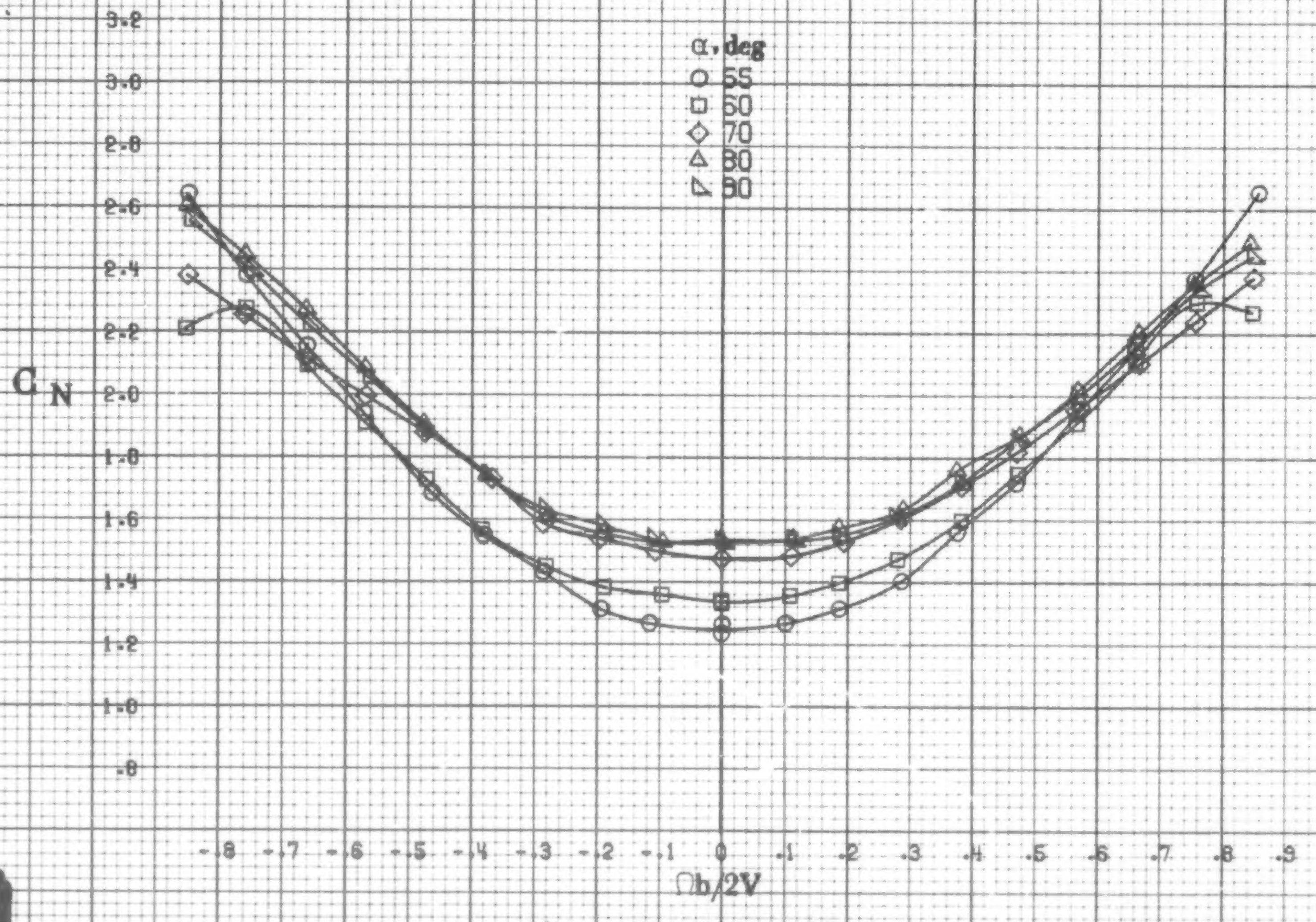

(d) α = 55 to 90 deg, SR = 0.

Figure A46.-Concluded.